

Dynamic Composition of Myelin Basic Protein mRNA-containing Ribonucleoprotein Complexes

Dissertation

zur Erlangung des Grades
Doktor der Naturwissenschaften

am Fachbereich Biologie
der Johannes Gutenberg-Universität Mainz

Peter Hoch-Kraft

geboren am 24.06.1984 in Mainz

Mainz, September 2015

Dekan:

1. Berichterstatterin:

2. Berichterstatter:

Tag der mündlichen Prüfung:

17. November 2015

Table of Contents

Summary	5
List of Figures	7
List of Tables.....	8
Abbreviations	9
1 Introduction.....	11
1.1 Central nervous system myelination in health and disease.....	11
1.1.1 Oligodendrocytes are the myelinating cells in the CNS	11
1.1.2 Myelination of axonal fibers in the CNS.....	13
1.1.3 Adaptive myelination as a component of neuronal network plasticity	15
1.1.4 Dysfunctional myelin impairs the integrity of the neuronal network.....	16
1.2 Myelin basic protein is a fundamental element to organize CNS myelin	17
1.2.1 Expression und functions of classical MBP isoforms.....	17
1.2.2 Spotlight on MBP exon 2-containing isoforms.....	19
1.3 MBP expression is precisely regulated at the posttranscriptional level	20
1.3.1 RNA localization and mRNP complex assembly	20
1.3.2 MBP mRNA is localized to the myelin compartment	21
1.3.3 Transacting factors mediate the MBP mRNA fate in oligodendrocytes.....	22
1.3.4 Axonal signals initiate the spatiotemporal synthesis of MBP	24
1.3.5 Cytoplasmic RNA granule composition dynamically reacts to cellular cues	25
1.4 Identification of novel MBP mRNA-associated proteins.....	26
1.4.1 The multifunctional DEAD Box RNA Helicase 5 (DDX5).....	27
1.4.2 The ALS-associated RNA binding protein Fused in Sarcoma (FUS)	30
1.5 MS2 – a system to dynamically label and isolate RNAs <i>in vivo</i>	32
1.6 Aim of the study	34

2	Material & methods	35
2.1	Material resources	35
2.1.1	Equipment	35
2.1.2	Materials, chemicals and commercial Kits	36
2.1.3	Buffers and Media	38
2.1.4	Software	39
2.2	Antibodies	39
2.3	Molecular biology.....	41
2.3.1	General molecular biological methods	41
2.3.2	Cloning strategy for MBP-MS2 constructs	43
2.3.3	Cloning strategy for <i>firefly</i> luciferase constructs	44
2.3.4	Site directed mutagenesis of DDX5 ^{K144N}	46
2.3.5	Plasmids.....	46
2.4	Cell culture	47
2.4.1	Preparation and culture of primary oligodendrocytes	47
2.4.2	Oli- <i>neu</i> cell culture	47
2.4.3	Transfection methods	48
2.4.4	Generation of MBP14-MS2 stable cell lines.....	49
2.4.5	Incorporation of labeled amino acids into MBP14-MS2 cells for SILAC quantitative proteomics	50
2.5	Proteinbiochemistry.....	50
2.5.1	Cell lysis and subcellular fractionation.....	50
2.5.2	SDS-PAGE and protein visualization	50
2.5.3	Western blotting and immunodetection of selected proteins	51
2.5.4	Optiprep® density gradient centrifugation	51
2.5.5	DDX5 RNA Immunoprecipitation (RIP)	52
2.5.6	MBP14-MS2 streptavidin affinity purification (SA-AP)	53
2.5.7	SILAC quantitative proteomics of MBP14-MS2 affinity purification.....	54
2.5.8	Fluorescent immunocytochemistry	55

2.6	RNA analysis	55
2.6.1	Isolation of total RNA from cultured cells	55
2.6.2	Reverse transcription cDNA Synthesis	56
2.6.3	Quantitative PCR (qPCR)	56
2.7	In situ hybridization techniques	57
2.7.1	Stellaris® single molecule fluorescent in situ hybridization (smFISH).....	57
2.7.2	MS2-RNA visualization by fluorescent in situ hybridization (FISH).....	58
2.8	Luciferase-based MBP translation assay	58
2.9	Online databases and prediction algorithms	59
2.9.1	RBPmap binding site prediction	59
2.9.2	SFmap binding site prediction.....	60
2.9.3	RNAfold, secondary structure prediction.....	60
2.9.4	PANTHER classification of Gene Ontologies (GO)	60
2.9.5	Brain Cell RNAseq database	61
2.10	Statistics	61
3	Results.....	62
3.1	MBP mRNA visualization by single molecule FISH	62
3.2	Structural analysis of the MBP mRNA sequence.....	64
3.2.1	MBP mRNA secondary structure prediction	66
3.3	Establishment of MBP mRNA labeling using the MS2-system.....	67
3.3.1	MBP-MS2 stable cell line generation and subcellular expression	68
3.3.2	Attempted visualization of MBP-MS2-mRNA using tagged MCPs	69
3.3.3	Streptavidin-mediated MBP-MS2 RNA affinity purification.....	70
3.3.4	Identification of proteins associating with MBP14-MS2 mRNA under oxidative stress conditions using SILAC-based quantitative proteomics.....	74
3.4	The role of DDX5 in the posttranscriptional regulation of MBP expression	81
3.4.1	DDX5 is expressed in primary OL and decreases during differentiation.....	81
3.4.2	Cytoplasmic association of DDX5 with MBP mRNA RNP complexes	83

3.4.3	Size fractionation of RNA granules using Optiprep density gradient centrifugation....	85
3.4.4	Knockdown of DDX5 in primary oligodendrocytes increases MBP expression.....	87
3.4.5	Knockdown of DDX5 affects MBP isoform abundance in primary OL	89
3.4.6	Impact of DDX5-siRNA knockdown on oligodendroglial proliferation.....	90
3.4.7	Posttranscriptional regulation of MBP is dependent on the DDX5 helicase activity....	91
3.4.8	Impact of DDX5 on MBP-3'UTR-containing luciferase reporter systems.....	94
3.5	The RNA-binding protein FUS in maintaining MBP mRNA levels.....	95
3.5.1	Consequences of altered FUS levels in oligodendrocytes.....	96
3.5.2	FUS in the response of oligodendroglial cells to oxidative stress	99
4	Discussion	103
4.1	MBP mRNA localization in cultured oligodendroglial cells	103
4.2	Sequence analysis of MBP mRNA predicts secondary structures and a global RBP association profile	103
4.3	MBP mRNA labeling using the MS2-system.....	105
4.4	MS2-based affinity purification of MBP14-MS2-associated factors	106
4.5	MBP14-MS2 affinity purification yields novel targets in stress-dependent MBP mRNP complex remodeling.....	107
4.6	FUS contributes to maintaining MBP mRNA levels in health and disease?.....	109
4.7	DDX5-containing cytoplasmic RNP complexes in oligodendrocytes.....	110
4.8	DDX5 inhibits MBP expression at the posttranscriptional level	113
4.9	DDX5 as a factor regulating alternative splicing in oligodendrocytes?.....	116
4.10	The dual role of DDX5 in the regulation of MBP expression.....	119
4.11	Future Perspectives.....	120
	References.....	123
	Appendix	I
A.	Danksagung	I
B.	Curriculum Vitae.....	II
C.	Publications and presentations.....	Fehler! Textmarke nicht definiert.
D.	Eidesstattliche Erklärung.....	IV

Summary

Myelin Basic Protein (MBP) is a major component of the myelin sheath orchestrating the assembly of compact myelin in the central nervous system and thus ensuring saltatory signal propagation and maintenance of the neuronal network. MBP expression is precisely regulated at the posttranscriptional level and depends on the assembly of MBP mRNA-containing granules, which mediate transport and localized translation at the axoglial contact site. This study focused on the identification of the dynamic composition of these RNP complexes and a detailed functional analysis of the previously identified potential MBP mRNA-associating proteins DDX5 and FUS.

DDX5 was shown to associate with MBP mRNA in subpopulations of cytoplasmic RNP complexes. In oligodendroglial cells DDX5 functioned as an inhibitor of MBP protein synthesis, acting at the posttranscriptional level and depending on the DDX5 helicase activity. Consequently, knockdown of DDX5 in primary OL correlates with the elevation of MBP protein levels and an imbalance of the known MBP-associating RNA-binding proteins hnRNP A2 and hnRNP F. In addition, DDX5-knockdown selectively increased the expression of the exon 2-containing MBP isoforms 17.22-kDa and 21.5-kDa, possibly by affecting alternative splicing of the pre-mRNA.

Alteration of FUS levels did not show a major impact on the myelin protein expression, although MBP mRNA levels were slightly reduced in line with changes in the expression of MBP mRNA-associated proteins hnRNP A2 and DDX5. During oxidative stress, FUS localized to oligodendroglial stress granules and FUS levels inversely correlated with MBP RNA stability upon increasing concentrations of sodium arsenite.

To further examine the dynamic composition of MBP mRNA complexes in a more RNA-centric approach, the MS2-RNA-labeling system was adapted to MBP mRNA. The introduction of MS2 hairpin loops into the MBP transcript allowed its visualization and the purification of associated MBP mRNP complexes. Oligodendroglial cell lines stably expressing moderate levels of MS2-labeled MBP14-MS2 mRNA were generated and single molecule FISH confirmed localization and the physiological behavior of the transcript, which reacted to cellular cues such as oxidative stress. The following affinity purification of MBP14-MS2 mRNP complexes under oxidative stress conditions resulted in the identification of numerous candidates potentially playing a role in stress-dependent RNA granule formation and the regulation of

MBP. This list includes several proteins connected to neurodegenerative or psychiatric diseases and may thus aid in shedding light on mechanisms regulating MBP expression during OL maturation and myelination in health and disease.

List of Figures

1. Introduction

Figure 1-1. Markers of oligodendrocyte differentiation and myelination.....	12
Figure 1-2. Myelination in the central nervous system.....	14
Figure 1-3. Myelin Basic Protein is the “executive” molecule in myelination.....	18
Figure 1-4. Overview of murine MBP isoforms and the role of exon 2.....	19
Figure 1-5. MBP mRNA is transported to the axoglial contact site.....	22
Figure 1-6. MBP mRNA is translationally silent during translocation.....	23
Figure 1-7. MBP mRNA transport and local translation at the axoglial contact site.....	24
Figure 1-8. Cytoplasmic RNA granule composition dynamically adapts to cellular cues.....	26
Figure 1-9. Conserved domains and binding sites of DEAD Box RNA helicases.....	28
Figure 1-10. DDX5 is a multitasking RNA helicase affecting numerous aspects of gene expression.....	29
Figure 1-11. Roles of FUS in the cellular RNA metabolism.....	31
Figure 1-12. Components and applications of the MS2 RNA labeling system.....	33

2. Material & Methods

Figure 2-1. Cloning strategy of MS2 labeled MBP constructs.....	44
Figure 2-2. <i>Firefly</i> luciferase constructs.....	45

3. Results

Figure 3-1. Single molecule fluorescent in situ hybridization (smFISH) of MBP mRNA in oligodendroglial cells..	63
Figure 3-2. Interactive positional mapping of predicted binding sites in murine MBP mRNA.....	65
Figure 3-3. MBP isoform-dependent RNAfold secondary structure prediction.....	67
Figure 3-4. Generation and expression analysis of stable MBP14-MS2 labeled oligodendroglial cell lines.....	69
Figure 3-5. Streptavidin-mediated affinity purification of MBP14-MS2-associated mRNPs.....	71
Figure 3-6. MBP14-MS2 affinity purification under oxidative stress conditions.....	73
Figure 3-7. SILAC-based proteomics to identify MBP14-MS2 RNP complex dynamics during oxidative stress...	74
Figure 3-8. Oxidative stress induced stress granule formation in SILAC-labeled MBP14-MS2 cell lines.....	75
Figure 3-9. PANTHER database classification of proteins identified in SILAC mass spectrometry.....	76
Figure 3-10. Expression and cytoplasmic localization of DDX5 in primary oligodendrocytes.....	82
Figure 3-11. RNA-immunoprecipitation (RIP) of DDX5 enriches MBP mRNA.....	83
Figure 3-12. Cytoplasmic localization of DDX5 and hnRNP A2B1 granules.....	84
Figure 3-13. Size fractionation of RNA granules using Optiprep density gradient centrifugation.....	86
Figure 3-14. DDX5-siRNA knockdown enriches MBP protein levels in primary oligodendrocytes.....	88
Figure 3-15. DDX5-siRNA knockdown results in a shift of the MBP isoform distribution.....	90
Figure 3-16. Impact of DDX5 knockdown on oligodendroglial proliferation.....	91
Figure 3-17. Overexpression of the DDX5 helicase mutant K144N in oligodendroglial cells.....	93
Figure 3-18. Impact of DDX5 on MBP-3’UTR-containing luciferase reporter systems in <i>Oli-neu</i> cells.....	95

Figure 3-19. Impact of FUS-knockdown on primary oligodendrocytes.	97
Figure 3-20. FUS-myc overexpression in primary oligodendrocytes.	98
Figure 3-21. Regulation and subcellular fractionation of selected RBPs after FUS-knockdown.	99
Figure 3-22. FUS localization to TIA1 positive foci in oligodendroglial cells.	100
Figure 3-23. Oxidative stress and FUS-knockdown in Oli-neu cells change.	101

4. Discussion

Figure 4-1. Working model of DDX5-mediated MBP silencing mechanisms.	114
Figure 4-2. Prediction of splicing factor binding sites in MBP exon 2-surrounding regulatory regions.	117
Figure 4-3. The dual role of DDX5 in the posttranscriptional regulation of MBP synthesis.	120

List of Tables

2. Material & Methods

Table 2-1. Cell culture equipment.	35
Table 2-2. Microscopes and objectives.	35
Table 2-3. Other lab equipment.	35
Table 2-4. Materials, chemicals and commercial Kits.	36
Table 2-5. Buffers, media and solutions.	38
Table 2-6. Software.	39
Table 2-7. Monoclonal primary antibodies.	39
Table 2-8. Polyclonal primary antibodies.	40
Table 2-9. Secondary antibodies.	40
Table 2-10. Primer pairs used in PCR.	41
Table 2-11. PCR cycler program.	41
Table 2-12. Plasmids.	46
Table 2-13. siRNA.	48
Table 2-14. Reverse transcription cycler program.	56
Table 2-15. Taqman® Gene Expression Assays.	57
Table 2-16. Primer pairs used in SYBR Green qPCR.	57
Table 2-17. FISH probe used for MS2-RNA visualization.	58
Table 2-18. Plasmid amounts for FuGENE HD transfections in MBP Luciferase Assays.	59

3. Results

Table 3-1. Proteins enriched to MBP14-MS2 complexes under oxidative stress conditions.	77
Table 3-2. Proteins enriched in MBP14-MS2 complexes in the absence of oxidative stress.	78
Table 3-3. Selected RNPs enriched in MBP14-MS2 complexes under oxidative stress conditions.	80

Abbreviations

3'UTR	3' untranslated region
5'UTR	5' untranslated region
A2RE	hnRNP A2 response element
ALS	Amyotrophic lateral sclerosis
AP	Affinity purification
ATP	Adenosine triphosphate
CDS	Coding sequence
CLIP	Cross-linking and immunoprecipitation
CNP	2',3'-Cyclic-nucleotide 3'-phosphodiesterase
CNS	Central nervous system
CPE	Cytoplasmic polyadenylation element
DIV	Days <i>in vitro</i>
DNA	Desoxyribonucleic acid
EGCG	Epigallocatechin-3-gallate
EJC	Exon Junction Complex
FISH	Fluorescent in situ hybridization
FMR1/FMRP	Fragile X mental retardation / Fragile X Mental Retardation Protein
FTLD	Frontotemporal lobar degeneration
FUS/TLS	Fused in Sarcoma/Translocated in Liposarcoma
FXS	Fragile X syndrome
GFP	Green fluorescent protein
HD	Huntingtons' disease
IP	Immunoprecipitation
KO	Knock-out
LUC	Luciferase
MACS	Magnetic Cell Separation
MBP	Myelin basic protein
MBS	MS2 binding site
MCP	MS2 coat protein
MOBP	Myelin-Associated Oligodendrocyte Basic Protein
MOG	Myelin Oligodendrocyte Glycoprotein

MS	Multiple Sclerosis
MSA	Multi system atropy
MT	Microtubule
NES	Nuclear export sequence
NLS	Nuclear localization sequence
NMD	Nonsense-mediated decay
OL	Oligodendrocyte
OPC	Oligodendrocyte progenitor cell
ORF	Open reading frame
PB	P-bodies, processing bodies
PLP	Proteolipid protein
pOL	Primary oligodendrocyte
QKI	Quaking
QRE	Quaking response element
RBP	RNA-binding protein
RIP	RNA immunoprecipitation
RISC	RNA-induced silencing complex
RLR	RNA localization region
RNA	Ribonucleic acid
RNP	Ribonucleoprotein (-complex)
RRM	RNA-recognition motif
SA	Streptavidin
SG	Stress granule
SILAC	Stable isotope labeling by/with amino acids in cell culture
TDP-43	Transactive response DNA-binding protein 43
TIA-1	T cell-induced antigen 1
TOG	Tumor overexpressed gene
uORF	upstream open reading frame

1 Introduction

1.1 Central nervous system myelination in health and disease

1.1.1 Oligodendrocytes are the myelinating cells in the CNS

The mammalian central nervous system (CNS) is composed of a complex network of synaptically interconnected neurons, embedded in an environment of supportive glial cell types. Glial cells classically comprise astrocytes, microglia, oligodendrocyte precursor cells (OPC) and oligodendrocytes (OL) and in humans by far outnumber neurons (Verkhratsky, 2010). As neurons are considered as the “executive cells” in the brain that process and store information, the simplistic view on glia has developed to a broad spectrum of cell type specific glial functions ensuring the functionality and plasticity of the whole neural network (Allen and Barres, 2009; Barres, 2008). Single-cell RNA sequencing recently has identified 47 molecularly distinct subclasses of neural cell types in the hippocampus and somatosensory cortex hinting to an extensive cellular heterogeneity. This study also revealed 6 subclasses of maturing oligodendrocytes, of which one subclass was almost exclusively observed in the somatosensory cortex (Zeisel et al., 2015). Discovery of a widespread spatial astrocyte heterogeneity moreover indicates a regional glial brain organization and function (Bayraktar et al., 2015) and supports the idea of a versatile ensemble of different neuronal and glial cell types orchestrating higher brain functions.

A striking feature of higher eukaryotic nervous systems is the evolution of myelination, which facilitates the fast conduction of neuronal signals and is believed to have been a prerequisite for the evolution of larger vertebrates including humans (Zalc et al., 2008). During the myelination process axonal nerve fibers are isolated with multiple layers of compact myelin membranes (internodes) and the formation of interspersed Nodes of Ranvier is the basis of fast saltatory signal propagation (Tasaki, 2007). The glial cell type responsible for the generation of CNS myelin is the oligodendrocyte, which originates from oligodendrocyte precursors (OPC). During embryonal development, OPC arise in sequential waves from distinct gliogenic zones in spinal cord and forebrain (Richardson et al., 2006). The proliferating cells extend their population, distribute throughout the CNS on migratory paths, finally settling the developing brain with a uniform spacing (Kirby et al., 2006) and adjusting appropriate numbers as a prerequisite for subsequent myelination (Barres and Raff, 1994). This

distribution is continuously maintained during adulthood, rendering OPCs as a stem cell in the adult brain (Hughes et al., 2013). When OPCs contact axons in prospective white matter areas, a polarization towards the axoglial contact site is orchestrated and differentiation into myelination-competent mature OL is initiated.

The differentiation program encompasses the upregulation of myelin specific proteins and lipids, accompanied with morphological changes from a bipolar progenitor to a multipolar cell with a branched network of oligodendrocyte processes that finally fuse to myelin sheets enwrapping up to 40 different axons simultaneously (Simons and Trotter, 2007). Cytoskeletal regulation plays an essential role during this processes and is highly dependent on extracellular and intracellular signals (Bauer et al., 2009). Cellular markers of oligodendroglial maturation are summarized in Figure 1-1, NG2 and PDGFR- α are classical proteins expressed in OPC, whereas upregulation of myelin proteins CNP, PLP, MBP or MOG indicates ongoing maturation of the cells (Baumann and Pham-Dinh, 2001). This intrinsic maturation program can also be recapitulated in isolated cultured cells in the absence of growth factors, while

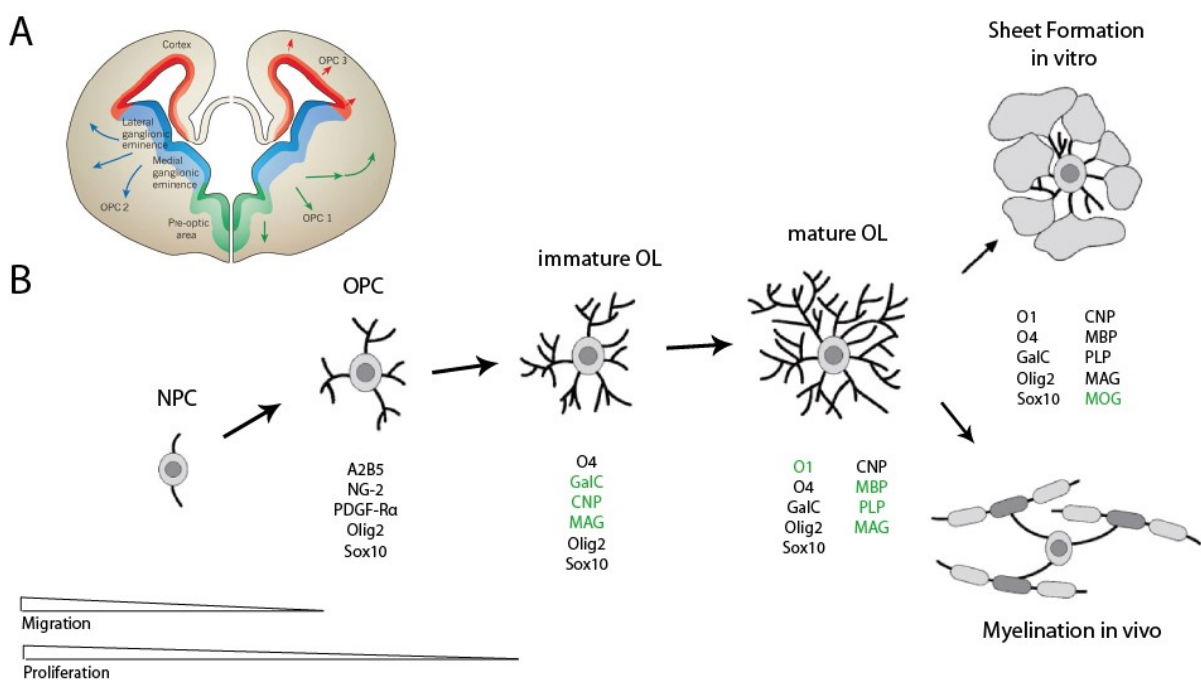


Figure 1-1. Markers of oligodendrocyte differentiation and myelination

(A) OPC generation and migration in the developing brain occurs in three waves emanating from gliogenic ventricular zones. Adapted from (Rowitch and Kriegstein, 2010). **(B)** OL differentiation encompasses the upregulation of myelin-specific proteins and lipids. This is accompanied by morphological changes from a bipolar progenitor to a multipolar cell with a branched network of oligodendrocyte processes that finally fuse to myelin sheets *in vitro* or give rise to myelination *in vivo*. Stage-specific markers are shown below the illustrations of the cells. Details are described in the text. Modified from (Gielen et al., 2006).

axonal signals are required to control timing and the extent of myelination *in vivo* (Barres and Raff, 1999). Extracellular signals, intracellular pathways and transcription factors regulating OPC specification, proliferation, migration and finally oligodendrocyte differentiation are well studied and excellently reviewed in detail by Ben Emery and colleagues (Mitew et al., 2014).

1.1.2 Myelination of axonal fibers in the CNS

Surprisingly, artificial nanofibers with a diameter of >400 nm can be a substrate for oligodendrocyte myelination in culture, hinting to an intrinsic, biophysically encoded program to at least initiate the wrapping process of axonal fibers (Lee et al., 2012b). However, proper compaction and myelination of smaller diameter fibers were usually not achieved, highlighting the importance of axonal signals and the interplay of repulsive and attractive signals to ensure selective axonal fiber selection and myelin initiation in the CNS. Indeed, organization of axoglial complexes (e.g. clustering of nodal sodium channels and adhesion molecules on the axon) is instructed by reciprocal cellular interactions and signaling cascades (Simons and Trajkovic, 2006; Susuki and Rasband, 2008).

Recent models, obtained by *in vivo* imaging techniques, suggest a mechanism of wrapping the myelin sheet by extending a leading inner tongue adjacent to the axon in a croissant-like manner, accompanied by lateral expansion of the internode (Snaidero et al., 2014; Sobottka et al., 2011). In zebrafish, an individual myelination process is accomplished in only 5 hours, highlighting the extensive synthesis of myelin components during this timeframe (Czopka et al., 2013). As the myelin sheath evolves, cytoplasmic areas are retracted from the stacked membranes and tight association of the inner leaflets of the OL plasma membrane lead to a compaction process, which is highly dependent on MBP (see also Chapter 1.2). During myelination the myelin sheet stays connected to the cell body via myelinic channels, which are microtubule filled routes for trafficking myelin components such as vesicles and mRNA transport granules to the adaxonal leading edge (Snaidero et al., 2014) and in part are retained after successful assembly of compacted myelin (Velumian et al., 2011). Wrapping continues until a final thickness of the myelin sheath is achieved, which increases concomitantly with axonal diameter and can be measured as a relatively stable g-ratio (axon diameter divided by the total diameter of the myelinated fiber).

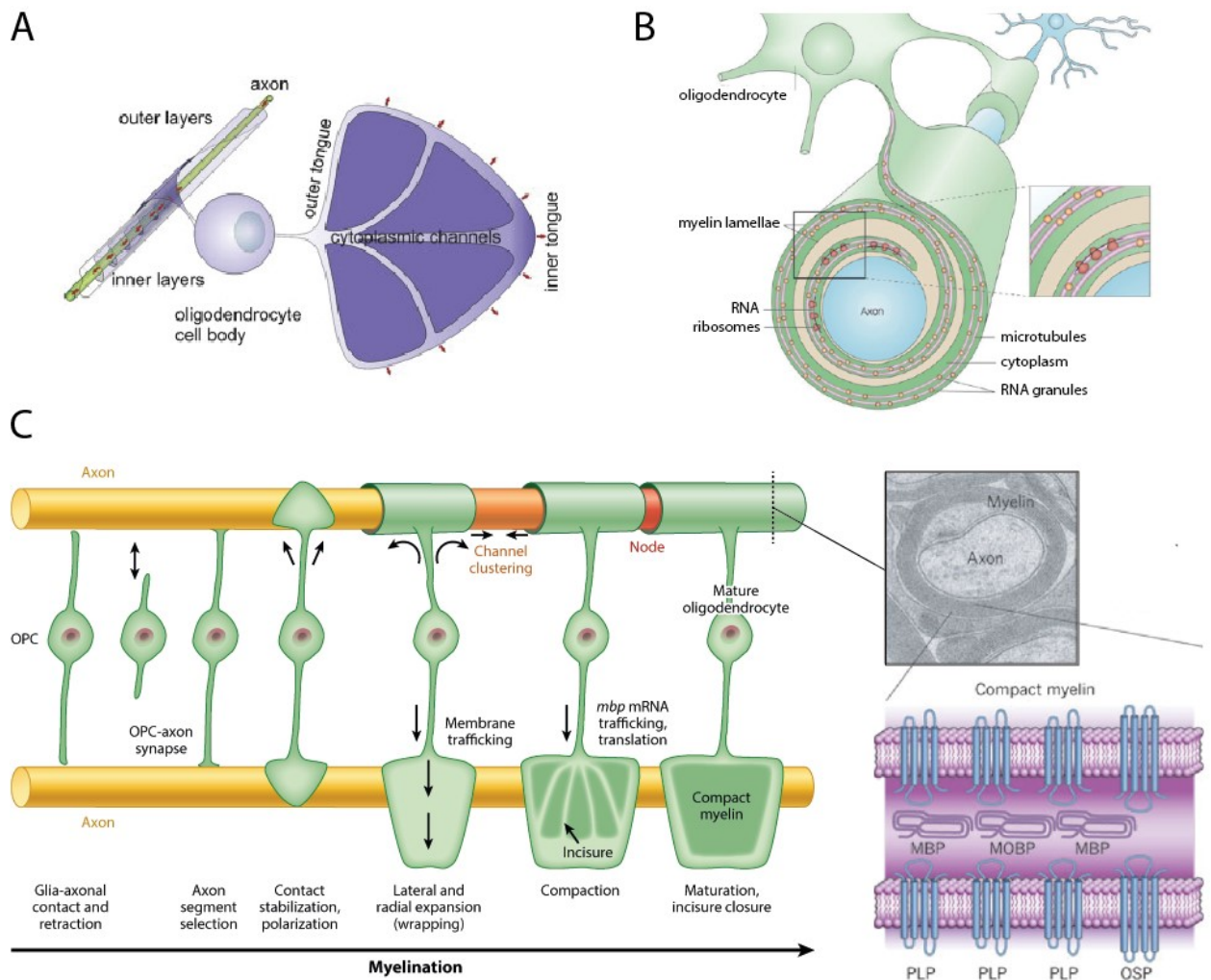


Figure 1-2. Myelination in the central nervous system

(A) Mechanism of axonal enwrapping. Extension of the leading inner tongue accompanied by lateral growth of the myelin sheet leads to a spiral wrapping of the axon. Adapted from (Snaidero et al., 2014). **(B)** Scheme of a growing myelin sheath with indicated RNA transport on microtubules along the cytoplasmic channels and local translation at the adaxonal membrane. Adapted from (Sherman and Brophy, 2005). **(C)** OL differentiation and myelination process from OPC to mature OL, from initial axonal contact to the formation of a compact myelin sheath, including an EM-micrograph of a dissected myelinated axon and schematic representation of compact myelin-associated proteins. Details are described in the text. Modified from (Nave, 2010; Nave and Werner, 2014).

The number of myelinated axons in a given area is variable, reliant on the brain region and the neuronal cell type. Recently, studies on the structural heterogeneity of myelinated tracts in the neocortex indicated that different intermittent myelination profiles may occur, leaving large intermediate axonal segments unmyelinated (Tomassy et al., 2014), challenging the view of myelin as simply a prerequisite for unidirectional saltatory nerve conduction (Fields, 2014).

Nevertheless, in line with its insulating properties, myelin membrane shows a unique composition of proteins and is highly enriched in lipids, especially in the glycosphingolipids galactosylceramide and -sulfatide, plasmalogens and cholesterol (Quarles, 2006). Proteomic

studies revealed a growing number of proteins associated with myelin (de Monasterio-Schrader et al., 2012; Jahn et al., 2009) and mRNAs have been shown to be transported to the myelin compartment as a source for rapid and extensive localized myelin protein synthesis (Colman et al., 1982).

In the axoglial complex, paranodal cytoplasmic channels remain open maintaining and possibly adapting myelin during adulthood (Velumian et al., 2011). In addition to myelination, accumulating evidence suggests a major role of OL in providing metabolic support to axons (Funfschilling et al., 2012; Lee et al., 2012c; Nave, 2010). It is suggested that metabolites such as lactate or pyruvate can be shuttled to adjacent axons via the monocarboxylate transporter 1 (MCT1) and are used to generate ATP in axonal mitochondria. An alternative mechanism contributing to the axonal support could be the transfer of oligodendroglial exosomes, that may carry demanded proteins or nucleic acids to the neuron in response to axonal glutamate signaling (Frohlich et al., 2014; Fruhbeis et al., 2012; Fruhbeis et al., 2013).

1.1.3 Adaptive myelination as a component of neuronal network plasticity

Oligodendroglial biology is highly interconnected to neuronal activity ensuring selective myelination and long-term axonal integrity. OPC can receive synaptic input from neurons (Bergles et al., 2010; Bergles et al., 2000) and OPC not only respond to, but are also able to modulate the neuronal network activity in response (Sakry et al., 2014). In rodents, oligodendrogenesis and de novo myelination continues into adulthood (Young et al., 2013) and may contribute to myelin plasticity. As myelination determines the signal transmission rate of associated neurons, dynamically changing the degree of myelination has the potential to modulate the network activity, influencing learning and cognition (Fields, 2008). Indeed, electrical activity of the target axon affects myelination *in vitro* and *in vivo* (Demerens et al., 1996; Gibson et al., 2014; Wake et al., 2011) and in living zebrafish, sheet number of individual OL is directly correlated with the activity-dependent release of synaptic vesicles (Mensch et al., 2015). Moreover, initiation of myelination is autonomous in individual OL processes and dependent on a non-synaptic release of neurotransmitters from corresponding electrically active axons, leading to a localized translation of MBP (Wake et al., 2015). In humans, performing complex tasks like piano playing changes patterns of myelination in corresponding brain areas (Bengtsson et al., 2005) and by blocking production of newly born adult OL and consequently myelination, learning of new motor skills in adult mice is impaired (McKenzie et al., 2014).

1.1.4 Dysfunctional myelin impairs the integrity of the neuronal network

Consequences of adaptive myelination, especially in humans remain poorly understood, but open an exciting field of mechanisms controlling extra-neuronal plasticity in the central nervous system. Today, a wide range of psychiatric disorders including autism, depression or schizophrenia (reviewed in (Fields, 2008) have been linked to oligodendrocyte or myelin dysfunction and early social deprivation during childhood, a major risk factor for psychiatric diseases, leads to changes in myelination patterns in the prefrontal cortex (Toritsuka et al., 2015). Integrated research, implying the interplay of cellular networks is a challenging task, but indispensable to understand pathologic mechanisms in the CNS.

The most frequent white matter disease is still multiple sclerosis (MS), where autoimmune reactions lead to focal demyelination and eventually a decline of associated neurons (Compston and Coles, 2008). Loss of myelin can be compensated by remyelination, that shares characteristics with developmental myelination (Fancy et al., 2011), but is limited during progressing disease. Even if remyelination seems more robust than anticipated (Powers et al., 2013), the restrictive environment in MS lesions must be overcome to initiate the remyelination program (Fancy et al., 2010). The presence of OPC in chronic MS lesions, but a reduction or absence of mature OL, indicates impaired differentiation as a source for failing remyelination (Kuhlmann et al., 2008). Overcoming this brake could improve remyelination, prevent neuronal degeneration and finally attenuate disease progression.

Accumulating evidence also links OL dysfunction to the pathogenesis of various neurodegenerative diseases. In amyotrophic lateral sclerosis (ALS), degeneration of OL precedes the loss of affected motor neurons (Kang et al., 2013) and regenerated OL seem dysfunctional (Philips et al., 2013). Furthermore, classical neurodegenerative diseases like Alzheimer's disease (AD), Huntington's disease (HD) or multiple system atrophy (MSA) show a wide contribution at the oligodendroglial level, reviewed by (Ettle et al., 2015).

Dysfunctionality or loss of myelin, but also the disturbance of myelin-independent oligodendroglial functions may play a role in numerous pathogenic conditions (Bercury and Macklin, 2015) and encourage a reconsideration of the contribution of myelin and oligodendrocytes to the neural network homeostasis in health and disease.

1.2 Myelin basic protein is a fundamental element to organize CNS myelin

Myelin Basic Protein (MBP) is one of the most abundant myelin proteins (Jahn et al., 2009) and co-evolved together with myelination itself (Nawaz et al., 2013). Several animal models, like *shiverer* mice (Readhead and Hood, 1990), Long Evans shaker rats (O'Connor et al., 1999) or *mbp(jive)* mice (Staats et al., 2015) lack appropriate MBP expression and show severe dysmyelination phenotypes and premature death, highlighting the fundamental importance of MBP in myelination and CNS integrity.

1.2.1 Expression und functions of classical MBP isoforms

The classical murine MBP isoforms arise from a locus called *genes of oligodendrocyte lineage (golli)* and range from 14 kDa to 21.5 kDa in mass (Campagnoni et al., 1993). The generation of at least 6 classical isoforms is dependent on alternative splicing of MBP exon II and exons V/VI (de Ferra et al., 1985; Newman et al., 1987; Takahashi et al., 1985) and leads to a set of basic myelin proteins with essential functions in oligodendrocytes and myelination (Harauz and Boggs, 2013). As a second family, *golli* proteins arise from a different transcription start site, show a more ubiquitous expression in the immune and nervous system, can include exons of the classical MBP isoforms, but are not associated with myelin. *Golli* knock-out mice do not show a severe dysmyelination phenotype, but OL maturation is affected and the mice exhibit hypomyelination in selected brain areas (Jacobs et al., 2005).

Classical MBPs have been described to be multifunctional proteins, with an extraordinary degree of posttranslational modification, affecting binding properties and functions (Boggs, 2006) and the membrane-bound MBP is well-studied as part of myelin formation. MBP is an intrinsically disordered protein (IDP), which adapts its conformation dependent on interacting molecules (Harauz et al., 2004). The high proportion of basic amino acids favors adherence to the negatively charged lipids and facilitates myelin compaction and formation of the major dense line (Bakhti et al., 2014). Upon lipid binding, phase transition from soluble MBP protein to a protein meshwork at the inner leaflets of the myelin lipids tightly zippers the membranes together (Aggarwal et al., 2013) and the highly ordered association of MBP forms a 'molecular sieve' that restricts diffusion of membrane-associated proteins into compacted sheets (Aggarwal et al., 2011). MBP also influences the composition of lipids (Fitzner et al., 2006) and polarizes the membrane towards the compacted myelin insulation. Furthermore, recent

studies provide evidence that during axonal enwrapping F-actin turnover at the leading edge is essential for the protrusion and spreading of the membrane and disassembly of the actin cytoskeleton is a key factor in myelin wrapping (Nawaz et al., 2015; Zuchero et al., 2015). Interestingly, the disassembly of actin filaments is highly dependent on MBP and its absence leads to defects in the axonal wrapping mechanism (Zuchero et al., 2015). In the mature myelin sheath, MBP is maintaining the compacted structure and has been found to be one of the most stable proteins in the brain, with a half-life of several months (Savas et al., 2012).

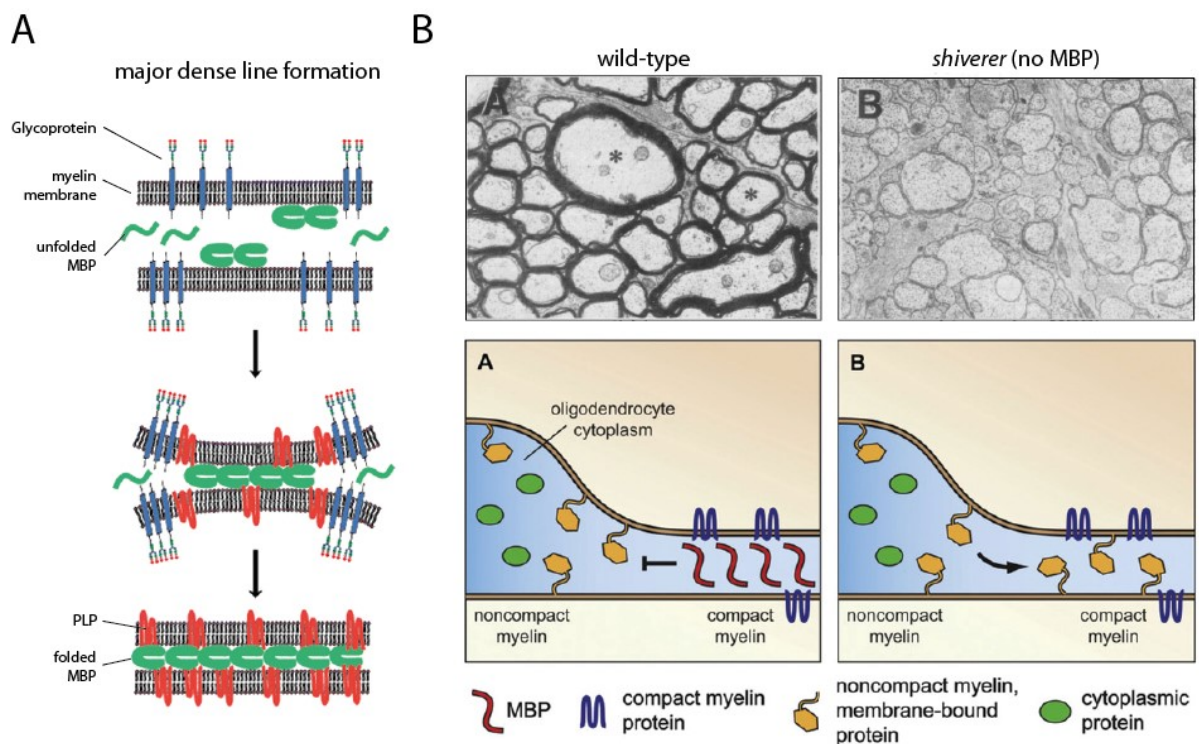


Figure 1-3. Myelin Basic Protein is the “executive” molecule in myelination

(A) Model of MBP-induced compaction at the inner leaflets of the OL myelin membrane. Association of folded MBP zippers the membranes together and leads to formation of the major dense line. Modified from (Bakhti et al., 2014). **(B)** MBP in the compacted myelin acts as a molecular sieve that restricts the diffusion of non-compact myelin proteins and lipids into the sheets. Loss of MBP in the *shiverer* mouse model leads to free diffusion of non-myelin associated proteins and leads to a loss of compact myelin, visible in the EM-micrographs below. Adapted from (Readhead et al., 1987; Zuchero and Barres, 2011).

In addition, numerous reports on the molecular functions of MBP suggest important roles in organizing the cytoskeleton, tethering proteins containing SH3-domains or Calmodulin, participating in Fyn-kinase-mediated signaling and regulation of cellular Ca^{2+} homeostasis (Harauz and Boggs, 2013).

1.2.2 Spotlight on MBP exon 2-containing isoforms

Inclusion of MBP exon 2 into the mature protein can be a major determinant of the protein function. Classical MBP isoforms containing exon 2 are expressed earlier in OL development (Barbarese et al., 1978) and become re-expressed in OL prior remyelination in MS lesions (Capello et al., 1997).

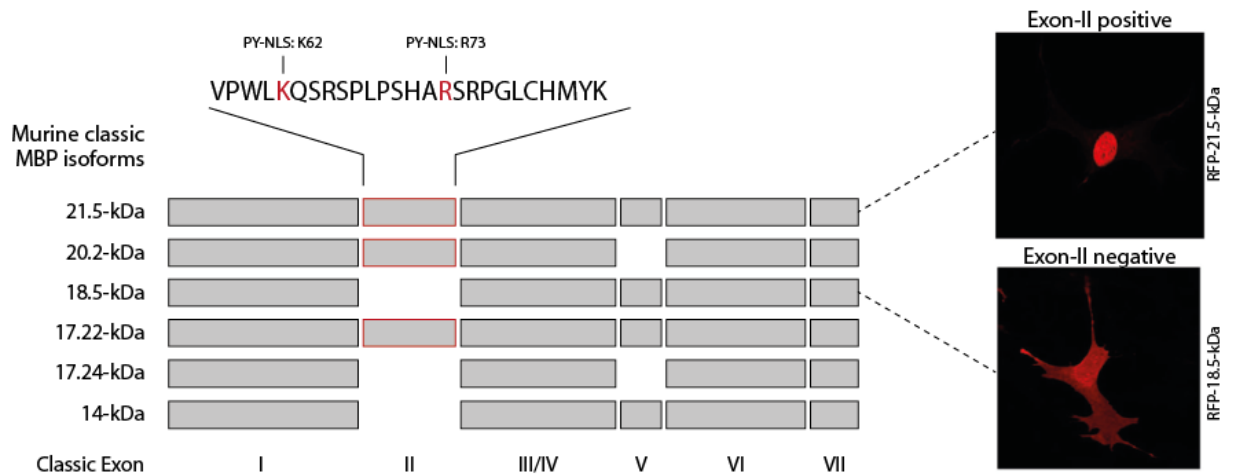


Figure 1-4. Overview of murine MBP isoforms and the role of exon 2

Exon-composition of the 6 classic MBP isoforms in the mouse. The sequence of exon 2 is enlarged and amino acids (K62, R73) essential for nuclear localization are highlighted in red (Smith et al., 2012). Fluorescently RFP-labeled 18.5-kDa or 21.5-kDa MBP expressed in N19-OLGs indicate subcellular localization dependent on presence of MBP exon 2. Modified from (Pedraza et al., 1997; Smith et al., 2013).

In contrast to classical exon 2-lacking isoforms, exon 2-positive proteins localize diffusely in the cytoplasm and to the nucleus of transfected Hela cells (Staugaitis et al., 1990) as well as oligodendrocytes (Allinquant et al., 1991; Pedraza, 1997; Pedraza et al., 1997). A single study even suggests extensive cytoplasmic and nuclear MBP localization in OL in adult as well as developing mouse brain (Hardy et al., 1996). The nuclear translocation is based on active transport (Pedraza et al., 1997) that is mediated by a non-traditional P-Y nuclear localization signal within the exon 2 sequence (Smith et al., 2012). Localization correlates with proliferation and density of the cells in culture and on the activation of intracellular signaling cascades (Ozgen et al., 2014; Pedraza et al., 1997; Smith et al., 2013). Nevertheless, consequences of nuclear MBP localization, especially *in vivo*, remain enigmatic. In culture, 21.5-kDa MBP overexpression increases proliferation of oligodendroglial cell lines, dependent on a secreted factor or cell-cell contacts (Smith et al., 2013), and co-culture with the neuronal cell line N2a increases neurite outgrowth and branching, dependent on the nuclear

translocation of the exon 2 sequence in the 21.5-MBP expressing glial cells (Smith et al., 2013). Furthermore, a newly discovered exon 2-bearing isoform (16-kDa eMBP), expressed also in non-myelinating cells has been shown to regulate proliferation (Ozgen et al., 2014).

Despite the observed differences, exon 2-lacking as well as exon 2-containing isoforms associate with myelin (Karthigasan et al., 1996) and seemingly each can partly rescue the *shiverer* phenotype after reintroduction (Kimura et al., 1998; Readhead et al., 1987). This indicates a certain degree of redundancy and highlights the fundamental role and plasticity of the intrinsically disordered myelin basic proteins.

1.3 MBP expression is precisely regulated at the posttranscriptional level

The synthesis of MBP protein is an essential factor during OL maturation and myelin formation and has been shown to be precisely regulated on the posttranscriptional level. In particular, MBP mRNA was one of the first mRNAs described to be transported and locally translated in the myelin compartment (Ainger et al., 1993; Colman et al., 1982; Landry et al., 1994; Trapp et al., 1987).

1.3.1 RNA localization and mRNP complex assembly

Localized translation saves time and energy by generating multiple proteins from one localized mRNA and seems to play a much more fundamental role in the cell than previously thought. More than 70% of transcripts appear to be localized in *Drosophila* (Lecuyer et al., 2007) and transcriptome analysis of neuropil-associated mRNAs in rodent hippocampus (Cajigas et al., 2012) or sequencing of growth cone-associated mRNAs (Zivraj et al., 2010) also rendered a picture of extensive RNA localization patterns. The localization of mRNA is a prerequisite for a fast and spatial reaction to cellular signals, such as synaptic transmission at dendritic spines, where it is a major contributor to development and synaptic plasticity (Holt and Schuman, 2013).

A specific mRNA fate is basically regulated by the arrangement of interacting RNA binding proteins (RBP) and non-coding RNAs with the target mRNA, which bind to cis-acting motifs or secondary structures in the RNA sequence and build up heterogeneous ribonucleoprotein (RNP) complexes. Recent discoveries highlight the role of prion-like low complexity domains in most RBP, which can promote aggregation in RNP complexes (Han et al., 2012; Kato et al., 2012) and together with specific RNA-binding domains realize target recognition and assembly

of RNA granules. A growing number of proteins have been implicated in RNA binding (Baltz et al., 2012; Castello et al., 2012), whereas many of these >800 proteins were previously not implicated in RNA metabolism. On the other hand, high throughput methods to identify the repertoire of mRNAs binding to a given RBP have been developed and allow the identification of distinct RBP specific RNA binding motifs (Licatalosi et al., 2008). Despite the growing knowledge about the RNA-protein interactome, deciphering the “mRNP code” decorating a given RNA in a spatiotemporal resolution in the cell and its regulation remains a challenge.

1.3.2 MBP mRNA is localized to the myelin compartment

The classical MBP transcripts arise from a common pre-mRNA and are generated by alternative splicing of exons II, V and VI (de Ferra et al., 1985). Mechanisms controlling exon selection are largely unknown. All classical MBP mRNAs share an identical, relatively short 5'UTR and an exceptionally long 3'UTR (>1300 nucleotides) encoded by the invariant exon I and exon VII, respectively. An upstream open reading frame and potentially other regulatory elements are located in the MBP 5'UTR, influencing RNA stability and translation efficiency (Campagnoni et al., 1987; Ueno et al., 1994). As in most translocated mRNAs, the long MBP 3'UTR carries multiple sequence elements, regulating nuclear export, cytoplasmic transport, mRNA stability, translation efficiency and the MBP 3'UTR sequence is sufficient to target a random RNA to the OL periphery (Ainger et al., 1997). Translocation is mainly attributed to an 11 nucleotide short motif, named A2 response element (A2RE), which is selectively recognized by the transacting factor hnRNP A2 (Ainger et al., 1997; Hoek et al., 1998; Munro et al., 1999), whereas related proteins hnRNP A1, hnRNP A3 or CBF-A also can associate with the A2RE (Ma et al., 2002; Raju et al., 2008). Initially discovered in MBP mRNA, functional A2RE sequences are present in many RNAs and can also target neuronal mRNAs to dendrites (Gao et al., 2008; Raju et al., 2011), rendering the A2-pathway as a ubiquitous mechanism for RNA localization with implications in synaptic plasticity and learning. A critical component of A2RE granules is TOG (Francone et al., 2007), which might serve as a hub for multiplexing several hnRNP A2 proteins into the granule (Kosturko et al., 2005) and as a consequence, conditional knockout of TOG in neuronal cells shows severe defects in A2RE-dependent granule assembly and translation, leading to a reduction of synaptic plasticity-dependent memory formation (Barbarese et al., 2013).

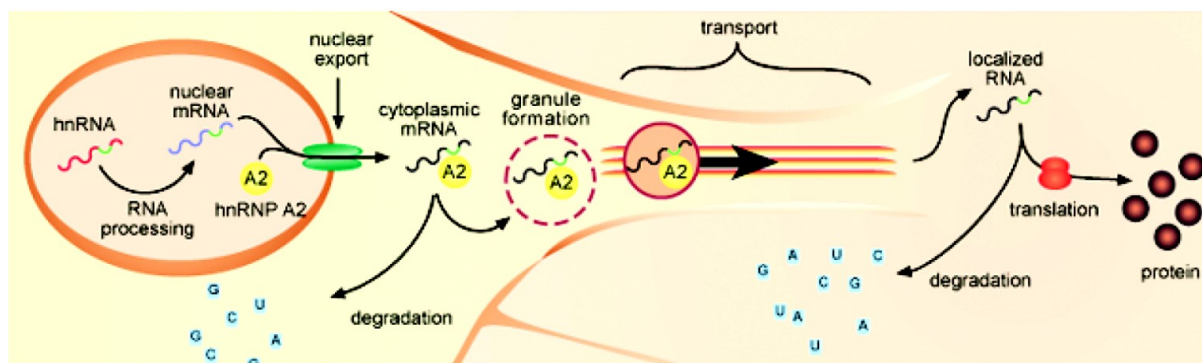


Figure 1-5. MBP mRNA is transported to the axogial contact site

After transcription and nuclear export, the mRNA associates in RNA transport granules in the cytoplasm and is translocated translationally silent to the axogial contact site, where local translation leads to synthesis of MBP protein. Adapted from (Smith, 2004).

In oligodendrocytes, hnRNP A2 binding to the MBP mRNA mediates the assembly of cytoplasmic transport granules, keeps the RNA in a translationally silenced state and directs the mRNA to the axogial contact site, reviewed in (Carson et al., 2001; Muller et al., 2013). The trafficking is rigorously dependent on the microtubule (MT) network, since MT depolymerization (Carson et al., 1997) or downregulation of the MT-organizing protein tau (Seiberlich et al., 2015) leads to impairment of MBP mRNA transport. In developing zebrafish, the MT-associated motor protein Kif1B has been shown to be indispensable for proper translocation of MBP mRNA (Lyons et al., 2009) and a genetic mutation in Kif1B is discussed as a risk factor for multiple sclerosis susceptibility (Aulchenko et al., 2008; International Multiple Sclerosis Genetics et al., 2010). Surprisingly, although sharing identical UTRs including the A2RE, inclusion of exon 2 into the MBP mRNA changes the subcellular RNA localization to a cytosol-restricted pattern (de Vries et al., 1997), in line with the localization of exon 2-containing MBP proteins (see above). The mechanism of targeting exon 2-containing mRNAs is not known, but must somehow rely on factors associating with the mRNA in a MBP exon 2-dependent manner.

1.3.3 Transacting factors mediate the MBP mRNA fate in oligodendrocytes

The fact that in OPCs MBP mRNA is expressed, but the synthesis of MBP protein is restricted and also in MS lesions MBP synthesis is inhibited (Bauer et al., 2012), implicates that translational inhibition may be a substantial step in regulating MBP expression. Several mechanisms keep MBP mRNA in a translationally silent state during transport, to guarantee

the correct spatio-temporal expression in myelinating OL. The hnRNP A2-dependent recruitment of hnRNP E1 to the MBP mRNP complex (Kosturko et al., 2006; Torvund-Jensen et al., 2014) and association of snRNA-715 to its corresponding binding site in the MBP 3'UTR (Bauer et al., 2012) are well studied factors of translational inhibition. Additionally, CPE elements in MBP mRNA (Du and Richter, 2005) have been identified, suggesting a CPEB-mediated regulation of polyadenylation-induced translation (Richter, 2007). Fragile X Syndrome (FXS)-related FMRP has been linked to MBP translational repression in premature OL (Li et al., 2001; Wang et al., 2004), though myelin abnormalities in patients caused by lack of FMRP expression in FXS could not be recapitulated in FMR1-KO mice (Giampetruzzi et al., 2013). Another important cis-acting element in the MBP 3'UTR is the quaking recognition element (QRE). MBP mRNA has been validated as a high affinity target for corresponding quaking (QKI) RNA-binding proteins, which play a key role in myelination and regulate mRNA stability, nuclear export and splicing in oligodendrocytes (Bockbrader and Feng, 2008; Larocque et al., 2002; Li et al., 2000). Several reports revealed further insight into MBP granule composition. Balanced levels of hnRNP F in the granule appear important for efficient translation at the axonal contact site (White et al., 2012) and remodeling of the RNP complex by an exchange of inhibitory hnRNP E1 to translation-promoting hnRNP K prior to the final stages of transport seems to be required for the subsequent initiation of MBP synthesis (Torvund-Jensen et al., 2014).

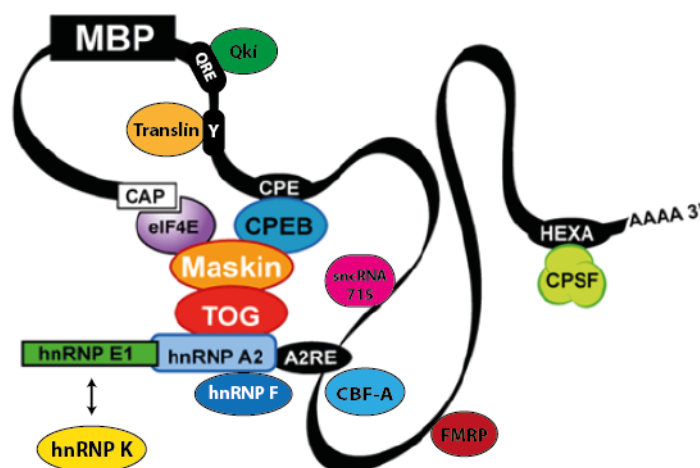


Figure 1-6. MBP mRNA is translationally silent during translocation.

The potential association of several cis-acting elements to RNA motifs or secondary structures in the MBP mRNA mediates translational silencing during mRNA transport. Details described in the text. Modified from (Carson et al., 2008).

1.3.4 Axonal signals initiate the spatiotemporal synthesis of MBP

To initiate translation, remodeling the MBP mRNA granule is essential to allow association with polyribosomes and this can be triggered by neuronal signals. A signaling complex comprising contactin and $\alpha 6 \beta 1$ -integrin integrates signals from the extracellular matrix (laminin) and the axonal surface (L1-CAM) and activates Fyn kinase at the oligodendroglial membrane (Laursen et al., 2009; White et al., 2008). Activation of Fyn kinase leads to an RNP complex remodeling towards translation initiation (White et al., 2008) dependent on hnRNP K (Laursen et al., 2011) and phosphorylation of MBP granule components hnRNP A2 and hnRNP F, leading to their dissociation from the granule and finally triggering MBP synthesis (White et al., 2012; White et al., 2008).

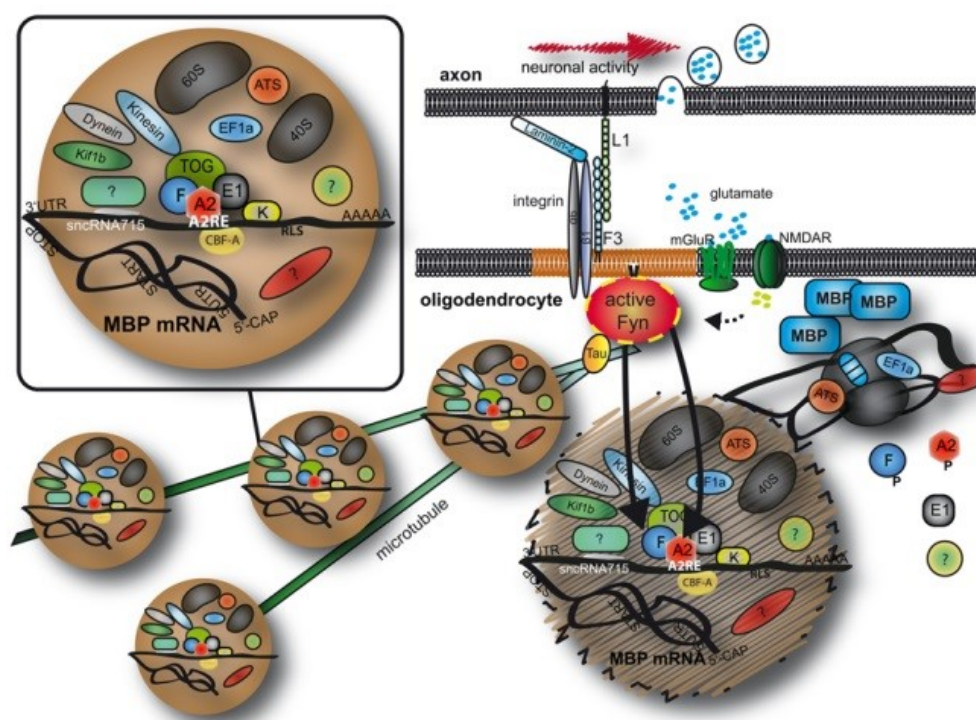


Figure 1-7. MBP mRNA transport and local translation at the axoglial contact site.

MBP mRNA is transported in RNA granules in a translationally silent manner. Components of the mRNP complex are shown schematically and comprise hnRNPs, motor proteins and scaffolds. Local translation occurs at the axoglial interface and is dependent on Fyn kinase activation. Further details are described in the text. Adapted from (Muller et al., 2013).

Fyn kinase activation and MBP synthesis have also been shown to transduce neuronal activity into myelin plasticity. Electrical stimulation of axons drives vesicular release of neurotransmitters and induces localized translation of MBP in the adjacent OL membrane, which can be blocked by reducing levels of Fyn kinase (Wake et al., 2011). In developing

zebrafish, manipulation of Fyn kinase activity regulates sheath number per oligodendrocyte (Czopka et al., 2013). Activation of Fyn kinase at the axoglial contact site (Kramer-Albers and White, 2011) is thought to be a key mechanism to control local MBP synthesis and becomes apparent in Fyn-KO mice (Goto et al., 2008; Lu et al., 2005; Sperber et al., 2001) that show extensive demyelination.

Furthermore, conditional knockout of ERK2 MAP Kinase in OL suggests an important role in the translational control of MBP, regulating remyelination in the adult brain (Michel et al., 2015) and also conditional knockout of mTOR components in OL selectively affects MBP levels posttranscriptionally, impeding mTORC1-dependent translation (Bercury et al., 2014; Lebrun-Julien et al., 2014). The interplay of these and other pathways in different brain regions, also in relation to Fyn kinase activation remains to be elucidated, but hints to redundant mechanisms to ensure execution of the myelination program.

1.3.5 Cytoplasmic RNA granule composition dynamically reacts to cellular cues

Cytoplasmic RNA granules are defined by their composition and function and can dynamically change these parameters during the RNA lifecycle in reaction to cellular cues. (Anderson and Kedersha, 2009a; Buchan, 2014). Oxidative stress, starvation, heat shock or translational arrest can lead to the transient formation of stress granules (SG) which harbor translationally-stalled mRNPs and specific SG factors that built up dynamic hubs for the maintenance of mRNAs and cell signaling during stress conditions (Anderson and Kedersha, 2009b; Kedersha et al., 2013). A major step in SG assembly is the phosphorylation of eIF2 α , resulting in inhibition of translational initiation with subsequent coalescence of the large irregular shaped granules (Kedersha et al., 1999). Major SG assembly promoting factors are prion-like LC domain containing TIA1 (T-cell internal antigen 1) and G3BP1 (Ras-GTPase-activating protein SH3-domain-binding protein 1), which are commonly used as marker proteins to identify SG.

A related class of cytoplasmic RNA granules are processing bodies (PB), where RNAs are sequestered, which are destined for degradation or translational silencing. Consequently, PB contain translational repressors and components of the mRNA decay machinery (Decker and Parker, 2012). SG and PB are very dynamic structures, shuttling RBPs and mRNAs in and out of these often adjacent RNA-protein complexes. The average retention time of components in SG is very short (order of a minute), compared to the visible SG persistence over hours after stress relief (Kedersha et al., 2005; Mollet et al., 2008). The transition and interconversion of

mRNPs between translating polysomes, PB and SG describes a model of an RNA cycle, which is linked to the cellular state and regulates the RNA fate in the cell (Decker and Parker, 2012). Interestingly, PB have been observed in dendrites in close interaction with transport granules and might be involved in the translational silencing and release in a neuronal activity-dependent manner (Zeitelhofer et al., 2008). In OL, MBP mRNA can accumulate in perinuclear aggregates after oxidative stress (Thomas et al., 2005) and Qki-6 is associated with MBP mRNA-containing SG after oxidative stress in primary rat OL (Wang et al., 2010).

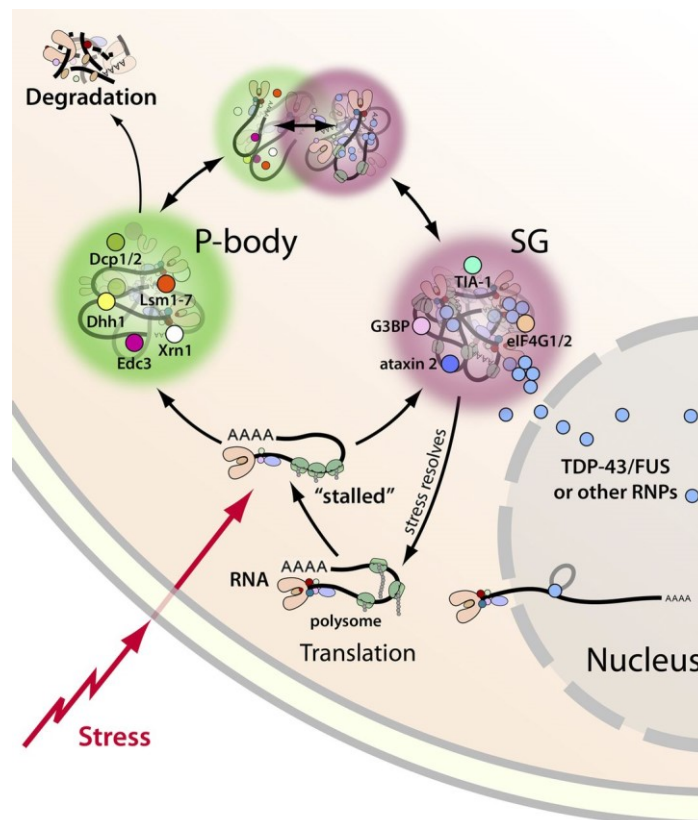


Figure 1-8. Cytoplasmic RNA granule composition dynamically adapts to cellular cues.

Translation occurs on polysomes associated with cellular mRNAs. Stress can lead to polysome dissociation and induces the transient formation of stress granules (SG), which comprise SG specific factors (e.g. TIA-1, G3BP-1) and stalled mRNPs during the stress condition. P-Bodies are sites of RNA degradation or translational inhibition. A given mRNA can cycle between the different cytoplasmic RNA granules dependent on cellular cues. Adapted from (Li et al., 2013).

1.4 Identification of novel MBP mRNA-associated proteins

The association of hnRNP A2 with MBP mRNA is a key step in the assembly of the corresponding cytoplasmic transport granules and a prerequisite for localized MBP synthesis.

To identify hnRNP A2 interaction partners that potentially also associate with MPB mRNA in an mRNP complex, mass spectrometry analysis following immunoprecipitation of hnRNP A2 from an oligodendroglial cell line was performed (Dissertation, (White, 2007)).

1.4.1 The multifunctional DEAD Box RNA Helicase 5 (DDX5)

DEAD Box RNA helicase 5 (DDX5, also commonly named p68 RNA helicase), a selected target from the screen described above was subjected to initial experiments (Dissertation Gonsior, 2011; Diploma thesis Hoch-Kraft, 2010) to assess the role of DDX5 in oligodendrocytes: Expression in oligodendroglial cells was analyzed and co-immunoprecipitation showed association with hnRNP A2. Furthermore, DDX5 seemed not to be a tyrosine phosphorylation target of Fyn kinase, compared to other MBP mRNA granule-associated RBPs like hnRNP A2 or hnRNP F (Gonsior, 2011) however siRNA knockdown and MBP-3'UTR-based luciferase assays hinted to DDX5 as a target potentially influencing MBP expression in oligodendroglial cells (Hoch-Kraft, 2010).

DDX5 is a prototypical member of the DEAD box RNA helicase protein family and has been shown to be an extraordinary multifunctional protein, fulfilling fundamental functions in the cell. Consequently, DDX5 knockout animals exhibit embryonic lethality at E11.5 (Fukuda et al., 2007). DDX5 has been shown to build homodimers and heterodimers with a closely related DEAD box family member DDX17, with partly overlapping functions (Ogilvie et al., 2003). DDX5 multifunctionality relies on its association with several macromolecular protein complexes, signaling molecules and a wide range of RNA species. A common feature of DEAD box helicases is the ATP-dependent unwinding of RNA substrates, whereas participating binding sites and functional domains have been characterized in detail (Linder and Jankowsky, 2011). DDX5 thus provides suitable key functions to realize the dynamic remodeling of RNP complexes. Two nuclear localization sequences (NLS) and two nuclear export sequences (NES) enable shuttling between nucleus and cytoplasm (Wang et al., 2009) and localization was correlated with the association of DDX3 in a cell cycle-dependent manner (Choi and Lee, 2012).

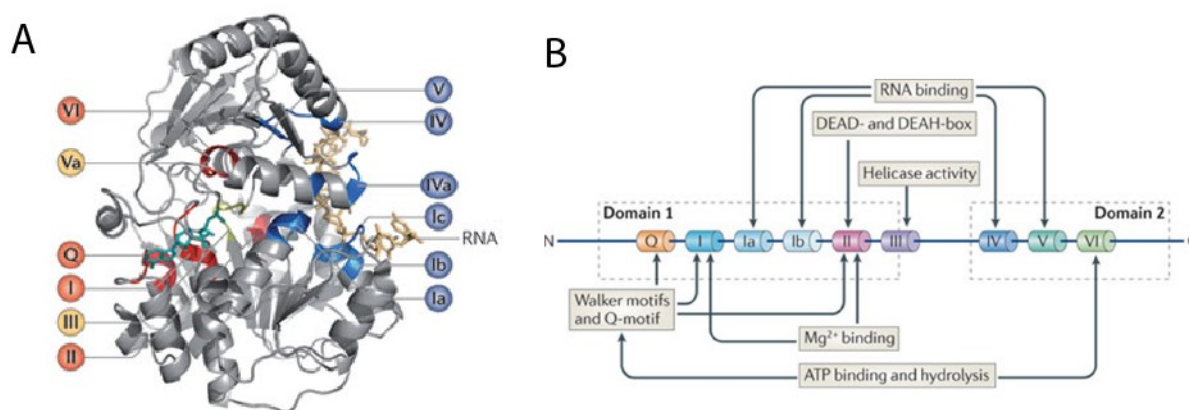


Figure 1-9. Conserved domains and binding sites of DEAD Box RNA helicases

(A) DEAD Box helicase protein structure, showing binding motifs for RNA binding (blue) and coordination of ATP and Mg^{2+} molecules (red). Adapted from (Linder and Jankowsky, 2011). **(B)** Domain architecture of DEAD Box helicases. Motifs and corresponding binding substrates or functions are indicated. Adapted from (Parsyan et al., 2011).

DDX5 has been described as an essential splicing factor, mediating dissociation of U1 snRNP from the 5' splice site (5'ss) and is needed for subsequent assembly of the mature spliceosome (Lin et al., 2005; Liu, 2002). Regulation of alternative splicing is target specific and has been shown to regulate several targets by different mechanisms (Camats et al., 2008; Dardenne et al., 2014; Kar et al., 2011). Independent of the helicase function, DDX5 acts as a potent transcriptional coactivator for various signaling pathways (Fuller-Pace, 2013), including hormone receptors (Clark et al., 2008a; Endoh et al., 1999; Watanabe et al., 2001), p53 (Bates et al., 2005), Notch (Jung et al., 2013; Lin et al., 2013) and Wnt-signaling (Guturi et al., 2014; Wang et al., 2015b; Yang et al., 2006). Furthermore, DDX5 can regulate gene expression epigenetically by recruiting HDACs (Wilson et al., 2004) or favoring HDAC dissociation (Carter et al., 2010) at target genes. Overexpression in various tumors and the role in proliferation, metastasis and tumor progression make DDX5 a highly researched target primarily in cancer biology (Dai et al., 2014; Janknecht, 2010). DDX5 may couple transcription to posttranscriptional RNA processing (Clark et al., 2008b; Germann et al., 2012) and in line with that, DDX5 not only acts as a transcriptional coactivator of estrogen receptor alpha ($ER\alpha$) and androgen receptor (AR) target genes, but also influences splicing of several key regulators, including GSK-3 β , rendering DDX5 (together with DDX17) as a cornerstone in these signaling pathways (Samaan et al., 2014).

Moreover, DDX5 can selectively control biogenesis of miRNAs as part of the DROSHA/DGCR8 miRNA processing machinery in the nucleus (Fukuda et al., 2007; Hong et al., 2013; Suzuki et

al., 2009) and DDX5 contributes also to biogenesis of the ribosome (Fukuda et al., 2007; Jalal et al., 2007; Saporita et al., 2011) via regulation of rRNA expression.

Recently, DDX5/17 have been proposed to be master regulators of cellular differentiation programs in epithelial cells and myoblasts, globally orchestrating transcription, miRNA expression, and alternative splicing patterns. In cooperation with hnRNP H/F at the 5'ss DDX5/17-dependent alternative splicing massively impacts on the cellular transcriptome outcome and is correlated with myoblast differentiation and epithelial mesenchymal transition (EMT) (Dardenne et al., 2014).

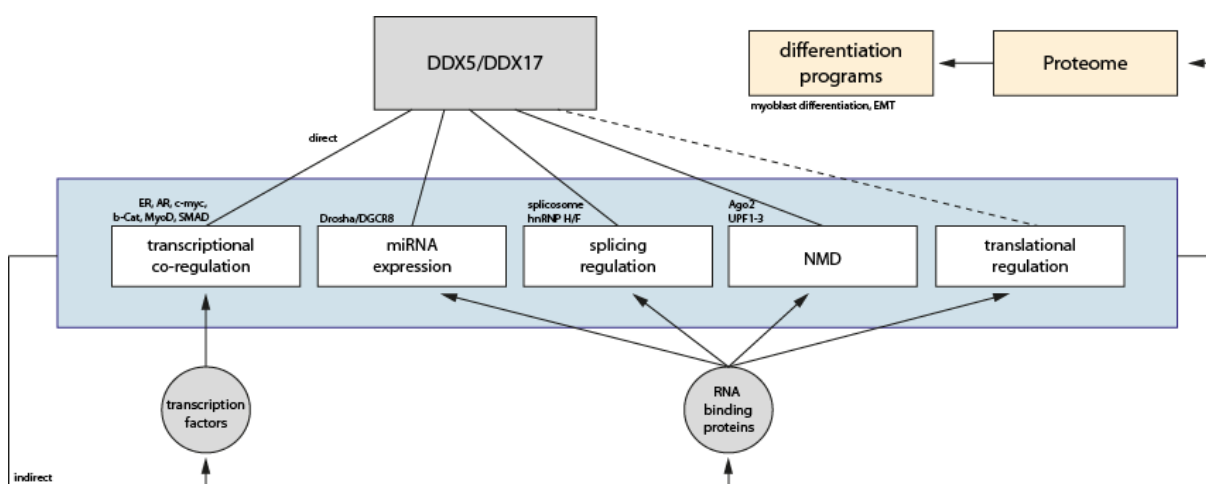


Figure 1-10. DDX5 is a multitasking RNA helicase affecting numerous aspects of gene expression

Diagram, illustrating the roles of DDX5 in controlling the cellular proteome on the transcriptional as well as the posttranscriptional level. DDX5 can directly influence the expression and splicing patterns of mRNAs or miRNAs. As a consequence, changing expression of transcription factors and RNA binding proteins, can indirectly alter the transcriptome outcome, orchestrating cellular differentiation programs. Details are explained in the text.

Increasing evidence suggests that factors assembling during splicing can remain associated with the mRNA in the cytoplasm thus additionally regulating gene expression (Moore, 2005). DDX5 has been identified in mRNPs on newly spliced mRNAs, together with deposition of exon junction complexes (EJC) (Merz et al., 2007) or can functionally replace the EJC (Geissler et al., 2013), potentially coupling nuclear RNA modification events to the RNA fate in the cytoplasm. Identification as a part of cytoplasmic RNP complexes in mouse brain and neuronal cells (Elvira et al., 2006; Kanai et al., 2004; Miller et al., 2009; Shelkownikova et al., 2014) and involvement in nonsense-mediated RNA degradation pathways (NMD) in mammalian cells as well as in yeast (Bond et al., 2001; Cloutier et al., 2012; Geissler et al., 2013; He and Jacobson, 1995) reveals its potential not only to control gene expression on the level of transcription and splicing, but also in mechanisms controlling the cytoplasmic mRNA fate.

On the molecular level, binding affinity and helicase activity favors interaction with ssRNA and dsRNA (Huang and Liu, 2002), although affinity for dsRNA seems to be much higher. Commonly, dsRNA structures are found in miRNA-precursors and are the basis for secondary structures in mRNAs, e.g. in RNA hairpin loops. The DDX5 RNA-binding capacity, helicase activity and transcriptional activation are highly dependent on posttranslational modifications like phosphorylation (Yang et al., 2005b) or sumoylation (Jacobs et al., 2007; Mooney et al., 2010), which can be dynamically regulated. Furthermore, DDX5 phosphorylation status correlates with cancer development (Yang et al., 2005a) and Ca^{2+} signaling can regulate DDX5 RNA helicase activity, by binding of Calmodulin and phosphorylation in the IQ-Domain (Buelter et al., 1994).

Importantly, the biologically active compound in green tea (-)-Epigallocatechin-3-gallate (EGCG) (Tanaka et al., 2011) and a newly developed anti-cancer drug RX-5902 (Kost et al., 2015) target DDX5 activity and allow the modulation of DDX5-mediated effects in humans.

1.4.2 The ALS-associated RNA binding protein Fused in Sarcoma (FUS)

A second target of the screen for MBP mRNA-associated proteins (White, 2007) was identified as the RNA-binding protein Fused in Sarcoma (FUS). FUS is a multifunctional RNA-binding protein, which has been studied intensively over the last years as a candidate gene causing Amyotrophic Lateral Sclerosis (ALS) and other neurodegenerative diseases (Deng et al., 2014). FUS mutations, primarily in the NLS of the protein lead to cytoplasmic mislocalization (Dormann et al., 2010; Sabatelli et al., 2013) and formation of ectopic stress granules (Andersson et al., 2008; Bosco et al., 2010; Lenzi et al., 2015; Shelkovnikova et al., 2013), which are suspected to be seeding points for aberrant protein aggregation. Several SG components are found in pathogenic FUS inclusions (Dormann et al., 2010) and cellular proteins and mRNAs can be sequestered into these structures ectopically (Takanashi and Yamaguchi, 2014). Also, hnRNP A2, hnRNP A1 and endogenous FUS trapped into mutant FUS SG (Takanashi and Yamaguchi, 2014) and moreover, the presence of mutant FUS proteins can alter SG dynamics (Baron et al., 2013). The perturbed subcellular localization is hypothesized to misregulate mRNA metabolism (Li et al., 2013) and in addition to the cytoplasmic gain of function, the nuclear loss of function can account for pathology (Haass, 2013), referring to the physiological role of FUS in transcription (Schwartz et al., 2012), splicing (Orozco et al., 2012), Drosha-

associated miRNA biogenesis (Morlando et al., 2012) and in the DNA damage response (Mastrocola et al., 2013).

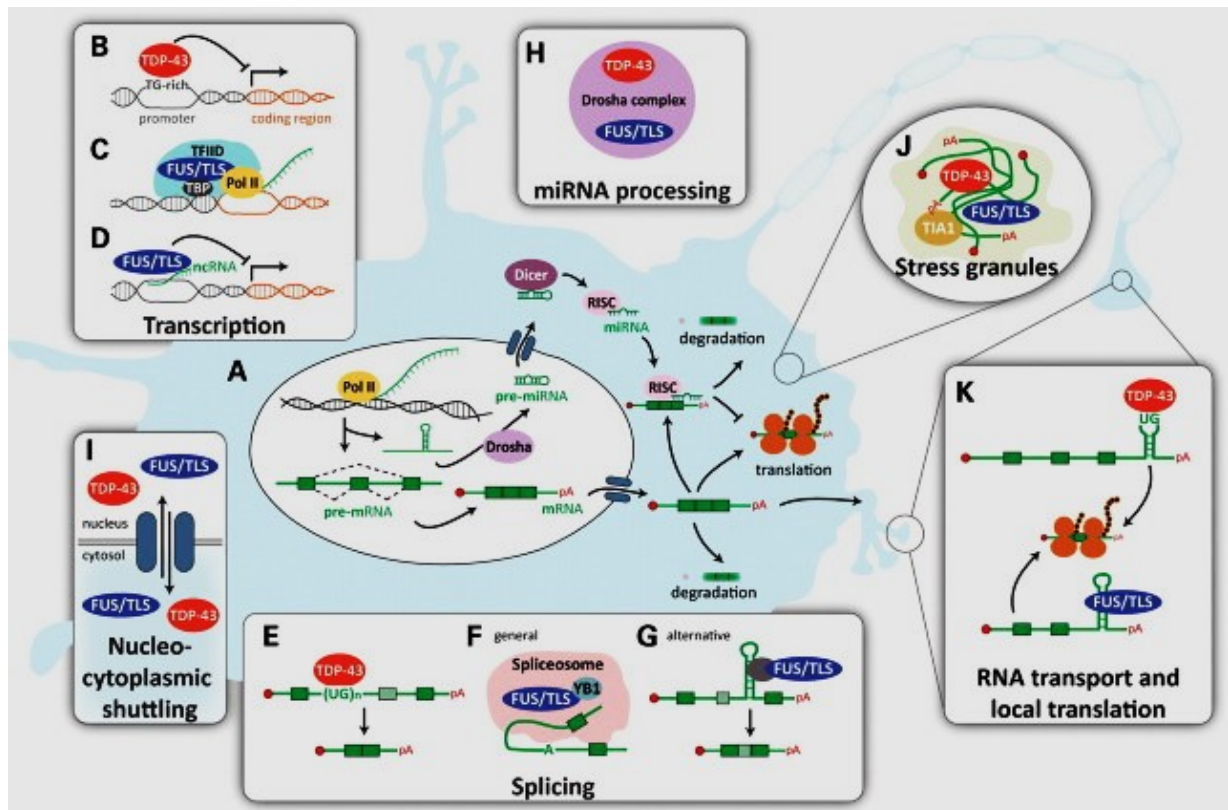


Figure 1-11. Roles of FUS in the cellular RNA metabolism

FUS affects several mechanisms involved in the cellular RNA metabolism from transcription (A-D), alternative splicing (F-G), miRNA processing (H), nucleo-cytoplasmic shuttling (I) to cytoplasmic RNA transport and local translation (K) and the formation of stress granules (J). Details are described in the text. Adapted from (Lagier-Tourenne et al., 2010).

FUS exhibits potential binding sites for a vast range of nucleic-acids with preference for specific RNA sequence motifs but also dependence on secondary structures (Wang et al., 2015a). High-throughput sequencing of FUS-associated mRNAs revealed diverse patterns of binding targets (Colombrita et al., 2012; Hoell et al., 2011; Lagier-Tourenne et al., 2012) and a large number of genes showed altered levels of splicing upon FUS depletion (Lagier-Tourenne et al., 2012; Rogelj et al., 2012). FUS selectively regulates splicing of other RBPs (Nakaya et al., 2013) and interestingly, is also involved in splicing of the DDX5 targets H-Ras and Tau (Camats et al., 2008; Orozco et al., 2012). Furthermore, as a component of neuronal transport granules FUS has been shown to transport mRNAs to the dendritic spines and to regulate local translation in an mGluR1/5 activity-dependent manner (Belly et al., 2005; Fujii et al., 2005; Sephton et al., 2014). A novel function has been allocated to FUS in adenomatous polyposis

coli (APC) protein-containing RNA granules, where FUS association supports the local translation in these stress granule-like structures (Yasuda et al., 2013). Recently, detailed characterization of FUS-containing cytoplasmic RNA granules (FG) dynamics has led to a multistep model of FUS aggregation (Shelkovnikova et al., 2014). Oxidative stress can lead to assembly of FUS aggregates (FA), that resemble, but are different to classical SGs. Interestingly, a marker to discriminate FA from SG is the presence of DDX5 (Shelkovnikova et al., 2014).

It has become clear that oligodendrocyte dysfunction contributes to the early pathogenesis of ALS and severity of motor neuron loss in the spinal cord is correlated to pathogenic hallmarks in OL (Brettschneider et al., 2014; Kang et al., 2013) challenging the classical view of glial cell involvement in ALS pathomechanisms (Valori et al., 2014). RNA-binding proteins also make up part of OL inclusions, altogether pointing to the interesting question how a misregulation of the oligodendroglial RNA metabolism may contribute to the disease.

1.5 MS2 – a system to dynamically label and isolate RNAs *in vivo*

A fundamental improvement in understanding cellular RNA metabolism was the development of high resolution detection of mRNA molecules *in situ*. Fluorescent in situ hybridization (FISH) has advanced to a detection of mRNA transcripts with single molecule resolution (Femino et al., 1998; Raj et al., 2008) and thereby allows quantitative imaging of RNA expression levels in individual cells (reviewed by (Kwon, 2013)). In spite of these advances, FISH requires fixation and hybridization protocols, which are not consistent with imaging in a temporal resolution. To overcome this limitation, genetically encoded RNA reporter systems were designed to label mRNA molecules in living cells and help to understand RNA localization (Buxbaum et al., 2015a; Tyagi, 2009).

A prominent method is based on a high-affinity protein-RNA interaction discovered in the bacteriophage MS2. In the genomic RNA, MS2-binding sites (MBS) are specifically recognized by a homodimer of MS2 coat proteins (MCP). Association of the MCP with the stem loop operon represses transcription of the phage replicase gene and directs packaging and assembly of the genomic RNA into the bacteriophage capsid structure (Fouts et al., 1997; Valegard et al., 1997). Tandem repeats of MBS can be introduced into selected mRNAs and co-expression of conjugated MCP finally decorates the RNA of interest with the MCP-conjugated reporter protein.

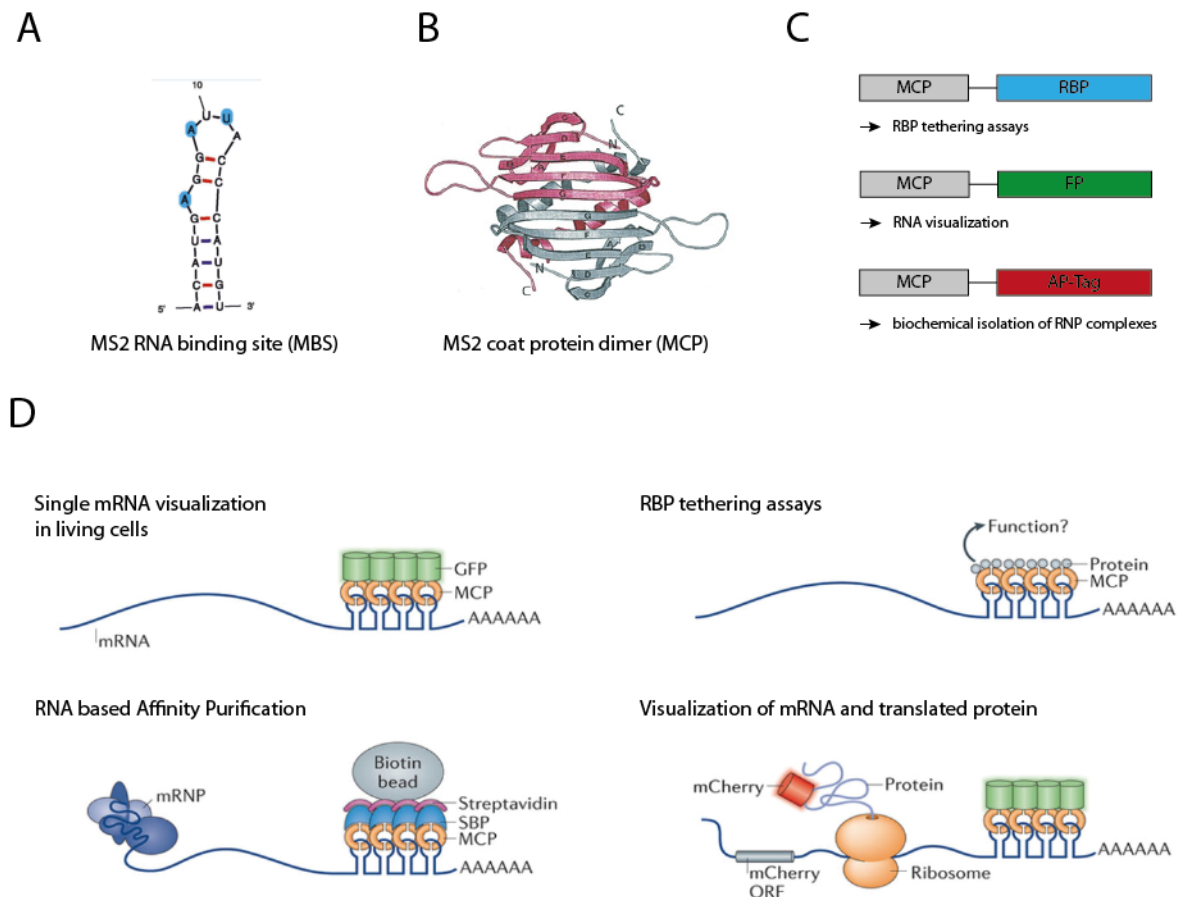


Figure 1-12. Components and applications of the MS2 RNA labeling system

(A) RNA stem loop structure of the MS2 binding site. Adapted from (Weil et al., 2010). **(B)** Protein structure of homodimeric MS2 coat proteins. Adapted from (Keryer-Bibens et al., 2008). **(C)** Overview of selected MCP-fusion constructs. FP=fluorescent protein, AP=affinity purification. **(D)** Applications of MS2-based techniques, details are described in the text. Modified from (Buxbaum et al., 2015a)

The MS2 system has initially been used in tethering assays, to study influences of MBS/MCP-directed RBP binding to reporter mRNAs (reviewed by (Keryer-Bibens et al., 2008)). In oligodendroglial cells, tethering of the RNA binding proteins hnRNP F/H to a location in exon 3B of PLP/DM20 splicing reporters was used to elucidate the role of hnRNP H/F in the PLP splicing mechanism (Wang and Cambi, 2009).

In pioneer work Bertrand et al. adapted the system for RNA visualization, fusing the MCP to green fluorescent protein (MCP-GFP) (Bertrand et al., 1998). Live cell imaging revealed transport and localization of labeled ASH1 mRNA in budding yeast cells. Subsequently, the system was transferred to β -actin mRNA and shed light on mechanisms of movement of single mRNA molecules in mammalian cells (Fusco et al., 2003). Today, RNA labeling has been applied to numerous mRNAs, e.g. hnRNP A2 pathway-associated mRNAs Arc and CaMKIIa (Gao et al., 2008) have been visualized in neuronal cells (Dictenberg et al., 2008; Dyne and Steward,

2007) revealing insights into mRNA dynamics, especially in transport and local translation at synapses (Buxbaum et al., 2015b). Recently, whole transgenic organisms, in which β -actin mRNA is fluorescently labeled in every cell of the living animal, are used for visualization of mRNA movement in mouse (Lionnet et al., 2011; Park et al., 2014) and zebrafish tissue (Campbell et al., 2015). Development of novel MS2-based techniques, such as the combination of split PP7/MS2 reporter systems (Wu et al., 2014), translational biosensors (Halstead et al., 2015) or the construction of new high affinity synonymous MS2 repeats (Wu et al., 2015), continuously improves the possibilities to study RNA dynamics.

Apart from RNA visualization with fluorescent proteins, alternatively tagged MCPs can be used to biochemically isolate labeled MS2-RNAs and identified *in vivo* interacting molecules like RBPs or non-coding RNAs (Gong and Maquat, 2015; Slobodin and Gerst, 2010; Tsai et al., 2011; Yoon et al., 2012). Taken together, the MS2-system is a powerful tool to study composition and dynamics of RNP complexes in living cells and led to the generation of general concepts of RNA localization and metabolism.

1.6 Aim of the study

The posttranscriptional regulation of MBP expression is an essential factor controlling myelination in the CNS. A major aim of this study was the identification of MBP mRNA-associated proteins and their role in regulating MBP mRNA dynamics. Previously identified candidates DDX5 and FUS (White, 2007) were to be subjected to further analysis elucidating their role in regulating MBP expression in oligodendroglial cells. Furthermore, novel tools should be established, including the adaptation of the MS2-RNA labeling system to MBP mRNA in order to visualize and isolate MBP mRNA complexes from oligodendroglial cells. Additional methods such as *in situ* hybridization with single molecule resolution and RNA affinity purification are valuable tools to analyze RNA localization and the dynamic composition of MBP mRNP complexes. Use of these novel RNA-centric methods should shed light on mechanisms that control the synthesis of myelin basic protein in oligodendroglial cells in health and disease.

2 Material & methods

2.1 Material resources

2.1.1 Equipment

Table 2-1. Cell culture equipment.

Type	Name	Manufacturer
Sterile working bench	SterilGARD III Advance Class II	The Baker Company
CO₂ incubator	C200 Incubator	Labotect
CO₂ incubator	CO ₂ incubator MCO-20AIC	Sanyo
Transfection device	AMAXA Nucleofector II	Lonza
Transfection device	AMAXA 4D Nucleofector Core Unit	Lonza
Transfection device	AMAXA 4D Nucleofector Y Unit	Lonza
Water bath	Water bath Z 383K	Hermle
Inverted microscope	Leica DM-IL	Leica
Centrifuge	Megafuge® 1.0R	Heraeus

Table 2-2. Microscopes and objectives.

Type	Name	Manufacturer
Fluorescence microscope	Leica DM6000B + DFC360 FX camera	Leica
Objective	HCX PLAN APO 20.0x0.70 DRY	Leica
Objective	HCX PLAN APO 40.0x0.75 DRY	Leica
Objective	HCX PL APO CS 100.0x1.40 OIL	Leica
Fluorescence microscope	Leica DM-LB + DFC350 FX camera	Leica
Objective	PL FLUOTAR 40.0x0.70 DRY	Leica

Table 2-3. Other lab equipment.

Type	Name	Manufacturer
Bacteria incubator	H15/500	Noctua
Luminometer	Infinite M200 Pro	Tecan
Real-Time PCR System	StepOne™ Real-Time PCR system 48-well	Applied Biosciences
pH meter	pH meter Lab 850	Schott
Centrifuge	Tabletop Biofuge® fresco	Heraeus
Centrifuge	Biofuge® 17RS	Heraeus
Ultracentrifuge (Rotor)	Optima™ L-90K Ultracentrifuge (SW41-Ti)	Beckman Coulter
Magnetic separation device	DynaMag-2®	Life Technologies
Refractometer	Refractometer T, Refractometer 2T	Atago
Heating thermomixer	Heating thermomixer HTMR-133	HLC, Bovenden

SDS-PAGE System	Mini-PROTEAN® TetraVertical Electrophoresis Cell	Bio-Rad
Western blot System	Mini Trans-Blot® Cell	Bio-Rad
SDS-PAGE System	XCell SureLock™ Mini-Cell Electrophoresis System	Invitrogen
Photospectrometer	Nanodrop™ 1000 Photospectrometer	Thermo Scientific
PCR Thermocycler	T3 Thermocycler	Biometra
X-Ray film processor	Optimax Typ TR X-Ray film processor	MS Laborgeräte
Scanner	Epson Perfection 1660	Epson

2.1.2 Materials, chemicals and commercial Kits

Glassware was purchased from VWR, cell culture plastics and consumables from Sarstedt or BD Falcon and reaction tubes and other consumables from Sarstedt or Eppendorf. Chemicals not listed in Table 2-4, were purchased from Roth or Sigma Aldrich or are described in the text individually.

Table 2-4. Materials, chemicals and commercial Kits.

Name	Item	Source
96-well Plates white (Luminescence)	#236105	Nunc
Agarose (low melt)	#6351.2	Roth
AMAXA AD1 Primary Cell 4D-Nucleofector™ Y Kit	#V4YP-1A24	Lonza
AMAXA Basic Nucleofector Kit for Primary Neurons	#VPI-1003	Lonza
BCA Protein Assay Kit	#71285-3	Novagen
Biotin	#B4639	Sigma Aldrich
BSA Nuclease-free 10%	#126615	Calbiochem
Chloroform	#3313.1	Roth
DAPI	#D9542	Sigma Aldrich
dbcAMP (N6,2'-O-Dibutyryl adenosine 3',5'-cyclic monophosphate sodium salt)	#D0627	Sigma Aldrich
Dextran sulfate	#D8906	Sigma Aldrich
Digitonin	#D141	Sigma Aldrich
Dual Glo® Luciferase Assay System	#E2920	Promega
Dynabeads M280 Streptavidin	#11205D	Life Technologies
Dynabeads Protein G	#10004D	Life Technologies
E. coli tRNA		Sigma Aldrich
EDTA	#8040.2	Roth
Ethanol	#9065.4	Roth
Fluoromount G™ with DAPI	#00-4959-52	eBioscience
Formamide	#F9037	Sigma Aldrich
H₂O Ultrapure	#W4502	Sigma Aldrich
Halt Phosphatase Inhibitor Cocktail	#78420	Pierce

Halt Protease Inhibitor Cocktail	#1860932	Thermo Fisher
Magnesium chloride	#M2670	Sigma Aldrich
MicroAmp® 48-Well Optical Adhesive Film	#4375323	Life Technologies
MicroAmp® Fast Optical 48-Well Reaction Plate	#4375816	Life Technologies
Mowiol 4-88 reagent	#475904	Calbiochem
NE-PER Nuclear/Cytoplasmic Extraction Kit	#78833	Pierce
Nonidet™ P 40 Substitute	#74385	Fluka
NuPAGE® LDS Sample Buffer (4x)	#NP0007	Invitrogen
NuPAGE® MES SDS Running Buffer (20X)	#NP0002	Life technologies
NuPAGE® MOPS SDS Running Buffer (20X)	#NP0001	Life technologies
NuPAGE® Novex® 4-12% Bis-Tris Protein Gels	#NP0335BOX	Life technologies
O´GeneRuler 1kb DNA Ladder	#SM1163	Thermo Scientific
Optiprep Density Gradient Solution 60%	#D1556	Sigma Aldrich
PJK Beetle-Juice Luciferase assay	#102511	PJK GmbH
PJK Renilla GLOW-Juice Luciferase assay	#102532	PJK GmbH
Polyallomer Centrifuge Tubes SW41 (14 x 95 mm)	#331374	Beckman Coulter
Propanol ROTIPURAN®	#6752.2	Roth
Protein A Sepharose CL-4B	#17078001	Amersham
Pure Link HiPure Maxiprep Kit	#K2100	Invitrogen
QIAzol Lysis Reagent	#79306	Qiagen
RNase A	#12091-039	Invitrogen
RNase-free DNase Set	#79254	Qiagen
RNaseZAP	#R2020	Sigma Aldrich
RNasin® Plus RNase Inhibitor	#N2611	Promega
Roti®-Histofix	#P087.3	Roth
SOC Medium	#S1797	Sigma Aldrich
Sodium chloride	#S3014	Sigma Aldrich
SSC 20x Ultrapure	#15557044	Gibco
SYBR® Green PCR Master Mix	#4344463	Life Technologies
T₁₀E₁ buffer pH=8	#AM9849	Ambion
TaqMan® Gene Expression Master Mix	#4369016	Life Technologies
Tris	#4855.1	Roth
Triton X-100	#3.051	Roth
Tween 20	#9127.2	Roth
Vanadylribonucleoside complex	#94742	Sigma Aldrich
Yeast tRNA (10 mg/ml)	#AM7119	Ambion

2.1.3 Buffers and Media

Table 2-5. Buffers, media and solutions.

Buffer/Medium/Solution	Composition
10 x Poly-L-Lysine (PLL)	0.1 % PLL (Sigma, #P1524) in ddH ₂ O
Sato 1.0-1.5 % HS (Oli-<i>neu</i> culture medium)	13.4 g/l DMEM (Invitrogen, #52100-039), 2 g/l NaHCO ₃ , 0.01 g/l transferrin, 100 µg/l insulin, 100 µM putrescine, 200 nM progesterone, 500 nM TIT, 220 nM Sodium-selenite, 520 mM L-thyroxine, 1.0-1.5% (v/v) horse serum
SILAC light medium, (modified Sato 1% HS)	DMEM high glucose, no glutamine, no lysine, no arginine (Gibco, #A14431), 2 g/l NaHCO ₃ , 0.01 g/l transferrin, 100 µg/l insulin, 100 µM putrescine, 200 nM progesterone, 500 nM TIT, 220 nM Sodium-selenite, 520 mM L-thyroxine, 4 mM L-Glutamine, 1% (v/v) horse serum, 73 mg/l Lysine, 42 mg/l Arginine
SILAC heavy medium, (modified Sato 1% HS)	DMEM high glucose, no glutamine, no lysine, no arginine (Gibco, #A14431), 2 g/l NaHCO ₃ , 0.01 g/l transferrin, 100 µg/l insulin, 100 µM putrescine, 200 nM progesterone, 500 nM TIT, 220 nM Sodium-selenite, 520 mM L-thyroxine, 4 mM L-Glutamine, 1% (v/v) horse serum, 73 mg/l heavy Lysine-8, 42 mg/l heavy Arginine-10
B27 1% HS (pOL basic culture medium)	13.4 g/l DMEM, 2 g/l NaHCO ₃ , 20 ml/l B27 supplement, 0.011% pyruvate, 500 nM TIT, 520 mM L-thyroxine, 0.05% gentamycine, 1% (v/v) horse serum
B27 1% HS + growth factors (pOL plating medium)	13.4 g/l DMEM, 2 g/l NaHCO ₃ , 20 ml/l B27 supplement, 0.011% pyruvate, 500 nM TIT, 520 mM L-thyroxine, 0.05% gentamycine, 1% (v/v) horse serum, 10 ng/ml PDGF-AA (PeproTech, #100-13B), 5 ng/ml bFGF (PeproTech, #100-18B)
HBSS⁺	500 ml HBSS (1x) + 7.5 ml 10% MgSO ₄
1% trypsin (cell dissociation)	100 ml 2,5% (v/v) trypsin, 15 ml HBSS (10x), 125 mg DNase I, with 135 ml H ₂ O to 250 ml in total, pH=7.8
Trypsin/EDTA „low“	0.01% trypsin, 0.02% EDTA in HBSS
Freezing medium	20% (v/v) FCS, 10% (v/v) DMSO in RPMI 1640
50 x TAE buffer	242 g Tris (2M), 100 ml 0.5 M EDTA pH 8.0 (50mM), 57.1 ml acetic acid, fill to 1000 ml with ddH ₂ O
LB medium	10 g trypton, 5 g yeast extract, 10 g NaCl, fill to 1000 ml with ddH ₂ O, pH=7.4
LB agar	4.5 g agar-agar in 300 ml LB medium
PBS	150 mM NaCl, 8 mM Na ₂ HPO ₄ , 1.7 mM NaH ₂ PO ₄ , pH=7.2
TBS	150 mM NaCl, 50 mM Tris, pH=7.2
TBST	0.1% (v/v) Tween 20 in TBS
Modified RIPA Lysis buffer	50 mM Tris-HCl pH=7.4, 150 mM NaCl, 1 mM EDTA, 1% (v/v) NP-40 Substitute, Halt [®] Protease and/or Phosphatase Inhibitor Cocktails (Thermo Fisher)
NP40-RIP Lysis buffer	50 mM Tris-HCl pH=7.4, 150 mM KCl, 3 mM MgCl ₂ , 1% (v/v) NP-40, Halt [®] Protease and/or Phosphatase Inhibitor Cocktails (Thermo Fisher)
NP40-AP Lysis buffer	50 mM Tris-HCl pH=7.4, 100 mM NaCl, 5 mM MgCl ₂ , 10% (v/v) glycerol, 0.5% (v/v) NP-40 Substitute in nuclease-free H ₂ O, Halt [®] Protease and Phosphatase Inhibitor Cocktails (Thermo Fisher), 50 U/ml RNAsin
Optiprep 5% gradient buffer	5 % (v/v) Optiprep solution, 50 mM Tris-HCl pH=7.4, 150 mM NaCl, 1 mM EDTA, 1% (v/v) NP-40 Substitute
Optiprep 25% gradient buffer	25 % (v/v) Optiprep solution, 50 mM Tris-HCl pH=7.4, 150 mM NaCl, 1 mM EDTA, 1% (v/v) NP-40 Substitute
4x sample buffer	200 mM Tris-HCL, pH=6.8, 10% (w/v) SDS, 0.4% (w/v) bromphenol blue, 40% (v/v) glycerol, 400 mM DTT
SDS running buffer for electrophoresis (5x)	125 mM Tris, 1.25 M glycine, 0.5 % (w/v) SDS, pH=8.3
Western blot transfer buffer	24 mM Tris, 192 mM glycine, 20% ethanol in dH ₂ O

WB blocking buffer	4 % (w/v) dry milk powder in TBST
Homemade ECL solution	Solution A: 50 mg luminol in 200 ml 0.1 M Tris-HCl pH=8.6 Solution B: 11 mg para-hydroxy coumaric acid in 10 ml DMSO (dark) ECL solution: combine 1 ml solution A + 100 µl solution B + 0.3 µl H ₂ O ₂
2X SSC	10 % 20x SSC in nuclease-free H ₂ O
Stellaris hybridization buffer	100 mg/mL dextran sulfate, 10 % formamide in 2X SSC
Stellaris wash buffer	10 % formamide in 2X SSC
Singer hybridization buffer	100 mg/mL dextran sulfate, 50 % formamide, 40 µg E. coli tRNA, 2 mM vanadylribonucleoside complex, 0.02% RNase-free BSA in 2X SSC
Singer wash buffer	50 % formamide in 2X SSC
DAPI stain	1 µg/µl DAPI (#D9542, Sigma) in PBS
Mounting medium	2.4 g moviol 4-88, 6 g glycerol, 6 ml ddH ₂ O, 12 ml 0.2 M Tris pH=8.5

2.1.4 Software

Following software was used with licenses of the University of Mainz:

Table 2-6. Software.

Software	Developer
Microsoft Office 2013	Microsoft
Illustrator CS5, Photoshop CS5	Adobe
StepOne Software 2.2.2	Applied Biosystems
Endnote X5	Thomson Reuters
FinchTV	Geospiza
ImageJ	Open source, NIH
Clone Manager 9 Professional	Sci-Ed Software
LAS AF Microscope Software	Leica
SPSS 23	International Business Machines Corporation (IBM)

2.2 Antibodies

Table 2-7. Monoclonal primary antibodies. (WB = Western blot, ICC = Immunocytochemistry).

Antigen	Antibody Name	Host Species	Application	Source
hnRNP A2	DP3B3	mouse	1:2000 (WB)	Sigma-Aldrich
CNP	11-5B	mouse	1:500 (WB)	Sigma-Aldrich
FUS	4H11	mouse	1:500 (WB) 1:400 (ICC)	Santa Cruz
Fyn	25	mouse	1:250 (WB)	BD Biosciences
His-Tag	penta-His	mouse	1:1000 (WB)	Qiagen
Histone H1	[34] ab11079	mouse	1:500 (WB)	Abcam
hnRNP A2	EF67	mouse	1:500 (WB) 1:100 (ICC)	Dr. Rigby, Dartmouth Medical School, USA

hnRNP K	F45-P9-C7	mouse	1:1000 (WB)	Abcam
MBP	MCA409S	rat	1:500 (WB) 1:500 (ICC)	Serotec
MOG	8-18C5	mouse	1:100 (WB)	Dr. Linington, Glasgow
Myc-tag	-	mouse	1:500 (WB)	Sigma-Aldrich
NG2	-	rat	1:100 (WB) 1:100 (ICC)	Hybridoma culture supernatant
Ki-67	B56	mouse	1:200 (ICC)	BD Biosciences

Table 2-8. Polyclonal primary antibodies. (WB = Western blot, ICC = Immunocytochemistry, IP = immunoprecipitation).

Antigen	Antibody Name	Host Species	Application	Source
Control -IgG	sc-2027	Rabbit	IP	Santa Cruz
DDX5	A300-523A	rabbit	1:5000 (WB) 1:200 (ICC), IP	Bethyl Laboratories
G3BP1	13057-2-AP	rabbit	1:2000(WB) 1:500 (ICC)	Proteintech
GAPDH	A300-641A	rabbit	1:3000 (WB)	Bethyl Laboratories
hnRNP E1	T18	goat	1:100 (WB)	Santa Cruz
hnRNP F	ab50982	rabbit	1:1500 (WB)	Abcam
Olig-2	AB9610	rabbit	1:1000 (ICC)	Milipore
PABP-C1	-	rabbit	1: 5000 (WB)	Gift from P. Macchi, Trento
RPLP0	Ab101279	Rabbit	1:4000 (WB)	Abcam
Tia-1	C-20	goat	1:400 (ICC)	Santa Cruz

Table 2-9. Secondary antibodies. (WB = Western blot, ICC = Immunocytochemistry).

Target species	Host species	Conjugation	Application	Source
rabbit	goat	Alexa 488	1:400 (ICC)	Invitrogen
rabbit	donkey	Alexa 488	1:400 (ICC)	Invitrogen
mouse	donkey	Alexa 546	1:400 (ICC)	Invitrogen
rabbit	goat	Cy3	1:1000 (ICC)	Dianova
mouse specific	goat	Cy3	1:800 (ICC)	Dianova
rat	goat	Cy3	1:800 (ICC)	Dianova
goat	donkey	Cy5	1:100 (ICC)	Dianova
goat	bovine	HRP	1:10000 (WB)	Dianova
mouse	goat	HRP	1:10000 (WB)	Dianova
rabbit	goat	HRP	1:10000 (WB)	Dianova
rat	goat	HRP	1:10000 (WB)	Dianova

2.3 Molecular biology

2.3.1 General molecular biological methods

Polymerase Chain Reaction

Polymerase chain reaction (PCR) was used to amplify DNA fragments from cellular cDNA libraries or plasmid DNA. Recognition sequences for restriction enzymes may be included into sequence specific primer pairs. All reactions were set up with the DNA polymerase Pfu Turbo (Stratagene), according to the manufacturers' suggestions and primer pairs described in Table 2-10.

Table 2-10. Primer pairs used in PCR

Target sequence	Forward primer (5' → 3')	Reverse primer (5' → 3')
MBP-14-kDa (Mus)	GTCAAGCTTGATGTGATGGCATCACAG	ACTGGATCCTCAGCGTCTCGCCATG
MBP-17-kDa (Mus)	GTCAAGCTTGATGTGATGGCATCACAG	ACTGGATCCTCAGCGTCTCGCCATG
DDX5^{K144N} mutation	GCTCAGACTGGATCTGGGAAC- ACATTATCTTATTTGCTGCC	GGCAGCAAATAAGATAATGTGTT CCCAGATCCAGTCTGAGC
MBP 5'UTR (Mus)	GATGCTAGCTTTTCCCGAGATGC	GATAAGCTTCAGGCCTCCGGAAG
MBP 3'UTR (Mus)	ACAGATCTGAGCCCTCCCCGCTCAGC	CACTCGAGTACCGTCGACTGCAGAGTTCGG
mCherry FP	CAGTTAAGCTTGCCACCATGGTG	CGAATGGATCCTTACTTGTACAGCTCG

Initial denaturation for 1 min at 95°C was followed by repeated cycling of Steps 2-4 for 20-36 times. After final extension of 10 min, reaction was cooled to 4°C and subsequently analyzed or stored at -20°C.

Table 2-11. PCR cycler program

Function	Temperature	Time	Step
Initial denaturation	95°C	1-2 min	1
Denaturation	95°C	30 sec	2
Primer annealing	60-65°C	30 sec	3
Extension	72°C	1 min / kb	4, go to Step 2 (19x- 35x)
Final extension	72°C	10 min	5

DNA purification and analysis

The QIAquick® PCR Purification Kit (Qiagen) was used to remove primers, buffers and enzymes between working steps. DNA was eluted with nuclease-free H₂O, concentration was determined with the Nanodrop® 1000 photospectrometer (Thermo Scientific) and PCR products were subjected to analytical agarose gel electrophoresis.

Agarose gel electrophoresis

Agarose gel electrophoresis was used to separate DNA molecules according to size. 1-2 % (w/v) agarose was dissolved in TAE-buffer by boiling in a microwave oven. After application of 6 µg/ml ethidium bromide to the cooled solution, the gel was poured into a horizontal gel chamber. DNA samples were mixed with 6x loading dye (Fermentas), loaded on the gel and run together with the Gene ruler 1 kb DNA ladder (Fermentas) until desired separation was achieved. Afterwards, gels were photographed and printed with a UV-based gel documentation system. Alternatively, selected DNA bands were excised from the agarose gel and purified using the QIAquick Gel Extraction Kit (Qiagen) according to the manufacturers' instructions.

DNA restriction digestion and vector dephosphorylation

DNA restriction was performed with indicated restriction enzymes (NEB) according to the manufacturer's protocol, including double digest suggestions. To minimize recirculization of digested vectors, dephosphorylation with Antarctic Phosphatase (NEB) was performed according to the manufacturers' protocol. The reaction was set up for 15 min at 37°C followed by incubation at 70°C for 5 min to deactivate the enzyme.

Ligation and Transformation

Ligation of DNA inserts with the desired vector backbone was performed using the T4 DNA Ligase (Promega) according to the manufacturer's suggestions. Ligation products were amplified in transformation competent TOP10F' Escherichia coli cells (Invitrogen) or recombination-resistant MAX Efficiency® Stbl2™ Competent cells (Invitrogen). For transformation of TOP10F' cells, 14 µl of ligation product was combined with 50 µl cell suspension and a 30 min incubation on ice was followed by heat-shock at 37°C for one minute, inducing uptake of the plasmid. After adding 1 ml of 37°C pre-warmed LB medium, cells were incubated for 30 min at 37°C before an appropriate volume was spread on ampicillin-containing LB-Agar plates. Bacteria were cultured overnight at 37°C in a bacteria incubator. MAX Efficiency® Stbl2™ Competent Cells were transformed according to manufacturer's protocol. Reactions were diluted in SOC medium and plated on LB-Agar plates containing the corresponding antibiotic. Growth took place overnight at 30°C in a bacteria incubator. Individual clones were selected for plasmid amplification and preparation.

Plasmid preparation

Plasmid preparation from transformed bacteria cultures was performed using the PureLink™ Quick Plasmid Miniprep Kit (Invitrogen) or the PureLink™ HiPure Plasmid Maxiprep Kit (Invitrogen) according to the manufacturers' protocols. To prepare Miniprep cultures, individual bacterial colonies from the agar plates were picked and incubated in 4 ml LB medium. To set up Maxiprep cultures, 100 µl of Miniprep culture or a filter tip covered with bacterial glycerol stocks were added to 100 ml of LB medium. Each culture was supplemented with the corresponding antibiotic. Cultures were incubated overnight at 37°C or 30°C (dependent on the bacteria used) and 225 RPM in a shaking bacteria incubator and subjected to the plasmid preparation protocols indicated above. Plasmids were eluted from the Miniprep column with 30 µl and precipitated plasmid DNA from the Maxiprep procedure was resuspended in 100-200 µl of nuclease-free H₂O, respectively. DNA concentration was determined using the Nanodrop® 1000 photospectrometer (Thermo Scientific) and the plasmid DNA was stored at -20°C. Miniprep DNA was routinely analyzed by restriction digestion and agarose gel electrophoresis.

2.3.2 Cloning strategy for MBP-MS2 constructs

The pSL-24xMS2 plasmid containing 24 MS2-loops was a kind gift of Robert Singer (Albert Einstein College, New York) and Yaron Shav-Tal (Bar-Ilan University, Tel-Aviv). The MBP14-3'UTR-IRES-YFP construct was kindly provided by Mika Simons (MPI for experimental medicine, Göttingen). Cloning was carried out in collaboration with Constantin Gonsior (JGU, Mainz). Murine MBP 3'UTR was amplified by PCR (Primers, Table 2-10) from MBP14-3'UTR-IRES-YFP and cloned into the pSL-24xMS2 vector using BglII and XhoI sites, creating the pSL-24xMS2-MBP3'UTR construct. All plasmids containing MS2-loops were amplified in MAX Efficiency® Stbl2™ Competent cells, to minimize recombination. Next, the 24xMS2-MBP-3'UTR sequence was cloned into a pcDNA3.1-Zeo(+) backbone using BamHI and XhoI restriction sites (Zeo-24xMS2-MBP-3'UTR). Murine CDS of 14-kDa-MBP or 17.22-kDa-MBP were amplified from oligodendroglial cDNA libraries by PCR (Primers, Table 2-10) and cloned into Zeo-24xMS2-MBP-3'UTR using HindIII and BamHI sites. This created MBP constructs with 24 MS2-loops inserted between MBP CDS and 3'UTR and a Zeocin resistance gene for selection in mammalian cells (Zeo-MBP14-24xMS2-MBP-3'UTR, Zeo-MBP17-24xMS2-MBP-3'UTR). As a control, the CDS of *mCherry* was amplified by PCR from pAMCBA-mCherry-WPRE-bGHpA (kind gift of AG Lutz, JGU Mainz) and cloned into the pcDNA3.1-Zeo(+) backbone (Zeo-mCherry).

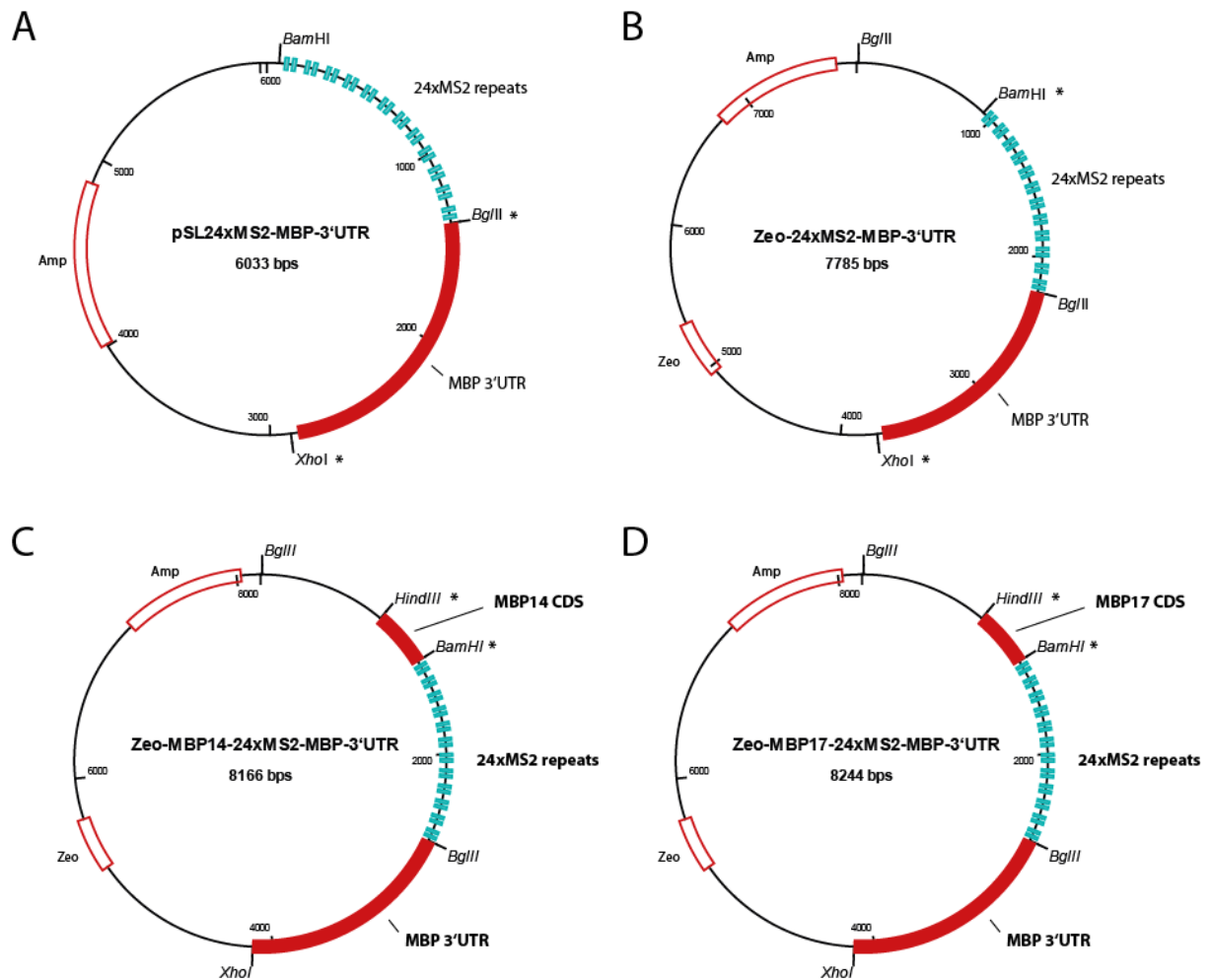


Figure 2-1. Cloning strategy of MS2 labeled MBP constructs.

Schematically drawn vector maps of the cloned plasmids, including restriction sites used for cloning (indicated with asterisks) and resistance genes (Zeo = Zeocin, Amp = Ampicilin). **(A)** pSL-24xMS2-MBP-3'UTR plasmid. **(B)** Zeo-24xMS2-MBP-3'UTR. **(C)** Zeo-MBP14-24xMS2-MBP-3'UTR. **(D)** Zeo-MBP17-24xMS2-MBP-3'UTR. Cloning steps are described in the text.

2.3.3 Cloning strategy for *firefly* luciferase constructs

As a control in MBP luciferase assays, an additional *Firefly* luciferase construct lacking the MBP-3'UTR was generated. The MBP-3'UTR was excised from pCMV-Firefly-MBP-3'UTR-FL using Eco RI-HF and XhoI sites and the vector only including the *Firefly* CDS was extracted and purified from the agarose gel. Single-stranded overhangs of 1 μ g of the purified plasmid were blunted using the DNA Polymerase-I Large Klenow Fragment (#M0210S, NEB) according to the manufacturers' instructions. After DNA purification the vector was re-ligated, producing the pCMV-*Firefly* construct. To study contribution of the MBP 5' untranslated region (5'UTR) on

MBP translation, the murine MBP 5'UTR was amplified from an oligodendroglial cDNA library by PCR (Primers, Table 2-10) and cloned into pCMV-Firefly-MBP-3'UTR or pCMV-Firefly upstream of the luciferase ORF using the restriction sites *NheI* and *HindIII*. The pCMV-Firefly-MBP-3'UTR and pCMV-Firefly constructs were used in luciferase assays (Chapter 2.8), while experiments done with 5'UTR constructs were not included in this thesis.

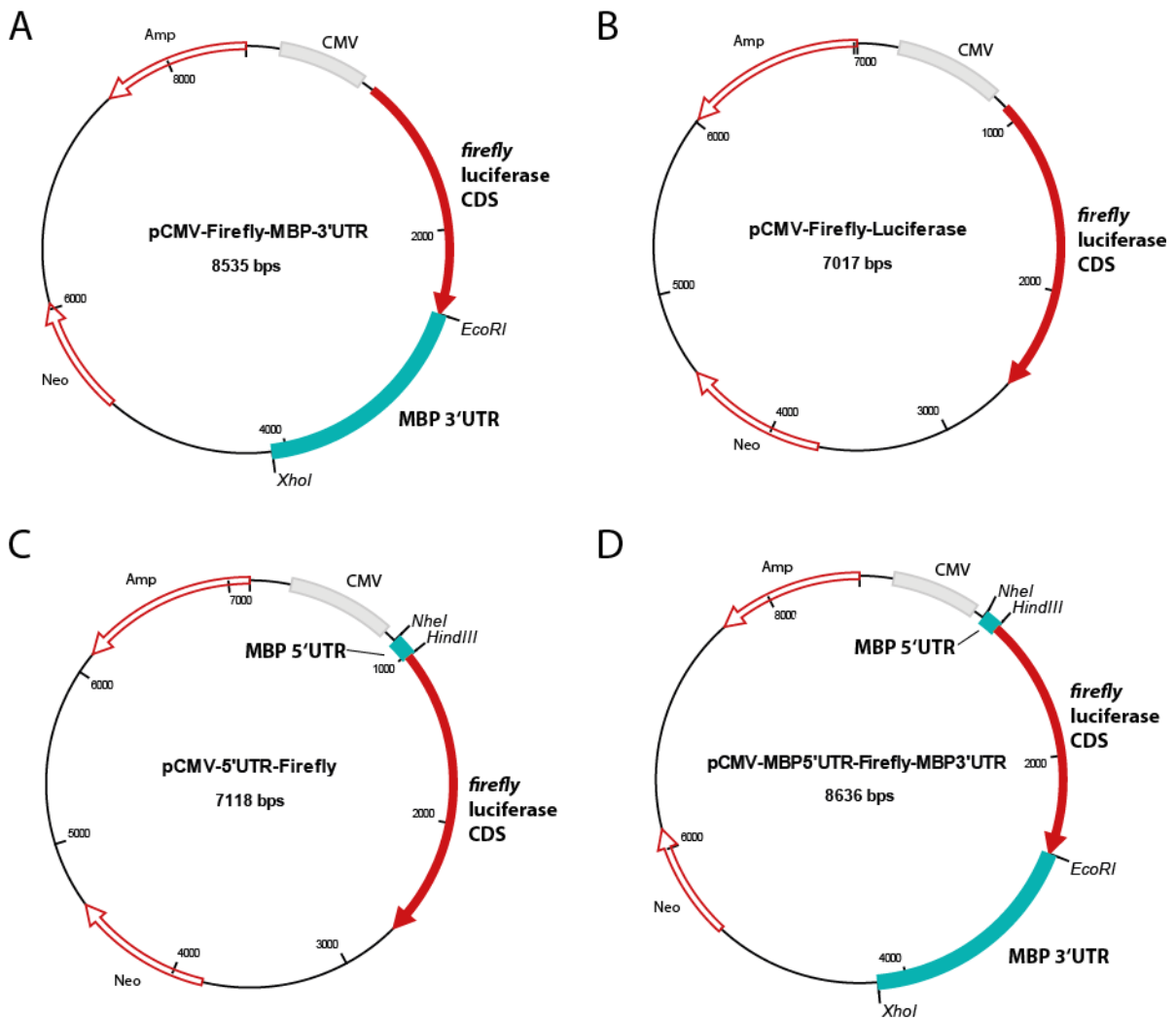


Figure 2-2. Firefly luciferase constructs.

Schematically drawn vector maps of the cloned plasmids, including restriction sites used for cloning, CMV promoter region and resistance genes (Neo = Neomycin, Amp = Ampicilin). **(A)** pCMV-Firefly-MBP-3'UTR. **(B)** pCMV-Firefly. Restriction sites *EcoRI* and *XhoI* were lost during blunting and re-ligation. **(C)** pCMV-MBP-5'UTR-Firefly. **(D)** pCMV-MBP-5'UTR-Firefly-MBP-3'UTR. Cloning strategy is described in the text.

2.3.4 Site directed mutagenesis of DDX5^{K144N}

Mutations of DDX5 have been created and evaluated in several publications (Jalal et al., 2007; Pause and Sonenberg, 1992; Saporita et al., 2011). Selective mutation of the amino acids Lysine (K) to Asparagine (N) at position 144 abolished ATP binding and the helicase activity of DDX5. The Quickchange II site directed mutagenesis Kit (Agilent, #200524) was used to insert this mutation into the pCMV-DDX5-myc vector. The PCR was performed according to the manufacturers' protocol using 125 ng of each primer including the desired mutation (Table 2-10) and 30 ng of the DDX5-myc plasmid. DpnI digestion was carried out for 1.5 hours at 37°C. Transformation of XL-Blue supercompetent cells was performed with minor changes (SOC medium used instead of NZY+ broth medium) and 250 µl of the transformation reaction was spread on Ampicillin containing LB-Agar plates, which were incubated overnight at 37°C. Selection, plasmid preparation and subsequent DNA sequencing confirmed the correct mutation in the DDX5^{K144N} plasmid.

2.3.5 Plasmids

Table 2-12. Plasmids

Plasmid	Source	Reference
pCMV-DDX5-myc	Constantin Gonsior, Mainz	
pCMV-DDX5-K144N-myc	Constructed in the context of this thesis	Chapter 2.3.4
pCMV-FUS-myc	Diploma thesis, Hoch-Kraft, 2010	Hoch-Kraft, 2010
MBP14-3'UTR-IRES-YFP	Mika Simons, Göttingen	
pSL-24xMS2	Kind gift from Yaron Shav-Tal, Tel Aviv with permission from Robert Singer, New York City	
pCMV-MBP14-24xMS2-MBP-3'UTR	Constructed in the context of this thesis	Chapter 2.3.2
pCMV-MBP17-24xMS2-MBP-3'UTR	Constructed in the context of this thesis	Chapter 2.3.2
pCMV-mCherry	Constructed in the context of this thesis	Chapter 2.3.2
L30-MCP-YFP-NLS	Kind gift from Yaron Shav-Tal, Tel Aviv with permission from Robert Singer, New York City	
L30-MCP-YFP-NLS-NES	Kind gift from Yaron Shav-Tal, Tel Aviv with permission from Robert Singer, New York City	
phage-ubc-NLS-HA-tdMCP-GFP	Kind gift from Robert Singer (Addgene plasmid # 40649)	Wu et. al 2012
MS2-HB (MCP-HBTH)	Kind gift from Marian Waterman (Addgene plasmid # 35573)	Tsai et 2011
pCMV-Firefly-MBP-3'UTR-FL	Constantin Gonsior, Mainz	Gonsior, 2011
pCMV-Firefly	Constructed in the context of this thesis	Chapter 2.3.3
pCMV-Firefly-MBP-5'-UTR-3'UTR-FL	Constructed in the context of this thesis	Chapter 2.3.3

pCMV-Renilla	Stefan Hüttelmaier, Halle
pAM-CBA-mCherry-WPRE-bGHpA	Stefan Guggenhuber, AG Lutz (JGU Medical Center, Mainz)

2.4 Cell culture

2.4.1 Preparation and culture of primary oligodendrocytes

Primary mouse oligodendrocytes (pOL) were prepared as described before (Trotter et al., 1989) with minor modifications. C57BL/6 mice were obtained from the animal facility of the Johannes Gutenberg-University Mainz. Embryonic brains (E14-16) were collected from the embryos, meninges were removed and pre-digestion was performed in 1% trypsin in HBSS for 3-5 min at 37°C. After two washing steps with HBSS+, brains were dissociated by resuspension in 0.05% DNase I solution (Roche, #104159) with Pasteur pipets of decreasing diameter. The obtained single cell suspension was pelleted for 10 min at 130 g, 4°C and after two HBSS+ washing steps resuspended in DMEM 10% HS. 10 ml containing 3 - 3.5 x 10⁷ cells were plated in PLL-coated T80 Flasks and cultured at 37°C, 8% CO₂. Neurons were depleted after 5 days in culture by a complement mediated immune cytolysis using monoclonal M5 antibodies (1:10, 358-hybridoma supernatant) and guinea pig complement (1:15), cell debris were removed by washing twice with DMEM 10% HS. 2-3 days later medium was exchanged to DMEM 10% HS supplemented with 5µl/10ml Insulin (Sigma, #I-5500). After 11 days in culture, gentle shaking removed microglia resting loosely on the mixed culture and retained pOL growing on an astrocyte cell layer. On day 14 after preparation, pOL were isolated from the mixed culture by intense shaking (oligoshake). Primary oligodendrocyte pellets were resuspended in pOL plating medium and seeded on PLL-coated cell culture dishes, coverslips or were directly used for nucleofection with siRNA.

2.4.2 Oli-*neu* cell culture

The oligodendroglial cell line Oli-*neu* was produced by infection of primary oligodendroglial precursor cells with replication deficient retroviruses bearing the constitutively active c-neu proto-oncogene (Jung et al., 1995). The dividing cell line exhibits characteristics of oligodendrocyte precursor cells, expressing marker molecules such as NG2 and can be differentiated into immature OL by a daily addition of 1 mM dibutyryl cyclic AMP (dbcAMP). Oli-*neu* cells were cultured in Sato 1.0-1.5% HS medium at 37°C and 8% CO₂ on PLL coated cell

culture vessels. Cells were grown sub-confluent before passaging, which includes detachment with pre-warmed TE low for 1-2 minutes (digestion was stopped by adding ice-cold PBS 10% HS), resuspension of the pelleted (10 min 130g 4°C) cells in culture medium and redistribution of desired volumes on PLL-coated culture dishes. For long term storage, *Oli-neu* cells were resuspended in freezing medium and transferred to -80°C and subsequently stored in liquid nitrogen.

2.4.3 Transfection methods

FuGene HD transfection of plasmid DNA

Transfection of plasmid DNA into *Oli-neu* cells was achieved by FuGene HD (Promega) according to the manufacturer's instructions. In general, 70 - 90 x 10³ cells were seeded into 6-well plate one day prior transfection. 2 µg of DNA were diluted in 100 µl DMEM and combined with 4 µl FuGene HD (2:4 ratio). Transfection complexes were mixed and immediately applied to the cells, which were analyzed 24-72 hours after transfection. The amounts could be scaled up to larger cell numbers and vessel diameters, keeping the transfection ratios constant.

Amaya Nucleofection of siRNA

RNAi was used to knockdown expression of selected target genes from *Oli-neu* cells or primary OL using the Amaya Basic Nucleofector® Kit for Primary Neurons according to the manufacturers' instructions. 1 x 10⁶ *Oli-neu* cells or 4 x 10⁶ primary OL from the "oligo-shake" were pelleted at 100 g at room temperature, resuspended in 100 µl AMAXA solution and combined with 160 pmol of siRNA cocktails (Table 2-13). Electroporation was carried out using program O-005 in the AMAXA Nucleofector II device, the cell suspension in the electroporation cuvette was immediately combined with the corresponding warm, CO₂-equilibrated plating medium and then carefully seeded in PLL-coated cell culture dishes. Culture medium was exchanged 3-5 hours post nucleofection and cells were analyzed 24-72 hours later.

Table 2-13. siRNA

Name	Catalogue Number	Source
siGENOME SMARTpool DDX5 siRNA	#M-06533-01-0005	GE Healthcare Dharmacon
siGENOME SMARTpool FUS siRNA	#M-051741-01-0005	GE Healthcare Dharmacon

Non-silencing control siRNA

#1022076

Qiagen

Amaxa 4D Nucleofection of plasmid DNA into adherent cells

Transfection of plasmid DNA into primary oligodendrocytes was achieved by the AMAXA AD1 Primary Cell 4D-Nucleofector™ Y Kit for adherent cells according to the manufacturer's instructions (Amaxa™ 4D-Nucleofector™ basic protocol for mammalian neural cells). Primary oligodendrocytes were plated into 24-well plates at a density of 5×10^5 cells / well. After 3 days in culture medium was removed, 10 µg plasmid DNA were mixed with 350 µl AD1 4D-Nucleofector™ Y solution and carefully applied to the cells. Then the 24-well dipping electrode array was inserted into the 24-well plate and electroporation was performed using program ED-158 in the AMAXA 4D Nucleofector Y-Unit. Preconditioned medium previously removed from the wells was stored, depleted from dead cells by brief centrifugation and mixed with fresh pre-equilibrated medium 1:1 prior reapplication by gentle pipetting after nucleofection. Cells were routinely analyzed 48 hours post transfection.

2.4.4 Generation of MBP14-MS2 stable cell lines

In order to keep the abundance of the MS2-labeled mRNA in the cell on a moderate level, polyclonal stable cell lines were established from Oli-*neu* cells in corporation with Constantin Gonsior. To promote a stable insertion of DNA fragments into the cellular genome, plasmids were linearized prior transfection. Digestions of 15 µg pCMV-MBP14-24xMS2-MBP-3'UTR, pCMV-MBP17-24xMS2-MBP-3'UTR and pCMV-mCherry were carried out with SapI (NEB) and linearized plasmids were purified from a 1 % agarose gel using the QIAquick Gel Extraction Kit (Qiagen). 2 µg of linearized plasmid DNA were introduced into Oli-*neu* cells using FuGene HD transfection. Cells were allowed to recover and express the *Zeo* resistance gene for three days before selection of plasmid-bearing cells was started by adding 200 µg/ml Zeocin (Invitrogen) to the culture medium. Selection was continued for 18 days and included several cell divisions and passages. Stocks of the stable cell lines MBP14-MS2, MBP17-MS2 and Zeo-mCherry were stored in liquid nitrogen for further use.

2.4.5 Incorporation of labeled amino acids into MBP14-MS2 cells for SILAC quantitative proteomics

DMEM (high glucose, no glutamine, no lysine, no arginine) was supplemented with heavy (SILAC heavy medium) or light (SILAC light medium) amino acids and the remaining components to obtain the modified SATO 1% HS culture media (Table 2-5). DMEM and amino acid mixtures were supplied by our collaborator Falk Butter (Proteomics Core Facility, IMB Mainz). MBP14-MS2 cell lines were cultured in the corresponding media for two weeks, leading to an incorporation of the heavy or light amino acids into the cellular proteome, respectively. Incorporation was validated by the Proteomics Core Facility and allowed the use of the cells in SILAC-based quantitative proteomics.

2.5 Proteinbiochemistry

2.5.1 Cell lysis and subcellular fractionation

Oli-neu cells or primary oligodendrocytes were lysed in order to analyze the cellular protein composition. Cells were placed on ice, washed twice with ice-cold PBS and an appropriate volume of indicated lysis buffer was added. After incubation for 10-45 minutes, cells were scraped with a rubber policeman, collected in 1.5 ml collection tubes and centrifuged at 1000 x g in a tabletop centrifuge at 4°C for 10 minutes. Pellets of nuclei and cellular debris were discarded and supernatant was collected, representing the post-nuclear supernatant (PNS). Optionally, protein concentrations were determined with BCA protein Assay Kit (Novagen) according to the “Enhanced Assay” protocol. For subcellular fractionation, NE-PER Nuclear/Cytoplasmic Extraction Kit (Thermo Scientific) was used according to the manufacturers’ instructions and yielded nuclear and cytosolic protein extracts.

2.5.2 SDS-PAGE and protein visualization

Proteins were separated by size using sodiumdodecylsulfate polyacrylamide gel electrophoresis (SDS-PAGE). Handmade gels were prepared according to “Molecular Cloning – A Laboratory Manual”, tables A8-9 and A8-10 in section A8.43, respectively (Sambrook, 2001) and poured using the Mini PROTEAN® 3 Gel Electrophoresis System (Bio-Rad).

Alternatively, proteins were analyzed with the Novex® NuPAGE® SDS-PAGE Gel system (Invitrogen) using 4-12% Bis-Tris gradient gels with MOPS or MES running buffer. Protein lysates were diluted in appropriate volumes of 4X sample buffer and heated to 90°C for 5 minutes prior loading into the gel pockets next to 5-10 µl of the Precision Plus Protein Standard (Bio-Rad). Electrophoresis was performed at 140-160V until the desired separation was achieved. Gels could be stained with the SilverQuest™ Silver Staining Kit (Invitrogen) according to the “Basic Staining” protocol or were routinely transferred on a PVDF membrane via Western blotting.

2.5.3 Western blotting and immunodetection of selected proteins

Proteins separated by SDS-PAGE were blotted on ethanol activated PVDF membranes using the Mini Trans-Blot® Electrophoretic Transfer Cell system (Bio-Rad). Transfer was performed for 3 hours at 200 mA or overnight (<15h) at 40-50 mA. Presence of the pre-stained protein standard indicated successful transfer and after rinsing the membrane with dH₂O twice, unspecific binding was minimized by blocking with blocking solution (4% w/v dry milk powder in TBST) for 60 min at room temperature. Primary antibodies were diluted in blocking solution and incubated at 4°C overnight or 2-3h at room temperature. After washing the membrane with TBST three times for at least 8 min each, species specific HRP-coupled secondary antibodies were diluted 1:10000 in blocking solution and incubated for 30 min at RT. Before enhanced chemiluminescence (ECL) detection, the membrane was washed twice with TBST and once with TBS. Incubation of the membrane in 1-2 ml homemade ECL solution for 2 minutes allowed the subsequent detection of emitted light from the HRP reaction with Hyperfilm ECL (GE healthcare) using a OptiMax X-Ray film processor. After ECL detection membranes could be used for detection with another primary antibody or were stored at -20°C for later use. Prior incubation with an additional primary antibody, the membrane was washed twice with TBST and again blocked for at least 15 min in blocking solution. Developed films were scanned and Western blot signals were quantified using the Image J software and Microsoft Excel.

2.5.4 Optiprep® density gradient centrifugation

Density gradient centrifugation was performed in collaboration with and according to the protocol established by Daniela Karra (Fritzsche et al., 2013). In SW41-sized polyallomer tubes,

5 ml Optiprep 25% gradient buffer were carefully overlaid and filled up with Optiprep 5% gradient buffer solution and sealed with parafilm. Tubes were incubated horizontally at 4°C, allowing diffusion and establishment of the density gradient. Before use, tubes were carefully rotated, placed on ice vertically and 2 ml were removed from the top prior loading of the cellular lysate. PNS of primary oligodendrocytes (DIV6) or differentiated Oli-*neu* cells were prepared and layered on top of the gradient. Samples were centrifuged at 280 000 x g for 2.5 h at 4°C in an ultracentrifuge, using a SW41-Ti Rotor (Beckmann Coulter). Fractions of 1 ml each were collected from the top of the gradient and analyzed via Western blot, by measurement of sucrose refractive index or RNA concentration. Optionally, RNase treatment of the lysates with 50 µg/ml RNase A (Invitrogen) for 20 min at 30°C was performed to disrupt RNP complexes.

2.5.5 DDX5 RNA Immunoprecipitation (RIP)

RNA immunoprecipitation was used to identify RNAs and proteins associating with DDX5 protein in oligodendroglial cells. All immunoprecipitation steps were performed on ice or at 4°C in RNase-free conditions and without interruptions to keep RNP dissociation as minimal as possible.

Sepharose-based RNA immunoprecipitation

Protein A-coupled sepharose beads are capable of tethering antibodies to the bead matrix, allowing the pulldown of specific proteins from cellular lysates. To form antibody-bead-complexes, 80 µl Protein A sepharose bead slurry (ca. 20 µl packed beads) were washed twice with PBS and incubated with 1 µg of polyclonal DDX5 antibody or normal rabbit IgG as a control in 500 µl PBS for 3 hours on a rotating wheel at 4°C. A washing step generally includes a brief centrifugation at 1000 x g in a table top centrifuge at 4°C and displacement of the supernatant. For immunoprecipitation, PNS was prepared from 2 days differentiated Oli-*neu* cells using RIP lysis buffer (1.5 ml in a 150-mm dish). To reduce unspecific binding, PNS was incubated with sepharose beads for 60 min at 4°C (Pre-clearing, PC). The pre-cleared lysate was split and combined with three times washed antibody-bead complexes (DDX5 or control) and immunoprecipitation was performed for 3 hours on a rotating wheel at 4°C. Supernatant was collected, depicting the unbound (UB) fraction. Beads were washed three times with RIP lysis buffer and one time with PBS, followed by the removal of residual PBS with a 27G needle. RNPs were eluted from the beads by incubation with RIP elution buffer (0.2% w/v SDS, 2% v/v

β -mercaptoethanol in 100 μ l nuclease-free H₂O) for 5 min at 70°C and 800 RPM on a shaking device. Supernatant was collected, 20 μ l were used for Western blotting and 70 μ l were stored in 700 μ l QIAzol[®] Lysis Reagent (Qiagen) at -80°C for RNA analysis. In addition, input PNS lysate (Total), PC precipitate (PC) and unbound proteins (UB) were analyzed by Western blotting.

Magnetic Dynabead-based RNA immunoprecipitation

MACS-sorted O4+ oligodendrocytes were prepared by Wen Ping Kuo from postnatal day 7 mice by using the Neural Tissue Dissociation Kit, gentleMACS dissociator, MACS Separator and anti-O4 MicroBeads (Miltenyi Biotec) according to manufacturer's instructions as described before (Frohlich et al., 2014). Typically three confluent 60-mm dishes were used for two immunoprecipitation experiments, including specific and control antibodies. PNS was prepared from O4+ pOL DIV3 using NP40-AP lysis buffer (300 μ l in a 60-mm dish). All steps were performed rapidly on ice under RNase-free conditions. 400 μ l lysate were combined with 2,5 μ g of polyclonal DDX5 antibody or normal rabbit IgG as a control and incubated for 90 min on a rotating wheel at 4°C. 50 μ l of Protein G coupled Dynabeads were washed three times with lysis buffer and incubated with the antibody-lysate mixture. Separation of the beads during washing steps was carried out using the DynaMag-2™ magnetic separation device (Life Technologies). Immunoprecipitation was performed for 45 min on a rotating wheel at 4°C. Supernatant was collected, depicting the unbound (UB) fraction. Beads were washed three times with lysis buffer and separated during the last washing step. 3/5 of the beads were boiled with 20 μ l 1x sample buffer at 90°C for 5 min and 800 RPM and supernatant was analyzed via Western blotting. 2/5 of the beads were combined with 700 μ l QIAzol[®] Lysis Reagent (Qiagen) and stored at -80°C for RNA analysis.

2.5.6 MBP14-MS2 streptavidin affinity purification (SA-AP)

The high affinity binding of streptavidin to biotin molecules was used to isolate MBP14-MS2 RNA and associated RBPs from oligodendroglial cells by affinity purification using a MCP coupled to an HTBH-tag. The HTBH-tag consists of two His-tags surrounding a TEV cleavage site and an *in vivo* biotinylation signal. Addition of Biotin to the culture medium led to biotinylation of the HTBH-tag and allows the purification of the MCP-bound MS2-labeled mRNA. The MS2-HB plasmid was a kind gift from Marian Waterman (Addgene plasmid # 35573) and has been described before (Tsai et al., 2011). For affinity purification, stable

MBP14-MS2 or Zeo-mCherry (Control) cell lines were seeded at a density of 25×10^4 cells in a 60-mm dish and transfected with FuGENE HD the following day. To obtain moderate expression levels, HTBH plasmid was diluted, 1.25 μg MS2-HTBH and 3.75 μg empty control vector were combined to reach 5 μg DNA in total. DNA was mixed with 250 μl DMEM and 10 μl FuGENE, maintaining the 2:4 transfection ratio. Culture medium was exchanged the following day and 1 mM dbcAMP and 5 μM biotin were added to induce differentiation and biotinylation, respectively. 48 hours after transfection, cells were lysed with NP40-AP lysis buffer for 15 min and PNS was prepared by centrifugation for 10 minutes at $2000 \times g$ at 4°C . Optionally, cells were exposed to oxidative stress by addition of 0.1 mM sodium arsenite to the medium 45 min prior lysis. For each affinity purification, 30 μl streptavidin-coupled magnetic M280 Dynabeads were blocked for at least 1 hour with blocking buffer (0.1% BSA, 200 $\mu\text{g}/\text{ml}$ yeast tRNA in PBS) at 4°C on a rotating wheel. Separation of the beads during washing steps was carried out using the DynaMag-2™ magnetic separation device (Life Technologies). After two washing steps with blocking buffer and once with lysis buffer supplemented with 200 $\mu\text{g}/\text{ml}$ yeast tRNA and 0.1% BSA, M280 beads were combined with the PNS lysate. Affinity purification was performed for 1h hour at 4°C , supplemented with 200 $\mu\text{g}/\text{ml}$ yeast tRNA. Supernatant was collected, depicting the unbound (UB) fraction. Beads were washed three times with lysis buffer and separated during the last washing step. 7/8 of the beads were boiled with 20 μl 1x sample buffer at 90°C for 5 min and 800 RPM and supernatant was analyzed via Western blotting. 1/8 of the beads was combined with 700 μl QIAzol® Lysis Reagent (Qiagen) and stored at -80°C for RNA analysis.

2.5.7 SILAC quantitative proteomics of MBP14-MS2 affinity purification

Streptavidin affinity purification was performed as described above (Chapter 2.5.6) comparing MS2-HB pulldowns from MBP14-MS2 lines grown in either heavy or light SILAC culture medium (Chapter 2.4.5). Two experiments were performed in a cross control, either MBP14-MS2-heavy or MBP14-MS2-light cell lines were treated with 0.1 mM sodium arsenite and the difference in mass of the detected peptides allows the correlation to the oxidative stress condition in each experiment. After the final washing step of the AP, beads of heavy and light conditions were combined and proteins were eluted in 30 μl elution buffer (100 mM DTT in 1x LDS sample buffer). SILAC mass spectrometry, data acquisition and normalization were performed by Falk Butter (Proteomics Core Facility IMB, Mainz). SILAC ratios were retrieved

and the mean value was calculated from two experiments, using inverse SILAC ratios of the second experiment.

2.5.8 Fluorescent immunocytochemistry

Oli-*neu* cells or primary OL were grown until a desired density and differentiation state was reached, then coverslips were washed 2 times with PBS and fixed with Roti Histofix® 4% formaldehyde solution or 4 % Paraformaldehyde in PBS for 10-15 min at room temperature. After two washing steps, coverslips were transferred into a humidified chamber and cells were permeabilized with 0.1% Triton X100 in PBS for 2 minutes or 5 µg/ml digitonin (stock 50 mg/ml solved in DMSO) in PBS for 5 minutes. Permeabilization with digitonin leaves the nuclear membrane intact and prevents antibody staining in the nucleus (Tissera et al., 2010). After three washing steps with PBS, cells were incubated in blocking solution (10 % horse serum in PBS) for 60 minutes. Primary antibodies were diluted in blocking solution and incubated with the cells over night at 4°C. The next day, after 3 washing steps, species matching fluorescently labeled secondary antibodies were diluted in blocking solution and incubated for 20-30 min at room temperature. FITC-conjugated streptavidin molecules could be applied 1:50 during the secondary antibody incubation step, fluorescently labeling biotin in the cell. Optionally, nuclear counterstaining with DAPI was introduced for 2 min. After three final washing steps, coverslips were rinsed in distilled water and mounted upside down in Mowiol on a glass slide and imaged using a Leica DM6000B fluorescence microscope.

2.6 RNA analysis

2.6.1 Isolation of total RNA from cultured cells

Oli-*neu* cells or primary oligodendrocyte cultures were scraped on ice in lysis buffer supplemented with RNAsin (50 U / ml) and appropriate volumes were mixed with 700 µl QIAzol Lysis reagent, vortexed for 15 seconds and stored at -80°C. Alternatively, magnetic Dynabeads or eluates from immuno- or affinity purifications or cells were directly mixed with 700 µl QIAzol. Total RNA, also containing small RNAs, was prepared with the miRNeasy® Mini Kit (Qiagen) according to the manufacturer's instructions, including DNase digestion using the RNase-free DNase Kit (Qiagen). RNA was eluted with 30 µl of nuclease-free water,

concentration was determined using Nanodrop® 1000 and samples were stored at -80°C immediately or used for cDNA synthesis.

2.6.2 Reverse transcription cDNA Synthesis

RNA was reverse transcribed by the Transcriptor First Strand cDNA Synthesis Kit (Roche) according to the manufacturer's instructions with minor modifications. Initially, 12.85 µl of RNA and 0.4 µl of random hexamer primers were heated for 10 min at 65°C and immediately placed on ice. The RT master mix, including 5U of Transcriptor Reverse Transcriptase was added and RT reaction was performed according to Table 2-14 in a thermal cycler, yielding cDNA libraries directly used in quantitative real time PCR or normal PCR reactions.

Table 2-14. Reverse transcription cyler program

Process	Temperature	Time
Annealing	25°C	10 min
Reverse Transcription	55°C	30 min
RT Enzyme deactivation	85°C	5 min
Storage	4°C	end

2.6.3 Quantitative PCR (qPCR)

Taqman® Gene Expression Assays

The cDNA libraries (Chapter 2.6.2) were analyzed with gene specific Taqman® Gene Expression Assays (Table 2-15) using the Taqman® Gene Expression Master Mix (Applied Biosystems) according to the manufactures' instructions and a total reaction volume of 10 µl. In each reaction 0.5-1.0 µl cDNA was used and samples were run in duplicate or triplicate on a StepOne™ Real-Time PCR system in standard "Taqman Gene Expression Assay" configuration. In no template-controls (NTC) cDNA was replaced by nuclease-free water. Relative gene expression was calculated by the $\Delta\Delta C_t$ method with the StepOne Software 2.2.2 using *Pgk1* or *Rs18s* as a reference gene.

SYBR Green qPCR

Real-time PCR based RNA quantification of MBP-3'UTR Luciferase assays was performed using the SYBR Green PCR Mastermix (Applied Biosystems). Primers for *Renilla* and *Firefly* luciferase were purchased from Sigma as described before (Lin et al., 2011). Briefly, 2 µl of cDNA or H₂O (NTC) were combined with 10 µl of 2x SYBR Green PCR Mastermix (Applied Biosystems) and 4

µl of each primer (200 nM) in a 20 ml reaction volume. Quantitative PCR was run on a StepOne™ Real-Time PCR system 48-well (Applied Biosystems) with standard SYBR Green settings, including melt curve analysis.

Table 2-15. Taqman® Gene Expression Assays

Target gene	Isoform specificity	Catalogue number	Source
Axin2	-	Mm00443610_m1	Applied Biosystems
CNP	-	Mm01306640_m1	Applied Biosystems
Cspg4 (NG2)	-	Mm00507256_m1	Applied Biosystems
hnRNP A2B1	-	Mm01325931_g1	Applied Biosystems
Mbp	All classic isoforms	Mm01262037_m1	Applied Biosystems
Mbp	Exon 2-containing isoforms	Mm01262035_m1	Applied Biosystems
Mbp	Exon 2-lacking isoforms	Mm00521980_m1	Applied Biosystems
Mog	-	Mm00447824_m1	Applied Biosystems
Olig2	-	Mm01210556_m1	Applied Biosystems
Pgk1	-	Mm00435617_m1	Applied Biosystems
Rn18s	-	Mm03928990_g1	Applied Biosystems
Rplp0	-	Mm00725448_s1	Applied Biosystems
β-actin	-	Mm00607939_s1	Applied Biosystems

Table 2-16. Primer pairs used in SYBR Green qPCR

Target gene	Forward Primer (5'→ 3')	Reverse Primer (5'→ 3')
Firefly luciferase	TCAAAGAGGCGAACTGTG	TCAATCAAGGCGTTGGTC
Renilla luciferase	GGGTGCTTGTTGGCATTTC	GGCCATTCATCCCATGATTC
Pgk1	CTTCGACCTCACGGTGTTG	CAACGGACTTGGCTCCATTG

2.7 In situ hybridization techniques

2.7.1 Stellaris® single molecule fluorescent in situ hybridization (smFISH)

Custom Stellaris® FISH probes were calculated by the Stellaris® FISH Probe Designer (<https://www.biosearchtech.com/stellarisdesigner/>), recognizing murine MBP exons 1, 3, 4 and 7. Probes are shown in Figure 3-1 aligned to the MBP sequence. Buffers were made (Table 2-5) and in situ hybridization was performed according to the manufacturer's suggestions (General Protocol & Protocol for Adherent Cells). Dried oligonucleotides were redissolved in 200 µl of TE buffer pH=8 (Ambion), to create a 25 µM stock solution. Cells were grown on

coverslips and fixed with 4 % PFA in PBS for 15 min at room temperature. After washing with nuclease-free PBS, coverslips were incubated in 70 % Ethanol at 4°C at least overnight. Prior FISH procedure, cells were rehydrated in Stellaris wash buffer for 10 min and coverslips were transferred into 24-well plates for hybridization. Stellaris MBP probes were diluted in hybridization buffer (1:200) and incubated with the cells (60 – 80 μ l / coverslip) over night at 37°C. 24-well plates were covered with MicroAmp® 96-Well Optical Adhesive Film (Applied Biosciences) and additionally sealed with Parafilm to exclude evaporation. After 2 washing steps with 2x SSC at 37°C for 30 minutes, coverslips were rinsed with nuclease-free H₂O and mounted upside down in Mowiol on a glass slide. Cells were imaged with a DFC360 FX camera, using Leica DM6000B widefield microscope equipped with a HCX PL APO CS 100.0x1.40 OIL objective.

2.7.2 MS2-RNA visualization by fluorescent in situ hybridization (FISH)

To visualize MS2-labeled mRNA in situ, an Alexa 546-conjugated oligonucleotide targeting the repetitive MS2-loop structure, described in (Ben-Ari et al., 2010), was purchased from Sigma (Table 2-17), binding 11 times to the 24xMS2 repeats. Dried oligonucleotides were redissolved nuclease-free H₂O to create a 500 ng/ μ l stock solution. Buffers were made (Table 2-5) and in situ hybridization was performed according to the Singer lab in situ hybridization protocol for mammalian cells (<http://www.singerlab.org/protocols>).

Table 2-17. FISH probe used for MS2-RNA visualization.

Name	Sequence (5' → 3')
MS2-A546	CTAGGCAATTAGGTACCTTAGGATCTAATGAACCCGGGAATACTGCAGAC-Alexa 546

In situ hybridization procedure was performed practically as described for Stellaris smFISH above. Changes include the composition of hybridization (Singer hybridization buffer) and wash buffers (Singer wash buffer) and the use of 45 ng of the MS2-A546 probe (0.75 ng/ μ l in Singer hybridization buffer) for *in situ* hybridization with the labeled MS2-RNA.

2.8 Luciferase-based MBP translation assay

Luciferase reporter assays were used to measure MBP-3'UTR dependent translational regulation in *Oli-neu* cells. Reporter plasmids comprise a *firefly* luciferase reporter conjugated

with the full length MBP 3'UTR (pCMV-Firefly-MBP-3'UTR) and a reporter bearing only the *firefly* luciferase coding region (pCMV-Firefly). As internal control, *renilla* luciferase was included in the assay. Transfection of 2 µg of DNA was carried out with FuGene HD according to Table 2-18 in a 2:4 transfection ratio.

Table 2-18. Plasmid amounts for FuGENE HD transfections in MBP Luciferase Assays. (ng Plasmid)

Plasmid	DDX5 ^{WT}	DDX5 ^{WT}	DDX5 ^{K144N}	DDX5 ^{K144N}	Control	Control
DDX5 ^{WT} -myc	1650	1650	0	0	0	0
DDX5 ^{K144N} -myc	0	0	1650	1650	0	0
pCMV-Firefly-MBP-3'UTR	250	0	250	0	250	0
pCMV-Firefly	0	250	0	250	0	250
pcDNA3.1 backbone	0	0	0	0	1650	1650
Renilla	100	100	100	100	100	100

After two days of dbcAMP induced differentiation cells were scraped on ice in 350 µl ice-cold PBS and divided in three parts, 100 µl were used for Western blotting (mixed with 4x sample buffer, stored at -20°C), 100 µl were used for RNA quantification (mixed in 700 µl Qiazol, stored at -80°C) and 150 µl were used to determine luciferase activity in triplicates. To measure luciferase activity DualGlo[®] Luciferase Assay (Promega) or Beetlejuice/Renilla GLOW-juice Luciferase Assay system (PJK GmbH) were performed according the manufacturer's instructions. Luminescence was measured with an Infinite M200 Pro reader (Tecan) with standard "luminescence" settings. Finally, *Firefly* luciferase activity was normalized to *renilla* values and compared between experimental conditions.

2.9 Online databases and prediction algorithms

2.9.1 RBPmap binding site prediction

The RBPmap server (<http://rbpmap.technion.ac.il/>) uses a database of 165 experimentally retrieved RNA binding motifs to realize an accurate prediction and mapping of RBP binding sites in a given mRNA (Paz et al., 2014). The mRNA sequence of murine 21.5-kDa MBP (NM_001025251) was analyzed in a GRCm38/mm10 background with stringency level on the highest setting, conservation filter turned on and with all Human/Mouse motifs selected for mapping. The prediction summary was saved and processed further in Microsoft Excel 2013

to generate a graphical output, dependent on the nucleotide position in MBP mRNA and linked to the annotated exons and additional RNA binding motifs and regions in MBP mRNA. The interactive map is available on request.

2.9.2 SFmap binding site prediction

The SFmap server Version 1.8 (<http://sfmap.technion.ac.il/>) has been designed for mapping binding sites of known splicing factors and their consensus motifs to a selected genomic region (Paz et al., 2010). The mRNA sequence of murine 21.5-kDa MBP (NM_001025251) exon 2 with a flanking intronic region of 300 bp each was analyzed in a mm9 background with stringency level of COS(WR) on “high” and with all motifs selected for mapping. The prediction summary was saved and a graphical output in the UCSC genome browser shows binding sites in the context of MBP exon 2 (Figure 4-2).

2.9.3 RNAfold, secondary structure prediction

Vienna RNA Web services (Gruber et al., 2008) allow the thermodynamic secondary structure prediction of RNA molecules. Different murine MBP isoforms, 21.5-kDa (NM_001025251), 18-kDa (NM_001025255), 17.22-kDa (NM_001025256) and 14-kDa (NM_001025259) were analyzed with the standard configuration of the software. The minimum free energy (MFE) structure predictions are displayed as a graphical readout. Base-pairing probabilities are color-coded and reflect the reliability of the given association. In addition, RNAalifold (Bernhart et al., 2008) was used to analyze conserved MBP secondary structures and MBP-21.5-kDa orthologues of human (NM_001025081), rat (NM_001025291) and mouse (NM_001025251) were aligned and processed with standard settings.

2.9.4 PANTHER classification of Gene Ontologies (GO)

The PANTHER (protein annotation through evolutionary relationship) classification system (<http://www.pantherdb.org/>) is a database that combines gene function and ontology to analyze protein classes of a group of proteins (Mi et al., 2013). Gene IDs were retrieved from the SILAC quantitative proteomics of proteins associated to MBP14-MS2 in stressed or unstressed conditions. The gene list was processed in a *Mus musculus* background and the functional classification was displayed in a pie chart.

2.9.5 Brain Cell RNAseq database

The Brain Cell RNA-seq website provides a platform for analyzing and comparing transcription and alternative splicing profiles for individual cell types in the cerebral cortex (http://web.stanford.edu/group/barres_lab/brain_rnaseq.html), including OPCs, newly formed OL and myelinating OL (Zhang et al., 2014). Expression profiles for DDX5 were retrieved and the RNA abundance between the different cell types was compared.

2.10 Statistics

Experimental data was presented in diagrams generated in Microsoft Excel 2013 and statistical analysis was performed using SPSS23 software. For assumed normally distributed data, two-tailed student's t-tests were performed. Otherwise, Wilcoxon signed rank test was applied. Experimental replicates (n) are individually indicated in the figures and error bars commonly represent the standard error of the mean (SEM).

3 Results

Myelin Basic Protein (MBP) is one of the major myelin proteins and indispensable for proper assembly of the CNS myelin sheath. The polarized cellular architecture of oligodendrocytes (OL) serves as an excellent model system to study mRNA localization and post-transcriptional regulation. Indeed, MBP mRNA dynamics have been studied intensely for over two decades and shaped the idea of A2RE-dependent mRNA transport and localized translation in the myelin compartment (Chapter 1.3). To better understand the regulatory mechanisms that control MBP expression, further knowledge of the variability and dynamics of associated RNP complexes would be valuable. Unraveling this precise regulation as a key factor in OL maturation could also help in understanding the pathology of leukodystrophies in central nervous system.

In this thesis, the posttranscriptional regulation of MBP expression was addressed with focus on the potential MBP mRNA-associated proteins DDX5 and FUS, initially reported in (White, 2007). Furthermore, the application of the MS2 RNA-labeling to MBP mRNA established a system to monitor and isolate MBP mRNA complexes from oligodendroglial cells. Finally, *in situ* hybridization of single MBP mRNA molecules was introduced as a method and database information and *in silico* analysis tools were consulted to identify motifs in the MBP RNA sequence with focus on secondary structures and RBP binding sites, which together mediate posttranscriptional regulation of MBP synthesis.

3.1 MBP mRNA visualization by single molecule FISH

In situ hybridization has classically been used to visualize MBP mRNA distribution in oligodendrocytes and revealed the RNA localization to the myelin compartment (Colman et al., 1982; de Vries et al., 1997; Trapp et al., 1987). Newly developed techniques now allow the imaging of single RNA molecules which have been used in this thesis project to confirm the MBP mRNA distribution in cell culture systems. Here, 46 individual fluorescently labeled probes covering the sequence of murine MBP were designed and single molecule FISH (smFISH) was performed in primary OL as well as differentiated Oli-*neu* cells (Figure 3-1). High signal to noise ratios potentially allow the detection down to one single mRNA molecule, thus the bright spots obtained by smFISH (Figure 3-1) can be considered as MBP mRNA granules, containing one or more MBP transcripts. In primary oligodendrocytes MBP mRNA granules

are very abundant and show expected distributions in the soma as well as in the peripheral processes and myelin-like membranes (Figure 3-1, primary OL).

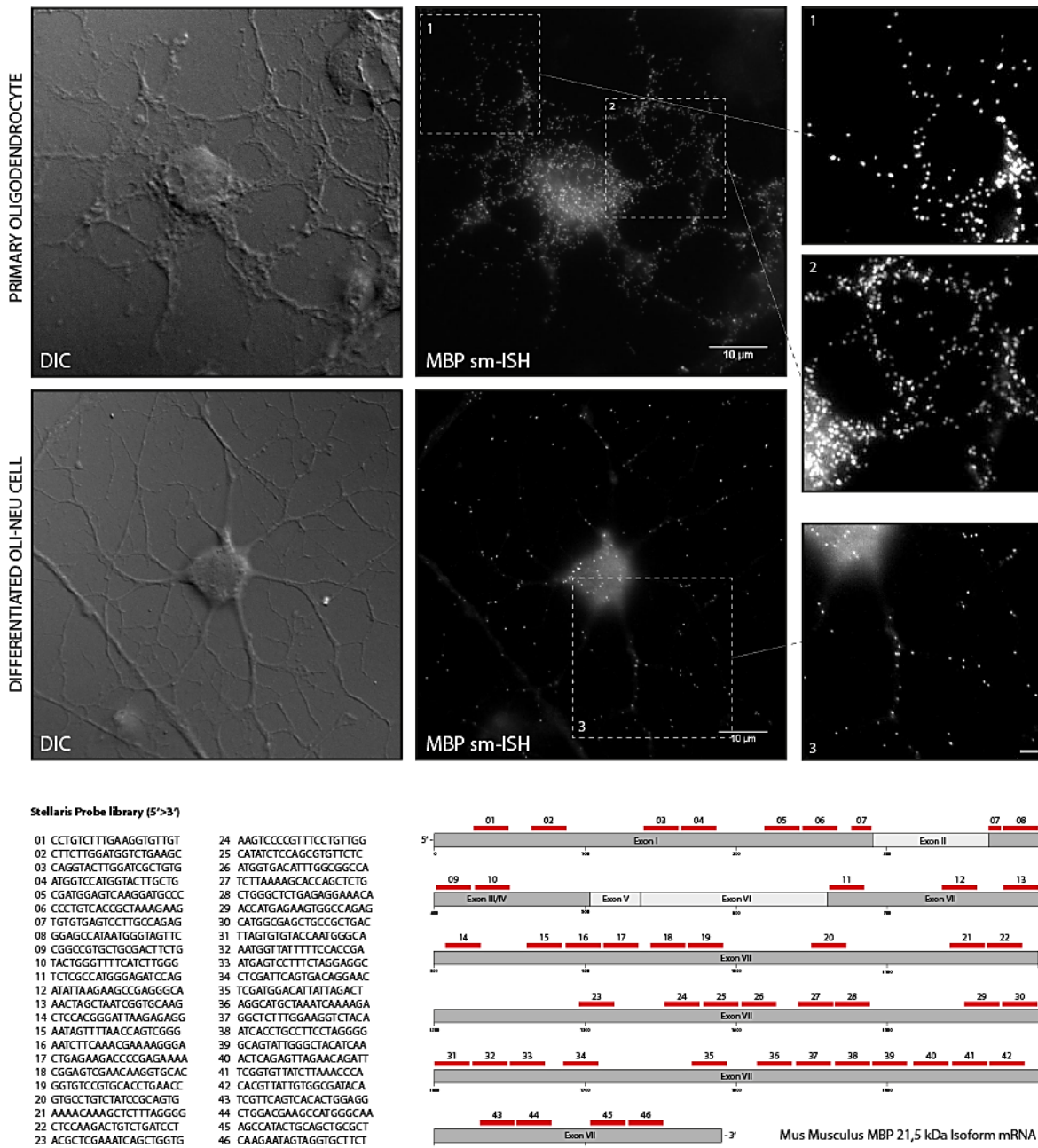


Figure 3-1. Single molecule fluorescent in situ hybridization (smFISH) of MBP mRNA in oligodendroglial cells.

To detect MBP mRNA molecules in oligodendroglial cells, 46 fluorescent antisense probes (Stellaris custom FISH probe library, Biosearchtech) were designed covering the sequence of murine MBP, excluding the exons 2, 5 and 6. Individual probe sequences and their alignment to the MBP sequence are shown schematically. MBP in situ hybridization (MBP smFISH) shows typical dot like patterns in primary oligodendrocytes as well as in differentiated Oli-*neu* cells, every dot potentially representing at least one individual mRNA molecule. Cellular morphology is displayed in the DIC image in the left column. Numbered boxes (1-3) show magnifications of indicated areas from the MBP smFISH pictures. MBP hybridization events in primary OL outnumber counts in Oli-*neu* cells, but both cell types share similarities in localization to the cell body as well as to distal processes.

Expression was restricted to cells that could be identified as oligodendrocytes by morphology or co-immunocytochemistry of MBP protein. As a negative control, cells positive for GFAP protein never showed MBP smFISH signals, neither did HEK293 cells, which both lack MBP expression (data not shown).

The immortalized oligodendroglial cell line *Oli-neu* (Jung et al., 1995) is a commonly used experimental *in vitro* system (Raju et al., 2008; Wang et al., 2012; White et al., 2008) and has been shown to express MBP mRNA abundantly, but subcellular localization was not addressed so far. Distribution of MBP mRNA in differentiated *Oli-neu* cells was analyzed in comparison to primary OL. smFISH events in *Oli-neu* cells were less frequent compared to primary OL but could still account for more than 300 granules/cell, consistent with the fact that *Oli-neu* cells represent a precursor state and are not as differentiated as mature primary OL. The number of granules increases with dbcAMP-induced differentiation of the cells, identified by a more complex process branching. While spots were fewer in number, the localization pattern was similar to primary cells, showing granules in the cell body and along the branched processes (Figure 3-1, *Oli-neu*). Dots at the tips of the processes represents mRNAs that could be transported more than 50 μm from the soma of the cell and hint to functional assembly of MBP transport granules in *Oli-neu* cells.

3.2 Structural analysis of the MBP mRNA sequence

The sequence of a given RNA molecule contains most of the information determining its fate in the cell. Secondary structures and binding motifs for RBPs or small noncoding RNAs are prerequisites for the proper assembly of RNP complexes, which regulate all aspects of mRNA metabolism. Recent advantages in experimental mapping of binding sites by different CLIP techniques (Hafner et al., 2010; Licatalosi et al., 2008; Ule et al., 2003) and the development of corresponding software tools, offers the opportunity to apply this experimental results to any mRNA of interest. Sequencing data, obtained from *in vivo* CLIP-experiments, integrates information from short RNA motifs associated to the corresponding RBP and allows the calculation of a consensus binding site. Using RBPmap server 1.0 (Paz et al., 2014), consensus binding sites for 94 RBPs in the murine 21.5-kDa-MBP sequence were retrieved and mapped according to their position into an interactive diagram, which can be used as a compendium to localize these binding motifs and regions to the MBP mRNA sequence. A screenshot is given in Figure 3-1 and includes all binding sites obtained.



Figure 3-2. Interactive positional mapping of predicted binding sites in murine MBP mRNA (snapshot of interactive Excel 2013 diagram).

The diagram shows a snapshot of an interactive positional map of binding sites in full length MBP mRNA. To display individual binding sites and exact position the interactive full .xlsx-file is available on request. Predicted binding sites for 94 RNA binding proteins were retrieved from RBPmap server 1.0 (Paz et al., 2014; <http://rbpmap.technion.ac.il/index.html>), based on the sequence of murine 21.5-kDa MBP (NM_001025251). They were mapped to the corresponding position in MBP mRNA, every bar representing the starting point of an RBP specific binding site. The Z-score gives a measure for the reliability compared to background datasets, with stringency set to the highest level. Experimentally validated binding sites were collected from literature, adjusted to positions in MBP 21.5-kDa and included as black bars above the MBP scheme. Translation regulatory units, hnRNP E1, hnRNP K (Torvund-Jensen et al., 2014). snc715 (Bauer et al., 2012). Y-element (Han et al., 1995). A2 response element (A2RE) and RNA localization Region RLR (Ainger et al., 1997; Munro et al., 1999).

The Z-score accounts for the reliability of each binding site compared to background datasets, with stringency set to the highest level. Experimentally retrieved binding sites were collected from literature (Ainger et al., 1997; Bauer et al., 2012; Han et al., 1995; Torvund-Jensen et al., 2014), adjusted to positions in 21.5-kDa-MBP mRNA and included as black bars and red lines into the related MBP scheme. To display individual binding sites and exact positions the interactive .xlsx-file is available on request.

3.2.1 MBP mRNA secondary structure prediction

Vienna RNA Web services (Gruber et al., 2008) allow the thermodynamic secondary structure prediction of RNA molecules. RNAfold server was used to analyze the RNA structure of different murine MBP isoforms (Figure 3-3, A, C) and RNAalifold was used to predict a conserved consensus structure based on the sequence alignment of mouse, rat and human 21.5-kDa-MBP (Figure 3-3, B). Graphical output of RNAfold predictions shows minimum free energy (MFE) secondary structures for different murine MBP isoforms (Figure 3-3, A+C). Base-pairing probabilities are color-coded from purple (0, lowest probability) to red (1, highest probability) and reflect the reliability of the given association.

The predicted secondary structure of 14-kDa-MBP was complemented with selected binding sites known from the literature (Figure 3-3, A). The secondary structure prediction appears subdivided in 2-4 major “branches” determined by complementary sequence stretches at the stem. Interestingly, most motifs associated with the translational regulation and transport of the RNA, are located on the lower “branch”, with the A2RE located in an exposed unstructured region (indicated by the low base-pairing probability) in the most distal part. Within the branch, a stem loop including the binding site for the sncRNA-715 (white arrows, magnified in Figure 3-3, A), as well as a second stem loop, containing parts of the RLR, is preserved in all isoforms analyzed. The sequence alignment of mouse, rat and human 21.5-kDa-MBP was used to calculate a conserved MBP secondary structure by RNAalifold algorithms and also shows these features, indicating a conservation of these secondary structures (Figure 3-3, B). Comparison of the different MBP isoforms shows a variability matching the combination of exons used. Exon 2-lacking isoforms 14-kDa-MBP and 18.5-kDa-MBP are similar in most parts, while exon 2-positive isoforms are diverging with the largest overall difference in 17.22-kDa-MBP, showing no “branching” at all. Nevertheless, all isoforms share the identical structure of the C-terminal 3’UTR and specific local hairpin loops (Figure 3-3, dotted blue lines).

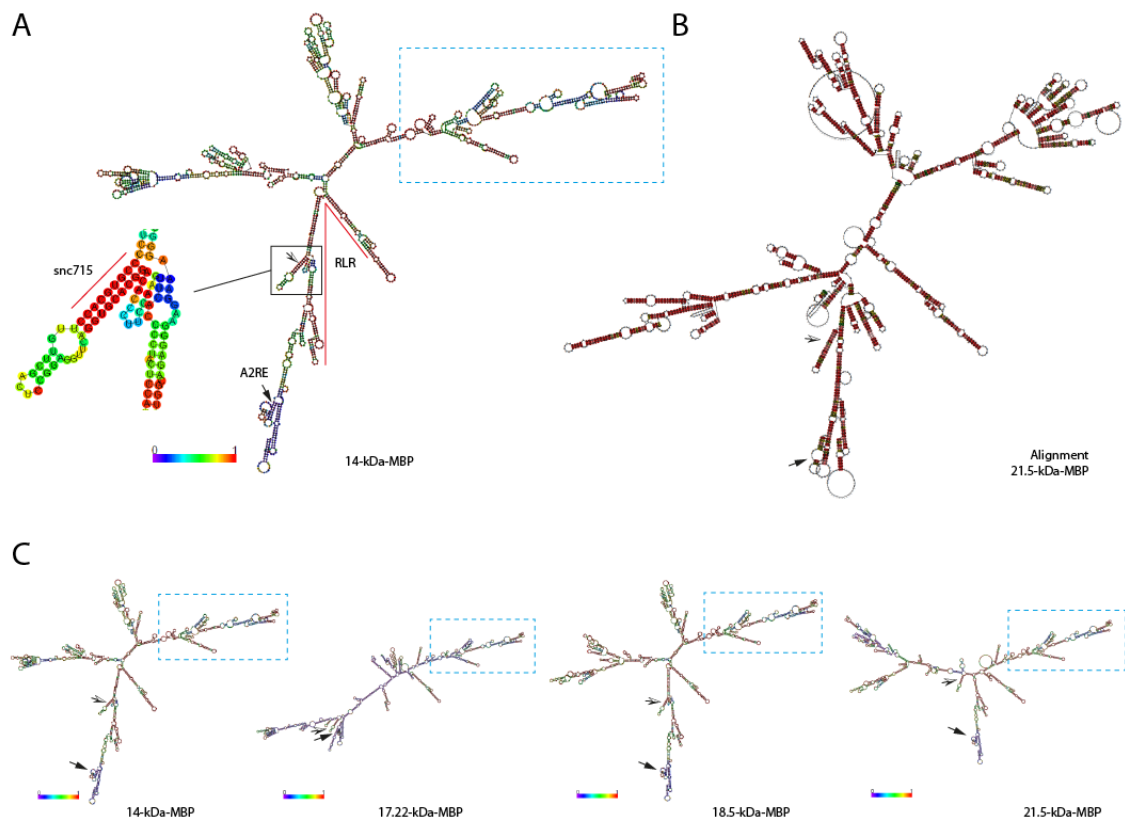


Figure 3-3. MBP isoform-dependent RNAfold secondary structure prediction.

RNAfold server was used to predict MBP mRNA secondary structures based on minimum free energy (MFE) calculations. **(A)** Secondary structure of 14-kDa-MBP is displayed with an enlarged insert of the snc715 binding site, revealing the RNA sequence and the color coded base pair probability (purple=0 to red=1). The A2RE (black arrows), the binding site for sncRNA-715 (white arrows) and the RLR (red line) are signposted. **(B)** The sequence alignment of mouse, rat and human 21.5-kDa-MBP was used to calculate a conserved secondary structure by the RNAalifold algorithm. **(C)** The secondary structures of different murine MBP isoforms are compared. Dotted blue rectangles indicate the part of the distal 3'UTR which is identical in all isoforms. (A2RE=A2 response element, RLR=RNA localization region, snc715=binding site for sncRNA-715).

3.3 Establishment of MBP mRNA labeling using the MS2-system

During the last decades visualization of RNA advanced to the level of high resolution single molecule in situ hybridization, but live cell imaging of endogenous RNA or *ex vivo* RNA co-purification techniques are still lacking. To overcome this limitation, different systems are used to label RNA molecules (Buxbaum et al., 2015a; Tyagi, 2009). A prominent method utilizes the bacteriophage MS2-system, where MS2 RNA stem-loops are recognized by high affinity and specifically binding proteins derived from the MS2 bacteriophage coat proteins (MCP) that tether the genomic RNA to the bacteriophage capsid structure. With our interest in MBP mRNA, we adapted the MS2-system to MBP mRNA, which not only facilitates

visualizing translocation of MBP mRNA transcripts in living cells, but also can be used to elucidate the dynamic composition of MBP mRNA-associated complexes by affinity purification.

3.3.1 MBP-MS2 stable cell line generation and subcellular expression

To generate a labeled MBP transcript, MS2 stem-loops were introduced between the MBP coding sequence of murine 14-kDa-MBP or 17.22-kDa-MBP and the corresponding MBP 3'UTR (Figure 3-4, A). Overall abundance of the MS2-labeled RNA in the cell should be kept comparable to endogenous MBP mRNA levels to guarantee appropriate RNP complex formation. To ensure physiological expression levels, we established polyclonal stable cell lines by transfecting linearized MBP14-MS2 and MBP17-MS2 plasmids (Figure 3-4, A) into *Oli-neu* cells and carried out a selection with Zeocin for cells that incorporated copies of the plasmid DNA into the genome (Figure 3-4, B). Using an Alexa546-conjugated in situ hybridization probe recognizing each of the 24 MS2-loops simultaneously, allowed the visualization of the MS2-labeled RNA with similar sensitivity to MBP smFISH (Figure 3-1). Both procedures were carried out in parallel to compare the localization of labeled and endogenous MBP mRNA, respectively. 24xMS2-FISH in the MBP14-MS2 cell line revealed a pattern similar to the endogenous MBP distribution, transcripts being localized in the perinuclear cytoplasm and along the processes of the cells (Figure 3-4, C). In a negative control, no specific MS2-FISH signal could be observed in *Oli-neu* cells lacking the MS2-labeled RNA (Figure 3-4, D). In addition, MBP smFISH was carried out in MBP14-MS2 cells and also reflects the distribution described above, albeit not discriminating between endogenous or labeled MBP transcripts (Figure 3-4, E). Furthermore, MS2-FISH after sodium arsenite-induced oxidative stress in MBP14-MS2 cells revealed a cytoplasmic aggregation of the labeled transcript in a pattern that is very reminiscent of stress granules in *Oli-neu* cells (personal communication, Constantin Gonsior).

Taken together, the MS2-labeled MBP transcripts are expressed in stable MBP14-MS2 cell lines and associate in RNP complexes capable of translocation and response to cellular cues, such as oxidative stress.

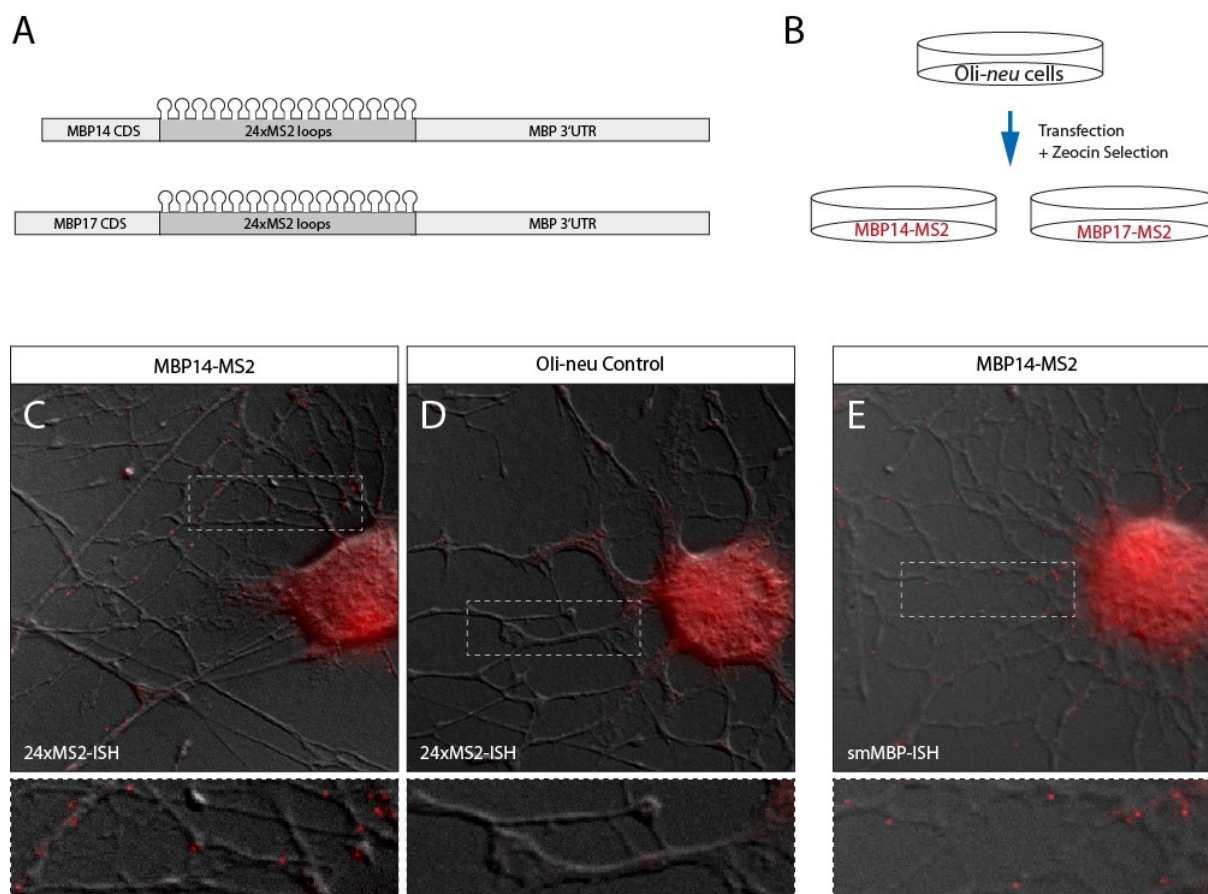


Figure 3-4. Generation and expression analysis of stable MBP14-MS2 labeled oligodendroglial cell lines.

(A) To adapt the MS2 labeling system to MBP mRNA 24xMS2 stem-loops were introduced between MBP14- or MBP17-CDS and the MBP 3'UTR. (B) *Oli-neu* cells were transfected with the MBP-MS2 constructs and polyclonally selected to generate cell lines stably expressing the labeled transcripts. (C-E) In situ hybridization specific for the MS2-loops or smMBP were performed to analyze the expression and subcellular distribution MS2-ISH shows typical dot-like pattern in MBP14-MS2 cell lines (C), but not in untransfected *Oli-neu* cells as a control (D). smMBP ISH in MBP14-MS2 cells showed a similar staining along oligodendrocyte processes (E).

3.3.2 Attempted visualization of MBP-MS2-mRNA using tagged MCPs

To dynamically visualize MS2-tagged MBP mRNA we transiently transfected different fluorochrome-conjugated MCPs into MBP14-MS2-bearing cells and analysed the subcellular distribution in fixed samples. Different plasmids were used and comprised L30-MCP-YFP-NLS, L30-MCP-YFP-NLS-NES and a modified high affinity tandem tdMCP-GFP-NLS (see Table 2-12. Plasmids). Nuclear localization signals are added to prevent fluorescence of unbound MCP in the cytoplasm. Although nuclear expression combined with occasional aggregation of GFP was observed, specific cytoplasmic signals could not be clearly identified compared to *Oli-neu* cells lacking expression of labeled MBP14-MS2 transcripts, possibly due to background fluorescence of unbound MCPs. Initial MCP-YFP-immunoprecipitation experiments led to

enrichment of MBP mRNA compared to precipitates of YFP alone in cells transfected with labeled MBP14-MS2, indicating that the MCPs indeed associated with the target mRNA, but the desired visualization was not successful (data not shown). Cytoplasmic background intensity may be overcome in the future by stable transfection of the fluorescently labeled MCPs and live cell imaging could additionally increase the probability of identifying MBP14-MS2 mRNA granules due to their characteristic movement along microtubules.

3.3.3 Streptavidin-mediated MBP-MS2 RNA affinity purification

The use of alternatively tagged MCPs from the MS2 toolkit moreover allows a biochemical isolation of MS2-RNA and simultaneous co-purification of interacting molecules like RBPs or non-coding RNAs. We used a tandem MCP coupled to a HTBH-tag, created by the lab of Marian Waterman (Tsai et al., 2011) to isolate MBP14-MS2 mRNA from the stable MBP-MS2 cell lines. The HTBH-tag is composed of two His-tags surrounding a TEV cleavage site and a biotinylation signal (Figure 3-5, A). Addition of Biotin to the cell culture medium leads to *in vivo* biotinylation of the HTBH-tag, subsequently allowing a streptavidin-mediated affinity purification (SA-AP) of MBP-MS2-associated mRNP complexes. MBP14-MS2 mRNA-associated RNP complexes were isolated with streptavidin-coupled M280 Dynabeads from MCP-HTBH-transfected MBP14-MS2 stable cell lines and analyzed via SDS-PAGE and qPCR (Figure 3-5, B). Silverstaining of the SDS-PAGE gel revealed a band pattern strikingly different to the input sample and the intensity of distinct bands in the pulldown was decreased by RNase-treatment (Figure 3-5, C), although many proteins were still present after this treatment. Detection with the indicated antibodies shows an efficient pulldown of the His-tagged MCP which was independent of the treatment with RNase A (Figure 3-5, D). In the MBP14-MS2-dependent SA-pulldown (SA-AP), known MBP mRNA-associated proteins like hnRNP A2, hnRNP F and DDX5 were detected, which showed a reduced or abolished association when treated with RNase A (SA-AP +RNase). Note, that in the case of hnRNP A2B1, only the isoforms B1 and A2 could be detected in the pulldown while the lower molecular weight isoform B0 was absent, although it was abundant in the input lysate. As a control, abundant cytoplasmic proteins, such as FUS and GAPDH could not be detected in the pulldown. MBP mRNA was highly enriched in the SA-AP (related to the input sample and compared to Pgk-1) indicating an efficient pulldown of the MBP14-MS2 transcript (Figure 3-5, E). As a control, Taqman Gene Expression Assays amplifying only exon 2-containing MBP mRNA were not enriched and serve as an additional

internal control for the binding of endogenous MBP mRNA, carrying the identical 3'UTR sequence (Figure 3-5, E). These results show that RNP complexes can be isolated from the MBP14-MS2 cell lines, containing the tagged MBP14-MS2 transcript and expected MBP mRNA binding proteins, in an RNase-sensitive manner.

RNA affinity purification has been reported to be biased by a high degree of unspecific binding by RBPs and other abundant cellular proteins. In pulldown experiments with Zeo-mCherry lines lacking the tagged MBP-MS2 construct as a control, we attempted to reduce the unspecific binding by varying affinity purification conditions (Chapter 2.5.6). Comparison between Control- and MBP14-MS2-SA-AP shows that using this optimized protocol, RNA-

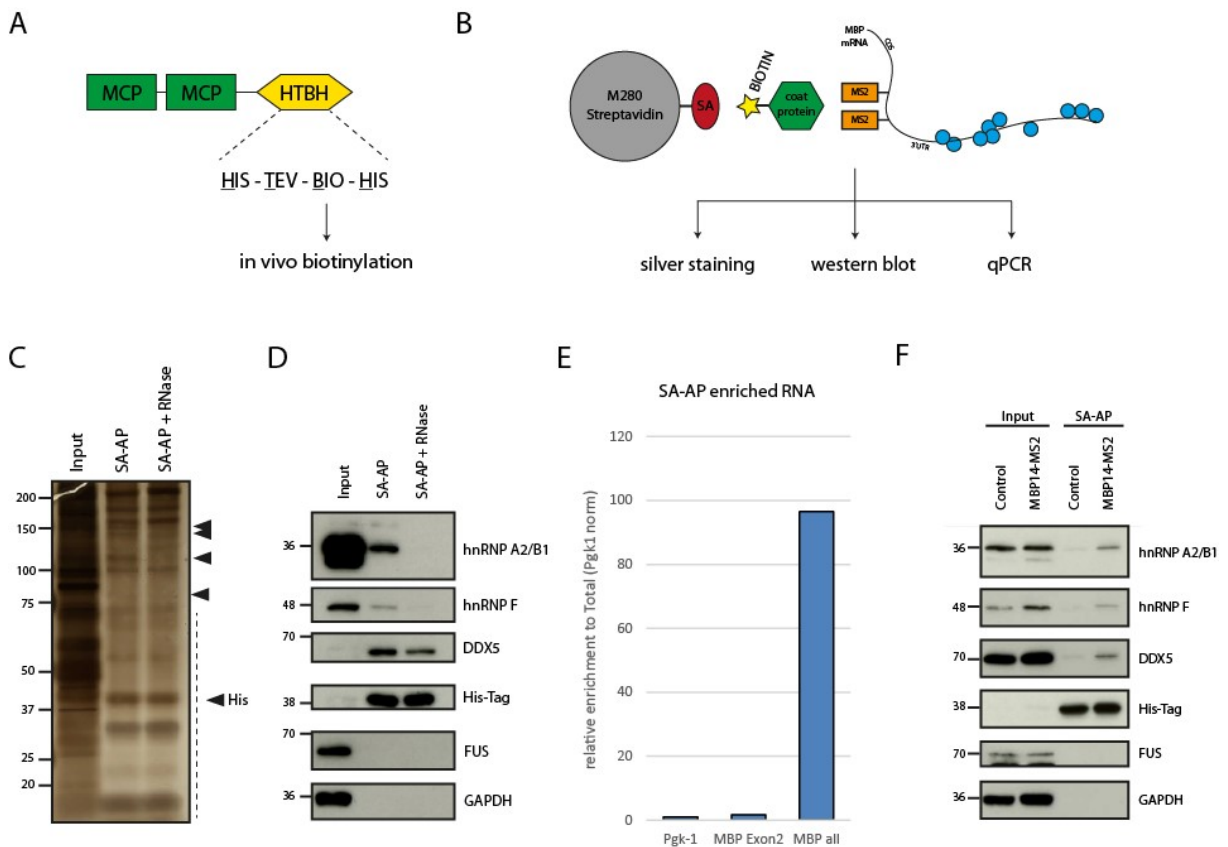


Figure 3-5. Streptavidin-mediated affinity purification of MBP14-MS2-associated mRNPs.

(A) A tandem MCP coupled to a HTBH-tag was used for streptavidin mediated affinity purification (SA-AP). **(B)** MBP14-MS2-associated RNP complexes were isolated with Streptavidin-coupled M280 Dynabeads from MCP-HTBH-transfected MBP14-MS2 stable cell lines and analyzed by SDS-PAGE and qPCR. **(C)** A silverstained SDS-PAGE gel and the corresponding Western blot **(D)** indicate the protein composition of the MBP-MS2 pulldown (SA-AP) and an RNase A-treated control. **(E)** RNA quantification by qPCR validated an enrichment of MBP mRNA (MBP all), but not endogenous MBP exon 2-positive isoforms in the SA-AP. **(F)** SA-AP after protocol optimization compares SA-AP composition from the MBP14-MS2 cell line with Zeo-mCherry control cells and shows enrichment of MBP mRNA-associated proteins hnRNP A2, hnRNP F and DDX5 in MBP14-MS2 pulldowns.

binding proteins hnRNP A2, hnRNP F and DDX5 are enriched in the MBP14MS2-AP, while the unspecific binding in APs from control cells could be reduced to an acceptable level (Figure 3-5, F).

RNP complexes undergo dramatic changes in composition during the life time of an mRNA, thus mediating localization, storage, translation or decay. The formation of stress granules is a specific event, which can protect RNA messages by segregation and translational silencing under conditions of cellular stress (Anderson and Kedersha, 2009b). To evaluate if our system can detect such dynamic changes in RNP composition, we applied oxidative stress prior to MBP14-MS2 affinity purification and compared the protein composition to unstressed cells and additional control conditions. These conditions are indicated above the Western blots shown in Figure 3-6 and again comprise *Oli-neu-mCherry* cell lines without the labeled transcript, RNase treatment and MBP14-MS2 cells transfected with an empty vector instead of MCP-HTBH.

In all MCP-HTBH-transfected SA-APs an efficient pulldown was achieved (Figure 3-6, A-C, His-Tag) and the expression levels varied between different conditions. RNA quantification of MBP transcripts via qPCR indicated an efficient pulldown of MBP14-MS2 compared to control cells (Figure 3-6, D), while no signal or no enrichment was detected in RNase-treated or untransfected controls, respectively (not shown). A silverstained SDS-PAGE gel gives an overall impression of the SA-AP protein composition in the different conditions (Figure 3-6, C) and reflects an enrichment of proteins in the MBP14-MS2 pulldown compared to control cells (Control mCh). In the MBP14-MS2-AP of cells subjected to oxidative stress, the pattern of associated proteins showed distinct changes compared to unstressed controls and in RNase-treated samples or APs from untransfected cells numerous bands were absent (Figure 3-6, C). Similarly, detection of MBP mRNA-associated proteins hnRNP A2, hnRNP F, hnRNP K or DDX5 via Western blot revealed an enrichment of these proteins in the MBP14-MS2 SA-AP, especially under oxidative stress conditions, but a reduced or abolished association with MBP14-MS2 RNA in RNase-treated or untransfected cells (Figure 3-6, A-B). Additionally, a weak signal for the stress granule marker G3BP1 in the MBP14-MS2 SA-AP of stressed cells was detected (Figure 3-6, A) and may indicate an assembly of MBP14-MS2-containing stress granules. Differences in the MBP14-MS2-associated protein composition under oxidative stress conditions were addressed further in a SILAC-based proteomic approach (Chapter 3.3.4).

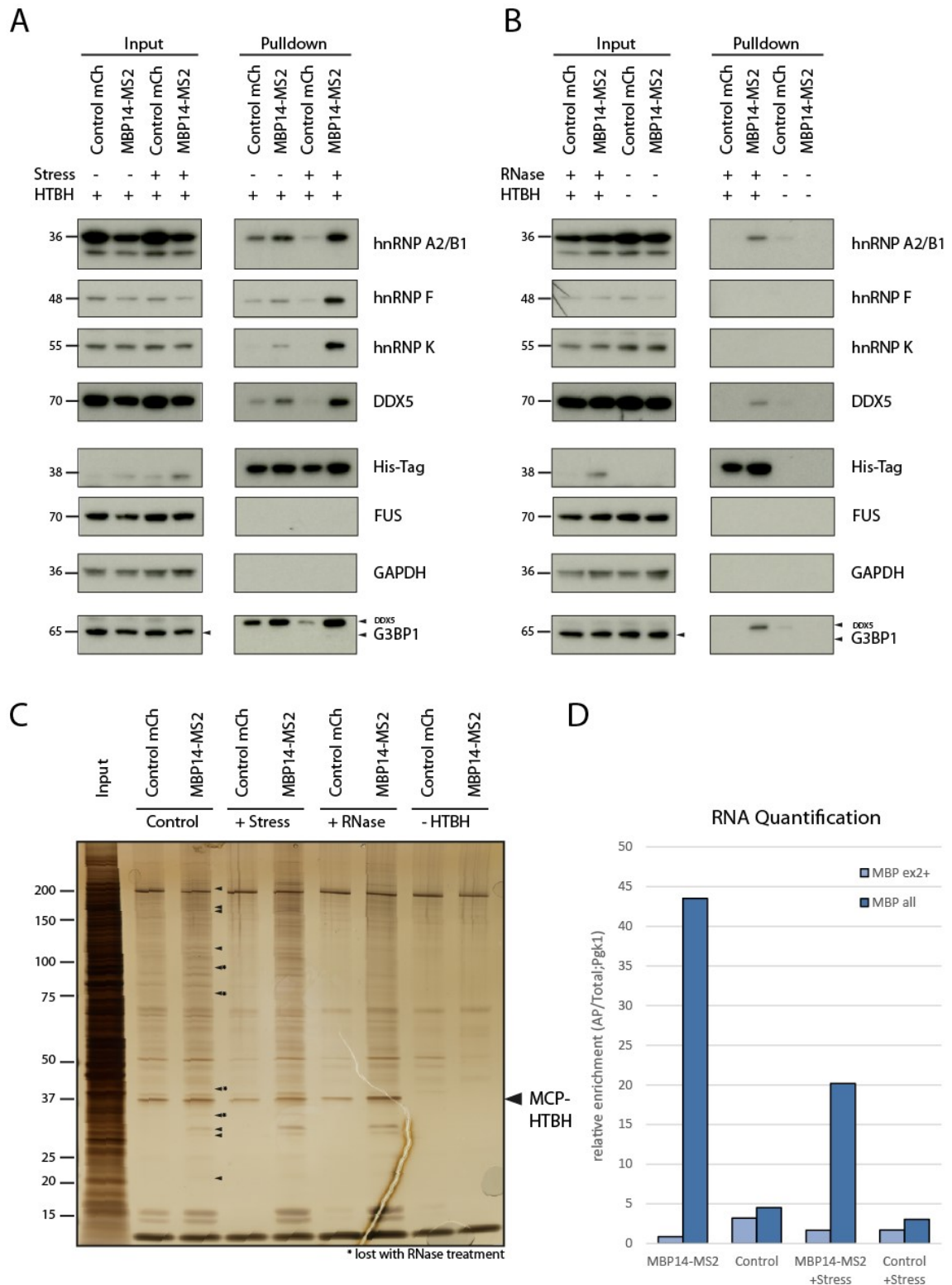


Figure 3-6. MBP14-MS2 affinity purification under oxidative stress conditions.

MBP14-MS2-associated RNP complexes were isolated with Streptavidin-coupled M280 Dynabeads from MCP-HTBH transfected MBP14-MS2 or Zeo-mCherry control cells and analyzed by SDS-PAGE and qPCR. **(A)** Oxidative stress was applied prior AP. **(B)** APs were treated with RNase or were performed from untransfected cells, as indicated. **(C)** Silverstained SDS-PAGE gel shows protein abundance in APs in the different conditions. Arrows indicate bands that are visible in the MBP14-MS2-APs but not in RNase-treated samples. **(D)** RNA quantification shows the relative enrichment of MBP transcripts in indicated conditions normalized to Pgk1 and to the input total RNA.

3.3.4 Identification of proteins associating with MBP14-MS2 mRNA under oxidative stress conditions using SILAC-based quantitative proteomics

SILAC (stable isotope labeling with amino acids in cell culture) mass spectrometry is a quantitative proteomic technique which allows identification and simultaneous quantitation of proteins between defined experimental conditions. It is based on a differential labeling of amino acids with stable non-radioactive isotopes. The difference in mass of detected peptides allows the exact correlation between the experimental conditions and their ratio displays the change in abundance. We applied this method to identify changes in the protein composition of MBP14-MS2 RNP complexes under oxidative stress conditions by comparing

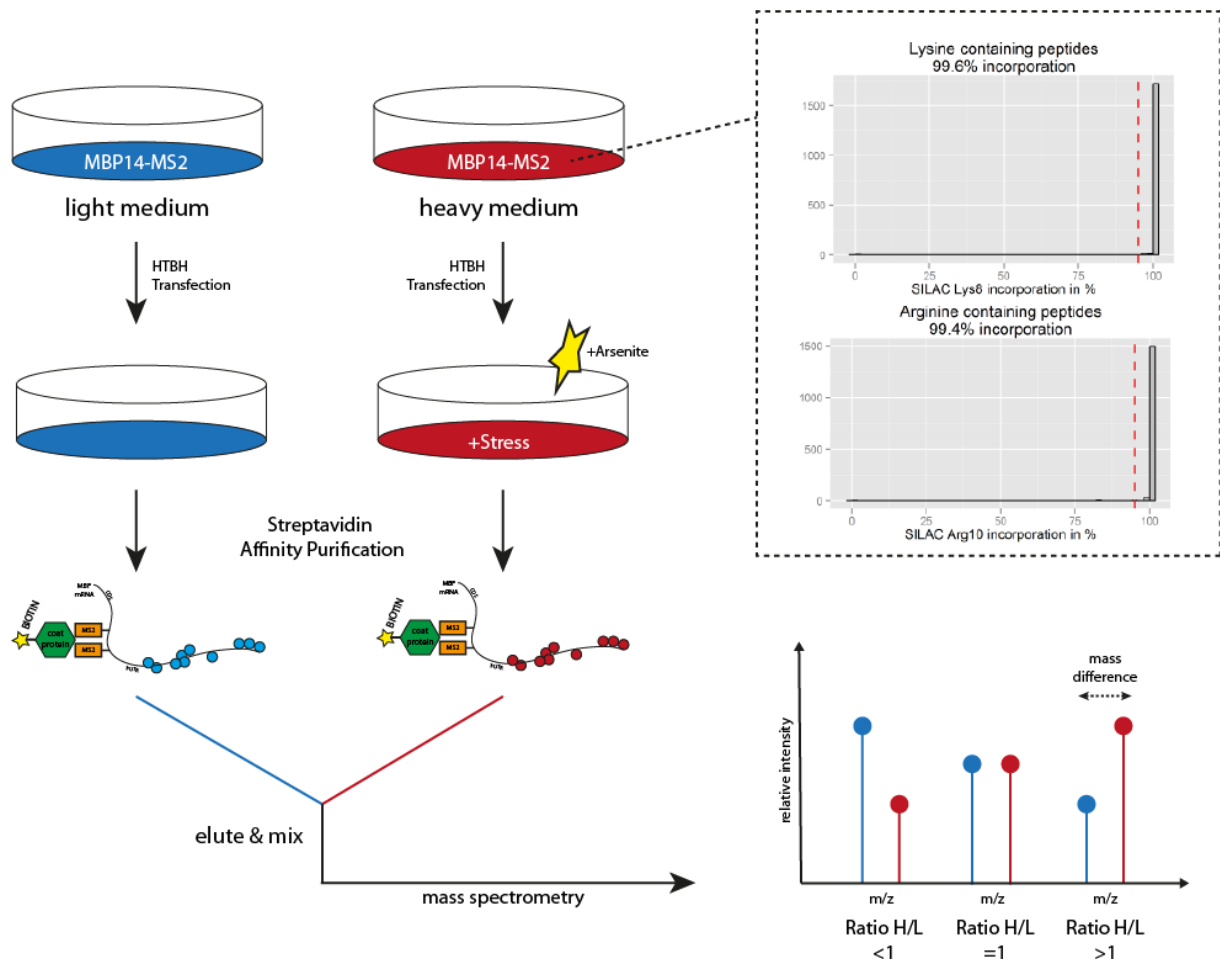


Figure 3-7. SILAC-based proteomics to identify MBP14-MS2 RNP complex dynamics during oxidative stress.

MBP14-MS2 cells were grown in medium supplemented with heavy or light amino acids, successful incorporation of heavy isotopes was confirmed after 2 weeks in culture (Falk Butter, dotted box). After SA-AP, mass spectrometry was used to identify proteins associated with the MBP14-MS2-RNA in stressed or control cells. Mass difference in detected peptides allows the correlation of identified proteins with the experimental conditions and ratios of heavy to light peptides demonstrates their change in abundance.

peptides found in RNA affinity purifications after sodium arsenite treatment compared to control conditions. Generally, we observed a distinct degree of unspecific protein binding in the RNA affinity purifications, even after protocol optimization (Figure 3-5 and Figure 3-6, control cells). However, a major advantage of SILAC-based mass spectrometry is the inclusion of unspecifically-binding proteins into the normalization procedure, highlighting only differences between the experimental conditions. SILAC experiments were performed in collaboration with Falk Butter (Proteomics Core Facility, IMB Mainz). MBP14-MS2 stable cell lines were grown in modified SATO medium supplemented with heavy or light amino acids (Chapter 2.4.5). Incorporation was validated after two weeks in culture and revealed that the heavy isotopes had been incorporated efficiently in nearly all cellular proteins (Figure 3-7, dotted Box, evaluated by the Proteomics Core Facility).

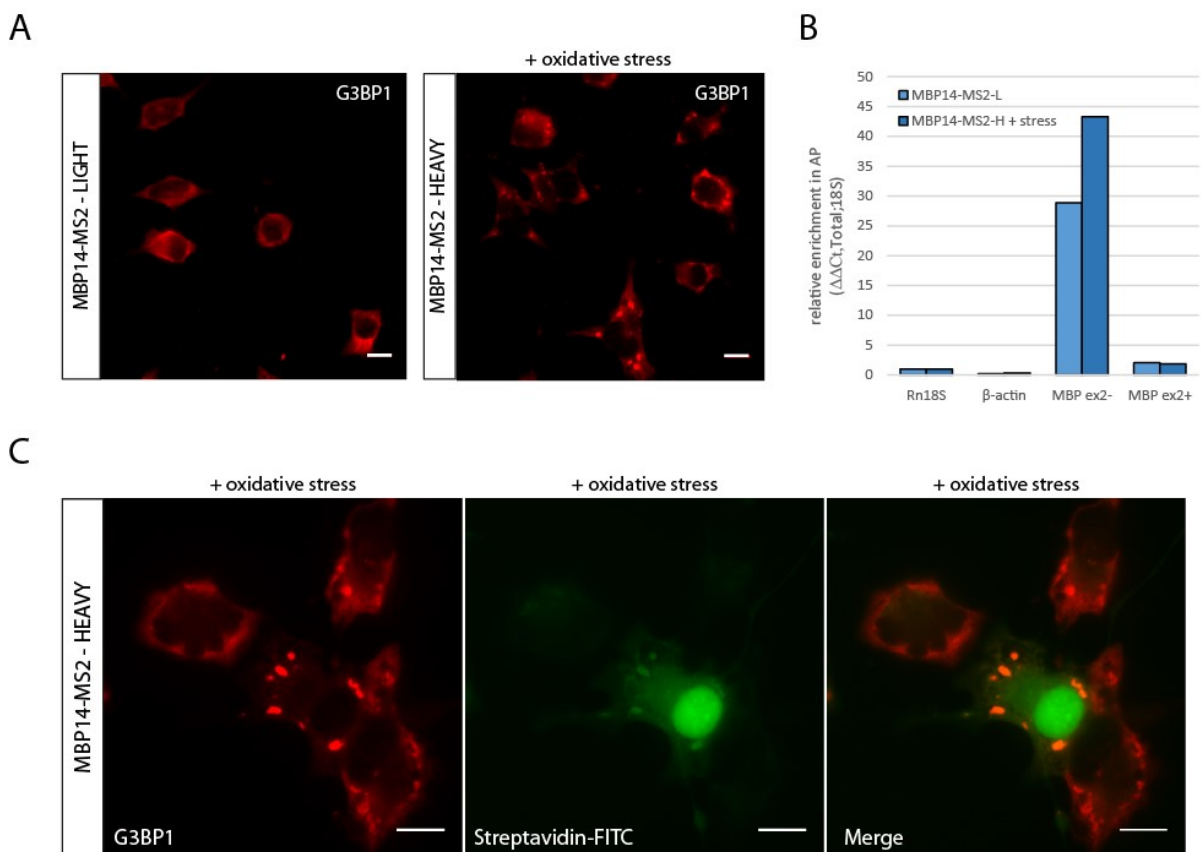


Figure 3-8. Oxidative stress induced stress granule formation in SILAC-labeled MBP14-MS2 cell lines.

(A) Stress granule formation in MBP14-MS2 cells was clearly demonstrated by clustering of G3BP1 in arsenite treated MBP14-MS2-heavy, but not in MBP14-MS2-light control cells. **(B)** RNA enrichment of MBP exon 2-negative transcripts or control RNAs (β -actin, MBP exon2+) in AP related to the input samples and normalized to Rn18S indicates an efficient pulldown of MBP14-MS2 RNP complexes. **(C)** Streptavidin-FITC, recognizing the biotinylated HTBH-tagged MCP, localizes to G3BP1-positive stress granules in transfected MBP14-heavy cells.

The MBP14-MS2 affinity purification was carried out as described schematically in Figure 3-7. MBP14-MS2-heavy and MBP14-MS2-light cell lines were transfected with MCP-HTBH and selectively treated with 0.1 mM sodium arsenite prior streptavidin affinity purification. Three independent experiments were performed in parallel, two experiments were analyzed in SILAC mass spectrometry and one experiment was used to validate stress conditions and pulldown efficiency. Stress granule formation was confirmed by immunocytochemistry of G3BP1, which appeared in cytoplasmic clusters around the nuclei of MBP14-MS2-heavy cells treated with sodium arsenite (Figure 3-8, A). Streptavidin-FITC, binding the biotinylated HTBH-tagged MCP, co-localizes with these G3BP1-positive stress granules in transfected cells (Figure 3-8, C) and robust enrichment of the MBP transcript (MBP exon 2-negative) in the SA-AP compared to mRNAs of β -actin or exon 2-positive MBP indicated an efficient pulldown of MBP14-MS2 RNP complexes (Figure 3-8, B). The two SILAC affinity purification experiments were performed in cross controls, either MBP14-MS2-heavy or MBP14-MS2-light cell lines were stressed, thus excluding experimental variations by the artificial amino acids and allowing the calculation of a mean value (Chapter 2.5.7). SILAC mass spectrometry, data acquisition and normalization were performed by Falk Butter (Proteomics Core facility, IMB Mainz).

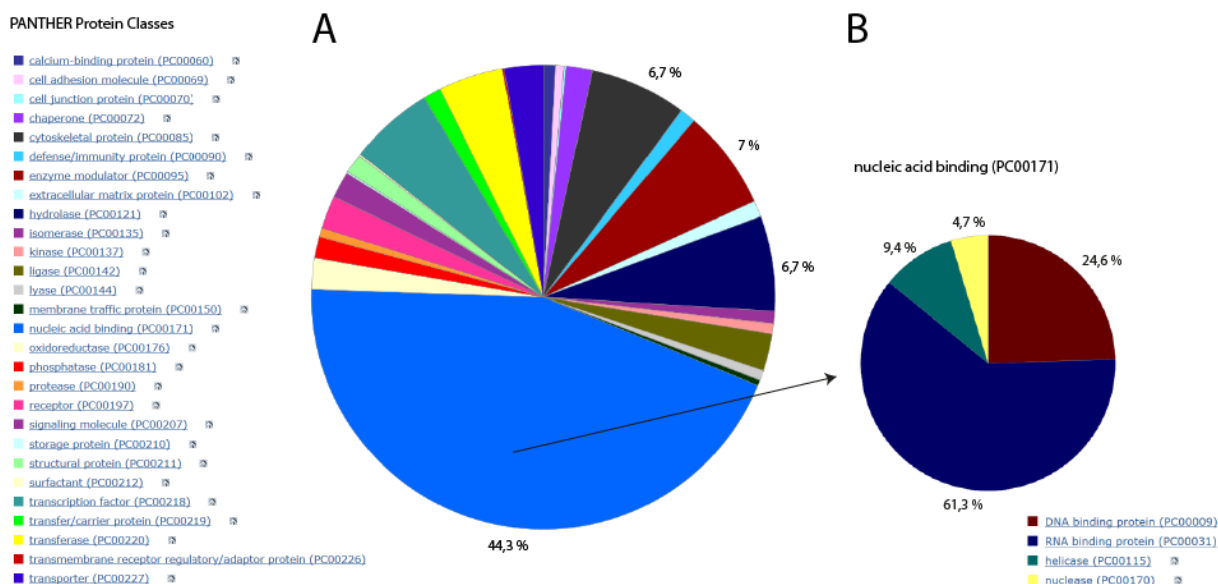


Figure 3-9. PANTHER database classification of proteins identified in SILAC mass spectrometry.

In total, 735 proteins were identified in both mass spectrometry experiments. **(A)** PANTHER classification (Mi et al., 2013) revealed a heterogeneous distribution of GO annotations with the largest group corresponding to nucleic acid binding proteins. **(B)** Subsequent analysis of this group renders RNA binding proteins as the biggest subgroup. Percent values (%) describe the proportion of total proteins identified. Details are described in the text.

In total, 735 proteins could be identified in both SILAC experiments. Panther database information (Mi et al., 2013) was used to classify the proteins according to their annotated GO Protein Class (Figure 3-9). The majority (44.3%) of hits represents the class of nucleic acid binding proteins (Figure 3-9, A), most of them binding to RNA (Figure 3-9, B). Additional groups comprise enzyme modulators (7%), cytoskeletal proteins (6.7%), and hydrolases (6.7%). The protein composition is a snapshot of all proteins identified and most probably includes unspecific-binding proteins during stressed and unstressed conditions, but displayed an anticipated distribution for an RNA-pulldown experiment.

The mass difference in detected peptides facilitates the correlation of identified proteins with the experimental condition. The ratio of heavy to light peptides indicates their change in abundance according to the condition (stress or control). Consequently, SILAC ratios >1 reflect increased protein association and SILAC ratios <1 reflect release from the target MBP14-MS2 RNP complex under stress conditions. A ratio around 1 is considered as background binding (due to equal binding characteristics in both conditions) but could also imply that the protein associates with MBP14-MS2 RNA independent of stress condition (Figure 3-7). The peptides with the highest SILAC ratios are listed in Table 3-1 and correspond to proteins that selectively associated with the MBP14-MS2 transcript under oxidative stress conditions.

Coronin-1c (14.5-fold) and Filamin-A (13.0-fold) showed the highest change in abundance in response to oxidative stress. They are described as actin-binding and -modulating proteins (Feng and Walsh, 2004; Iizaka et al., 2000). In addition, several scaffolding and cytoskeleton-associated proteins (Pdlim5, Tns3, Flnb, Actn4) are present among the most enriched peptides. Several RNA-binding proteins enriched with oxidative stress have previously been linked to stress granules or translational repression: TDP-43, FMRP, Fxr1, Fxr2, PABPC1 and components of the eIF3-complex were found associated with stress granules in mammalian cells (Buchan and Parker, 2009) and support the concept that MBP14-MS2 RNA sequesters to these structures. Cnot1 and DDX6 constitute CCR4-NOT complexes, which have been shown to mediate RISC-mediated gene silencing (Rouya et al., 2014). Interestingly, several enriched genes, such as Phldb1, Pdlim5, Gtf2i, FMRP or TDP-43 have been connected to neural disorders or tumor formation and will be discussed in Chapter 4.5.

Table 3-1. Proteins enriched to MBP14-MS2 complexes under oxidative stress conditions.

SILAC ratios (peptide abundance after stress/peptide abundance unstressed) are displayed as a mean of two SILAC affinity purifications (AP) with the corresponding standard derivation (SD). The table displays the TOP 35

proteins with corresponding gene annotations, enriched in APs of MBP14-MS2 RNA under conditions of oxidative stress. Underlined genes are discussed in the text.

Protein	Gene	SILAC Ratio	SD
Coronin-1C	<u>Coro1c</u>	14,52	4,98
Filamin-A	<u>Flna</u>	13,03	3,25
tRNA (uracil-5-)-methyltransferase homolog A	Trmt2a	9,15	0,84
Proliferating cell nuclear antigen	Pcna	8,12	0,73
PDZ and LIM domain protein 5	<u>Pdlim5</u>	6,73	3,60
CCR4-NOT transcription complex subunit 1	<u>Cnot1</u>	5,63	2,67
Tensin-3	<u>Tns3</u>	5,61	2,91
Pleckstrin homology-like domain family B member 1	<u>Phldb1</u>	5,51	1,40
Heterogeneous nuclear ribonucleoprotein A0	Hnrnpa0	4,99	0,32
Peroxiredoxin-1	Prdx1	4,83	1,12
Galectin-1	Lgals1	4,64	3,12
Fragile X mental retardation protein 1 homolog	<u>Fmr1</u>	4,30	0,39
Exportin-5	Xpo5	4,29	1,84
Acidic leucine-rich nuclear phosphoprotein 32 family member E	Anp32e	4,14	1,81
Filamin-B	<u>Flnb</u>	4,08	0,04
Polyadenylate-binding protein 1	<u>Pabpc1</u>	3,89	1,64
High mobility group protein B2	Hmgb2	3,77	2,41
Fragile X mental retardation syndrome-related protein 2	<u>Fxr2</u>	3,60	1,52
General transcription factor II-I	<u>Gtf2i</u>	3,56	1,53
Fragile X mental retardation syndrome-related protein 1	<u>Fxr1</u>	3,41	1,20
Alpha-actinin-4	<u>Actn4</u>	3,41	0,06
Peroxiredoxin-2	Prdx2	3,39	1,36
Eukaryotic translation initiation factor 3 subunit C	<u>Eif3c</u>	3,12	2,47
26S proteasome non-ATPase regulatory subunit 11	Psm11	3,11	1,45
Eukaryotic translation initiation factor 3 subunit A	<u>Eif3a</u>	3,11	1,84
Liprin-beta-1	Ppfbp1	3,08	1,17
Small ubiquitin-related modifier 2	Sumo2	3,07	1,86
TAR DNA-binding protein 43	<u>Tardbp</u>	3,06	0,31
Replication factor C subunit 1	Rfc1	3,05	1,98
High mobility group protein B1	Hmgb1	3,00	2,22
Inter-alpha-trypsin inhibitor heavy chain H2	Itih2	3,00	3,97
Eukaryotic translation initiation factor 3 subunit L	<u>Eif3l</u>	2,94	1,79
Y-box-binding protein 1-3	Ybx1-3	2,91	0,77
Probable ATP-dependent RNA helicase DDX6	<u>Ddx6</u>	2,91	2,58

Table 3-2. Proteins enriched in MBP14-MS2 complexes in the absence of oxidative stress.

SILAC ratios (peptide abundance after stress/peptide abundance unstressed) are displayed as a mean of two SILAC affinity purifications (AP) with the corresponding standard derivation (SD). The table displays the TOP 20

proteins with corresponding gene annotations, enriched in APs of MBP14-MS2 RNA under control conditions without oxidative stress. Underlined genes are discussed in the text.

Protein	Gene	SILAC Ratio	SD
Plasminogen activator inhibitor 1 RNA-binding protein	<u>Serbp1</u>	0,41	0,03
Plectin	Plec	0,54	0,10
DNA (cytosine-5)-methyltransferase 1	Dnmt1	0,55	0,06
Alpha-adducin	Add1	0,59	0,05
Bromodomain-containing protein 2	Brd2	0,61	0,04
Gamma-adducin	Add3	0,61	0,04
Suppressor of SWI4 1 homolog	Ppan	0,63	0,55
40S ribosomal protein S12	<u>Rps12</u>	0,65	0,15
Zinc finger CCCH domain-containing protein 14	Zc3h14	0,69	0,02
Acetyl-CoA carboxylase 1;Biotin carboxylase	<u>Acaca</u>	0,71	0,13
40S ribosomal protein S19	<u>Rps19</u>	0,71	0,13
60S ribosomal protein L37a	<u>Rpl37a</u>	0,72	0,28
Zinc finger CCCH domain-containing protein 11A	Zc3h11a	0,72	0,03
DNA (cytosine-5)-methyltransferase 3A	Dnmt3a	0,72	0,01
Propionyl-CoA carboxylase alpha chain, mitochondrial	<u>Pcca</u>	0,73	0,18
Ras-related protein Rab-5A-C	Rab5a-c	0,73	-
Methylcrotonoyl-CoA carboxylase subunit alpha, mitochondrial	<u>Mccc1</u>	0,73	0,24
Heterochromatin protein 1-binding protein 3	Hp1bp3	0,73	0,23
Propionyl-CoA carboxylase beta chain, mitochondrial	<u>Pccb</u>	0,73	0,17
Spectrin beta chain, non-erythrocytic 1	Sptbn1	0,74	0,07

Far less proteins appeared to be specifically released during oxidative stress conditions (SILAC Ratio < 1), peptides with the lowest SILAC ratios are listed in Table 3-2. The peptide most decreased in amount was identified as Serbp1, an RNA binding protein that is also associated with stress granule formation in mammalian cells (Lee et al., 2014). Furthermore, in the absence of stress, more ribosomal proteins of the 40S and 60S ribosomal subunit appear to be associated with the transcript, which could indicate ongoing translation. Finally, contamination by endogenously biotin-associated proteins (Acaca, Pcca, Mccc1, Pccb) is noticeable, most probably as these bind to streptavidin coupled Dynabead matrix.

Several proteins previously associated with the regulation of MBP mRNA were also identified in MBP14-MS2-related SILAC mass spectrometry and are displayed in Table 3-3 with their calculated SILAC ratios.

Table 3-3. Selected RNPs enriched in MBP14-MS2 complexes under oxidative stress conditions.

SILAC ratios (peptide abundance after stress/peptide abundance unstressed) are displayed as mean of two SILAC affinity purifications (AP) with the corresponding standard derivation (SD). The table displays a selection of previously analyzed MBP-associated RBPs with corresponding gene annotations, enriched in APs of MBP14-MS2 RNA under conditions of oxidative stress.

Protein	Gene	SILAC Ratio	SD
Heterogeneous nuclear ribonucleoprotein K	Hnrnpk	2,17	0,09
Heterogeneous nuclear ribonucleoprotein F	Hnrnpf	1,70	0,07
Poly(rC)-binding protein 1 (alias hnRNP E1)	Pcbp1	1,46	0,22
Ras GTPase-activating protein-binding protein 1	G3bp1	1,36	0,50
Probable ATP-dependent RNA helicase DDX5	Ddx5	1,32	0,35
Heterogeneous nuclear ribonucleoproteins A2/B1	Hnrnpa2b1	0,96	0,32

In summary, MBP14 mRNA was successfully labeled with MS2-loops. A moderate expression of the transcript was achieved, which resembles the endogenous localization of MBP mRNA and is capable of reacting to cellular cues such as oxidative stress. MBP14-MS2 complexes were successfully isolated and analysis of the protein composition revealed enrichment of known MBP mRNA-associated proteins such as hnRNP A2 and hnRNP F. Furthermore, novel MBP14-MS2 RNA-associated proteins were identified using SILAC mass spectrometry during oxidative stress, leading to candidates potentially playing a role in MBP mRNA-containing mRNP complexes that form in response to oxidative stress.

3.4 The role of DDX5 in the posttranscriptional regulation of MBP expression

DEAD box RNA helicases are multifunctional enzymes, which have been described as modulators of RNA secondary structures and are involved in the formation of RNP complexes on target mRNAs (Linder and Jankowsky, 2011). In a screen for potential MBP mRNA-associated protein complexes, the DEAD box RNA Helicase 5 (DDX5) was identified (White, 2007). Initial experiments to assess the role of DDX5 in oligodendrocytes were subsequently performed in our group (Gonsior, 2011; Hoch-Kraft, 2010) and hinted that DDX5 could potentially influence MBP protein expression in oligodendroglial cells. During this thesis work, experiments addressing the functional role of DDX5 were intensified and mechanisms elucidating a potential regulation of MBP in oligodendrocytes on a post-transcriptional level, were investigated.

3.4.1 DDX5 is expressed in primary OL and decreases during differentiation

DDX5 expression has been reported to be developmentally regulated in several cell lines and tissues (Stevenson et al., 1998). Western blotting of lysates obtained from differentiating OL *in vitro*, indicates a decrease in DDX5 expression with ongoing maturation of the cells, as evidenced by upregulation of the myelin proteins CNP or MBP (Figure 3-10, A). The brainRNA-seq database harbors comprehensive information about changes in the cellular transcriptome during oligodendrocyte differentiation (Zhang et al., 2014). Expression data for DDX5 was extracted and revealed a decline in DDX5 expression also at the level of transcription (Figure 3-10, B). A predominant localization of DDX5 to the cell nucleus (Figure 3-12, A) hinders the detection of DDX5 protein in adjacent cytoplasmic regions. A permeabilization with digitonin was included in the staining protocol to prevent such nuclear staining, leaving the nuclear membrane intact (Tissera et al., 2010). Co-immunocytochemistry with NG2 and MBP antibodies confirmed the cytoplasmic localization pattern of DDX5 in OPCs and mature OL, respectively. Most DDX5 appears in a granular distribution around the nucleus (Figure 3-10, C-D), but can be localized along the OL processes of OPCs (Figure 3-10, C) and prospective membrane sheets of the mature OL (Figure 3-10, D).

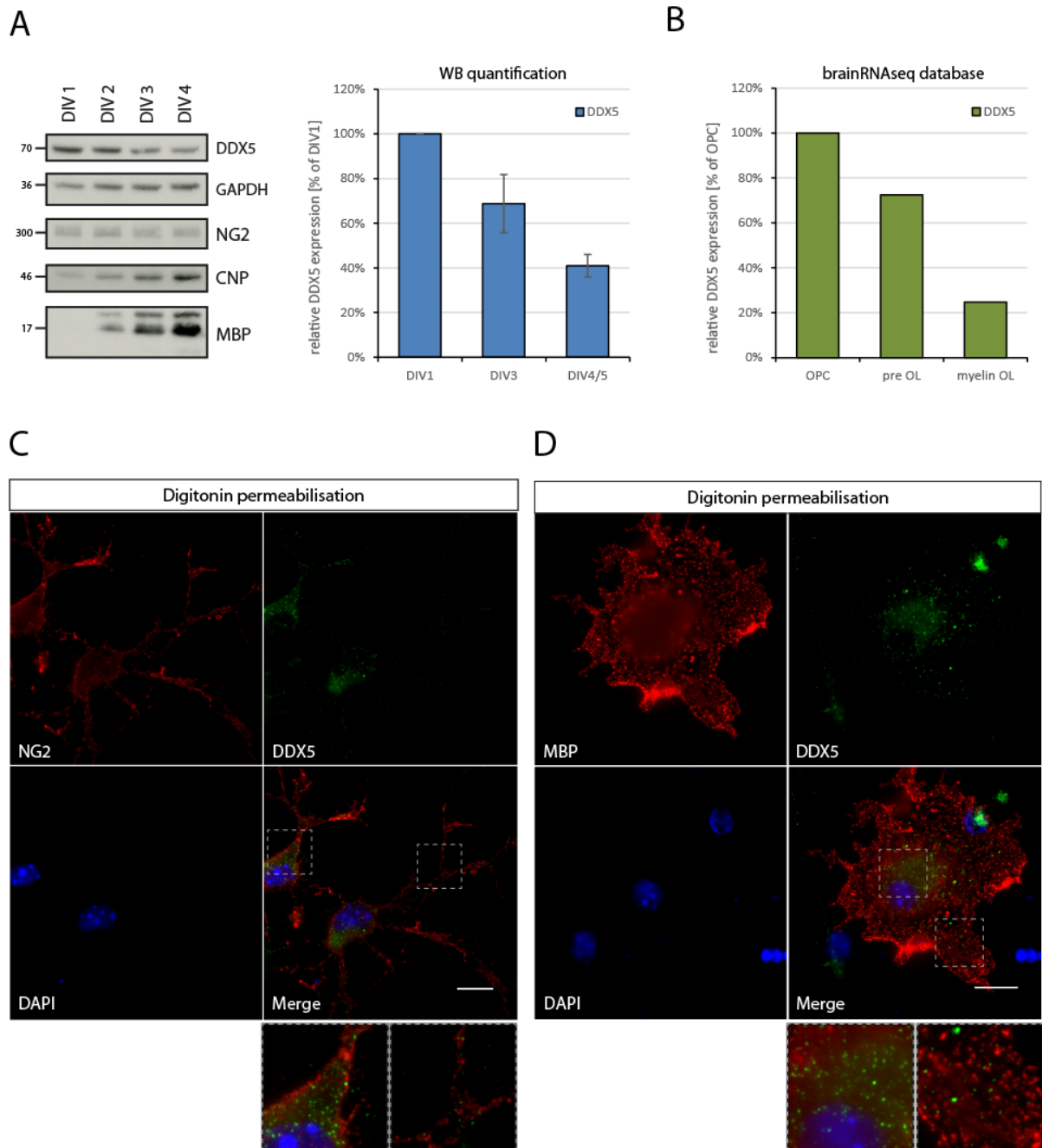


Figure 3-10. Expression and cytoplasmic localization of DDX5 in primary oligodendrocytes

(A) Cell lysates of primary oligodendrocytes after 1, 2, 3, 4 or 5 DIV are analyzed via Western blot. A representative Western blot and quantification of DDX5 signals shows a decrease in DDX5 protein levels with ongoing differentiation (GAPDH normalized, $n=3$, SEM). (B) DDX5 RNA expression data, obtained from the brainRNAseq database (Zhang et al., 2014), also indicating a decrease in DDX5 expression. (C-D) On the subcellular level, DDX5 expression was analyzed in digitonin-permeabilized primary oligodendrocytes by co-immunocytochemistry with (C) NG2 or (D) MBP antibodies to identify OPCs or mature OL, respectively. Magnifications of indicated areas (dotted squares) is displayed below the merged images. Scale bar = 10 μm

3.4.2 Cytoplasmic association of DDX5 with MBP mRNA RNP complexes

To verify an association with MBP mRNA, DDX5 immunoprecipitations (IP) were performed and mRNA abundance was analyzed with Taqman Gene Expression Assays in *Oli-neu* cells and MACS-sorted O4+ primary OL (Figure 3-11). In line with an efficient pulldown of DDX5 protein from differentiated *Oli-neu* cells (Figure 3-11, A), MBP mRNA exhibited a significant enrichment in DDX5 pulldowns compared to immunoprecipitations with isotype matching control antibodies (displayed in relation to Pgk-1 mRNA). As a control, mRNAs for the cytoplasmic myelin protein CNP and the ZBP1-transport pathway-associated β -actin mRNA were not enriched (Figure 3-11, B). Furthermore, using specific Taqman Gene Expression Assays for MBP exon 2-positive (MBP exII+) and MBP exon 2-negative (MBP exII-) isoforms (Figure 3-11, D), a significant preference for MBP isoforms that do not contain exon 2 was detected (Figure 3-11, B).

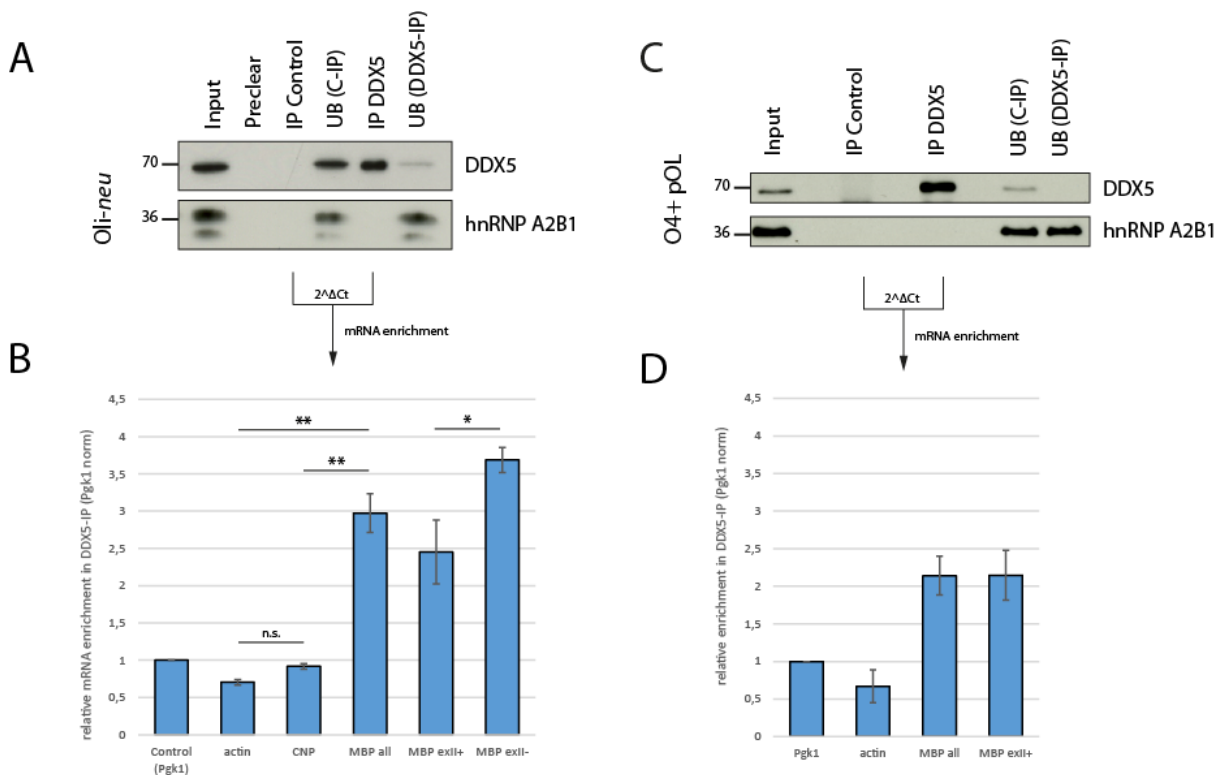


Figure 3-11. RNA-immunoprecipitation (RIP) of DDX5 enriches MBP mRNA.

RNA co-immunoprecipitations with antibodies directed against DDX5 (IP DDX5) or isotype matching control antibodies (IP Control) were performed and enrichment of associated mRNAs was analyzed by qPCR. To assess relative mRNA enrichment, fold-changes of indicated mRNAs between DDX5 IP and Control IP precipitates were calculated and normalized to Pgk-1 as a control. Precipitations were performed with protocols using Protein A coupled Sepharose beads from differentiated *Oli-neu* cells (A-B, n=4) and Protein G-coupled magnetic Dynabeads from O4-sorted primary OL (C-D, n=3). Mean values are displayed, error bars indicate SEM; * = $p < 0.05$; ** = $p < 0.01$ (paired two-tailed students t-test).

Co-immunoprecipitation experiments were additionally carried out with MACS sorted O4-expressing primary oligodendrocytes using an alternative protocol comprising Protein G coupled Dynabeads (Chapter 0). RNA quantification similarly indicated an enrichment of MBP mRNA in the DDX5 precipitates under these experimental conditions (Figure 3-11, C+D). Surprisingly, in both approaches hnRNP A2B1 proteins could not be detected in DDX5 immunoprecipitations (Figure 3-11, A+C), although MBP mRNA was enriched (Figure 3-11, B+D). To compare the subcellular localization of hnRNP A2 and DDX5, immunostaining of oligodendroglial cells was performed and the cytoplasmic distribution was analyzed (Figure 3-12). Both proteins show a typical nuclear accumulation and a granular appearance in

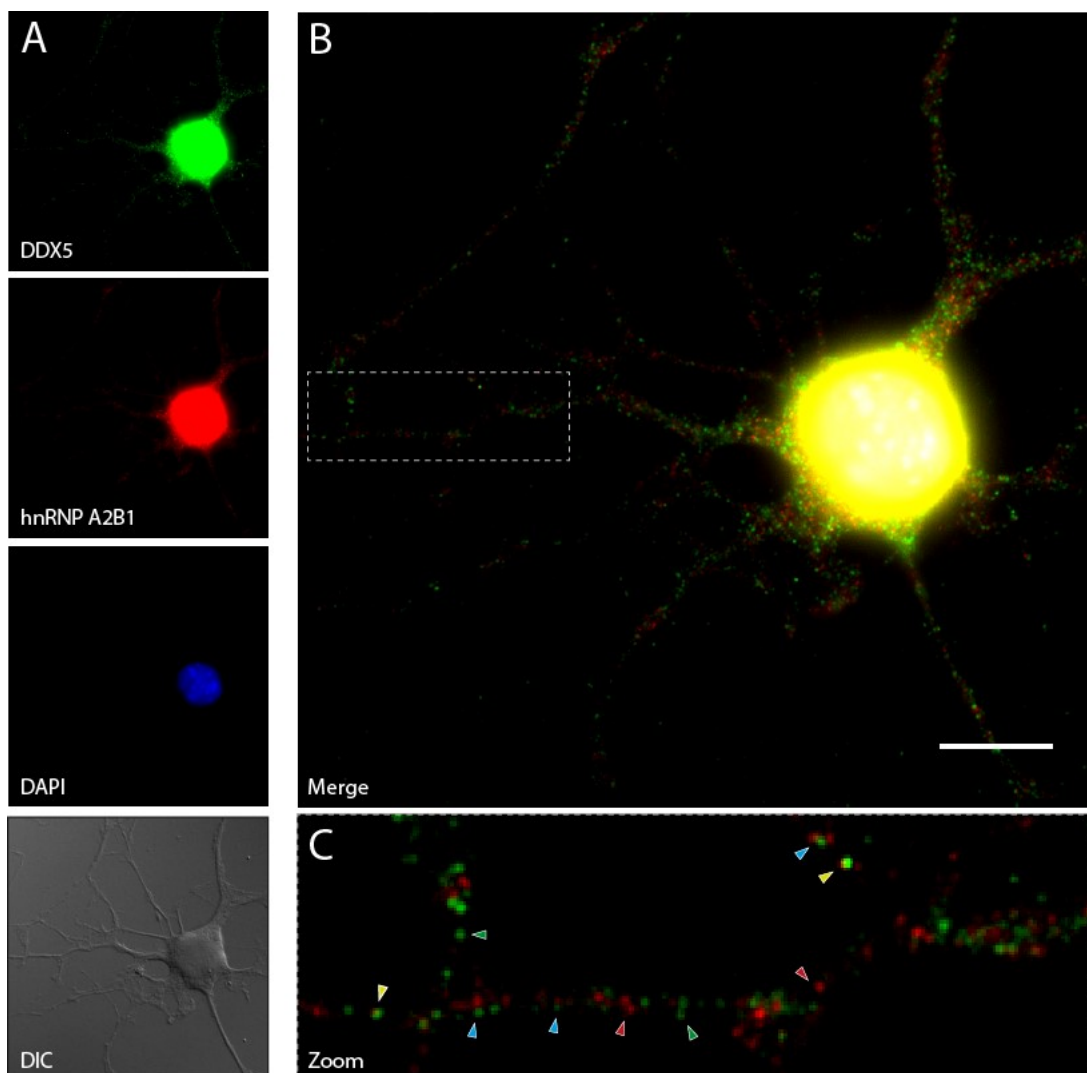


Figure 3-12. Cytoplasmic localization of DDX5 and hnRNP A2B1 granules.

(A) Oli-*neu* cells were allowed to differentiate for 4 days and fixed cells were subsequently subjected to immunocytochemistry with antibodies directed against DDX5, hnRNPA2 and stained with DAPI. **(B)** Merged picture of the DDX5 and hnRNP A2 staining. **(C)** Magnified view showing the granule distribution in an Oli-*neu* process. Arrows indicate individual DDX5 (green) or hnRNP A2 (red) positive spots or an adjacent (blue) or overlapping (yellow) localization of the signals. Scale bar=10 μ m.

cytoplasmic processes. The majority of granules appeared as individual DDX5+ or hnRNP A2+ spots (Figure 3-12, C, green and red arrows, respectively), often adjacent and separated by a distance of <500 nm (Figure 3-12, C, blue arrows) and signals rarely tended to overlap (Figure 3-12, C, yellow arrows).

These results raise the question of a MBP mRNA complex heterogeneity and suggest that DDX5 is present in subpopulations of MBP mRNA-associated RNP complexes, which may be separate from those containing hnRNP A2. The exact nature of these RNP complexes remains to be elucidated.

3.4.3 Size fractionation of RNA granules using Optiprep density gradient centrifugation

Density gradient centrifugation has been used to isolate endogenous RNP complexes from neuronal cells to decipher the molecular basis of RNA transport granule localization (Fritzsche et al., 2013) and is similarly used in polysome profiling to subdivide fractions of distinct ribosomal RNP complexes. In collaboration with Daniela Karra, we adapted the protocols in order to isolate RNP complexes from oligodendroglial cells. Experiments were carried out together with Constantin Gonsior.

Primary oligodendrocytes or *Oli-neu* cells were subjected to Optiprep density centrifugation (Chapter 2.5.4). Fractions were collected from the top of the gradient and analyzed via Western blot and by measurement of the sucrose refractive index and total RNA concentrations (Figure 3-13, A). Optionally, lysates were treated with RNase A, to disrupt RNP complexes as a control. To identify segregation and association with distinct RNP complexes, DDX5, hnRNP A2, hnRNP F and indicated markers were detected in the Western blot fractions (Figure 3-13, B-C).

In general, the distribution of DDX5 and other RNPs varied between experiments (data not shown), an example for fractionation of complexes derived from primary OL (Figure 3-13, B) or differentiated *Oli-neu* cells (Figure 3-13, C) is represented and highlights common characteristics of the RBP distribution. The main protein peak is allocated to the first three fractions, where soluble cytoplasmic proteins, like GAPDH, and most RBPs are enriched (Figure 3-13, C). The presence of poly-A binding protein (PABP) and ribosomal protein L0 (RPLP0) in heavier fractions indicates the preservation of RNP complexes containing mRNAs

or ribosomal subunits, respectively. In the heaviest fraction at the bottom of the gradient, RBP and RNA abundance indicates accumulation of large RNP complexes, like polysomes or multiplexed RNA transport granules, whereas the absence of GAPDH (as a control) excludes contamination by light fractions during manual fraction collection. As a control, RNase treatment shifted RBPs to lighter fractions and indicates the dissociation of the RNP complexes (Figure 3-13, C +RNase).

Protein composition in individual fractions of primary oligodendrocytes is correlated with Optiprep density and RNA concentration in Figure 3-13, B. Fractions 5-6 and 9-10 indicate peaks of RNA concentration and fractions 9-10 show signals for the ribosomal Protein L0, as a marker for 60S ribosomal subunit. In the light RNA-enriched fraction 5 (Figure 3-13B, fractions 5) low amounts of hnRNP A2 co-migrated together with hnRNP F and DDX5, but not with RPLP0. A second RNA-enriched fraction (Figure 3-13B, fractions 9-10) is enriched for RPLP0, includes DDX5 and hnRNP F, but no hnRNP A2.

Similar results were obtained with differentiated *Oli-neu* cells (Figure 3-13, C), whereas enrichment of RNPs in higher density fractions appeared to correlate with cell complexity and viability during multiple experiments. Again, in contrast to hnRNP A2, DDX5 was repeatedly present in heavier fractions and shared similar distributions with PAPB and hnRNP F, being also present in fractions enriched in RPLP0. Interestingly, an hnRNP A2B1 isoform with higher molecular weight (ca. 40 kDa) behaves differently to the predominant hnRNP A2B1 isoforms, being shifted to heavier fractions 5-6.

Taken together, these results demonstrate that heterogeneous RNP complexes could be isolated from oligodendroglial cells. Fractionation revealed different distributions for distinct RNA-binding proteins, such as DDX5 or hnRNP A2 and could be used in various experimental approaches as an initial purification step of RNP complexes, away from the main protein peak.

3.4.4 Knockdown of DDX5 in primary oligodendrocytes increases MBP expression

As DDX5 is associated with MBP mRNA, we analyzed the consequences of DDX5 knockdown in primary oligodendrocytes. DDX5-targeting or control siRNAs were introduced into primary mouse oligodendrocytes via the AMAXA Nucleofection system and the consequences were

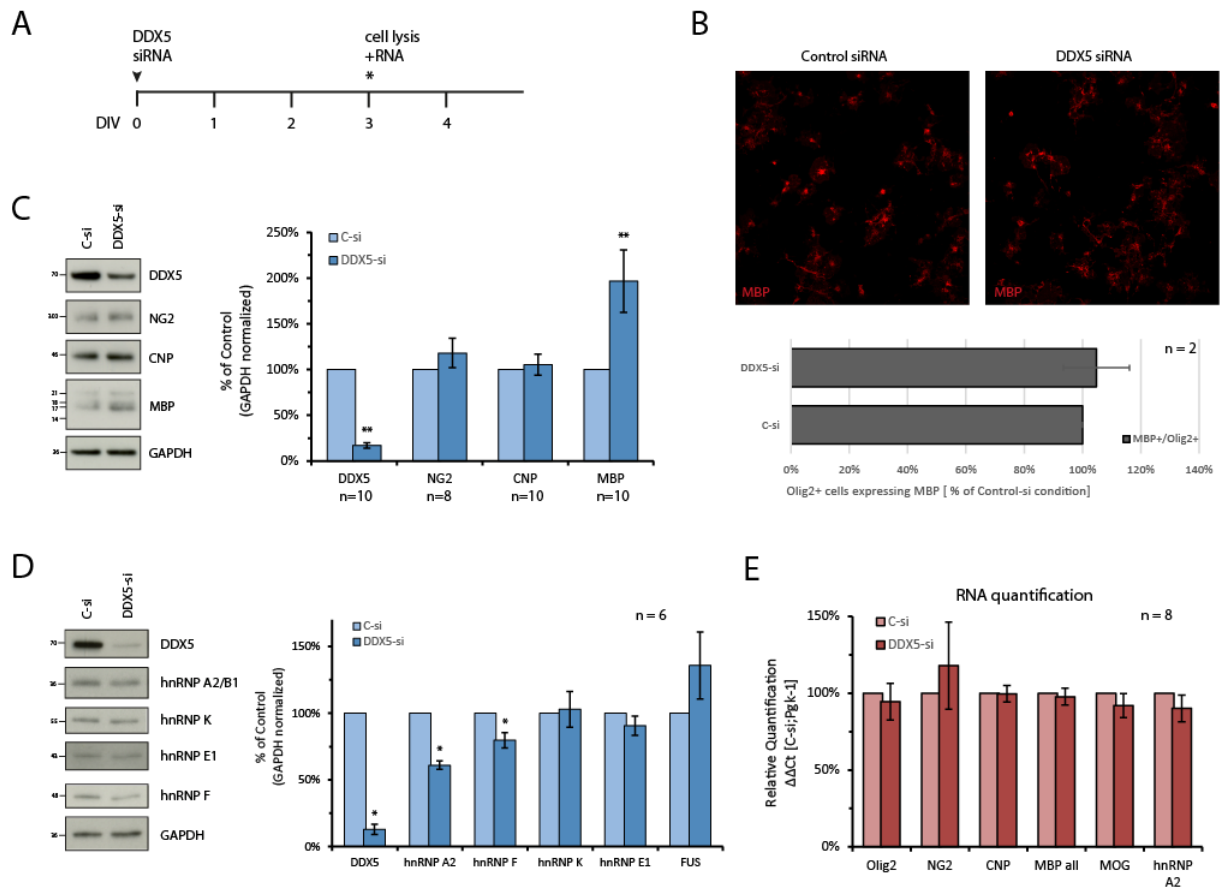


Figure 3-14. DDX5-siRNA knockdown enriches MBP protein levels in primary oligodendrocytes.

(A) Primary mouse oligodendrocytes were nucleofected with a siRNA cocktail targeting DDX5 or a Control-siRNA. After 3 days of differentiation *in vitro*, cells were harvested and analyzed via Western blot, qPCR and immunocytochemistry. (B) Coverslips were fixed and immunostained using antibodies against Olig2 and MBP, respectively. Olig2+ cells expressing MBP were counted per area and compared between DDX5 knockdown and control conditions. At least 24 images were counted for each condition from 2 individual experiments. (C-D) Western blot signals of (C) OL-specific proteins or (D) selected RBPs were densitometrically quantified, normalized to GAPDH levels and mean values are displayed in bar charts. (E) RNA levels were measured via qPCR and $\Delta\Delta Ct$ values were calculated using Pgk1 mRNA and C-si values for normalization. Number of experiments is shown individually, n=2-7, error bars indicate SEM (* = $p < 0.05$; ** = $p < 0.01$; Wilcoxon signed rank test).

studied via Western blot, immunocytochemistry and qPCR after 3 days in culture (Figure 3-14. A). DDX5 siRNA transfection efficiently reduced levels of DDX5 protein and correlated with a significant elevation of MBP protein (Figure 3-14, C). Oligodendroglial proteins NG2 and CNP were not reproducibly altered, indicating that the number of OL was not changed. In line with this observation, Olig2+ cells were counted and percentage of concurrently MBP+ cells revealed no change after DDX5 knockdown (Figure 3-14, B). Additionally, quantification of corresponding RNA levels via qPCR did not show obvious changes, indicating that primarily posttranscriptional effects were responsible for the elevation of MBP protein after DDX5 knockdown (Figure 3-14, F). Posttranscriptional effects are regulated by the ensemble of RBPs associated with the target transcript. Detection of RBPs with well-known roles in regulating

MBP metabolism, revealed a selective reduction in hnRNP A2 and hnRNP F protein levels, leaving hnRNP K, hnRNP E1 or FUS untouched (Figure 3-14, D). Taken together, knockdown of DDX5 from primary OL correlates with the reduction of MBP-associated RBPs and the elevation of MBP protein levels by post-transcriptional mechanisms.

3.4.5 Knockdown of DDX5 affects MBP isoform abundance in primary OL

During Western blot analysis of MBP protein in multiple DDX5-siRNA experiments, an alteration of bands correlating with the different MBP isoforms attracted our attention (Figure 3-15, A). Since the exon 2-bearing 17.22-kDa-MBP isoform largely contributed to the increase in MBP protein levels, the alteration of the other isoforms was analyzed individually focusing on exon 2-dependent differences. Signals from the 17/18-kDa-MBP doublet could not be quantified individually, but hinted at a shift towards the 17-kDa isoform inside the doublet (Figure 3-15, A) and the collective quantification demonstrated a significant increase after DDX5-si treatment (Figure 3-15, B). Comparison of 21.5-kDa-MBP (ex2+) and 14-kDa-MBP (ex2-) protein showed a selective enrichment for the exon 2-containing 21.5-kDa-MBP isoform. Calculation of the ratio between exon 2-positive and exon 2-negative protein expression levels suggests an isoform-related switch in MBP expression as a result of DDX5 knockdown (Figure 3-15, C).

Consequently, RNA analysis with Taqman Gene Expression Assays specific for individual MBP isoforms (Figure 3-15, D) revealed an increase in MBP transcripts bearing exon 2 accompanied with a decrease in exon 2-negative isoforms, underlining the observed effect at the protein level. The inverse correlation of MBP isoform levels suggests a regulatory effect of DDX5 knockdown on MBP splicing, rather than an individually altered stability of exon 2-positive versus exon 2-negative transcripts. Several reports suggest that DDX5 is involved in the regulation of alternative splicing (Camats et al., 2008; Kar et al., 2011; Lin et al., 2005). Recently, Dardenne and Espinosa revealed a role of DDX5 and its close relative DDX17 as “master orchestrators” of switching between splicing programs during cell differentiation (Dardenne et al., 2014), which raises the question of a similar contribution in the oligodendrocyte lineage.

In summary, DDX5 knockdown in primary oligodendrocytes altered the MBP isoform abundance elevating the levels of the exon 2-positive MBP isoforms 17.22-kDa and 21.5-kDa.

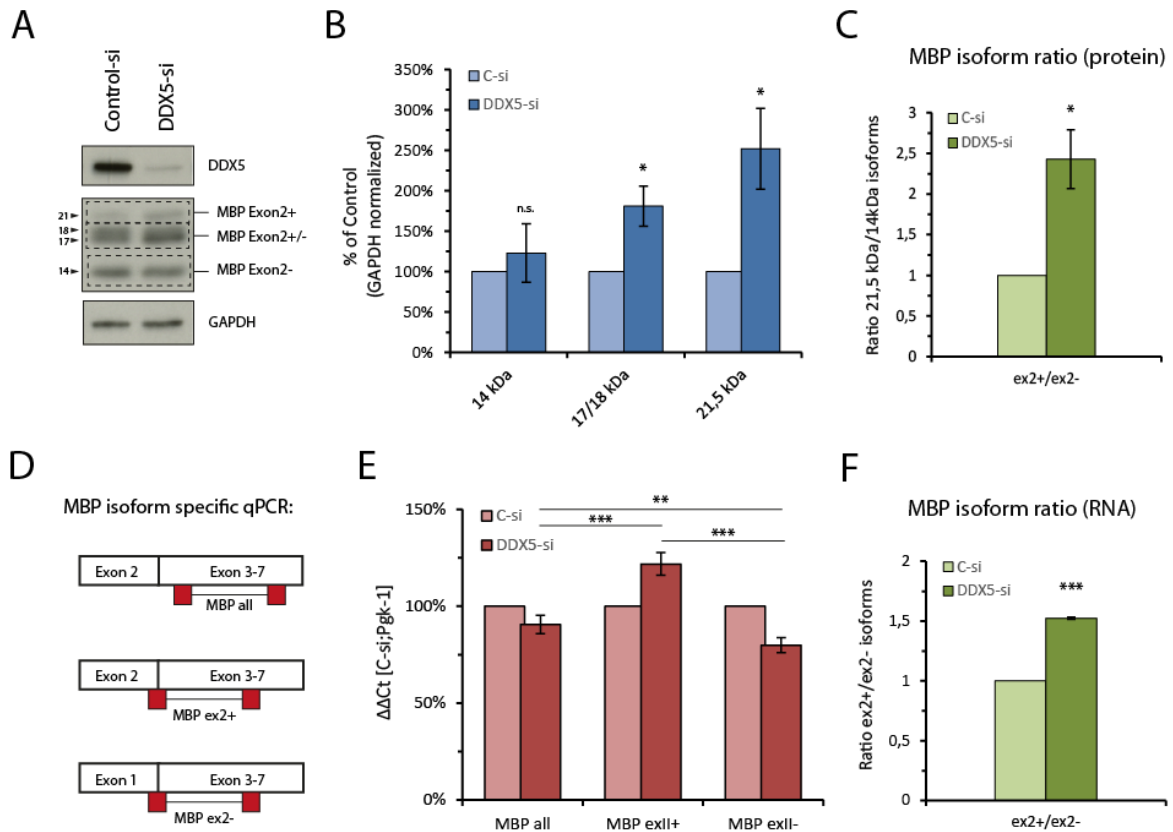


Figure 3-15. DDX5-siRNA knockdown results in a shift of the MBP isoform distribution

DDX5-siRNA knockdown experiments in primary OL were analyzed with focus on the distribution of MBP isoforms. **(A)** Western blot showing a shift of MBP isoforms towards exon 2-positive isoforms 21.5-kDa and 17.22-kDa. **(B)** Quantification of the individual bands (A, dotted boxes) according to MBP isoforms (n=8). **(C)** Ratio of the 21.5-kDa-MBP to the 14-kDa-MBP protein isoform. **(D)** Taqman Gene expression assays specific for MBP isoforms bearing (ex2+) or lacking exon 2 (ex2-) were used to quantify RNA abundance of the MBP isoforms. **(E)** RNA levels were measured via qPCR and $\Delta\Delta C_t$ values were calculated using Pgk1 mRNA and C-si for normalization (n=5). **(F)** Ratio of exon 2+ to exon 2- isoforms at the RNA level. Error bars indicate SEM. (* = $p < 0.05$; ** = $p < 0.01$; *** = $p < 0.001$; Wilcoxon signed rank test: B,C,F – two-tailed student's paired t-test: E).

3.4.6 Impact of DDX5-siRNA knockdown on oligodendroglial proliferation

Although MBP proteins have been studied intensively, MBP exon 2-specific protein functions are not well understood (Chapter 1.2.2). Nevertheless, according to the literature MBP exon 2-positive isoforms appear capable of increasing intrinsic proliferation of oligodendroglial cells, possibly by releasing a proliferation-promoting factor (Ozgen et al., 2014; Smith et al., 2013). On the other hand, DDX5 was suggested to positively regulate cellular proliferation (Jalal et al., 2007; Yang et al., 2005a), raising the question of the impact of a DDX5 knockdown (increasing expression of MBP exon 2-positive isoforms) on oligodendroglial proliferation. Immunocytochemistry with Ki67 antibodies allows the identification of proliferating cells and was applied to oligodendroglial cultures. Consequently, cell nuclei positive for Olig2 and Ki67

were counted and compared between DDX5- or Control-siRNA treatment after 3 DIV (Figure 3-16, B). In general, Ki67-positive cells appeared in clusters indicating a recent cell division and co-expression of Olig2 identifies these as oligodendroglial cells. Figure 3-16A shows typical distributions of Olig2+ and Ki67+ cells, respectively. Total numbers of Olig2+ and Ki67+ cells are displayed in Figure 3-16C and indicate increased numbers of cells per area after DDX5-siRNA treatment compared to control (Figure 3-16, C), but normalization to Olig2+ cell numbers (Ki67+/Olig2+) revealed only a negligible increase in actively dividing oligodendroglial cells after DDX5-knockdown (Figure 3-16, D).

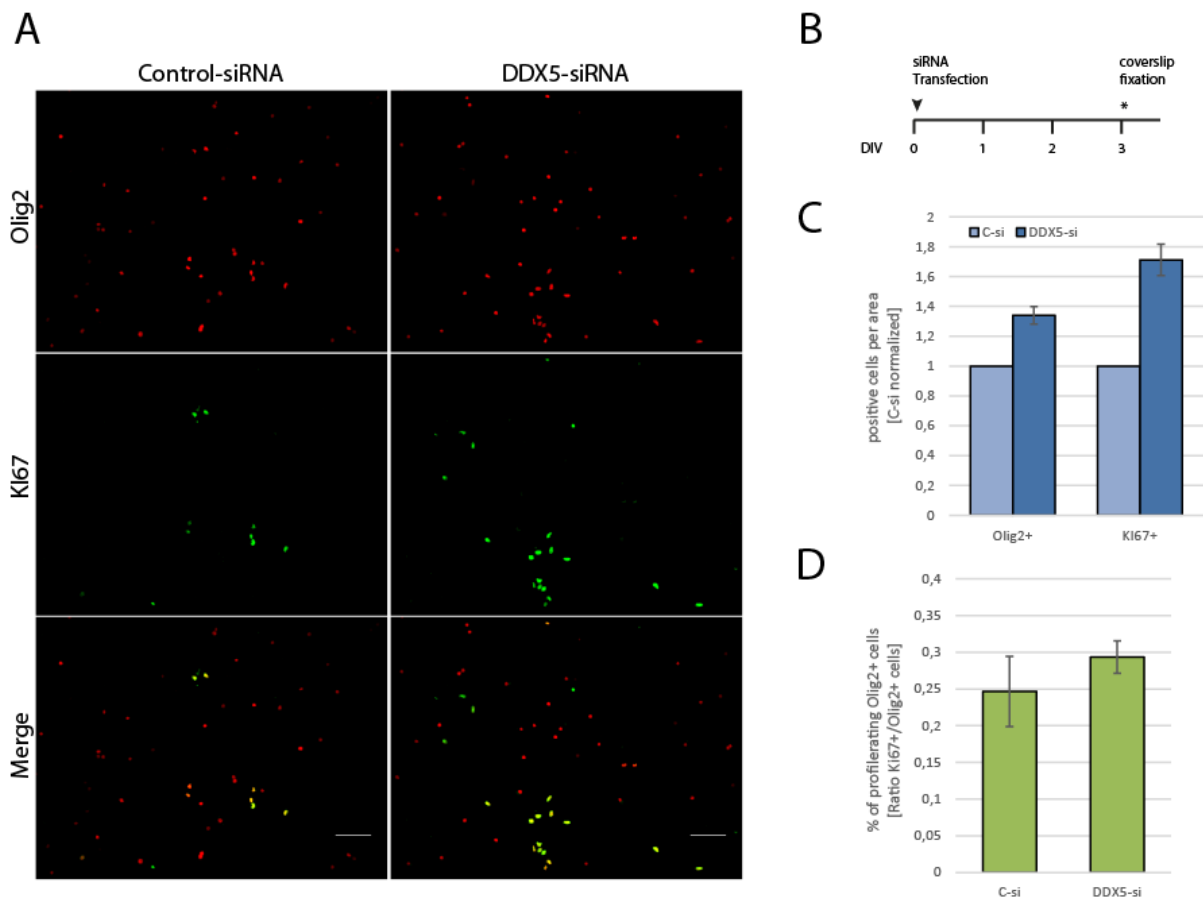


Figure 3-16. Impact of DDX5 knockdown on oligodendroglial proliferation.

(A-B) Primary mouse oligodendrocytes were nucleofected with a siRNA cocktail targeting DDX5 or a Control-siRNA. After 3 days of differentiation *in vitro*, cells were harvested and analyzed via immunocytochemistry. Coverslips were fixed and immunostained using antibodies against Olig2 and Ki67, respectively. (C) Olig2+ and Ki67+ cells were counted (cells per area) and compared between DDX5 knockdown and control conditions. At least 24 images were counted for each condition from 3 individual experiments. (D) Ratio of Ki67+/Olig2+ cells after DDX5-knockdown. Bar charts indicate the mean +/- SEM, n=3. Scale bar=10 μ m.

3.4.7 Posttranscriptional regulation of MBP is dependent on the DDX5 helicase activity

DEAD box helicases have been studied intensively and in the course of deciphering their molecular characteristics, several mutations were established to alter the enzymatic function

and binding abilities of the helicase (Jalal et al., 2007; Pause and Sonenberg, 1992; Saporita et al., 2011). Substitution of the amino acid Lysine to Asparagine at position 144 (K144N) abolishes ATP-binding and the RNA helicase activity of DEAD box helicases (Figure 3-17, A). This K144N mutation was inserted in our DDX5-myc construct by site directed mutagenesis (Chapter 2.3.4) and the consequences of this enzymatic impairment were evaluated in primary OL and *Oli-neu* cells.

DDX5-myc, K144N-myc or eGFP as a control, were transfected into primary OL at 3 DIV using the AMAXA 4D Nucleofection system (Chapter 2.4.3). Consequences of the overexpression were monitored via Western blot and qPCR after 2 days in culture corresponding to DIV 5 (Figure 3-17, B). Detection of the myc-tag facilitates the identification of plasmid-mediated DDX5/K144N expression via Western blot (Figure 3-17, C). Analysis of myelin proteins after DDX5-myc overexpression revealed a reduction in MBP protein levels, but in addition also a decrease in other OL proteins like CNP or MOG, while NG2 was not altered in a reproducible fashion (Figure 3-17, D). This inverse correlation fits well to the observed elevation of MBP protein after DDX5 knockdown, but is extended to other myelin proteins, unlike the knockdown condition, which left CNP unaffected (Figure 3-14, C). In contrast, overexpression of K144N did not yield comparable changes in the levels of the late myelin proteins MBP and MOG, MBP levels even were slightly increased (Figure 3-17, E). Solely CNP, a myelin protein expressed early in the OL lineage, exhibits a similar tendency in response to K144N and DDX5 overexpression.

RNA quantification of OL-specific transcripts after DDX5 or K144N overexpression did not show a change in the level of the mRNAs (Figure 3-17, F), linking the observed regulatory effects to post-transcriptional mechanisms. Moreover, MBP isoform-specific qPCRs also did not detect any alterations in the expression of MBP exon 2-containing isoforms (Figure 3-17, F-G). Overexpression of DDX5 or the mutated K144N in *Oli-neu* cells led to inconsistent results on the protein levels of RNA-binding proteins and CNP (Figure 3-17, H-I). Nevertheless, overexpression of both proteins revealed a minor but significant effect on the MBP isoform ratio towards exon 2-negative MBP isoforms, independent of the DDX5 helicase function (Figure 3-17, J).

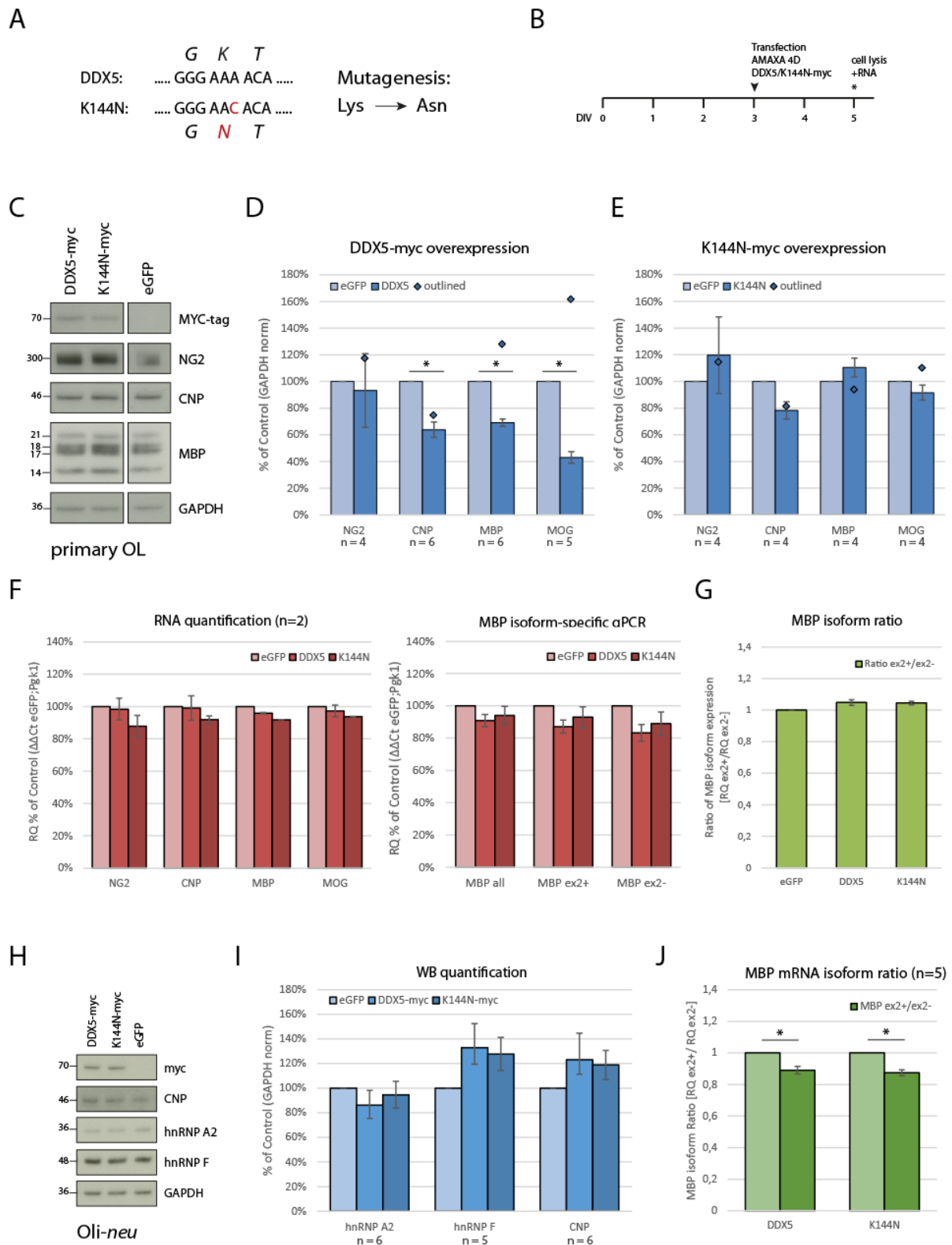


Figure 3-17. Overexpression of the DDX5 helicase mutant K144N in oligodendroglial cells

(A) The K144N mutation was introduced by the change of a single base (A>C) using site directed mutagenesis, leading to an exchange of Lys to Asp at position 144 in the translated DDX5 protein sequence, abolishing the DDX5 helicase function. (B) Primary oligodendrocytes were transfected with DDX5-myc, K144N-myc or eGFP as a control using AMAXA 4D nucleofection system at 3 DIV. 2 days later cells were harvested and analyzed via Western blot or qPCR. (C-E) Western blot bands were densitometrically quantified, normalized to GAPDH levels and displayed in bar charts (D-E, n=4-6, +/- SEM), one experiment is displayed as outlined data points (n=1,

diamonds). **(F)** RNA levels were measured via qPCR and $\Delta\Delta\text{Ct}$ values were calculated using Pgk1 mRNA and eGFP control for normalization (F, n=2, SEM). **(G)** Ratios of the MBP mRNA isoform abundance is displayed **(H-I)** Oli-*neu* cells were transfected with indicated plasmids by FuGene HD reagent and were analyzed via Western blot and **(J)** corresponding MBP mRNA levels were measured and MBP isoform ratios were calculated. * = $p < 0.05$; Wilcoxon signed rank test.

Taken together, DDX5 helicase activity in oligodendroglial cells decreased myelin protein expression of MBP, CNP and MOG at a post-transcriptional level, whereas a slight regulation of the MBP isoform ratio in Oli-*neu* cells appears to be independent of the DDX5 RNA helicase function.

3.4.8 Impact of DDX5 on MBP-3'UTR-containing luciferase reporter systems

The previous results indicate that post-transcriptional mechanisms are responsible for altered levels of MBP upon overexpression or knockdown of DDX5. Standardized assays, measuring luciferase activities have been used to identify changes in MBP translation efficiencies (White et al., 2012; White et al., 2008). Thus, luciferase assays were used to analyze the effect of DDX5 and K144N on translation of a MBP-3'UTR containing reporter construct (Chapter 2.8). Oli-*neu* cells were transfected with *firefly* luciferase reporter constructs, with or without the MBP 3'UTR attached (Chapter 2.3.3). In parallel, *renilla* luciferase was used to normalize for transfection efficiency or varying cell densities. Ratios of Firefly to Renilla luciferase activity give a measure for the translational output under given experimental conditions.

Relative luciferase activities are displayed after overexpression of DDX5-myc or K144N-myc, respectively (Figure 3-18, B-C). The activity of LUC-MBP-3'UTR was reduced by half independent of the helicase function (Figure 3-18, B). Surprisingly, a LUC-control construct, not bearing the MBP-3'UTR, revealed almost identical results (Figure 3-18, C). Analyzing RNA levels of the corresponding *firefly* or *renilla* luciferase reporters with SYBR Green qPCR assays uncovered a major impact on RNA stability. *Renilla* levels, used for intrinsic normalization of the system were increased up to 6-fold compared to control conditions (Figure 3-18, D). Similarly, *firefly* expression was also altered and even more pronounced in the case of LUC-Control constructs (Figure 3-18, E). These changes in the overall expression of the reporter transcripts does prevent a conclusion and luciferase assays appear not be a suitable method for measuring translational activity in combination with DDX5. Nevertheless, the discrepancies might point to a role of DDX5 in plasmid based-transcription or RNA decay that remains to be elucidated.

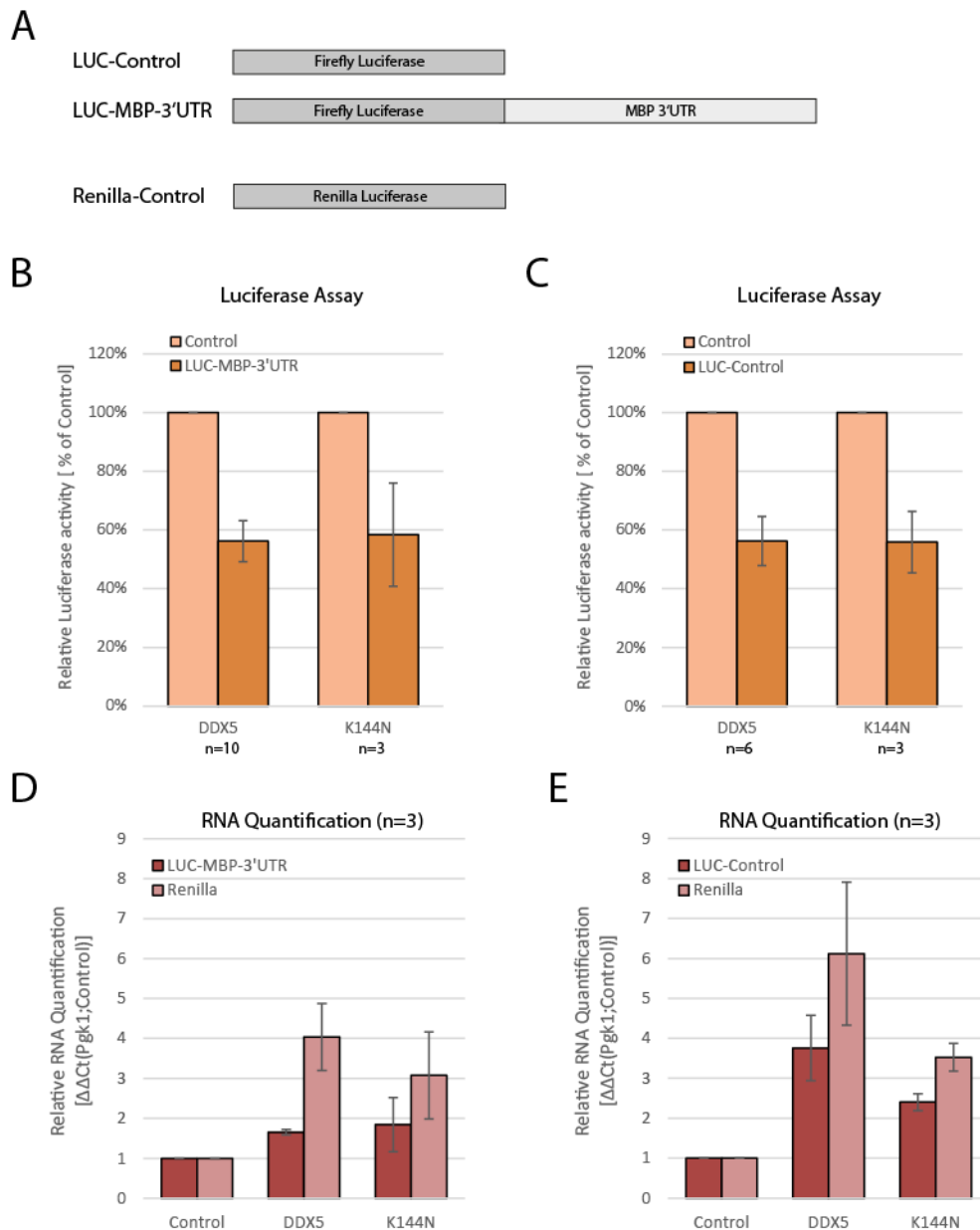


Figure 3-18. Impact of DDX5 on MBP-3'UTR-containing luciferase reporter systems in *Oli-neu* cells.

(A) Luciferase-based assays were used to measure the post-transcriptional regulation of MBP-3'UTR reporters. *Oli-neu* cells were transfected with DDX5-myc, K144N-myc or empty vector (Control) in combination with *firefly* luciferase reporters with attached MBP-3'UTR (LUC-MBP3'UTR) or without (LUC-control) and *renilla* luciferase as an internal control. After 24-48h cells were harvested and analyzed in Luciferase Assays or qPCR. **(B-C)** Relative luciferase activity is calculated by normalization of Firefly- to Renilla-based luminescence and displayed for LUC-MBP-3'UTR (B) and LUC-Control (C) as a mean \pm SEM. **(D-E)** Corresponding RNA levels were measured via SYBR Green qPCR and $\Delta\Delta$ Ct values were calculated using Pgk1 mRNA and empty vector control for normalization (D-E, n=3, \pm SEM).

3.5 The RNA-binding protein FUS in maintaining MBP mRNA levels

FUS is a multifunctional RNA binding protein that has been studied intensively over the last years (Chapter 1.4.2) as a candidate gene causing familiar cases of Amyotrophic Lateral Sclerosis (ALS) and other neurodegenerative diseases (Deng et al., 2014). In ALS, the

involvement of oligodendrocyte death in the early pathology was revealed recently (Kang et al., 2013) and raises the question of the contribution of an oligodendroglial mRNA misregulation to the disease progress or myelination in general. As we identified FUS as a protein potentially associated with MBP mRNA (White, 2007), we carried out preliminary experiments analyzing the functional role of FUS in oligodendrocytes (Hoch-Kraft, 2010). Our earlier results showed that oligodendroglial expression of FUS was predominantly nuclear, with the formation of RNA granule-like structures after overexpression. Co-immunoprecipitation experiments showed RNA-dependent association with hnRNP A2 and a tendency to co-localize, especially in cytoplasmic branch points of oligodendroglial processes. Moreover, knockdown of FUS in oligodendrocytes appeared to influence MBP protein levels. During this thesis, additional experiments were addressed to shed further light on the role of misbalanced FUS in oligodendrocytes, potentially impacting on myelination or neurodegenerative diseases.

3.5.1 Consequences of altered FUS levels in oligodendrocytes

To examine the consequences of misbalanced FUS levels in oligodendroglial cells, siRNA-mediated knockdown or FUS overexpression were addressed. FUS-targeting or control siRNAs were introduced into primary mouse oligodendrocytes via the AMAXA Nucleofection system. Cells were harvested after 2, 3 or 4 days of differentiation and were analyzed via Western blot and qPCR (Figure 3-19, A). Initial work during the diploma thesis pointed to an influence of siRNA-mediated FUS knockdown on the expression of MBP protein in primary OL. FUS siRNA experiments were repeated at DIV2 (n=2), DIV3 (n=4), in addition performed at DIV 4 (n=3) and summarized in Figure 3-19.

FUS knockdown in primary cells led to an average reduction of FUS protein to about 45% of control levels, and was comparable between different time points of cell lysis (Figure 3-19, B-E). MBP protein levels changed marginally in amount, yet an increase to 126% of control at DIV 3 was statistically significant (Figure 3-19, D). CNP was not significantly altered, independent of the time point analyzed. In contrast, analysis of DDX5 protein levels shows a robust rise after FUS knockdown, gently declining at 4 DIV. Although analyzed in only two experiments at 4 DIV, hnRNP A2 protein levels were notably reduced. Quantification of mRNA levels at 4 DIV additionally reveals a slight reduction in MBP and CNP expression

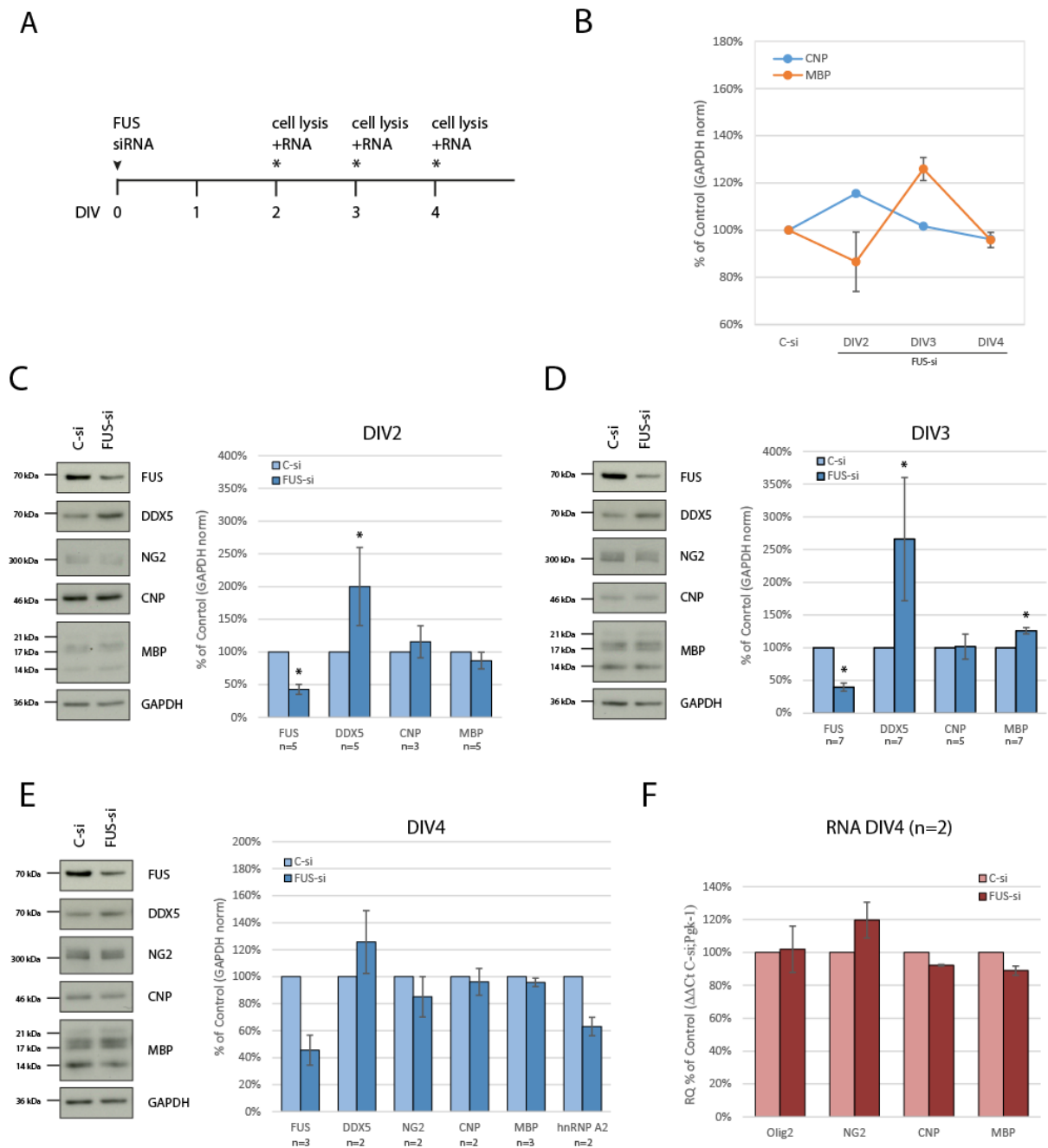


Figure 3-19. Impact of FUS-knockdown on primary oligodendrocytes.

(A) Primary mouse oligodendrocytes were nucleofected with a siRNA cocktail targeting FUS or Control-siRNA. After 2-4 days of differentiation *in vitro*, cells were harvested and analyzed via Western blot or qPCR. (C-E) Western blot bands were densitometrically quantified, normalized to GAPDH levels and displayed in bar charts subdivided in different timepoints. (F) RNA levels were measured via qPCR and $\Delta\Delta Ct$ values were calculated using Pgk1 mRNA and C-si for normalization. (B) Summary of CNP and MBP expression levels after FUS knockdown. The number of analyzed experiments is shown individually, n=2-7, error bars indicate SEM, * = $p < 0.05$ in Wilcoxon signed rank test.

(Figure 3-19, F). Overexpression of FUS in primary oligodendrocytes was performed using the AMAXA 4D nucleofection system. Plasmids, carrying myc-tagged murine FUS-CDS or eGFP as a control were introduced and after 2 days cells were lysed analyzed via Western blot and qPCR (Figure 3-20). Transfected FUS-myc protein was detected with a monoclonal antibody

recognizing the myc-tag (Figure 3-20, A). Protein levels of myelin proteins and hnRNP A2 were compared with the control condition, one experiment was considered as an outlier, but is displayed as additional data points (Figure 3-20, B). In the remaining experiments, FUS-myc overexpression lead to a moderate reduction in levels of the myelin proteins CNP and MBP and more pronounced decrease of hnRNP A2 (Figure 3-20, A-B). Comparable to FUS knockdown, a minor reduction of CNP and MBP could be recapitulated at the RNA level (Figure 3-20, C).

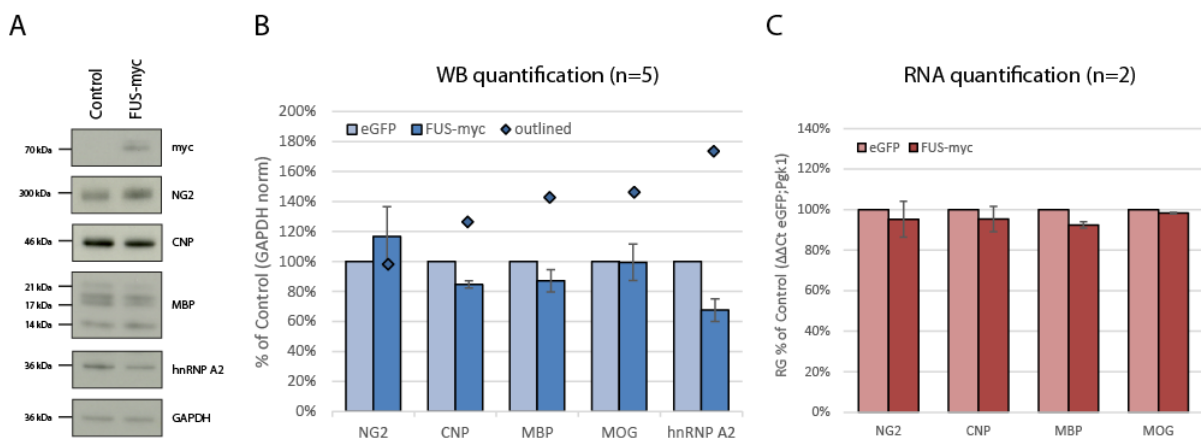


Figure 3-20. FUS-myc overexpression in primary oligodendrocytes.

Primary oligodendrocytes were transfected with FUS-myc or eGFP as a control using AMAXA 4D nucleofection system after 3 DIV. 2 days later cells were harvested and analyzed via Western blot or qPCR. **(A-B)** Western blot bands were densitometrically quantified, normalized to GAPDH levels and displayed in bar charts (n=4, SEM), one experiment is displayed as outlined data points (n=1, diamonds). **(C)** RNA levels were measured via qPCR and $\Delta\Delta C_t$ values were calculated using Pgl1 mRNA and eGFP control for normalization (C, n=2, SEM).

To further study the effects of misbalanced FUS, levels of the MBP mRNA-associated proteins hnRNP A2, hnRNP F and DDX5 were analyzed. Since FUS has been shown to shuttle between the nucleus and cytoplasm (Zinszner et al., 1997), siRNA treated cells were additionally subjected to a nuclear and cytosolic fractionation, to detect possible changes in subcellular localization of the RNA-binding proteins (Figure 3-21, C). Compared to primary cells, siRNA mediated knockdown in Oli-*neu* cells further reduced FUS levels to about 30% of control (Figure 3-21, A,C). As already observed in primary OL, DDX5 protein levels were elevated up to 300% in all subcellular fractions analyzed. Enrichment in cytosolic, as well as nuclear fractions, excludes mislocalization of the protein as a source for the observed increase (Figure 3-21, C). The RNA-binding protein hnRNP A2 was hardly detectable in the cytosolic fraction and did not display a reduction in response to low levels of FUS, in contrast to primary cells

(Figure 3-19). Quantification of RNA levels revealed a statistically significant reduction in CNP and MBP after FUS knockdown, whereas hnRNP A2 and Axin2 (as controls) were not altered.

Taken together, alteration of FUS levels did not show a major impact on the protein expression of CNP or MBP, though MBP mRNA levels tended to be reduced in line with changes in the expression of MBP mRNA-associated proteins hnRNP A2 and DDX5.

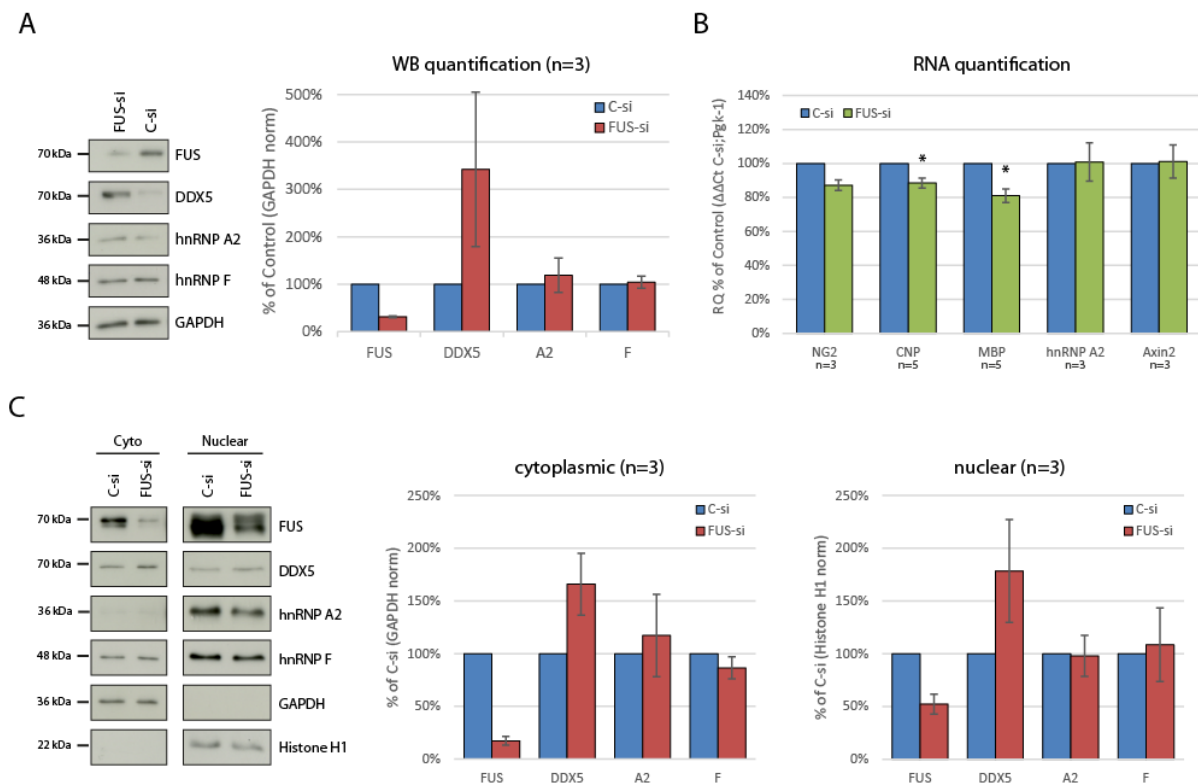


Figure 3-21. Regulation and subcellular fractionation of selected RBPs after FUS-knockdown.

(A-B) Oli-neu cells were nucleofected with siRNAs targeted against FUS or Control-siRNA. After 2 days of dbcAMP treatment, cells were harvested and analyzed via Western blot or qPCR. (A) Western blot bands were densitometrically quantified, normalized to GAPDH levels and displayed in bar charts, including data from unstressed controls in Fig. 4-23. (B) RNA levels were measured via qPCR and $\Delta\Delta C_t$ values were calculated using Pgk1 mRNA and Control-si samples for normalization. (C) Cell fractionation was performed using the NE-PER Fractionation Kit (Pierce). Cytosolic protein levels were normalized to GAPDH, nuclear protein levels to Histone H1, respectively. (n=3-5, SEM). * = $p < 0.05$ in the Wilcoxon signed rank test).

3.5.2 FUS in the response of oligodendroglial cells to oxidative stress

FUS has been shown to cluster in stress granules (SG) after cytoplasmic mislocalization, dependent on mutations in the NLS region of the protein (Chapter 1.4.2). We showed that MBP mRNA was sorted to SG (personal communication Constantin Gonsior) in line with previous reports (Thomas et al., 2005; Wang et al., 2010). Consequently, we verified the

association of FUS with oligodendroglial SG and analyzed the influence on MBP mRNA during oxidative stress conditions, in combination with FUS knockdown.

Oxidative stress was induced in *Oli-neu* cells by application of 0.5 mM sodium arsenite, after 45 minutes coverslips were fixed and stained for FUS and the stress granule marker TIA-1 (experiments were performed in collaboration with Constantin Gonsior). Indeed, FUS protein showed redistribution to Tia1-positive SG after sodium arsenite treatment (Figure 3-22, upper cell). The stress granule association was not ubiquitous, but was restricted to individual cells in the culture, hinting to selectivity and also excluding a cross-reactivity of secondary antibodies. In addition, although FUS is difficult to detect in perinuclear cytoplasmic areas of primary OL, faint signals pointed to localization to G3BP1-positive stress granules (data not shown).

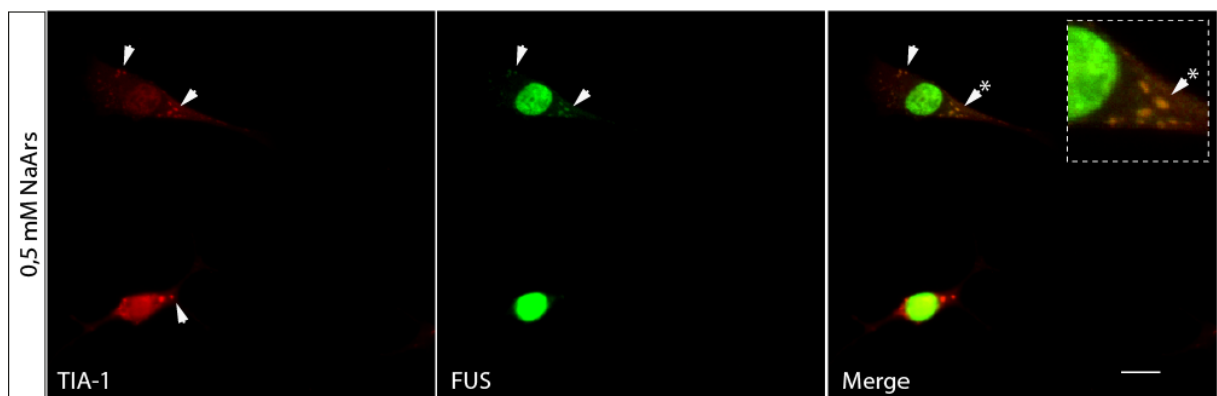


Figure 3-22. FUS localization to TIA1 positive foci in oligodendroglial cells.

Oli-neu cells were differentiated 2 days by adding dbcAMP, before applying oxidative stress for 45 minutes (0.5 mM sodium arsenite) followed by fixation with 4% paraformaldehyde. Co-immunocytochemistry of FUS protein with the stress granule marker TIA-1 was performed and imaged using widefield microscopy. FUS localizes in stress granules in distinct cells in culture and arrows depict the overlap of FUS and TIA1 signal in cytoplasmic stress granules (scale bar=10 μ m).

As FUS is a component of oligodendroglial SG and potentially associated with MBP mRNA, we addressed the role of FUS in the metabolism of MBP mRNA during stress conditions. FUS was knocked down in *Oli-neu* cells prior exposure to indicated sodium arsenite concentrations. Levels of MBP mRNA-associated proteins and RNA levels of myelin proteins were analyzed after 45 minutes of oxidative stress.

In control cells, MBP mRNA levels generally declined with elevated stress (Figure 3-23C, C-si). After FUS knockdown, MBP mRNA levels were already lowered in unstressed cells (Figure 3-21, A; Figure 3-23, C), but remained constant during mild stress conditions (0.1 mM arsenite). FUS knockdown thus appeared to attenuate MBP reduction during mild stress conditions, but had no beneficial effect with high arsenite concentrations (0.5 mM), revealing an additive reduction of MBP mRNA to 70%. CNP mRNA levels were more stable only differing slightly between siRNA knockdown conditions and after 0.5 mM arsenite.

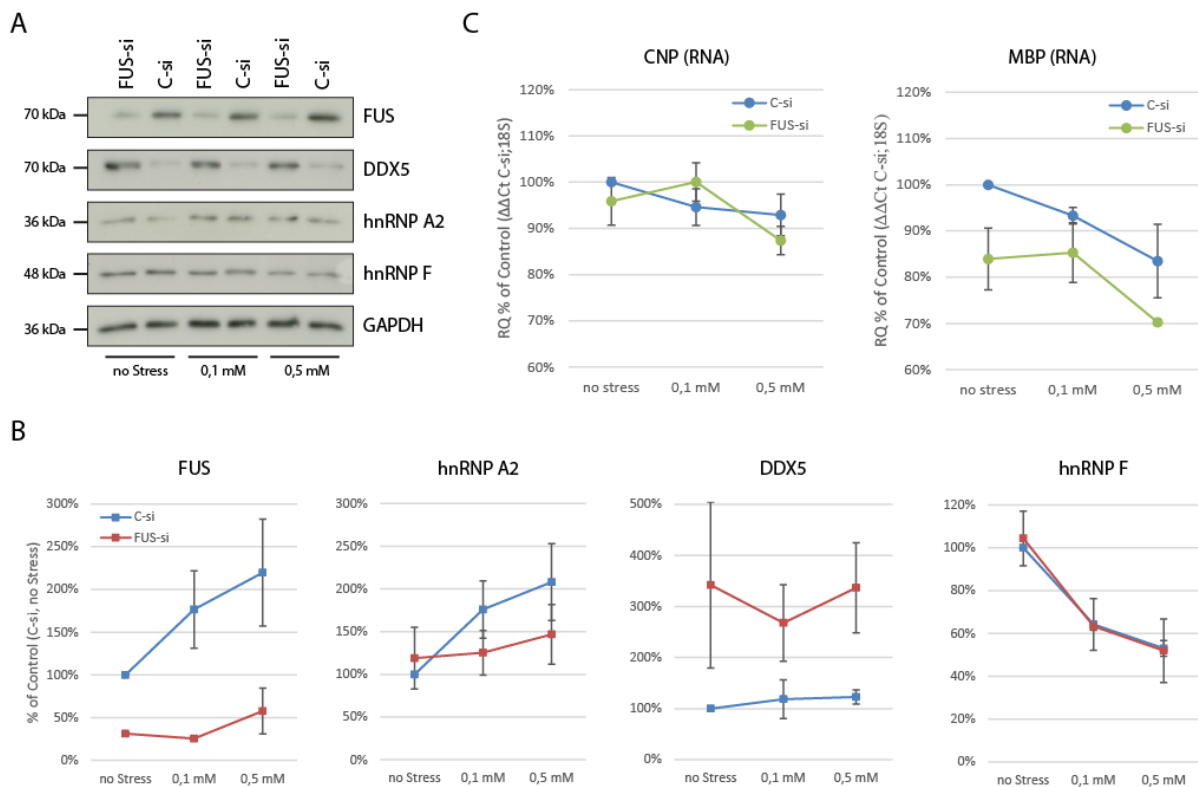


Figure 3-23. Oxidative stress and FUS-knockdown in Oli-neu cells change.

Oli-*neu* cells were nucleofected with siRNAs targeted against FUS or Control-siRNA. After 2 days of dbcAMP treatment, cells were stressed for 45 minutes with 0, 0.1 mM or 0.5 mM sodium arsenite, harvested and analyzed via Western blot or qPCR. **(A-B)** Western blot bands were densitometrically quantified, normalized to GAPDH levels and displayed in point diagrams individually for each protein. **(C)** RNA levels were measured via qPCR and $\Delta\Delta Ct$ values were calculated using 18S rRNA and unstressed C-si for normalization. $n=3$, error bars indicate SEM.

On the protein level, oxidative stress raised the levels of hnRNP A2 and FUS proteins, which increased more than 2-fold and shared similar characteristics with progressing sodium arsenite concentrations (Figure 3-23, B). In FUS-si treated cells, FUS protein was reduced as anticipated, but remained constant during mild stress conditions with a slight increase of high arsenite concentrations, in a course comparable to hnRNP A2. In the case of DDX5, the generally observed increase after FUS knockdown was maintained independent of oxidative

stress and hnRNP F was markedly decreased with elevated stress concentrations, but showed no difference in the absence of FUS.

Comparing protein levels of FUS and hnRNP A2 to levels of MBP mRNA during progressing stress concentrations, revealed an inverse correlation. Upregulation of either protein was accompanied by a decrease in MBP mRNA. This becomes particularly apparent when comparing cells after FUS knockdown, where these levels stayed constant during mild stress conditions and inversely shifted with application of high arsenite concentrations.

Taken together, the results suggest that oxidative stress reduced levels of MBP mRNA in oligodendroglial cells, FUS knockdown attenuated the MBP reduction under mild stress conditions and FUS levels inversely correlated with MBP RNA stability upon increasing concentrations of sodium arsenite. In addition, RNA-binding proteins previously described in MBP mRNA metabolism also reacted to oxidative stress and may play a role in the stabilization of MBP mRNA during the stress response.

4 Discussion

4.1 MBP mRNA localization in cultured oligodendroglial cells

Myelin basic protein is essential for the assembly of CNS myelin and a precise spatiotemporal regulation on the post-transcriptional level assures RNA translocation and synthesis at the axoglial contact site. MBP mRNA has classically been visualized by in situ hybridization in oligodendrocytes and revealed a developmental translocation towards the myelin compartment during maturation (Colman et al., 1982; Trapp et al., 1987). Here, the MBP distribution was analyzed with single molecule resolution in primary OL and *Oli-neu* cells (Figure 3-1). Localization in distal processes of differentiated *Oli-neu* cells as well as primary OL indicates that mRNA localization is efficient in both cell types and mRNA abundance reflects the maturation status (Figure 3-1). *Oli-neu* cells are immortalized oligodendroglial cells that show characteristics of OPCs and early premyelinating OL (Jung et al., 1995). MBP mRNA is abundant, but MBP protein expression is rigorously repressed, providing an environment where MBP mRNA-associated RNP complexes most likely represent a translationally silent state. Accumulating mRNA in the absence of translated MBP protein is also a hallmark of stalled progenitors in MS lesions (Bauer et al., 2012) and might contribute to the proposed differentiation brake operating on OPCs (Kuhlmann et al., 2008) impairing remyelination during progressing disease. Elucidation of the MBP mRNP complex composition will help to shed further light onto mechanisms of mRNA transport and the translational inhibition of MBP synthesis, while efficient MBP granule assembly and translocation render *Oli-neu* and primary oligodendrocytes potent systems to study MBP mRNA metabolism.

4.2 Sequence analysis of MBP mRNA predicts secondary structures and a global RBP association profile

The mRNA fate in the cell is basically determined by the association with defined proteins to form mRNP complexes that dynamically accompany the mRNA during its life cycle from transcription to decay. The genomically encoded mRNA sequence harbors intrinsic binding motifs and secondary structures, mediating RNP complex formation. Software-based prediction of RNA secondary structures by the RNAfold server (Gruber et al., 2008) revealed conserved secondary structures in MBP mRNA (Figure 3-3). Although sequence-based algorithms neglect the influence of RNA-associated factors, they can still provide insight into

potential structures of nascent RNAs. Adjacent complementary sequences favor the formation of hairpin loops and long stretches of potential base-pairing are likely to define subdomains in the RNA molecule. Interestingly, most motifs implicated in RNA transport and translational regulation in the 14-kDa MBP 3'UTR are located in a distinct "branch" (Figure 3-3, A). In contrast, the presence of MBP exon 2 in 17.22-kDa-MBP interferes with this secondary structure (Figure 3-3, C), favoring alternative folding properties. Intramolecular interactions between the variable CDS and the MBP 3'UTR, altering overall secondary structures in an isoform-dependent manner, might allow the association of different RNA-binding factors thus leading to an isoform-specific localization and regulation of MBP mRNAs (de Vries et al., 1997). The exposed localization of the A2RE in the distal part of the "branch" is compatible with the interconnection to the microtubule cytoskeleton via kinesin motors (Carson et al., 1997), or a TOG/hnRNP A2-dependent RNA multiplexing (Carson et al., 2008; Kosturko et al., 2005) and might be less effective in exon 2-containing 17.22-kDa MBP, which does not show this predicted structural subdivision. hnRNP A2 has been reported to bind a ssRNA motif (Shan et al., 2000) and since secondary structures in the distal part show a very low basepairing probability, the ssRNA A2RE motif seems more accessible for trans-acting factors like hnRNP A2 (Hoek et al., 1998) or CBF-A (Raju et al., 2008). Furthermore, the binding site of the MBP-silencing sncRNA-715 (Bauer et al., 2012) is predicted to lie within a conserved hairpin loop (Figure 3-3, A), suggesting stem loop formation as a potential mechanism regulating binding of this small non-coding RNA.

Secondary structures and binding motifs are a prerequisite for RNA-associating factors, but the local concentration of RBPs and the accessibility of their corresponding binding sites finally determine the formation of the RNP complex. Modification of RBPs (e.g. phosphorylation) or co-association of cooperative interaction partners can alter RNA-binding affinity and dynamically influence the RNP composition (Huttelmaier et al., 2005; White et al., 2008). As introduced in Chapter 1.3.3, distinct binding motifs and interacting molecules have already been identified as associating with MBP mRNA (Figure 1-6). In addition, the RBPmap server (Paz et al., 2014) was used to predict potential binding sites in MBP mRNA from available CLIP-seq libraries, revealing an unbiased global association profile of selected RBPs (

Figure 3-2). In the interactive diagram provided in Microsoft Excel 2014, predicted binding sites can be linked to the annotated regions of MBP mRNA. The predictions did not match with the known binding sites for hnRNP A2, hnRNP E1, or hnRNP K (Munro et al., 1999; Torvund-

Jensen et al., 2014), because motifs used in the prediction differ from the MBP-specific A2RE/K-motifs. The motifs are rather based on a large scale analysis of RNA association *in vivo* and could hint to functionally relevant global RBP association profiles. The lack of predicted binding sites around the A2RE might for example indicate a predominant association of hnRNP A2-based RNP complexes, which evolutionary excluded the binding of common RBPs in this area. In close proximity downstream to the snRNA-715 site, a binding site for PCBP1/hnRNP E1 is predicted, potentially linking the binding of hnRNP E1 to the snRNA-715-mediated translational inhibition (Bauer et al., 2012; Kosturko et al., 2006). Ongoing improvement of bioinformatical tools, including data from an increasing number of novel CLIP-seq experiments in relation with miRNA-binding prediction and secondary structure information would open possibilities to study the composition of MBP-associated RNP complexes *in silico* with increasing accuracy.

4.3 MBP mRNA labeling using the MS2-system

RNA labeling with MS2-loops has advanced to a commonly used technique to study RNA dynamics and MS2-labeling of MBP mRNA offers the opportunity to study transport dynamics and localization to the myelin compartment in living cells. The cloning, expression and the creation of stable cell lines moderately expressing the MBP14-MS2 transcript has been accomplished (Figure 3-4) facilitating its use in various experimental setups. The assembly of transport granules is a prerequisite for MBP14-MS2 localization to the processes of the cells and suggests a successful formation of RNP complexes, despite the presence of the artificial MS2-loops. Even if the transcript can be shown to be localized to distal processes up to 60 μm from the soma reminiscent of endogenous MBP smFISH (Figure 3-1 & Figure 3-4), initial attempts to visualize the message with fluorescently labeled MCPs were not successful. Possible reasons converge on the inability to detect a granule-specific GFP signal and better signal-to-noise ratios are needed to overcome the background fluorescence of unbound MCP-GFP. Generation of cell lines stably expressing both constructs could help to ensure appropriate levels of MBP mRNA and MCP-tagged protein and establishment of live cell imaging might reduce influences arising from the fixation procedure. Recently, modifications and improvements of the MS2 system have been developed. Split-GFP molecules, used in a combination with MS2 and PP7 labeling (Wu et al., 2014) or the generation of new

synonymous MS2-loops (Wu et al., 2015) could be used to improve the visualization of MBP mRNA in living cells.

4.4 MS2-based affinity purification of MBP14-MS2-associated factors

In addition to the visualization of mRNAs in living cells, MS2-labeled MBP mRNA can be used to isolate associated mRNP complexes and has been used here to analyze the dynamic MBP mRNP complex composition during oxidative stress. MS2 *in vivo* biotin-tagged RNA affinity purification (MS2-BioTRAP) has previously been used to capture *in vivo*-assembled IRES-interacting protein complexes with a MCP coupled to an HTBH-tag (Tsai et al., 2011). A similar approach named RaPiD (RNA-binding protein purification and identification) was developed in yeast and yielded the coexistence of different RNA species within the same RNP complex (Slobodin and Gerst, 2010). Here, the MCP-HTBH (Tsai et al., 2011) was used to purify RNP complexes from MBP14-MS2 stable cell lines (Figure 3-5, A-B) and yielded efficient pulldown of tagged MBP14 mRNA (Figure 3-5). Lack of exon 2-containing isoforms in the pulldown acts as an endogenous control, and additionally hinted against a prevalence of multiplexed MBP mRNAs (Carson et al., 2008) in the granules, but could also be due to a stoichiometrically lower abundance of the endogenous isoforms. Several previously described MBP mRNA-associated proteins were co-purified and validated via Western blot, including hnRNP A2, hnRNP F and DDX5 (Figure 3-5 & Figure 3-6), indicating an appropriate specificity of the affinity purification. To elucidate the MBP mRNP composition in a more unbiased way, we decided to aim for a global proteomic approach. With the expertise in RBP isolation by aptamer-tagged RNA motifs as bait and SILAC-based quantitative proteomics (Butter et al., 2009), isolation and mass spectrometric analysis of MBP mRNA complexes were performed in collaboration with Falk Butter (Proteomics Core Facility, IMB Mainz). Association of MBP mRNA to oligodendroglial stress granules (Thomas et al., 2005; Wang et al., 2010) and stress induced perinuclear aggregation of MBP14-MS2-labeled RNAs (personal communication, Constantin Gonsior) suggested that we could examine stress-associated MBP mRNP complex remodeling to evaluate the method.

4.5 MBP14-MS2 affinity purification yields novel targets in stress-dependent MBP mRNP complex remodeling

More than 700 targets could be identified in the pulldown experiments during stressed and unstressed conditions, including a repertoire of common RNA-binding proteins and proteins previously not connected to RNA metabolism. The largest fraction, according to GO terms, belongs to the group of nucleic acid-binding proteins (Figure 3-9), suitable to the experimental setup. The results most probably display a subfraction of the MBP mRNA-specific interactome since the 5'UTR lacking MBP14-MS2 message does not undergo endogenously regulated transcription, is not spliced due to the lack of introns and a crosslinking step was not included in the experiments. Nevertheless, factors known to associate with the MBP 3'UTR were co-purified (Table 3-3) and the recruitment of the MS2-tagged mRNA to G3BP1-positive SG under oxidative stress conditions shows that this RNP composition is sufficient to yield discrete localization of the RNA (Figure 3-8). Moreover, although it may include proteins which bind unspecifically, SILAC-based mass spectrometry highlights specific differences between the defined experimental conditions, using internal normalization procedures.

Oxidative stress massively decreases the translation rates of most mRNAs in the cell and sorting into stress granules (SG), P-bodies (PB) or yet undefined RNPs goes hand in hand with an extensive RNP remodeling, orchestrating mRNA maintenance, storage, translation, or decay (Anderson and Kedersha, 2009a). In our experiments, SILAC Ratios (SR) of numerous ribosomal proteins were <1 , demonstrating a reduced association with MBP mRNA under stress conditions and possibly reflecting decreased translation rates of MBP. The concurrent enrichment of known SG components of the eIF3 complex, PABP-C1, TDP43, Fmr, Fxr1/2, Y-box-binding proteins 1-3, or components of the DDX6/CCR4-NOT silencing complex (Buchan and Parker, 2009), indicate instead the recruitment of stress-related complexes to MBP mRNA.

The MBP mRNA-binding hnRNP A2 has previously been described to associate with SG in oligodendrocytes (Gonsior, 2011) and a SR of 0.96 ± 0.32 indeed indicates that it remains associated with MBP mRNA under oxidative stress conditions, similar to PCBP1/hnRNP E1 (SR 1.46 ± 0.22) and hnRNP F (SR 1.70 ± 0.07), which were only slightly enriched. The MBP mRNA-associated protein hnRNP K (Laursen et al., 2011), which exhibited enriched binding during stress (SR 2.17 ± 0.09) has also been reported to participate in SG formation before (Fukuda

et al., 2009). However, a convenient role in the stress-mediated silencing of MBP remains to be elucidated, since in previous studies hnRNP K promoted rather than inhibited MBP translation (Laursen et al., 2011; Torvund-Jensen et al., 2014). Surprisingly, another stress granule-associated RNA-binding protein, Serbp1 (Lee et al., 2014) displayed the lowest SR observed ($SR\ 0.41 \pm 0.03$), indicating a dissociation from constitutive MBP mRNPs with a possible competing function in SG.

Most targets identified have not been previously connected to RNA metabolism or the formation of stress-induced mRNPs and may thus represent novel candidates playing a role in SG and MBP biology. The enrichment of Sumo2 ($SR\ 3.07 \pm 1.86$) indicates a stress-dependent sumoylation of MBP mRNA-associated proteins and the presence of the proteasomal subunit Psm2 ($SR\ 2.79 \pm 0.27$) may link RNA decay with protein degradation of damaged or dispensable RBPs during oxidative stress. The molecular function of Trmt2a ($SR\ 9.15 \pm 0.84$) is not known, but it shares homology with RNA methyl transferase domains (Guarguaglini et al., 1997). Several cytoskeleton-associated proteins are enriched under oxidative stress conditions (Table 3-1; Coro1c, Flna, Pdim5, Tns3, Flnb, Actn4). SG and PB are highly dynamic structures that rely on the interaction with an intact cytoskeleton, permitting assembly, coalescence, movement, disassembly and the rapid exchange of factors in and out of the granules (Aizer et al., 2008; Bartoli et al., 2011; Rajgor and Shanahan, 2014). F-actin-based motors Myosin H9 ($SR\ 1.45 \pm 0.71$) and Myosin L6 ($SR\ 1.36 \pm 0.28$), as well as the MT based motor dynein ($SR\ 1.40 \pm 0.08$) were slightly augmented during oxidative stress, possibly mediating retrograde transport of remaining MBP mRNA towards SG or PB.

The highly enriched Coronin-1C ($SR\ 14.52 \pm 4.98$) is a modulator of the actin network (Xavier et al., 2012; Ziemann et al., 2013) and co-localizes with actin filaments in perinuclear areas in Pop10 cells (Xavier et al., 2012), strongly reminiscent of the characteristic arrangement of SG around the nucleus. A potential function of actin-binding proteins could include the tethering of SG components to the local cytoskeleton or altering overall filament dynamics allowing the exchange of factors in and out of the granules. SG components have been identified in pathologic inclusions and SG persistence has been claimed to be a seeding point for aberrant protein aggregation in ALS (Li et al., 2013). In line with this, ALS-linked mutations in the actin-binding protein Profilin-1 alter stress granule dynamics, possibly linking pathogenic protein aggregation in ALS to actin cytoskeleton dynamics (Figley et al., 2014). Another well-known protein playing a role in the ALS pathogenesis and found targeted to MBP14-MS2 mRNA

during oxidative stress (SR 3.06 ± 0.31), is TDP43 (Colombrita et al., 2009; Lee et al., 2012a). Appearance of TDP43 inclusions in OL correlates with neuronal degeneration in the spinal cord (Brettschneider et al., 2014) and recruitment to MBP mRNA, which is highly abundant during myelination, might favor the aggregation properties in the cell. Myelination, as a system highly dependent on mRNA transport and local translation of MBP mRNA, could easily be affected by a dysregulation of the RNA metabolism, which has been proposed to be an important factor in a growing number of neurodegenerative diseases. Several candidates have been connected to disease before: Pdim5/ENH is associated with schizophrenia and bipolar disorders (Carter, 2007; Kato et al., 2005), Trmt2a/HTF9C with schizophrenia (Liu et al., 2007), Gtf2i with autism-related Willms–Beuren syndrome (Meyer-Lindenberg et al., 2006; Sakurai et al., 2011) and FMRP, Fxr1 or Fxr2 with Fragile X mental retardation syndrome (Santoro et al., 2012; Spencer et al., 2006). The link between these proteins and the regulation of MBP mRNA could indicate an oligodendroglial contribution to the respective pathology. FMRP has previously been linked to MBP mRNA repression (Li et al., 2001; Wang et al., 2004), but myelin abnormalities of FXS patients could not be recapitulated in FMR1-KO mice (Giampetruzzi et al., 2013). Since FMRP associates with MBP14-MS2 mRNA during oxidative stress (SL 4.30 ± 0.39), the role of FMRP in oligodendroglial stress granules might contribute to the observed myelin defect and a higher susceptibility of FXS patients to stress could explain the discrepancy between mice and men.

Taken together, a novel RNA-centric affinity purification method of RNP complexes associated with MBP mRNA under oxidative stress conditions has led to numerous candidates potentially playing a role in stress-dependent RNA granule formation and the regulation of MBP metabolism. Nevertheless, validation experiments with different independent methods are essential to clarify the role of the promising candidates in the regulation of MBP synthesis.

4.6 FUS contributes to maintaining MBP mRNA levels in health and disease?

FUS has been identified as an hnRNP A2-interacting protein in oligodendroglial cells, potentially associating with MBP mRNA (White, 2007). FUS was verified as associating with hnRNP A2 in an RNA-dependent manner (Hoch-Kraft, 2010). Three FUS binding sites are predicted in MBP mRNA (

Figure 3-2) and the protein has been implicated in neuronal mRNA localization before (Elvira et al., 2006; Fujii et al., 2005; Kanai et al., 2004), making it a likely contributor to the

posttranscriptional regulation of MBP. Against expectation, FUS could not be detected in MBP14-MS2 affinity purifications in normal or stressed conditions (Figure 3-5, Figure 3-6, Chapter 3.3.4). However, immunocytochemistry shows a co-localization with the SG marker TIA-1 in *Oli-neu* cells (Figure 3-22) and FUS knockdown slightly, but consistently, decreases levels of MBP mRNA in oligodendroglial cells (Figure 3-19, F; Figure 3-21, B). In contrast, destabilization of MBP mRNA during mild oxidative stress (0.1 mM arsenite) correlates with the upregulation of FUS protein and can be rescued by siRNA knockdown of FUS (Figure 3-23, C). As a multifunctional protein, FUS might fine-tune MBP expression by several independent transcriptional or posttranscriptional mechanisms. High-throughput sequencing of FUS-associated RNAs and FUS-knockout mice revealed a broad impact on cellular gene regulation and splicing (Lagier-Tourenne et al., 2012). FUS knockdown in primary oligodendrocytes also decreased levels of hnRNP A2 (Figure 3-19, E) and robustly elevates DDX5 protein (Figure 3-19, Figure 3-21, Figure 3-23). In addition, alternative splicing of hnRNP K and Fyn is affected in FUS-KO mice (Lagier-Tourenne et al., 2012) thus displaying several possibilities to regulate MBP expression.

Mutated FUS and the aberrant formation of stress granules has been linked to familiar cases of ALS (Kwiatkowski et al., 2009; Vance et al., 2009), but an involvement of oligodendrocytes, even though myelin defects have been reported (Kwiatkowski et al., 2009), has not been addressed so far. Since oligodendroglial death precedes the onset of neurodegeneration in mutant SOD mice (Kang et al., 2013) a putative impact of misbalanced FUS levels in oligodendrocytes could contribute to an RNA-related pathology. Impeding MBP expression or misregulated splicing of other myelin genes, like MOBP or MAG (Lagier-Tourenne et al., 2012) could lead to a substantial, FUS-related myelin defect. However, the role of FUS in oligodendrocytes still largely remains to be elucidated and might help to better understand mechanisms driving ALS pathogenesis or myelination in general.

4.7 DDX5-containing cytoplasmic RNP complexes in oligodendrocytes

DDX5 has been identified as an interaction partner of oligodendroglial hnRNP A2, potentially associating with MBP mRNA (White, 2007) and initial experiments (Gonsior, 2011; Hoch-Kraft, 2010) have been pointing to a role of DDX5 in the posttranscriptional regulation of MBP. During this project, the influence of DDX5 in oligodendroglial cells was further addressed and

revealed the contribution to diverse processes of posttranscriptional gene regulation in oligodendrocytes.

DDX5 has been reported to be included in cytoplasmic RNA granules in the brain by several groups (Elvira et al., 2006; Kanai et al., 2004; Miller et al., 2009; Shelkovernikova et al., 2014) which raised the question of an association with MBP mRNA granules in oligodendrocytes. Indeed, in immunoprecipitates of DDX5 the association with MBP mRNA could be validated (Figure 3-11) and the use of different immunoprecipitation methods from primary oligodendroglial or *Oli-neu* cells strengthens this observation. DDX5 has been co-precipitated with hnRNP A2 and vice versa before (Gonsior, 2011). Here, although in DDX5 pulldowns MBP mRNA was enriched, hnRNP A2 protein was not detectable (Figure 3-11). Lack of hnRNP A2 in the DDX5 immunoprecipitation could simply be due to detection limitations (sensitivity of the EF67 antibody) or might indicate the presence of hnRNP A2-independent MBP mRNA-associated RNP complexes in the cytoplasm, whereas such subpopulations of MBP mRNA-containing granules have not been described so far.

Immunofluorescence staining of DDX5 verifies a cytoplasmic distribution that resembles the granular staining of hnRNP A2, but co-staining only occasionally shows a close association of both proteins in oligodendroglial processes (Figure 3-12). Assuming a concerted association with MBP mRNA, recognition of the proteins buried in RNA granules could be limited by masking of the antibody epitopes, preventing access to both components in one densely packed granule simultaneously. Similarly, β -actin mRNA access by in situ hybridization is limited in neuronal transport granules and can be unmasked by neuronal activity (dendritic stimulation), leading to the remodeling of the granule (Buxbaum et al., 2014). The secondary structure prediction of MBP mRNAs (Figure 3-3), resulted in the exposure of the A2RE to distal regions of the folded mRNA and the proposed multiplexing to TOG (Kosturko et al., 2005) also necessitates a given accessibility of the associated hnRNP A2. A binding site of DDX5 is not known and might be hidden in the core of the MBP mRNP, less accessible for antibodies during immunofluorescence or immunoprecipitation. This hypothesis would imply that DDX5-positive granules represent RNP complexes which have undergone remodeling, leading to an exposure of the protein and allowing the visualization and pulldown of the complex. The nature and function of granule-associated DDX5 remains unclear and does not exclude a simultaneous role in multiple RNP complexes. Since numerous mRNAs seem to be localized (Lecuyer et al., 2007), certainly also in oligodendrocytes, the total pool of RNA granules is likely

to be heterogeneous, with only a small fraction containing MBP mRNA. Underlining this notion, hnRNP A2 or DDX5 positive granules (Figure 3-12) are far more abundant than MBP smFISH signals (Figure 3-1) in *Oli-neu* cells and the potential granule heterogeneity demands a more MBP mRNA-centric mode of analysis. A technically challenging high resolution smFISH in combination with immunofluorescent visualization of RBPs would be an indispensable tool to discriminate individual MBP mRNA subpopulations in oligodendrocytes and adding a temporal resolution could also identify dynamic processes during the MBP mRNA lifespan. Both could be achieved by live cell imaging of labeled MBP mRNA and corresponding fluorescently labeled RBPs, including DDX5 and hnRNP A2, on the way to the myelin compartment using the here established MBP-MS2 system.

Size fractionation of RNA granules via Optiprep density gradients (Fritzsche et al., 2013) moreover revealed divergent distributions of DDX5 and hnRNP A2. DDX5 accumulates in two independent RNA-enriched fractions, whereas at least in primary OL co-sedimentation of hnRNP A2 or RPLP0 seems to be mutually exclusive (Figure 3-13, B). The focused RPLP0 distribution is reminiscent of monosomal peaks in polysome profiles and the absence of hnRNP A2 suggests that it is not present in complexes including large ribosomal subunits, consistent with the translationally silent state of RNA transport granules. On the other hand, MBP transport granules have been reported to contain components of the translational machinery (Barbarese et al., 1995), allowing immediate translation at the axonal contact site. DDX5 has been proposed to be associated with various protein complexes, accounting for its multifunctionality in the cell (Ogilvie et al., 2003). The abundance of DDX5 in the “monosome fractions” could indicate an mRNA association along with 80S ribosomes, potentially regulating translation initiation, elongation or bridging termination to posttranslational mRNA remodeling events, in addition to hnRNP A2-containing, RPLP0-negative, transport granules. However, a presence in the same fraction does not necessarily imply a physical interaction of the proteins and could well be dependent on the inclusion in individual RNP complexes with similar sedimentation properties. In contrast, absence of a factor in a given fraction suggests that it is unlikely to contribute to a presumed complex. In summary, the nature of DDX5-containing MBP mRNA granules remains to be elucidated, a proteomic approach to identify components of DDX5 containing RNP complexes would be valuable, possibly reflecting the confinement to multiple complexes regulating MBP. Optiprep fractionation and subsequent immunoprecipitation allows a two-step purification method to identify RBP interactomes and

revealed an unexpected heterogeneity in RNP complex composition of neuronal transport granules (Fritzsche et al., 2013). The method could also be applied to precisely define hnRNP A2- or DDX5-containing MBP granules in a fraction-based manner. Preferably, in a more RNA-centric approach, pulldown of MS2-tagged MBP mRNA would allow the biochemical separation of distinct macromolecular complexes and would be a powerful tool to elucidate subpopulations of MBP mRNA-associated RNP complexes according to their sedimentation properties.

4.8 DDX5 inhibits MBP expression at the posttranscriptional level

To study effects of DDX5 in oligodendroglial cells, siRNA targeting DDX5 was used to diminish DDX5 expression in primary oligodendrocytes. The timeframe examined comprises 3 days of differentiation *in vitro*, defining an early stage of OL development where MBP expression starts, but late OL proteins like MOG are not yet apparent. Expression profiles of DDX5 suggest a high expression in early OL, declining with ongoing differentiation (Figure 3-10). Consequently, DDX5 modulation might particularly affect mechanisms regulating early OL development. The efficient knockdown of DDX5 selectively elevates expression of MBP in primary oligodendrocytes (Figure 3-14). At this early OL stage, 17-kDa-MBP is the predominant isoform expressed, also accounting primarily for the observed increase in total MBP levels (Note, that the isoform specific effects will be discussed in a separate chapter). Overexpression of myc-tagged DDX5 in more mature primary OL, decreases the expression of several myelin proteins, including MBP (Figure 3-17, C+D). In contrast, transfection of mutant DDX5^{K144N} did not cause a comparable impact on MBP, indicating that this decrease of MBP is dependent on the DDX5 helicase activity (Figure 3-17, C+E). Importantly, RNA quantification did not show overall changes in myelin gene expression (Figure 3-17, F+G), excluding an effect on oligodendroglial differentiation in general and clearly pointing to an inhibitory role for DDX5 at MBP synthesis on the posttranscriptional level. Unfortunately, luciferase assays measuring translational output of an MBP 3'UTR-containing reporter construct did not provide reliable results, due to a massive impact on intrinsic mRNA expression of the *renilla* and *firefly* luciferase reporters. Various factors, including androgen receptors (AR) and Ras-signaling, have been shown to affect the constitutive expression of *renilla* luciferase reporters (Shifera and Hardin, 2010), and might explain the variations dependent on DDX5 manipulation (Camats et al., 2008; Clark et al., 2008a).

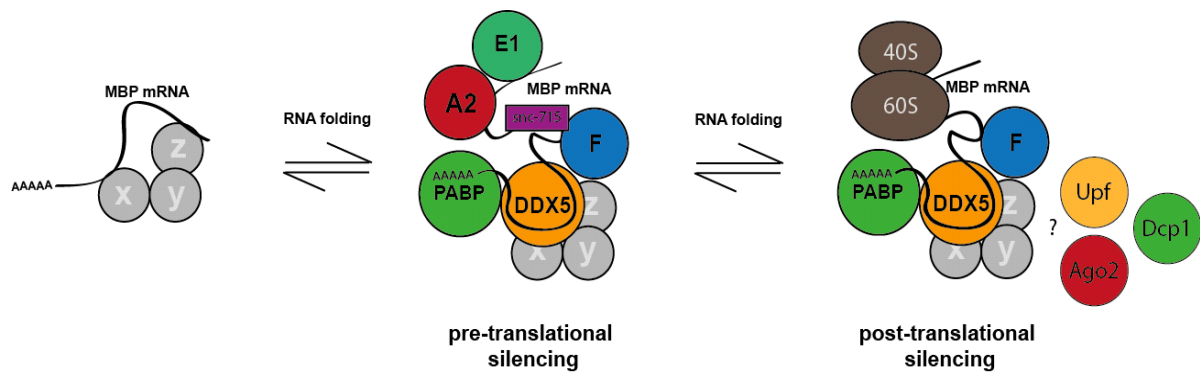


Figure 4-1. Working model of DDX5-mediated MBP silencing mechanisms.

Modulation of MBP mRNA secondary structures might lead to a dynamic association of MBP mRNA-associated factors, realizing inhibition of MBP protein expression. Details are described in the text. x, y, z = unknown factors. Upf = proteins of the NMD pathway; Dcp1 = proteins of the Decapping machinery; Ago2 = RNP complexes mediating non-coding RNA-dependent silencing or storage.

As an RNA helicase, DDX5 is capable of remodeling RNP complexes in the cell by generally modulating dsRNA formations frequently occurring in RNA secondary structures. Unwinding areas of dsRNA may permit or disrupt the association of RNA-binding factors, like RBPs or non-coding RNAs. The first step in remodeling the MBP RNP complex in the cytoplasm is during the assembly of transport granules in the perinuclear area after nuclear export (Ainger et al., 1993). Rearrangement and multiplexing of MBP RNP complexes leads to the formation of localization-competent granules that can travel along the microtubule cytoskeleton, in a translationally silent state (Carson et al., 2001). Since DDX5 knockdown in *Oli-neu* cells, as well as primary OL did not seem to alter the MBP mRNA or protein localization, the transport capability of the granule per se seems independent of DDX5 function. A well-studied factor mediating translation inhibition during MBP mRNA translocation is hnRNP E1 (Kosturko et al., 2006), associating with MBP mRNA in a fashion presumably dependent on hnRNP A2 and at least recognizing two binding motifs in the MBP 3'UTR (Torvund-Jensen et al., 2014). A DDX5-dependent unwinding of the RNA secondary structure might favor binding of hnRNP E1 (and/or additional inhibitors), securing the translationally silent state of MBP mRNA granules. Important mediators of translational inhibition are also small non-coding RNAs that mediate binding of RNA-induced silencing complexes (RISC) to target sequences in the mRNA. DDX5 is implicated in controlling parts of miRNA biogenesis as a component of nuclear DROSHA complexes (Fukuda et al., 2007), and has also been shown to influence miRNA expression levels on the transcriptional level (Dardenne et al., 2014). In a hypothetical scenario, DDX5

might also be involved in the targeting of the miRNAs to the mRNA binding site. In the MBP 3'UTR, the binding site for sncRNA-715 is located on a potential stem loop (Figure 3-3), regulating MBP expression (Bauer et al., 2012). DDX5 unwinding might open the dsRNA stem, allowing the recognition of the antisense sncRNA-715 and thereby mediating the RNA-based translational silencing. In addition, the predicted binding site for hnRNP E1 in the immediate vicinity (Fig 3-2) could contribute to the assembly of this silencing complex.

Furthermore, the translational silencing has to be maintained during ongoing RNP transport, although the granular structure could be modified on the way. A consecutive step of remodeling is thought to happen at process branch points, since knockdown of hnRNP K leads to accumulation of MBP transcripts at these areas (Laursen et al., 2011) where replacement of hnRNP E1 with hnRNP K is proposed to occur (Torvund-Jensen et al., 2014). It is tempting to speculate that the exchange from hnRNP E1 to hnRNP K represents a switch in transport at branchpoints that correlates with the translocation into compacted myelin sheets dependent on the RLR region in the MBP 3'UTR (Ainger et al., 1997), and hnRNP K is a part of this complex. If hnRNP E1 is released during this remodeling step, DDX5 might maintain translational silencing by recruiting translational silencers taking over hnRNP E1 function. The most important remodeling step occurs at the axoglial interface. Activation of Fyn kinase leads to phosphorylation of granule components hnRNP A2 and F, remodeling the granules towards translation initiation and MBP synthesis (Muller et al., 2013; Wake et al., 2011). DDX5 might act as a direct inhibitor of translation and also the co-sedimentation with RPLP0 in the Optiprep density gradient centrifugation may hint to an association with ribosomes.

The posttranslational fate of MBP mRNA has not been addressed in any study but also has to be tightly controlled to realize appropriate MBP synthesis in a spatiotemporal manner. This regulatory step is especially important for MBP expressed in the perinuclear cytoplasm, including exon 2-containing isoforms to prevent excessive translation in these areas. After translation the mRNA can be stored or degraded by remodeling of the MBP RNP complex. Interestingly, DDX5 has been reported to bind transcripts after their first round of translation and preferentially mRNAs with long 3'UTR are regulated by corresponding physiological NMD mechanisms (Geissler et al., 2013). Furthermore, DDX5 is co-localizing with Ago-2 in P-bodies of HeLa cells, hinting to a role in translational repression of mRNAs (Geissler et al., 2013). Live video microscopy in hippocampal neurons revealed docking of neuronal transport granules and P-bodies and assumed that P-bodies represent transient sites of mRNA storage in

dendrites that can be dissolved in response to synaptic activity (Zeitelhofer et al., 2008). The adjacent localization of DDX5 and hnRNP A2 (Figure 3-12, C) could be a hint to a similar interaction mechanism of RNP granules in the periphery of the cell, possibly balancing proportions of actively transported and locally stored RNA granules. Alternatively, DDX5 might associate after initial rounds of MBP translation, guiding the mRNA fate towards translational repression or decay.

The cytoplasmic association of DDX5 with MBP mRNA (Chapter 3.4.2) hints to a direct role in the posttranscriptional regulation of MBP expression, but does not exclude additional indirect effects on top. Accordingly, hnRNP A2 and hnRNP F that have been shown to play essential roles in the regulation of MBP synthesis (White et al., 2012; White et al., 2008) were concurrently reduced by DDX5-siRNA treatment (Figure 3-14, D). Nevertheless, decreased levels of hnRNP A2 and hnRNP F would rather be expected to result in an impairment of MBP synthesis, contradicting the here observed effects. DDX5, as an extraordinary multifunctional protein, may regulate MBP expression by multiple posttranscriptional mechanisms and its precise role remains to be elucidated.

4.9 DDX5 as a factor regulating alternative splicing in oligodendrocytes?

DDX5, as a prototypical DEAD box helicase, has been shown to determine cellular gene expression on various levels and recently has been proposed to orchestrate signaling pathways (Samaan et al., 2014) and whole cell differentiation programs (Dardenne et al., 2014), coordinately regulating transcription, miRNA biogenesis and splicing patterns.

The observed inverse switch in expression of MBP isoforms after the manipulation of DDX5 levels (Figure 3-15, D-F; Figure 3-17, G), hints to a regulatory role of DDX5 in alternative splicing of MBP exon 2. Although alternative splicing has been identified as a source for the developmentally regulated expression of the MBP isoforms (de Ferra et al., 1985), until today nothing is known about mechanisms regulating splicing decisions. In general, alternative splicing is mediated by the selective assembly of the spliceosome at core splicing motifs (5' and 3' splice sites, branch point, polypyrimidine tract), surrounding the variable exon. Association of trans-acting factors at exonic/intronic splicing enhancer or silencer sequences determines the exon-specific spliceosome assembly, and combinatorial or competitive association of activators and inhibitors leads to exon inclusion or skipping into the mature mRNA, respectively.

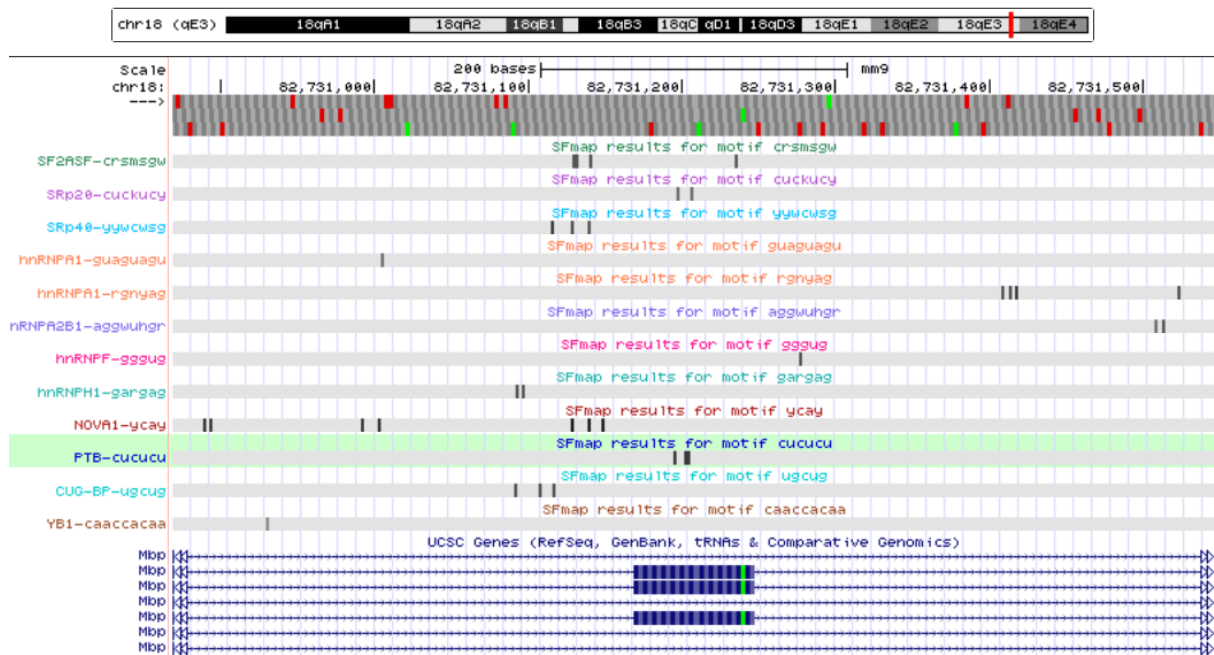


Figure 4-2. Prediction of splicing factor binding sites in MBP exon 2-surrounding regulatory regions.

The SFmap server (Paaz) was utilized to map binding sites of known splicing factors and their consensus motifs to murine MBP exon 2 with a flanking intronic region of 300 bp. The graphical output in the UCSC genome browser displays binding sites (black boxes) in the context of MBP exon 2 (blue boxes).

Sequence analysis of MBP exon 2 and its flanking intronic regions yields predicted binding sites of silencing factors (e.g. PTB, hnRNP A1), stimulating SR proteins (e.g. SC35, SF2ASF, SRp20, SRp40) and additional splicing regulators (e.g. hnRNP F/H, hnRNP A2B1, NOVA1, CUG-BP) in the regulatory regions around MBP exon 2 (Figure 4-2). DDX5 with its capability to alter RNA secondary structures could alter the balance of the silencing and stimulating factors associating with their corresponding binding motifs and knockdown of DDX5 consequently could promote spliceosome assembly leading to inclusion of MBP exon 2 into the mature mRNA. In H-Ras splicing, DDX5 knockdown favors inclusion of the exon IDX, by affecting RNA stemloop accessibility for hnRNP H (Camats et al., 2008). Global splicing pattern analysis in myoblasts and epithelial cells defined a huge number of “Class I” exons, which are included after DDX5/17 knockdown and commonly converge on hnRNP F/H splicing targets (Dardenne et al., 2014). In oligodendrocytes, global expression profiling and alternative splicing events regulated by hnRNP H/F pointed to a regulation of targets implicated in the transition from oligodendrocyte progenitor cells to oligodendrocytes (Wang et al., 2012). Similarly, components of MBNL1 splicing complexes from human myoblasts include hnRNP H, F, A2/B1, K, L, DDX5, DDX17, and DHX9 (Paul et al., 2011) and link DDX5-mediated splicing to several RBPs also relevant in the posttranscriptional regulation of MBP mRNA. In several reports the regulation of alternative splicing by DDX5 was dependent on its helicase activity, possibly

rearranging secondary structures at the 5' ss (Camats et al., 2008; Kar et al., 2011; Liu, 2002). Overexpression of DDX5 or the DDX5^{K144N} mutant both led to a comparable isoform shift in *Oli-neu* cells (Figure 3-17, J), indicating a regulatory mechanism independent of the helicase activity. Moreover, a comparable shift could not be recapitulated in more mature OL (Figure 3-17, F+G) and indicates that DDX5 might control alternative splicing only in immature oligodendrocytes, consistent with the high expression levels of DDX5 in these cells (Figure 3-10). Phosphorylation status, subcellular localization or the presence of cooperative factors could influence DDX5 function and certainly further studies are needed to elucidate mechanisms controlling the DDX5-dependent shift in MBP isoforms. In addition, hnRNP A2 and hnRNP F were decreased in DDX5-siRNA experiments (Figure 3-14), so DDX5 might impact on splicing also by modulating the activity of splicing factors, modifying the pattern of MBP isoforms indirectly.

Interestingly, another member of the DEAD box helicases recently has been implied in myelination and regulation of MBP synthesis. DDX54 is expressed in OL, associates with MBP protein and MBP mRNA and DDX54 knockdown in the mouse brain led to a reduction of MBP in the corpus callosum (Zhan et al., 2013). In the DDX54-knockdown brains, 21.5-kDa MBP is selectively reduced and co-transfection of DDX54 with MBP isoforms in HEK cells selectively increases nuclear translocation of 21.5-kDa MBP (Ueki et al., 2012). The results reflect a reverse effect on MBP compared to DDX5 knockdown and suggest an interplay of diverse DEAD box helicases in controlling MBP at the posttranscriptional level, yet the contribution of additional helicases remains to be elucidated. Changes in the MBP isoform ratios have also been described in QKI-mutant and in Fyn knockout mice, loss of Fyn leading to a decrease in exon 2-containing isoforms (Lu et al., 2005) and loss of quaking shifting the ratio towards MBP exon 2-positive isoforms in the brain (Li et al., 2000), in analogy to the observed DDX5 effect. Regulation of the MBP isoform pattern, may hypothesize DDX5, DDX54, Fyn and Quaking acting in connected pathways, whereas the underlying mechanisms, including the precise role of exon 2-containing isoforms themselves, remains unsolved. MBP exon 2-positive isoforms have been shown to increase proliferation of oligodendroglial cells (Ozgen et al., 2014; Smith et al., 2013). Here, proliferation was assessed after DDX5-knockdown and led to increased numbers of Olig2+ and KI67+ oligodendroglial cells (Figure 3-16, A+C), albeit ratios of actively dividing oligodendroglial cells (KI67+/Olig2) were not significantly altered (Figure 3-16, D). The increase in total cell numbers might result from increased proliferation rates during earlier

development dependent on DDX5-knockdown, presumably leading to elevated levels of exon 2-positive MBP isoforms. In contrast, previous studies have suggested that DDX5 positively regulates cellular proliferation (Jalal et al., 2007; Yang et al., 2005a) thus potentially counteracting the proposed 21.5-kDa-MBP effect due to the lack of DDX5. Moreover, 21.5-kDa-MBP-induced proliferation has been reported to be dependent on a secreted factor (Smith et al., 2013) thus possibly broadening the postulated impact of exon 2-containing MBP isoforms.

4.10 The dual role of DDX5 in the regulation of MBP expression

Nuclear RNA modification events can determine the cytoplasmic RNA fate (Moore, 2005), e.g. the deposition of exon junction complexes (EJC) during splicing has been shown to influence translation (Nott et al., 2004). Another example for the coupling of splicing events to translational regulation is given by the splicing factor SF2/ASF, which can accompany mRNAs into the cytosol and activates translation of associated transcripts (Michlewski et al., 2008). Interestingly, a SF2/ASF binding site in MBP exon 2 has been predicted, possibly linking the presence of MBP exon 2 to translation and localization in the perinuclear cytoplasm. Moreover, the DDX5-related DEAD box helicase eIF4AIII, a core EJC component, remains associated with neuronal mRNA granules and regulates translation-dependent RNA decay (Giorgi et al., 2007). MBP mRNA, with an upstream ORF in the 5' UTR and its long 3'UTR, could possibly be a target of regulation by physiological NMD and DDX5 is a known regulator of this process (Geissler et al., 2013). A dual role of DDX5 in alternative splicing of MBP and the association with mature MBP mRNAs in the cytoplasm might thus reflect a coordinated regulation of these posttranscriptional mechanisms and thus link the inclusion of MBP exon 2 into the mature mRNA to transport and translational regulation of the different MBP isoforms. The role of MBP exon 2 in oligodendroglial biology still remains enigmatic, the nuclear localization indicates functions in gene regulation and the re-expression in remyelinating OPCs hints to important functions in early OL differentiation (Capello et al., 1997; Pedraza et al., 1997). The inhibitory function of DDX5 in MBP synthesis might also contribute to the proposed differentiation brake of OPCs, and downregulation of DDX5 during maturation (Figure 3-10, A-B) may be a factor to ramp up large scale production of MBP proteins. Consequently, targeting DDX5 function could not only increase translation of MBP, promoting myelination or remyelination, but also might induce MBP exon 2-dependent proliferation of surrounding

OPCs. Compounds known to target DDX5 function (Kost et al., 2015; Tanaka et al., 2011) could be used in further studies and might help to shed light on mechanisms that contribute to oligodendrocyte biology in a DDX5-dependent manner.

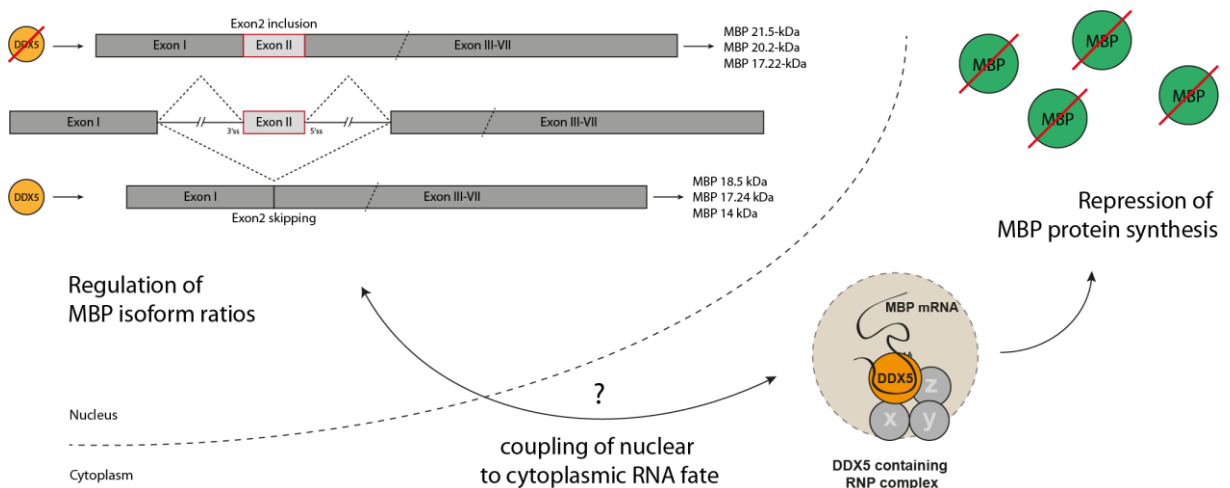


Figure 4-3. The dual role of DDX5 in the posttranscriptional regulation of MBP synthesis

Nuclear functions of DDX5 may alter MBP splicing decisions, favoring inclusion or skipping of MBP exon 2 and potentially link nuclear assembly of RNP complexes to the cytoplasmic repression of MBP protein synthesis. Details are described in the text.

4.11 Future Perspectives

Local synthesis of MBP occupies a key role in myelination not only in coordinating the compacted myelin membrane assembly (Aggarwal et al., 2011; Harauz and Boggs, 2013) and axonal wrapping (Zuchero et al., 2015), but possibly also in myelin maintenance and the transduction of neuronal activity into adaptive myelination due to local translation at the axoglial interface (Wake et al., 2011). Since overall absence of MBP (shiverer) leads to a severe dysmyelination phenotype, a focal misregulation might affect fine-tuning of the neuronal network activity, evoking problems in learning and memory or the manifestation of psychiatric diseases. Many pathologies already point to an oligodendroglial contribution (Ettle et al., 2015; Fields, 2008), and an exciting question would be the link to the Fyn-dependent posttranscriptional regulation of MBP, as a fundamental factor to control adaptive myelination mechanisms (Czopka et al., 2013; Wake et al., 2011). Redundancy and the polyvalent binding properties of most RBPs necessitate an RNA-centric analysis to assess the precise regulation of MBP mRNA. Thus, the established MBP-MS2 affinity purification system

could help to further decipher MBP mRNP complex dynamics orchestrating MBP synthesis and also to understand situations, where MBP synthesis is blocked (e.g. in stalled progenitors in MS-lesions). The MBP mRNP complex composition could be compared between numerous conditions, including stimulation with external cues (electrical activity, signaling molecules, stressors) or modulation of intracellular gene expression of related factors. Furthermore, the genetic modification of labeled MBP-MS2 constructs by mutational analysis of motifs or regions in the MBP 3'UTR, or the use of different MBP isoforms would allow to discriminate specific sets of associated RNA-binding proteins. In addition, co-purification of RNA species could illuminate multiplexed trafficking of mRNAs to the myelin compartment or the association of long or small non-coding RNAs regulating MBP synthesis. So far, MBP14-MS2 affinity purification under oxidative stress conditions has yielded several promising candidates potentially regulating MBP expression and might also help to shed light into general concepts of stress granule dynamics. In particular, candidates linked to psychiatric or neurodegenerative diseases have been identified and await further examination. Mutations in hnRNP A2 (Kim et al., 2013), FUS (Kwiatkowski et al., 2009; Vance et al., 2009) or TDP-43 (Sreedharan et al., 2008) already have been described to be causative for familiar forms of ALS and their connection to the regulation of MBP mRNA necessitates consideration of the oligodendroglial contribution to this disease pathology.

DDX5 has shown the capability to regulate MBP levels on the posttranscriptional level, but multifunctionality of the protein renders the identification of underlying mechanisms a challenging task. Direct association to MBP mRNA containing complexes may influence MBP synthesis dependent on the helicase-driven modulation of RNA secondary structures. A key aim will be to characterize the composition and corresponding biological role of the DDX5 containing RNP complexes and includes the elucidation of a possible MBP granule heterogeneity. In addition, studies should be extended to DDX17 that builds up heterodimers with DDX5 and has been shown to have redundant functions in the cell (Jalal et al., 2007; Ogilvie et al., 2003). Does DDX5 in cooperation with DDX17 act in a similar global way as in myocytes or epithelial cells (Dardenne et al., 2014), orchestrating differentiation programs from OPCs to mature OL thus implying a synergistic role of both proteins? To examine this and other questions, studies should also be translated into *in vivo* models. Interestingly, DDX5 protein is druggable (Kost et al., 2015; Tanaka et al., 2011) and can be targeted by compounds

already tested in human patients (Mahler et al., 2015) thus opening possibilities to study the role of DDX5 in myelination or remyelination *in vivo*.

References

- Aggarwal, S., N. Snaidero, G. Pahler, S. Frey, P. Sanchez, M. Zweckstetter, A. Janshoff, A. Schneider, M.T. Weil, I.A. Schaap, D. Gorlich, and M. Simons. 2013. Myelin membrane assembly is driven by a phase transition of myelin basic proteins into a cohesive protein meshwork. *PLoS biology*. 11:e1001577.
- Aggarwal, S., L. Yurlova, N. Snaidero, C. Reetz, S. Frey, J. Zimmermann, G. Pahler, A. Janshoff, J. Friedrichs, D.J. Muller, C. Goebel, and M. Simons. 2011. A size barrier limits protein diffusion at the cell surface to generate lipid-rich myelin-membrane sheets. *Developmental cell*. 21:445-456.
- Ainger, K., D. Avossa, A.S. Diana, C. Barry, E. Barbarese, and J.H. Carson. 1997. Transport and localization elements in myelin basic protein mRNA. *The Journal of cell biology*. 138:1077-1087.
- Ainger, K., D. Avossa, F. Morgan, S.J. Hill, C. Barry, E. Barbarese, and J.H. Carson. 1993. Transport and localization of exogenous myelin basic protein mRNA microinjected into oligodendrocytes. *The Journal of cell biology*. 123:431-441.
- Aizer, A., Y. Brody, L.W. Ler, N. Sonenberg, R.H. Singer, and Y. Shav-Tal. 2008. The dynamics of mammalian P body transport, assembly, and disassembly in vivo. *Molecular biology of the cell*. 19:4154-4166.
- Allen, N.J., and B.A. Barres. 2009. Neuroscience: Glia - more than just brain glue. *Nature*. 457:675-677.
- Allinquant, B., S.M. Staugaitis, D. D'Urso, and D.R. Colman. 1991. The ectopic expression of myelin basic protein isoforms in Shiverer oligodendrocytes: implications for myelinogenesis. *The Journal of cell biology*. 113:393-403.
- Anderson, P., and N. Kedersha. 2009a. RNA granules: post-transcriptional and epigenetic modulators of gene expression. *Nature reviews. Molecular cell biology*. 10:430-436.
- Anderson, P., and N. Kedersha. 2009b. Stress granules. *Current biology : CB*. 19:R397-398.
- Andersson, M.K., A. Stahlberg, Y. Arvidsson, A. Olofsson, H. Semb, G. Stenman, O. Nilsson, and P. Aman. 2008. The multifunctional FUS, EWS and TAF15 proto-oncoproteins show cell type-specific expression patterns and involvement in cell spreading and stress response. *BMC cell biology*. 9:37.
- Aulchenko, Y.S., I.A. Hoppenbrouwers, S.V. Ramagopalan, L. Broer, N. Jafari, J. Hillert, J. Link, W. Lundstrom, E. Greiner, A. Dessa Sadovnick, D. Goossens, C. Van Broeckhoven, J. Del-Favero, G.C. Ebers, B.A. Oostra, C.M. van Duijn, and R.Q. Hintzen. 2008. Genetic variation in the KIF1B locus influences susceptibility to multiple sclerosis. *Nature genetics*. 40:1402-1403.
- Bakhti, M., S. Aggarwal, and M. Simons. 2014. Myelin architecture: zippering membranes tightly together. *Cellular and molecular life sciences : CMLS*. 71:1265-1277.
- Baltz, A.G., M. Munschauer, B. Schwanhauser, A. Vasile, Y. Murakawa, M. Schueler, N. Youngs, D. Penfold-Brown, K. Drew, M. Milek, E. Wyler, R. Bonneau, M. Selbach, C. Dieterich, and M. Landthaler. 2012. The mRNA-bound proteome and its global occupancy profile on protein-coding transcripts. *Molecular cell*. 46:674-690.
- Barbarese, E., J.H. Carson, and P.E. Braun. 1978. Accumulation of the four myelin basic proteins in mouse brain during development. *Journal of neurochemistry*. 31:779-782.
- Barbarese, E., M.F. Ifrim, L. Hsieh, C. Guo, V. Tatavarty, M.J. Maggipinto, G. Korza, J.W. Tutolo, A. Giampetruzzi, H. Le, X.M. Ma, E. Levine, B. Bishop, D.O. Kim, S. Kuwada, and J.H. Carson. 2013. Conditional knockout of tumor overexpressed gene in mouse neurons affects RNA granule assembly, granule translation, LTP and short term habituation. *PLoS one*. 8:e69989.
- Barbarese, E., D.E. Koppel, M.P. Deutscher, C.L. Smith, K. Ainger, F. Morgan, and J.H. Carson. 1995. Protein translation components are colocalized in granules in oligodendrocytes. *Journal of cell science*. 108 (Pt 8):2781-2790.
- Baron, D.M., L.J. Kaushansky, C.L. Ward, R.R. Sama, R.J. Chian, K.J. Boggio, A.J. Quaresma, J.A. Nickerson, and D.A. Bosco. 2013. Amyotrophic lateral sclerosis-linked FUS/TLS alters stress granule assembly and dynamics. *Molecular neurodegeneration*. 8:30.
- Barres, B.A. 2008. The mystery and magic of glia: a perspective on their roles in health and disease. *Neuron*. 60:430-440.
- Barres, B.A., and M.C. Raff. 1994. Control of oligodendrocyte number in the developing rat optic nerve. *Neuron*. 12:935-942.

- Barres, B.A., and M.C. Raff. 1999. Axonal control of oligodendrocyte development. *The Journal of cell biology*. 147:1123-1128.
- Bartoli, K.M., D.L. Bishop, and W.S. Saunders. 2011. The role of molecular microtubule motors and the microtubule cytoskeleton in stress granule dynamics. *International journal of cell biology*. 2011:939848.
- Bates, G.J., S.M. Nicol, B.J. Wilson, A.M. Jacobs, J.C. Bourdon, J. Wardrop, D.J. Gregory, D.P. Lane, N.D. Perkins, and F.V. Fuller-Pace. 2005. The DEAD box protein p68: a novel transcriptional coactivator of the p53 tumour suppressor. *The EMBO journal*. 24:543-553.
- Bauer, N.G., C. Richter-Landsberg, and C. Ffrench-Constant. 2009. Role of the oligodendroglial cytoskeleton in differentiation and myelination. *Glia*. 57:1691-1705.
- Bauer, N.M., C. Moos, J. van Horssen, M. Witte, P. van der Valk, B. Altenhein, H.J. Luhmann, and R. White. 2012. Myelin basic protein synthesis is regulated by small non-coding RNA 715. *EMBO reports*. 13:827-834.
- Baumann, N., and D. Pham-Dinh. 2001. Biology of oligodendrocyte and myelin in the mammalian central nervous system. *Physiological reviews*. 81:871-927.
- Bayraktar, O.A., L.C. Fuentealba, A. Alvarez-Buylla, and D.H. Rowitch. 2015. Astrocyte development and heterogeneity. *Cold Spring Harbor perspectives in biology*. 7:a020362.
- Belly, A., F. Moreau-Gachelin, R. Sadoul, and Y. Goldberg. 2005. Delocalization of the multifunctional RNA splicing factor TLS/FUS in hippocampal neurones: exclusion from the nucleus and accumulation in dendritic granules and spine heads. *Neuroscience letters*. 379:152-157.
- Ben-Ari, Y., Y. Brody, N. Kinor, A. Mor, T. Tsukamoto, D.L. Spector, R.H. Singer, and Y. Shav-Tal. 2010. The life of an mRNA in space and time. *Journal of cell science*. 123:1761-1774.
- Bengtsson, S.L., Z. Nagy, S. Skare, L. Forsman, H. Forssberg, and F. Ullen. 2005. Extensive piano practicing has regionally specific effects on white matter development. *Nature neuroscience*. 8:1148-1150.
- Bercury, K.K., J. Dai, H.H. Sachs, J.T. Ahrends, T.L. Wood, and W.B. Macklin. 2014. Conditional ablation of raptor or rictor has differential impact on oligodendrocyte differentiation and CNS myelination. *The Journal of neuroscience : the official journal of the Society for Neuroscience*. 34:4466-4480.
- Bercury, K.K., and W.B. Macklin. 2015. Dynamics and mechanisms of CNS myelination. *Developmental cell*. 32:447-458.
- Bergles, D.E., R. Jabs, and C. Steinhauser. 2010. Neuron-glia synapses in the brain. *Brain research reviews*. 63:130-137.
- Bergles, D.E., J.D. Roberts, P. Somogyi, and C.E. Jahr. 2000. Glutamatergic synapses on oligodendrocyte precursor cells in the hippocampus. *Nature*. 405:187-191.
- Bernhart, S.H., I.L. Hofacker, S. Will, A.R. Gruber, and P.F. Stadler. 2008. RNAalifold: improved consensus structure prediction for RNA alignments. *BMC bioinformatics*. 9:474.
- Bertrand, E., P. Chartrand, M. Schaefer, S.M. Shenoy, R.H. Singer, and R.M. Long. 1998. Localization of ASH1 mRNA particles in living yeast. *Molecular cell*. 2:437-445.
- Bockbrader, K., and Y. Feng. 2008. Essential function, sophisticated regulation and pathological impact of the selective RNA-binding protein QKI in CNS myelin development. *Future neurology*. 3:655-668.
- Boggs, J.M. 2006. Myelin basic protein: a multifunctional protein. *Cellular and molecular life sciences : CMLS*. 63:1945-1961.
- Bond, A.T., D.A. Mangus, F. He, and A. Jacobson. 2001. Absence of Dbp2p alters both nonsense-mediated mRNA decay and rRNA processing. *Molecular and cellular biology*. 21:7366-7379.
- Bosco, D.A., N. Lemay, H.K. Ko, H. Zhou, C. Burke, T.J. Kwiatkowski, Jr., P. Sapp, D. McKenna-Yasek, R.H. Brown, Jr., and L.J. Hayward. 2010. Mutant FUS proteins that cause amyotrophic lateral sclerosis incorporate into stress granules. *Human molecular genetics*. 19:4160-4175.
- Brettschneider, J., K. Arai, K. Del Tredici, J.B. Toledo, J.L. Robinson, E.B. Lee, S. Kuwabara, K. Shibuya, D.J. Irwin, L. Fang, V.M. Van Deerlin, L. Elman, L. McCluskey, A.C. Ludolph, V.M. Lee, H. Braak, and J.Q. Trojanowski. 2014. TDP-43 pathology and neuronal loss in amyotrophic lateral sclerosis spinal cord. *Acta neuropathologica*. 128:423-437.
- Buchan, J.R. 2014. mRNP granules. Assembly, function, and connections with disease. *RNA biology*. 11:1019-1030.
- Buchan, J.R., and R. Parker. 2009. Eukaryotic stress granules: the ins and outs of translation. *Molecular cell*. 36:932-941.

- Buelt, M.K., B.J. Glidden, and D.R. Storm. 1994. Regulation of p68 RNA helicase by calmodulin and protein kinase C. *The Journal of biological chemistry*. 269:29367-29370.
- Butter, F., M. Scheibe, M. Morl, and M. Mann. 2009. Unbiased RNA-protein interaction screen by quantitative proteomics. *Proceedings of the National Academy of Sciences of the United States of America*. 106:10626-10631.
- Buxbaum, A.R., G. Haimovich, and R.H. Singer. 2015a. In the right place at the right time: visualizing and understanding mRNA localization. *Nature reviews. Molecular cell biology*. 16:95-109.
- Buxbaum, A.R., B. Wu, and R.H. Singer. 2014. Single beta-actin mRNA detection in neurons reveals a mechanism for regulating its translatability. *Science*. 343:419-422.
- Buxbaum, A.R., Y.J. Yoon, R.H. Singer, and H.Y. Park. 2015b. Single-molecule insights into mRNA dynamics in neurons. *Trends in cell biology*. 25:468-475.
- Cajigas, I.J., G. Tushev, T.J. Will, S. tom Dieck, N. Fuerst, and E.M. Schuman. 2012. The local transcriptome in the synaptic neuropil revealed by deep sequencing and high-resolution imaging. *Neuron*. 74:453-466.
- Camats, M., S. Guil, M. Kokolo, and M. Bach-Elias. 2008. P68 RNA helicase (DDX5) alters activity of cis- and trans-acting factors of the alternative splicing of H-Ras. *PLoS one*. 3:e2926.
- Campagnoni, A.T., M.J. Hunkeler, and J.E. Moskaitis. 1987. Translational regulation of myelin basic protein synthesis. *Journal of neuroscience research*. 17:102-110.
- Campagnoni, A.T., T.M. Pribyl, C.W. Campagnoni, K. Kampf, S. Amur-Umarjee, C.F. Landry, V.W. Handley, S.L. Newman, B. Garbay, and K. Kitamura. 1993. Structure and developmental regulation of Golli-mbp, a 105-kilobase gene that encompasses the myelin basic protein gene and is expressed in cells in the oligodendrocyte lineage in the brain. *The Journal of biological chemistry*. 268:4930-4938.
- Campbell, P.D., J.A. Chao, R.H. Singer, and F.L. Marlow. 2015. Dynamic visualization of transcription and RNA subcellular localization in zebrafish. *Development*. 142:1368-1374.
- Capello, E., R.R. Voskuhl, H.F. McFarland, and C.S. Raine. 1997. Multiple sclerosis: re-expression of a developmental gene in chronic lesions correlates with remyelination. *Annals of neurology*. 41:797-805.
- Carson, J.H., H. Cui, W. Krueger, B. Schlepchenko, C. Brumwell, and E. Barbarese. 2001. RNA trafficking in oligodendrocytes. *Results and problems in cell differentiation*. 34:69-81.
- Carson, J.H., Y. Gao, V. Tatavarty, M.K. Levin, G. Korza, V.P. Francone, L.D. Kosturko, M.J. Maggipinto, and E. Barbarese. 2008. Multiplexed RNA trafficking in oligodendrocytes and neurons. *Biochimica et biophysica acta*. 1779:453-458.
- Carson, J.H., K. Worboys, K. Ainger, and E. Barbarese. 1997. Translocation of myelin basic protein mRNA in oligodendrocytes requires microtubules and kinesin. *Cell motility and the cytoskeleton*. 38:318-328.
- Carter, C.J. 2007. eIF2B and oligodendrocyte survival: where nature and nurture meet in bipolar disorder and schizophrenia? *Schizophrenia bulletin*. 33:1343-1353.
- Carter, C.L., C. Lin, C.Y. Liu, L. Yang, and Z.R. Liu. 2010. Phosphorylated p68 RNA helicase activates Snail1 transcription by promoting HDAC1 dissociation from the Snail1 promoter. *Oncogene*. 29:5427-5436.
- Castello, A., B. Fischer, K. Eichelbaum, R. Horos, B.M. Beckmann, C. Strein, N.E. Davey, D.T. Humphreys, T. Preiss, L.M. Steinmetz, J. Krijgsveld, and M.W. Hentze. 2012. Insights into RNA biology from an atlas of mammalian mRNA-binding proteins. *Cell*. 149:1393-1406.
- Choi, Y.J., and S.G. Lee. 2012. The DEAD-box RNA helicase DDX3 interacts with DDX5, co-localizes with it in the cytoplasm during the G2/M phase of the cycle, and affects its shuttling during mRNP export. *Journal of cellular biochemistry*. 113:985-996.
- Clark, E.L., A. Coulson, C. Dalglish, P. Rajan, S.M. Nicol, S. Fleming, R. Heer, L. Gaughan, H.Y. Leung, D.J. Elliott, F.V. Fuller-Pace, and C.N. Robson. 2008a. The RNA helicase p68 is a novel androgen receptor coactivator involved in splicing and is overexpressed in prostate cancer. *Cancer research*. 68:7938-7946.
- Clark, E.L., F.V. Fuller-Pace, D.J. Elliott, and C.N. Robson. 2008b. Coupling transcription to RNA processing via the p68 DEAD box RNA helicase androgen receptor co-activator in prostate cancer. *Biochemical Society transactions*. 36:546-547.
- Cloutier, S.C., W.K. Ma, L.T. Nguyen, and E.J. Tran. 2012. The DEAD-box RNA helicase Dbp2 connects RNA quality control with repression of aberrant transcription. *The Journal of biological chemistry*. 287:26155-26166.
- Colman, D.R., G. Kreibich, A.B. Frey, and D.D. Sabatini. 1982. Synthesis and incorporation of myelin polypeptides into CNS myelin. *The Journal of cell biology*. 95:598-608.

- Colombrita, C., E. Onesto, F. Megiorni, A. Pizzuti, F.E. Baralle, E. Buratti, V. Silani, and A. Ratti. 2012. TDP-43 and FUS RNA-binding proteins bind distinct sets of cytoplasmic messenger RNAs and differently regulate their post-transcriptional fate in motoneuron-like cells. *The Journal of biological chemistry*. 287:15635-15647.
- Colombrita, C., E. Zennaro, C. Fallini, M. Weber, A. Sommacal, E. Buratti, V. Silani, and A. Ratti. 2009. TDP-43 is recruited to stress granules in conditions of oxidative insult. *Journal of neurochemistry*. 111:1051-1061.
- Compston, A., and A. Coles. 2008. Multiple sclerosis. *Lancet*. 372:1502-1517.
- Czopka, T., C. Ffrench-Constant, and D.A. Lyons. 2013. Individual oligodendrocytes have only a few hours in which to generate new myelin sheaths in vivo. *Developmental cell*. 25:599-609.
- Dai, T.Y., L. Cao, Z.C. Yang, Y.S. Li, L. Tan, X.Z. Ran, and C.M. Shi. 2014. P68 RNA helicase as a molecular target for cancer therapy. *Journal of experimental & clinical cancer research : CR*. 33:64.
- Dardenne, E., M. Polay Espinoza, L. Fattet, S. Germann, M.P. Lambert, H. Neil, E. Zonta, H. Mortada, L. Gratadou, M. Deygas, F.Z. Chakrama, S. Samaan, F.O. Desmet, L.C. Tranchevent, M. Dutertre, R. Rimokh, C.F. Bourgeois, and D. Auboeuf. 2014. RNA helicases DDX5 and DDX17 dynamically orchestrate transcription, miRNA, and splicing programs in cell differentiation. *Cell reports*. 7:1900-1913.
- de Ferra, F., H. Engh, L. Hudson, J. Kamholz, C. Puckett, S. Molineaux, and R.A. Lazzarini. 1985. Alternative splicing accounts for the four forms of myelin basic protein. *Cell*. 43:721-727.
- de Monasterio-Schrader, P., O. Jahn, S. Tenzer, S.P. Wichert, J. Patzig, and H.B. Werner. 2012. Systematic approaches to central nervous system myelin. *Cellular and molecular life sciences : CMLS*. 69:2879-2894.
- de Vries, H., J.C. de Jonge, C. Schrage, M.E. van der Haar, and D. Hoekstra. 1997. Differential and cell development-dependent localization of myelin mRNAs in oligodendrocytes. *Journal of neuroscience research*. 47:479-488.
- Decker, C.J., and R. Parker. 2012. P-bodies and stress granules: possible roles in the control of translation and mRNA degradation. *Cold Spring Harbor perspectives in biology*. 4:a012286.
- Demerens, C., B. Stankoff, M. Logak, P. Anglade, B. Allinquant, F. Couraud, B. Zalc, and C. Lubetzki. 1996. Induction of myelination in the central nervous system by electrical activity. *Proceedings of the National Academy of Sciences of the United States of America*. 93:9887-9892.
- Deng, H., K. Gao, and J. Jankovic. 2014. The role of FUS gene variants in neurodegenerative diseases. *Nature reviews. Neurology*. 10:337-348.
- Dicthenberg, J.B., S.A. Swanger, L.N. Antar, R.H. Singer, and G.J. Bassell. 2008. A direct role for FMRP in activity-dependent dendritic mRNA transport links filopodial-spine morphogenesis to fragile X syndrome. *Developmental cell*. 14:926-939.
- Dormann, D., R. Rodde, D. Edbauer, E. Bentmann, I. Fischer, A. Hruscha, M.E. Than, I.R. Mackenzie, A. Capell, B. Schmid, M. Neumann, and C. Haass. 2010. ALS-associated fused in sarcoma (FUS) mutations disrupt Transportin-mediated nuclear import. *The EMBO journal*. 29:2841-2857.
- Du, L., and J.D. Richter. 2005. Activity-dependent polyadenylation in neurons. *Rna*. 11:1340-1347.
- Dynes, J.L., and O. Steward. 2007. Dynamics of bidirectional transport of Arc mRNA in neuronal dendrites. *The Journal of comparative neurology*. 500:433-447.
- Elvira, G., S. Wasiak, V. Blandford, X.K. Tong, A. Serrano, X. Fan, M. del Rayo Sanchez-Carbente, F. Servant, A.W. Bell, D. Boismenu, J.C. Lacaille, P.S. McPherson, L. DesGroseillers, and W.S. Sossin. 2006. Characterization of an RNA granule from developing brain. *Molecular & cellular proteomics : MCP*. 5:635-651.
- Endoh, H., K. Maruyama, Y. Masuhiro, Y. Kobayashi, M. Goto, H. Tai, J. Yanagisawa, D. Metzger, S. Hashimoto, and S. Kato. 1999. Purification and identification of p68 RNA helicase acting as a transcriptional coactivator specific for the activation function 1 of human estrogen receptor alpha. *Molecular and cellular biology*. 19:5363-5372.
- Ettle, B., J.C. Schlachetzki, and J. Winkler. 2015. Oligodendroglia and Myelin in Neurodegenerative Diseases: More Than Just Bystanders? *Molecular neurobiology*.
- Fancy, S.P., J.R. Chan, S.E. Baranzini, R.J. Franklin, and D.H. Rowitch. 2011. Myelin regeneration: a recapitulation of development? *Annual review of neuroscience*. 34:21-43.
- Fancy, S.P., M.R. Kotter, E.P. Harrington, J.K. Huang, C. Zhao, D.H. Rowitch, and R.J. Franklin. 2010. Overcoming remyelination failure in multiple sclerosis and other myelin disorders. *Experimental neurology*. 225:18-23.
- Femino, A.M., F.S. Fay, K. Fogarty, and R.H. Singer. 1998. Visualization of single RNA transcripts in situ. *Science*. 280:585-590.

- Feng, Y., and C.A. Walsh. 2004. The many faces of filamin: a versatile molecular scaffold for cell motility and signalling. *Nature cell biology*. 6:1034-1038.
- Fields, R.D. 2008. White matter in learning, cognition and psychiatric disorders. *Trends in neurosciences*. 31:361-370.
- Fields, R.D. 2014. Neuroscience. Myelin--more than insulation. *Science*. 344:264-266.
- Figley, M.D., G. Bieri, R.M. Kolaitis, J.P. Taylor, and A.D. Gitler. 2014. Profilin 1 associates with stress granules and ALS-linked mutations alter stress granule dynamics. *The Journal of neuroscience : the official journal of the Society for Neuroscience*. 34:8083-8097.
- Fitzner, D., A. Schneider, A. Kippert, W. Mobius, K.I. Willig, S.W. Hell, G. Bunt, K. Gaus, and M. Simons. 2006. Myelin basic protein-dependent plasma membrane reorganization in the formation of myelin. *The EMBO journal*. 25:5037-5048.
- Fouts, D.E., H.L. True, and D.W. Celander. 1997. Functional recognition of fragmented operator sites by R17/MS2 coat protein, a translational repressor. *Nucleic acids research*. 25:4464-4473.
- Francone, V.P., M.J. Maggipinto, L.D. Kosturko, and E. Barbarese. 2007. The microtubule-associated protein tumor overexpressed gene/cytoskeleton-associated protein 5 is necessary for myelin basic protein expression in oligodendrocytes. *The Journal of neuroscience : the official journal of the Society for Neuroscience*. 27:7654-7662.
- Fritzsche, R., D. Karra, K.L. Bennett, F.Y. Ang, J.E. Heraud-Farlow, M. Tolino, M. Doyle, K.E. Bauer, S. Thomas, M. Planayavsky, E. Arn, A. Bakosova, K. Jungwirth, A. Hormann, Z. Palfi, J. Sandholzer, M. Schwarz, P. Macchi, J. Colinge, G. Superti-Furga, and M.A. Kiebler. 2013. Interactome of two diverse RNA granules links mRNA localization to translational repression in neurons. *Cell reports*. 5:1749-1762.
- Frohlich, D., W.P. Kuo, C. Fruhbeis, J.J. Sun, C.M. Zehendner, H.J. Luhmann, S. Pinto, J. Toedling, J. Trotter, and E.M. Kramer-Albers. 2014. Multifaceted effects of oligodendroglial exosomes on neurons: impact on neuronal firing rate, signal transduction and gene regulation. *Philosophical transactions of the Royal Society of London. Series B, Biological sciences*. 369.
- Fruhbeis, C., D. Frohlich, and E.M. Kramer-Albers. 2012. Emerging roles of exosomes in neuron-glia communication. *Frontiers in physiology*. 3:119.
- Fruhbeis, C., D. Frohlich, W.P. Kuo, J. Amphornrat, S. Thilemann, A.S. Saab, F. Kirchhoff, W. Mobius, S. Goebbels, K.A. Nave, A. Schneider, M. Simons, M. Klugmann, J. Trotter, and E.M. Kramer-Albers. 2013. Neurotransmitter-triggered transfer of exosomes mediates oligodendrocyte-neuron communication. *PLoS biology*. 11:e1001604.
- Fujii, R., S. Okabe, T. Urushido, K. Inoue, A. Yoshimura, T. Tachibana, T. Nishikawa, G.G. Hicks, and T. Takumi. 2005. The RNA binding protein TLS is translocated to dendritic spines by mGluR5 activation and regulates spine morphology. *Current biology : CB*. 15:587-593.
- Fukuda, T., T. Naiki, M. Saito, and K. Irie. 2009. hnRNP K interacts with RNA binding motif protein 42 and functions in the maintenance of cellular ATP level during stress conditions. *Genes to cells : devoted to molecular & cellular mechanisms*. 14:113-128.
- Fukuda, T., K. Yamagata, S. Fujiyama, T. Matsumoto, I. Koshida, K. Yoshimura, M. Mihara, M. Naitou, H. Endoh, T. Nakamura, C. Akimoto, Y. Yamamoto, T. Katagiri, C. Foulds, S. Takezawa, H. Kitagawa, K. Takeyama, B.W. O'Malley, and S. Kato. 2007. DEAD-box RNA helicase subunits of the Drosha complex are required for processing of rRNA and a subset of microRNAs. *Nature cell biology*. 9:604-611.
- Fuller-Pace, F.V. 2013. The DEAD box proteins DDX5 (p68) and DDX17 (p72): multi-tasking transcriptional regulators. *Biochimica et biophysica acta*. 1829:756-763.
- Funfschilling, U., L.M. Supplie, D. Mahad, S. Boretius, A.S. Saab, J. Edgar, B.G. Brinkmann, C.M. Kassmann, I.D. Tzvetanova, W. Mobius, F. Diaz, D. Meijer, U. Suter, B. Hamprecht, M.W. Sereda, C.T. Moraes, J. Frahm, S. Goebbels, and K.A. Nave. 2012. Glycolytic oligodendrocytes maintain myelin and long-term axonal integrity. *Nature*. 485:517-521.
- Fusco, D., N. Accornero, B. Lavoie, S.M. Shenoy, J.M. Blanchard, R.H. Singer, and E. Bertrand. 2003. Single mRNA molecules demonstrate probabilistic movement in living mammalian cells. *Current biology : CB*. 13:161-167.
- Gao, Y., V. Tatavarty, G. Korza, M.K. Levin, and J.H. Carson. 2008. Multiplexed dendritic targeting of alpha calcium calmodulin-dependent protein kinase II, neurogranin, and activity-regulated cytoskeleton-associated protein RNAs by the A2 pathway. *Molecular biology of the cell*. 19:2311-2327.
- Geissler, V., S. Altmeyer, B. Stein, H. Uhlmann-Schiffler, and H. Stahl. 2013. The RNA helicase Ddx5/p68 binds to hUpf3 and enhances NMD of Ddx17/p72 and Smg5 mRNA. *Nucleic acids research*. 41:7875-7888.

- Germann, S., L. Gratadou, E. Zonta, E. Dardenne, B. Gaudineau, M. Fougere, S. Samaan, M. Dutertre, S. Jauliac, and D. Auboeuf. 2012. Dual role of the ddx5/ddx17 RNA helicases in the control of the pro-migratory NFAT5 transcription factor. *Oncogene*. 31:4536-4549.
- Giampetruzzi, A., J.H. Carson, and E. Barbarese. 2013. FMRP and myelin protein expression in oligodendrocytes. *Molecular and cellular neurosciences*. 56:333-341.
- Gibson, E.M., D. Purger, C.W. Mount, A.K. Goldstein, G.L. Lin, L.S. Wood, I. Inema, S.E. Miller, G. Bieri, J.B. Zuchero, B.A. Barres, P.J. Woo, H. Vogel, and M. Monje. 2014. Neuronal activity promotes oligodendrogenesis and adaptive myelination in the mammalian brain. *Science*. 344:1252304.
- Gielen, E., W. Baron, M. Vandeven, P. Steels, D. Hoekstra, and M. Ameloot. 2006. Rafts in oligodendrocytes: evidence and structure-function relationship. *Glia*. 54:499-512.
- Giorgi, C., G.W. Yeo, M.E. Stone, D.B. Katz, C. Burge, G. Turrigiano, and M.J. Moore. 2007. The EJC factor eIF4AIII modulates synaptic strength and neuronal protein expression. *Cell*. 130:179-191.
- Gong, C., and L.E. Maquat. 2015. Affinity purification of long noncoding RNA-protein complexes from formaldehyde cross-linked mammalian cells. *Methods Mol Biol*. 1206:81-86.
- Gonsior, C. 2011. Fyn kinase targets in oligodendroglial physiology and myelination. In *Biology*. Johannes Gutenberg-University Mainz.
- Goto, J., T. Tezuka, T. Nakazawa, H. Sagara, and T. Yamamoto. 2008. Loss of Fyn tyrosine kinase on the C57BL/6 genetic background causes hydrocephalus with defects in oligodendrocyte development. *Molecular and cellular neurosciences*. 38:203-212.
- Gruber, A.R., R. Lorenz, S.H. Bernhart, R. Neubock, and I.L. Hofacker. 2008. The Vienna RNA websuite. *Nucleic acids research*. 36:W70-74.
- Guarguaglini, G., A. Battistoni, C. Pittoggi, G. Di Matteo, B. Di Fiore, and P. Lavia. 1997. Expression of the murine RanBP1 and Htf9-c genes is regulated from a shared bidirectional promoter during cell cycle progression. *The Biochemical journal*. 325 (Pt 1):277-286.
- Guturi, K.K., M. Sarkar, A. Bhowmik, N. Das, and M.K. Ghosh. 2014. DEAD-box protein p68 is regulated by beta-catenin/transcription factor 4 to maintain a positive feedback loop in control of breast cancer progression. *Breast cancer research : BCR*. 16:496.
- Haass, C. 2013. Cellular mechanisms of ALS mutations - a loss or a gain of function? *Drug research*. 63 Suppl 1:S17.
- Hafner, M., M. Landthaler, L. Burger, M. Khorshid, J. Hausser, P. Berninger, A. Rothballer, M. Ascano, Jr., A.C. Jungkamp, M. Munschauer, A. Ulrich, G.S. Wardle, S. Dewell, M. Zavolan, and T. Tuschl. 2010. Transcriptome-wide identification of RNA-binding protein and microRNA target sites by PAR-CLIP. *Cell*. 141:129-141.
- Halstead, J.M., T. Lionnet, J.H. Wilbertz, F. Wippich, A. Ephrussi, R.H. Singer, and J.A. Chao. 2015. Translation. An RNA biosensor for imaging the first round of translation from single cells to living animals. *Science*. 347:1367-1671.
- Han, J.R., G.K. Yiu, and N.B. Hecht. 1995. Testis/brain RNA-binding protein attaches translationally repressed and transported mRNAs to microtubules. *Proceedings of the National Academy of Sciences of the United States of America*. 92:9550-9554.
- Han, T.W., M. Kato, S. Xie, L.C. Wu, H. Mirzaei, J. Pei, M. Chen, Y. Xie, J. Allen, G. Xiao, and S.L. McKnight. 2012. Cell-free formation of RNA granules: bound RNAs identify features and components of cellular assemblies. *Cell*. 149:768-779.
- Harauz, G., and J.M. Boggs. 2013. Myelin management by the 18.5-kDa and 21.5-kDa classic myelin basic protein isoforms. *Journal of neurochemistry*. 125:334-361.
- Harauz, G., N. Ishiyama, C.M. Hill, I.R. Bates, D.S. Libich, and C. Fares. 2004. Myelin basic protein-diverse conformational states of an intrinsically unstructured protein and its roles in myelin assembly and multiple sclerosis. *Micron*. 35:503-542.
- Hardy, R.J., R.A. Lazzarini, D.R. Colman, and V.L. Friedrich, Jr. 1996. Cytoplasmic and nuclear localization of myelin basic proteins reveals heterogeneity among oligodendrocytes. *Journal of neuroscience research*. 46:246-257.
- He, F., and A. Jacobson. 1995. Identification of a novel component of the nonsense-mediated mRNA decay pathway by use of an interacting protein screen. *Genes & development*. 9:437-454.
- Hoch-Kraft, P. 2010. Charakterisierung der RNA-bindenden Proteine FUS und DDX5 in Oligodendrozyten. In *Diploma thesis Biology*. Vol. Diploma. Johannes Gutenberg-University Mainz.

- Hoek, K.S., G.J. Kidd, J.H. Carson, and R. Smith. 1998. hnRNP A2 selectively binds the cytoplasmic transport sequence of myelin basic protein mRNA. *Biochemistry*. 37:7021-7029.
- Hoell, J.I., E. Larsson, S. Runge, J.D. Nusbaum, S. Duggimpudi, T.A. Farazi, M. Hafner, A. Borkhardt, C. Sander, and T. Tuschl. 2011. RNA targets of wild-type and mutant FET family proteins. *Nature structural & molecular biology*. 18:1428-1431.
- Holt, C.E., and E.M. Schuman. 2013. The central dogma decentralized: new perspectives on RNA function and local translation in neurons. *Neuron*. 80:648-657.
- Hong, S., H. Noh, H. Chen, R. Padia, Z.K. Pan, S.B. Su, Q. Jing, H.F. Ding, and S. Huang. 2013. Signaling by p38 MAPK stimulates nuclear localization of the microprocessor component p68 for processing of selected primary microRNAs. *Science signaling*. 6:ra16.
- Huang, Y., and Z.R. Liu. 2002. The ATPase, RNA unwinding, and RNA binding activities of recombinant p68 RNA helicase. *The Journal of biological chemistry*. 277:12810-12815.
- Hughes, E.G., S.H. Kang, M. Fukaya, and D.E. Bergles. 2013. Oligodendrocyte progenitors balance growth with self-repulsion to achieve homeostasis in the adult brain. *Nature neuroscience*. 16:668-676.
- Huttelmaier, S., D. Zenklusen, M. Lederer, J. Dichtenberg, M. Lorenz, X. Meng, G.J. Bassell, J. Condeelis, and R.H. Singer. 2005. Spatial regulation of beta-actin translation by Src-dependent phosphorylation of ZBP1. *Nature*. 438:512-515.
- Iizaka, M., H.J. Han, H. Akashi, Y. Furukawa, Y. Nakajima, S. Sugano, M. Ogawa, and Y. Nakamura. 2000. Isolation and chromosomal assignment of a novel human gene, CORO1C, homologous to coronin-like actin-binding proteins. *Cytogenetics and cell genetics*. 88:221-224.
- International Multiple Sclerosis Genetics, C., D.R. Booth, R.N. Heard, G.J. Stewart, M. Cox, R.J. Scott, J. Lechner-Scott, A. Goris, R. Dobosi, B. Dubois, J. Saarela, V. Leppa, L. Peltonen, T. Pirttila, I. Cournu-Rebeix, B. Fontaine, L. Bergamaschi, S. D'Alfonso, M. Leone, A.R. Lorentzen, H.F. Harbo, E.G. Celius, A. Spurkland, J. Link, I. Kockum, T. Olsson, J. Hillert, M. Ban, A. Baker, A. Kemppinen, S. Sawcer, A. Compston, N.P. Robertson, P.L. De Jager, D.A. Hafler, L.F. Barcellos, A.J. Ivinson, J.L. McCauley, M.A. Pericak-Vance, J.R. Oksenberg, S.L. Hauser, D. Sexton, and J. Haines. 2010. Lack of support for association between the KIF1B rs10492972[C] variant and multiple sclerosis. *Nature genetics*. 42:469-470; author reply 470-461.
- Jacobs, A.M., S.M. Nicol, R.G. Hislop, E.G. Jaffray, R.T. Hay, and F.V. Fuller-Pace. 2007. SUMO modification of the DEAD box protein p68 modulates its transcriptional activity and promotes its interaction with HDAC1. *Oncogene*. 26:5866-5876.
- Jacobs, E.C., T.M. Pribyl, J.M. Feng, K. Kampf, V. Spreur, C. Campagnoni, C.S. Colwell, S.D. Reyes, M. Martin, V. Handley, T.D. Hiltner, C. Readhead, R.E. Jacobs, A. Messing, R.S. Fisher, and A.T. Campagnoni. 2005. Region-specific myelin pathology in mice lacking the golli products of the myelin basic protein gene. *The Journal of neuroscience : the official journal of the Society for Neuroscience*. 25:7004-7013.
- Jahn, O., S. Tenzer, and H.B. Werner. 2009. Myelin proteomics: molecular anatomy of an insulating sheath. *Molecular neurobiology*. 40:55-72.
- Jalal, C., H. Uhlmann-Schiffler, and H. Stahl. 2007. Redundant role of DEAD box proteins p68 (Ddx5) and p72/p82 (Ddx17) in ribosome biogenesis and cell proliferation. *Nucleic acids research*. 35:3590-3601.
- Janknecht, R. 2010. Multi-talented DEAD-box proteins and potential tumor promoters: p68 RNA helicase (DDX5) and its paralog, p72 RNA helicase (DDX17). *American journal of translational research*. 2:223-234.
- Jung, C., G. Mittler, F. Oswald, and T. Borggreffe. 2013. RNA helicase Ddx5 and the noncoding RNA SRA act as coactivators in the Notch signaling pathway. *Biochimica et biophysica acta*. 1833:1180-1189.
- Jung, M., E. Kramer, M. Grzenkowski, K. Tang, W. Blakemore, A. Aguzzi, K. Khazaie, K. Chlichlia, G. von Blankenfeld, H. Kettenmann, and et al. 1995. Lines of murine oligodendroglial precursor cells immortalized by an activated neu tyrosine kinase show distinct degrees of interaction with axons in vitro and in vivo. *The European journal of neuroscience*. 7:1245-1265.
- Kanai, Y., N. Dohmae, and N. Hirokawa. 2004. Kinesin transports RNA: isolation and characterization of an RNA-transporting granule. *Neuron*. 43:513-525.
- Kang, S.H., Y. Li, M. Fukaya, I. Lorenzini, D.W. Cleveland, L.W. Ostrow, J.D. Rothstein, and D.E. Bergles. 2013. Degeneration and impaired regeneration of gray matter oligodendrocytes in amyotrophic lateral sclerosis. *Nature neuroscience*. 16:571-579.
- Kar, A., K. Fushimi, X. Zhou, P. Ray, C. Shi, X. Chen, Z. Liu, S. Chen, and J.Y. Wu. 2011. RNA helicase p68 (DDX5) regulates tau exon 10 splicing by modulating a stem-loop structure at the 5' splice site. *Molecular and cellular biology*. 31:1812-1821.
- Karthigasan, J., J.S. Garvey, G.V. Ramamurthy, and D.A. Kirschner. 1996. Immunolocalization of 17 and 21.5 kDa MBP isoforms in compact myelin and radial component. *Journal of neurocytology*. 25:1-7.

- Kato, M., T.W. Han, S. Xie, K. Shi, X. Du, L.C. Wu, H. Mirzaei, E.J. Goldsmith, J. Longgood, J. Pei, N.V. Grishin, D.E. Frantz, J.W. Schneider, S. Chen, L. Li, M.R. Sawaya, D. Eisenberg, R. Tycko, and S.L. McKnight. 2012. Cell-free formation of RNA granules: low complexity sequence domains form dynamic fibers within hydrogels. *Cell*. 149:753-767.
- Kato, T., Y. Iwayama, C. Kakiuchi, K. Iwamoto, K. Yamada, Y. Minabe, K. Nakamura, N. Mori, K. Fujii, S. Nanko, and T. Yoshikawa. 2005. Gene expression and association analyses of LIM (PDLIM5) in bipolar disorder and schizophrenia. *Molecular psychiatry*. 10:1045-1055.
- Kedersha, N., P. Ivanov, and P. Anderson. 2013. Stress granules and cell signaling: more than just a passing phase? *Trends in biochemical sciences*. 38:494-506.
- Kedersha, N., G. Stoecklin, M. Ayodele, P. Yacono, J. Lykke-Andersen, M.J. Fritzler, D. Scheuner, R.J. Kaufman, D.E. Golan, and P. Anderson. 2005. Stress granules and processing bodies are dynamically linked sites of mRNP remodeling. *The Journal of cell biology*. 169:871-884.
- Kedersha, N.L., M. Gupta, W. Li, I. Miller, and P. Anderson. 1999. RNA-binding proteins TIA-1 and TIAR link the phosphorylation of eIF-2 alpha to the assembly of mammalian stress granules. *The Journal of cell biology*. 147:1431-1442.
- Keryer-Bibens, C., C. Barreau, and H.B. Osborne. 2008. Tethering of proteins to RNAs by bacteriophage proteins. *Biology of the cell / under the auspices of the European Cell Biology Organization*. 100:125-138.
- Kim, H.J., N.C. Kim, Y.D. Wang, E.A. Scarborough, J. Moore, Z. Diaz, K.S. MacLea, B. Freibaum, S. Li, A. Molliex, A.P. Kanagaraj, R. Carter, K.B. Boylan, A.M. Wojtas, R. Rademakers, J.L. Pinkus, S.A. Greenberg, J.Q. Trojanowski, B.J. Traynor, B.N. Smith, S. Topp, A.S. Gkazi, J. Miller, C.E. Shaw, M. Kottlors, J. Kirschner, A. Pestronk, Y.R. Li, A.F. Ford, A.D. Gitler, M. Benatar, O.D. King, V.E. Kimonis, E.D. Ross, C.C. Weihl, J. Shorter, and J.P. Taylor. 2013. Mutations in prion-like domains in hnRNPA2B1 and hnRNPA1 cause multisystem proteinopathy and ALS. *Nature*. 495:467-473.
- Kimura, M., M. Sato, A. Akatsuka, S. Saito, K. Ando, M. Yokoyama, and M. Katsuki. 1998. Overexpression of a minor component of myelin basic protein isoform (17.2 kDa) can restore myelinogenesis in transgenic shiverer mice. *Brain research*. 785:245-252.
- Kirby, B.B., N. Takada, A.J. Latimer, J. Shin, T.J. Carney, R.N. Kelsh, and B. Appel. 2006. In vivo time-lapse imaging shows dynamic oligodendrocyte progenitor behavior during zebrafish development. *Nature neuroscience*. 9:1506-1511.
- Kost, G.C., M.Y. Yang, L. Li, Y. Zhang, C.Y. Liu, D.J. Kim, C.H. Ahn, Y.B. Lee, and Z.R. Liu. 2015. A Novel Anti-Cancer Agent, 1-(3,5-Dimethoxyphenyl)-4-[(6-Fluoro-2-Methoxyquinoxalin-3-yl)Aminocarbonyl] Piperazine (RX-5902), Interferes With beta-Catenin Function Through Y593 Phospho-p68 RNA Helicase. *Journal of cellular biochemistry*. 116:1595-1601.
- Kosturko, L.D., M.J. Maggipinto, C. D'Sa, J.H. Carson, and E. Barbarese. 2005. The microtubule-associated protein tumor overexpressed gene binds to the RNA trafficking protein heterogeneous nuclear ribonucleoprotein A2. *Molecular biology of the cell*. 16:1938-1947.
- Kosturko, L.D., M.J. Maggipinto, G. Korza, J.W. Lee, J.H. Carson, and E. Barbarese. 2006. Heterogeneous nuclear ribonucleoprotein (hnRNP) E1 binds to hnRNP A2 and inhibits translation of A2 response element mRNAs. *Molecular biology of the cell*. 17:3521-3533.
- Kramer-Albers, E.M., and R. White. 2011. From axon-glia signalling to myelination: the integrating role of oligodendroglial Fyn kinase. *Cellular and molecular life sciences : CMLS*. 68:2003-2012.
- Kuhlmann, T., V. Miron, Q. Cui, C. Wegner, J. Antel, and W. Bruck. 2008. Differentiation block of oligodendroglial progenitor cells as a cause for remyelination failure in chronic multiple sclerosis. *Brain : a journal of neurology*. 131:1749-1758.
- Kwiatkowski, T.J., Jr., D.A. Bosco, A.L. Leclerc, E. Tamrazian, C.R. Vandenberg, C. Russ, A. Davis, J. Gilchrist, E.J. Kasarskis, T. Munsat, P. Valdmanis, G.A. Rouleau, B.A. Hosler, P. Cortelli, P.J. de Jong, Y. Yoshinaga, J.L. Haines, M.A. Pericak-Vance, J. Yan, N. Ticozzi, T. Siddique, D. McKenna-Yasek, P.C. Sapp, H.R. Horvitz, J.E. Landers, and R.H. Brown, Jr. 2009. Mutations in the FUS/TLS gene on chromosome 16 cause familial amyotrophic lateral sclerosis. *Science*. 323:1205-1208.
- Kwon, S. 2013. Single-molecule fluorescence in situ hybridization: quantitative imaging of single RNA molecules. *BMB reports*. 46:65-72.
- Lagier-Tourenne, C., M. Polymenidou, and D.W. Cleveland. 2010. TDP-43 and FUS/TLS: emerging roles in RNA processing and neurodegeneration. *Human molecular genetics*. 19:R46-64.
- Lagier-Tourenne, C., M. Polymenidou, K.R. Hutt, A.Q. Vu, M. Baughn, S.C. Huelga, K.M. Clutario, S.C. Ling, T.Y. Liang, C. Mazur, E. Wancewicz, A.S. Kim, A. Watt, S. Freier, G.G. Hicks, J.P. Donohue, L. Shiue, C.F. Bennett, J. Ravits, D.W. Cleveland, and G.W. Yeo. 2012. Divergent roles of ALS-linked proteins FUS/TLS and TDP-43 intersect in processing long pre-mRNAs. *Nature neuroscience*. 15:1488-1497.

- Landry, C.F., J.B. Watson, T. Kashima, and A.T. Campagnoni. 1994. Cellular influences on RNA sorting in neurons and glia: an in situ hybridization histochemical study. *Brain research. Molecular brain research*. 27:1-11.
- Larocque, D., J. Pilotte, T. Chen, F. Cloutier, B. Massie, L. Pedraza, R. Couture, P. Lasko, G. Almazan, and S. Richard. 2002. Nuclear retention of MBP mRNAs in the quaking viable mice. *Neuron*. 36:815-829.
- Laursen, L.S., C.W. Chan, and C. Ffrench-Constant. 2009. An integrin-contactin complex regulates CNS myelination by differential Fyn phosphorylation. *The Journal of neuroscience : the official journal of the Society for Neuroscience*. 29:9174-9185.
- Laursen, L.S., C.W. Chan, and C. Ffrench-Constant. 2011. Translation of myelin basic protein mRNA in oligodendrocytes is regulated by integrin activation and hnRNP-K. *The Journal of cell biology*. 192:797-811.
- Lebrun-Julien, F., L. Bachmann, C. Norrmen, M. Troztmuller, H. Kofeler, M.A. Ruegg, M.N. Hall, and U. Suter. 2014. Balanced mTORC1 activity in oligodendrocytes is required for accurate CNS myelination. *The Journal of neuroscience : the official journal of the Society for Neuroscience*. 34:8432-8448.
- Lecuyer, E., H. Yoshida, N. Parthasarathy, C. Alm, T. Babak, T. Cerovina, T.R. Hughes, P. Tomancak, and H.M. Krause. 2007. Global analysis of mRNA localization reveals a prominent role in organizing cellular architecture and function. *Cell*. 131:174-187.
- Lee, E.B., V.M. Lee, and J.Q. Trojanowski. 2012a. Gains or losses: molecular mechanisms of TDP43-mediated neurodegeneration. *Nature reviews. Neuroscience*. 13:38-50.
- Lee, S., M.K. Leach, S.A. Redmond, S.Y. Chong, S.H. Mellon, S.J. Tuck, Z.Q. Feng, J.M. Corey, and J.R. Chan. 2012b. A culture system to study oligodendrocyte myelination processes using engineered nanofibers. *Nature methods*. 9:917-922.
- Lee, Y., B.M. Morrison, Y. Li, S. Lengacher, M.H. Farah, P.N. Hoffman, Y. Liu, A. Tsingalia, L. Jin, P.W. Zhang, L. Pellerin, P.J. Magistretti, and J.D. Rothstein. 2012c. Oligodendroglia metabolically support axons and contribute to neurodegeneration. *Nature*. 487:443-448.
- Lee, Y.J., H.M. Wei, L.Y. Chen, and C. Li. 2014. Localization of SERBP1 in stress granules and nucleoli. *The FEBS journal*. 281:352-364.
- Lenzi, J., R. De Santis, V. de Turreis, M. Morlando, P. Laneve, A. Calvo, V. Caliendo, A. Chio, A. Rosa, and I. Bozzoni. 2015. ALS mutant FUS proteins are recruited into stress granules in induced pluripotent stem cell-derived motoneurons. *Disease models & mechanisms*. 8:755-766.
- Li, Y.R., O.D. King, J. Shorter, and A.D. Gitler. 2013. Stress granules as crucibles of ALS pathogenesis. *The Journal of cell biology*. 201:361-372.
- Li, Z., Y. Zhang, L. Ku, K.D. Wilkinson, S.T. Warren, and Y. Feng. 2001. The fragile X mental retardation protein inhibits translation via interacting with mRNA. *Nucleic acids research*. 29:2276-2283.
- Li, Z., Y. Zhang, D. Li, and Y. Feng. 2000. Destabilization and mislocalization of myelin basic protein mRNAs in quaking dysmyelination lacking the QKI RNA-binding proteins. *The Journal of neuroscience : the official journal of the Society for Neuroscience*. 20:4944-4953.
- Licatalosi, D.D., A. Mele, J.J. Fak, J. Ule, M. Kayikci, S.W. Chi, T.A. Clark, A.C. Schweitzer, J.E. Blume, X. Wang, J.C. Darnell, and R.B. Darnell. 2008. HITS-CLIP yields genome-wide insights into brain alternative RNA processing. *Nature*. 456:464-469.
- Lin, C., L. Yang, J.J. Yang, Y. Huang, and Z.R. Liu. 2005. ATPase/helicase activities of p68 RNA helicase are required for pre-mRNA splicing but not for assembly of the spliceosome. *Molecular and cellular biology*. 25:7484-7493.
- Lin, J., T. Lwin, J.J. Zhao, W. Tam, Y.S. Choi, L.C. Moscinski, W.S. Dalton, E.M. Sotomayor, K.L. Wright, and J. Tao. 2011. Follicular dendritic cell-induced microRNA-mediated upregulation of PRDM1 and downregulation of BCL-6 in non-Hodgkin's B-cell lymphomas. *Leukemia*. 25:145-152.
- Lin, S., L. Tian, H. Shen, Y. Gu, J.L. Li, Z. Chen, X. Sun, M.J. You, and L. Wu. 2013. DDX5 is a positive regulator of oncogenic NOTCH1 signaling in T cell acute lymphoblastic leukemia. *Oncogene*. 32:4845-4853.
- Linder, P., and E. Jankowsky. 2011. From unwinding to clamping - the DEAD box RNA helicase family. *Nature reviews. Molecular cell biology*. 12:505-516.
- Lionnet, T., K. Czaplinski, X. Darzacq, Y. Shav-Tal, A.L. Wells, J.A. Chao, H.Y. Park, V. de Turreis, M. Lopez-Jones, and R.H. Singer. 2011. A transgenic mouse for in vivo detection of endogenous labeled mRNA. *Nature methods*. 8:165-170.
- Liu, Y.L., C.S. Fann, C.M. Liu, C.C. Chang, W.C. Yang, J.Y. Wu, S.I. Hung, H.Y. Chan, J.J. Chen, M.H. Hsieh, T.J. Hwang, S.V. Faraone, M.T. Tsuang, W.J. Chen, and H.G. Hwu. 2007. HTF9C gene of 22q11.21 region associates with schizophrenia having deficit-sustained attention. *Psychiatric genetics*. 17:333-338.

- Liu, Z.R. 2002. p68 RNA helicase is an essential human splicing factor that acts at the U1 snRNA-5' splice site duplex. *Molecular and cellular biology*. 22:5443-5450.
- Lu, Z., L. Ku, Y. Chen, and Y. Feng. 2005. Developmental abnormalities of myelin basic protein expression in fyn knock-out brain reveal a role of Fyn in posttranscriptional regulation. *The Journal of biological chemistry*. 280:389-395.
- Lyons, D.A., S.G. Naylor, A. Scholze, and W.S. Talbot. 2009. Kif1b is essential for mRNA localization in oligodendrocytes and development of myelinated axons. *Nature genetics*. 41:854-858.
- Ma, A.S., K. Moran-Jones, J. Shan, T.P. Munro, M.J. Snee, K.S. Hoek, and R. Smith. 2002. Heterogeneous nuclear ribonucleoprotein A3, a novel RNA trafficking response element-binding protein. *The Journal of biological chemistry*. 277:18010-18020.
- Mahler, A., J. Steiniger, M. Bock, L. Klug, N. Parreidt, M. Lorenz, B.F. Zimmermann, A. Krannich, F. Paul, and M. Boschmann. 2015. Metabolic response to epigallocatechin-3-gallate in relapsing-remitting multiple sclerosis: a randomized clinical trial. *The American journal of clinical nutrition*. 101:487-495.
- Mastrocola, A.S., S.H. Kim, A.T. Trinh, L.A. Rodenkirch, and R.S. Tibbetts. 2013. The RNA-binding protein fused in sarcoma (FUS) functions downstream of poly(ADP-ribose) polymerase (PARP) in response to DNA damage. *The Journal of biological chemistry*. 288:24731-24741.
- McKenzie, I.A., D. Ohayon, H. Li, J.P. de Faria, B. Emery, K. Tohyama, and W.D. Richardson. 2014. Motor skill learning requires active central myelination. *Science*. 346:318-322.
- Mensch, S., M. Baraban, R. Almeida, T. Czopka, J. Ausborn, A. El Manira, and D.A. Lyons. 2015. Synaptic vesicle release regulates myelin sheath number of individual oligodendrocytes in vivo. *Nature neuroscience*. 18:628-630.
- Merz, C., H. Urlaub, C.L. Will, and R. Luhrmann. 2007. Protein composition of human mRNPs spliced in vitro and differential requirements for mRNP protein recruitment. *Rna*. 13:116-128.
- Meyer-Lindenberg, A., C.B. Mervis, and K.F. Berman. 2006. Neural mechanisms in Williams syndrome: a unique window to genetic influences on cognition and behaviour. *Nature reviews. Neuroscience*. 7:380-393.
- Mi, H., A. Muruganujan, J.T. Casagrande, and P.D. Thomas. 2013. Large-scale gene function analysis with the PANTHER classification system. *Nature protocols*. 8:1551-1566.
- Michel, K., T. Zhao, M. Karl, K. Lewis, and S.L. Fyffe-Maricich. 2015. Translational control of myelin basic protein expression by ERK2 MAP kinase regulates timely remyelination in the adult brain. *The Journal of neuroscience : the official journal of the Society for Neuroscience*. 35:7850-7865.
- Michlewski, G., J.R. Sanford, and J.F. Caceres. 2008. The splicing factor SF2/ASF regulates translation initiation by enhancing phosphorylation of 4E-BP1. *Molecular cell*. 30:179-189.
- Miller, L.C., V. Blandford, R. McAdam, M.R. Sanchez-Carbente, F. Badeaux, L. DesGroseillers, and W.S. Sossin. 2009. Combinations of DEAD box proteins distinguish distinct types of RNA: protein complexes in neurons. *Molecular and cellular neurosciences*. 40:485-495.
- Mitew, S., C.M. Hay, H. Peckham, J. Xiao, M. Koenning, and B. Emery. 2014. Mechanisms regulating the development of oligodendrocytes and central nervous system myelin. *Neuroscience*. 276:29-47.
- Mollet, S., N. Cougot, A. Wilczynska, F. Dautry, M. Kress, E. Bertrand, and D. Weil. 2008. Translationally repressed mRNA transiently cycles through stress granules during stress. *Molecular biology of the cell*. 19:4469-4479.
- Mooney, S.M., J.P. Grande, J.L. Salisbury, and R. Janknecht. 2010. Sumoylation of p68 and p72 RNA helicases affects protein stability and transactivation potential. *Biochemistry*. 49:1-10.
- Moore, M.J. 2005. From birth to death: the complex lives of eukaryotic mRNAs. *Science*. 309:1514-1518.
- Morlando, M., S. Dini Modigliani, G. Torrelli, A. Rosa, V. Di Carlo, E. Caffarelli, and I. Bozzoni. 2012. FUS stimulates microRNA biogenesis by facilitating co-transcriptional Drosha recruitment. *The EMBO journal*. 31:4502-4510.
- Muller, C., N.M. Bauer, I. Schafer, and R. White. 2013. Making myelin basic protein -from mRNA transport to localized translation. *Frontiers in cellular neuroscience*. 7:169.
- Munro, T.P., R.J. Magee, G.J. Kidd, J.H. Carson, E. Barbarese, L.M. Smith, and R. Smith. 1999. Mutational analysis of a heterogeneous nuclear ribonucleoprotein A2 response element for RNA trafficking. *The Journal of biological chemistry*. 274:34389-34395.
- Nakaya, T., P. Alexiou, M. Maragkakis, A. Chang, and Z. Mourelatos. 2013. FUS regulates genes coding for RNA-binding proteins in neurons by binding to their highly conserved introns. *Rna*. 19:498-509.
- Nave, K.A. 2010. Myelination and support of axonal integrity by glia. *Nature*. 468:244-252.

- Nave, K.A., and H.B. Werner. 2014. Myelination of the nervous system: mechanisms and functions. *Annual review of cell and developmental biology*. 30:503-533.
- Nawaz, S., P. Sanchez, S. Schmitt, N. Snaidero, M. Mitkovski, C. Velte, B.R. Bruckner, I. Alexopoulos, T. Czopka, S.Y. Jung, J.S. Rhee, A. Janshoff, W. Witke, I.A. Schaap, D.A. Lyons, and M. Simons. 2015. Actin Filament Turnover Drives Leading Edge Growth during Myelin Sheath Formation in the Central Nervous System. *Developmental cell*.
- Nawaz, S., J. Schweitzer, O. Jahn, and H.B. Werner. 2013. Molecular evolution of myelin basic protein, an abundant structural myelin component. *Glia*. 61:1364-1377.
- Newman, S., K. Kitamura, and A.T. Campagnoni. 1987. Identification of a cDNA coding for a fifth form of myelin basic protein in mouse. *Proceedings of the National Academy of Sciences of the United States of America*. 84:886-890.
- Nott, A., H. Le Hir, and M.J. Moore. 2004. Splicing enhances translation in mammalian cells: an additional function of the exon junction complex. *Genes & development*. 18:210-222.
- O'Connor, L.T., B.D. Goetz, J.M. Kwiecien, K.H. Delaney, A.L. Fletch, and I.D. Duncan. 1999. Insertion of a retrotransposon in Mbp disrupts mRNA splicing and myelination in a new mutant rat. *The Journal of neuroscience : the official journal of the Society for Neuroscience*. 19:3404-3413.
- Ogilvie, V.C., B.J. Wilson, S.M. Nicol, N.A. Morrice, L.R. Saunders, G.N. Barber, and F.V. Fuller-Pace. 2003. The highly related DEAD box RNA helicases p68 and p72 exist as heterodimers in cells. *Nucleic acids research*. 31:1470-1480.
- Orozco, D., S. Tahirovic, K. Rentzsch, B.M. Schwenk, C. Haass, and D. Edbauer. 2012. Loss of fused in sarcoma (FUS) promotes pathological Tau splicing. *EMBO reports*. 13:759-764.
- Ozgen, H., N. Kahya, J.C. de Jonge, G.S. Smith, G. Harauz, D. Hoekstra, and W. Baron. 2014. Regulation of cell proliferation by nucleocytoplasmic dynamics of postnatal and embryonic exon-II-containing MBP isoforms. *Biochimica et biophysica acta*. 1843:517-530.
- Park, H.Y., H. Lim, Y.J. Yoon, A. Follenzi, C. Nwokafor, M. Lopez-Jones, X. Meng, and R.H. Singer. 2014. Visualization of dynamics of single endogenous mRNA labeled in live mouse. *Science*. 343:422-424.
- Parsyan, A., Y. Svitkin, D. Shahbazian, C. Gkogkas, P. Lasko, W.C. Merrick, and N. Sonenberg. 2011. mRNA helicases: the tacticians of translational control. *Nature reviews. Molecular cell biology*. 12:235-245.
- Paul, S., W. Dansithong, S.P. Jog, I. Holt, S. Mittal, J.D. Brook, G.E. Morris, L. Comai, and S. Reddy. 2011. Expanded CUG repeats Dysregulate RNA splicing by altering the stoichiometry of the muscleblind 1 complex. *The Journal of biological chemistry*. 286:38427-38438.
- Pause, A., and N. Sonenberg. 1992. Mutational analysis of a DEAD box RNA helicase: the mammalian translation initiation factor eIF-4A. *The EMBO journal*. 11:2643-2654.
- Paz, I., M. Akerman, I. Dror, I. Kosti, and Y. Mandel-Gutfreund. 2010. SFmap: a web server for motif analysis and prediction of splicing factor binding sites. *Nucleic acids research*. 38:W281-285.
- Paz, I., I. Kosti, M. Ares, Jr., M. Cline, and Y. Mandel-Gutfreund. 2014. RBPmap: a web server for mapping binding sites of RNA-binding proteins. *Nucleic acids research*. 42:W361-367.
- Pedraza, L. 1997. Nuclear transport of myelin basic protein. *Journal of neuroscience research*. 50:258-264.
- Pedraza, L., L. Fidler, S.M. Staugaitis, and D.R. Colman. 1997. The active transport of myelin basic protein into the nucleus suggests a regulatory role in myelination. *Neuron*. 18:579-589.
- Philips, T., A. Bento-Abreu, A. Nonneman, W. Haeck, K. Staats, V. Geelen, N. Hersmus, B. Kusters, L. Van Den Bosch, P. Van Damme, W.D. Richardson, and W. Robberecht. 2013. Oligodendrocyte dysfunction in the pathogenesis of amyotrophic lateral sclerosis. *Brain : a journal of neurology*. 136:471-482.
- Powers, B.E., D.L. Sellers, E.A. Lovelett, W. Cheung, S.P. Aalami, N. Zapertov, D.O. Maris, and P.J. Horner. 2013. Remyelination reporter reveals prolonged refinement of spontaneously regenerated myelin. *Proceedings of the National Academy of Sciences of the United States of America*. 110:4075-4080.
- Quarles, M., Morell 2006. Myelin Formation, Structure and Biochemistry *In* Basic Neurochemistry: Molecular, Cellular and Medical Aspects. Siegel, editor. Elsevier Academic Press
- Raj, A., P. van den Bogaard, S.A. Rifkin, A. van Oudenaarden, and S. Tyagi. 2008. Imaging individual mRNA molecules using multiple singly labeled probes. *Nature methods*. 5:877-879.
- Rajgor, D., and C.M. Shanahan. 2014. RNA granules and cytoskeletal links. *Biochemical Society transactions*. 42:1206-1210.

- Raju, C.S., N. Fukuda, C. Lopez-Iglesias, C. Goritz, N. Visa, and P. Percipalle. 2011. In neurons, activity-dependent association of dendritically transported mRNA transcripts with the transacting factor CBF-A is mediated by A2RE/RTS elements. *Molecular biology of the cell*. 22:1864-1877.
- Raju, C.S., C. Goritz, Y. Nord, O. Hermanson, C. Lopez-Iglesias, N. Visa, G. Castelo-Branco, and P. Percipalle. 2008. In cultured oligodendrocytes the A/B-type hnRNP CBF-A accompanies MBP mRNA bound to mRNA trafficking sequences. *Molecular biology of the cell*. 19:3008-3019.
- Readhead, C., and L. Hood. 1990. The dysmyelinating mouse mutations shiverer (shi) and myelin deficient (shimld). *Behavior genetics*. 20:213-234.
- Readhead, C., B. Popko, N. Takahashi, H.D. Shine, R.A. Saavedra, R.L. Sidman, and L. Hood. 1987. Expression of a myelin basic protein gene in transgenic shiverer mice: correction of the dysmyelinating phenotype. *Cell*. 48:703-712.
- Richardson, W.D., N. Kessaris, and N. Pringle. 2006. Oligodendrocyte wars. *Nature reviews. Neuroscience*. 7:11-18.
- Richter, J.D. 2007. CPEB: a life in translation. *Trends in biochemical sciences*. 32:279-285.
- Rogelj, B., L.E. Easton, G.K. Bogu, L.W. Stanton, G. Rot, T. Curk, B. Zupan, Y. Sugimoto, M. Modic, N. Haberman, J. Tollervey, R. Fujii, T. Takumi, C.E. Shaw, and J. Ule. 2012. Widespread binding of FUS along nascent RNA regulates alternative splicing in the brain. *Scientific reports*. 2:603.
- Rouya, C., N. Siddiqui, M. Morita, T.F. Duchaine, M.R. Fabian, and N. Sonenberg. 2014. Human DDX6 effects miRNA-mediated gene silencing via direct binding to CNOT1. *Rna*. 20:1398-1409.
- Rowitch, D.H., and A.R. Kriegstein. 2010. Developmental genetics of vertebrate glial-cell specification. *Nature*. 468:214-222.
- Sabatelli, M., A. Moncada, A. Conte, S. Lattante, G. Marangi, M. Luigetti, M. Lucchini, M. Mirabella, A. Romano, A. Del Grande, G. Bisogni, P.N. Doronzio, P.M. Rossini, and M. Zollino. 2013. Mutations in the 3' untranslated region of FUS causing FUS overexpression are associated with amyotrophic lateral sclerosis. *Human molecular genetics*. 22:4748-4755.
- Sakry, D., A. Neitz, J. Singh, R. Frischknecht, D. Marongiu, F. Biname, S.S. Perera, K. Endres, B. Lutz, K. Radyushkin, J. Trotter, and T. Mittmann. 2014. Oligodendrocyte precursor cells modulate the neuronal network by activity-dependent ectodomain cleavage of glial NG2. *PLoS biology*. 12:e1001993.
- Sakurai, T., N.P. Dorr, N. Takahashi, L.A. McInnes, G.A. Elder, and J.D. Buxbaum. 2011. Haploinsufficiency of Gtf2i, a gene deleted in Williams Syndrome, leads to increases in social interactions. *Autism research : official journal of the International Society for Autism Research*. 4:28-39.
- Samaan, S., L.C. Tranchevent, E. Dardenne, M. Polay Espinoza, E. Zonta, S. Germann, L. Gratadou, M. Dutertre, and D. Auboeuf. 2014. The Ddx5 and Ddx17 RNA helicases are cornerstones in the complex regulatory array of steroid hormone-signaling pathways. *Nucleic acids research*. 42:2197-2207.
- Sambrook, J.R., D.W. . 2001. Molecular Cloning: A laboratory Manual. Cold Spring Harbor Laboratory Press Cold Spring Harbor, New York.
- Santoro, M.R., S.M. Bray, and S.T. Warren. 2012. Molecular mechanisms of fragile X syndrome: a twenty-year perspective. *Annual review of pathology*. 7:219-245.
- Saporita, A.J., H.C. Chang, C.L. Winkler, A.J. Apicelli, R.D. Kladney, J. Wang, R.R. Townsend, L.S. Michel, and J.D. Weber. 2011. RNA helicase DDX5 is a p53-independent target of ARF that participates in ribosome biogenesis. *Cancer research*. 71:6708-6717.
- Savas, J.N., B.H. Toyama, T. Xu, J.R. Yates, 3rd, and M.W. Hetzer. 2012. Extremely long-lived nuclear pore proteins in the rat brain. *Science*. 335:942.
- Schwartz, J.C., C.C. Ebmeier, E.R. Podell, J. Heimiller, D.J. Taatjes, and T.R. Cech. 2012. FUS binds the CTD of RNA polymerase II and regulates its phosphorylation at Ser2. *Genes & development*. 26:2690-2695.
- Seiberlich, V., N.G. Bauer, L. Schwarz, C. Ffrench-Constant, O. Goldbaum, and C. Richter-Landsberg. 2015. Downregulation of the microtubule associated protein Tau impairs process outgrowth and myelin basic protein mRNA transport in oligodendrocytes. *Glia*. 63:1621-1635.
- Sephton, C.F., A.A. Tang, A. Kulkarni, J. West, M. Brooks, J.J. Stubblefield, Y. Liu, M.Q. Zhang, C.B. Green, K.M. Huber, E.J. Huang, J. Herz, and G. Yu. 2014. Activity-dependent FUS dysregulation disrupts synaptic homeostasis. *Proceedings of the National Academy of Sciences of the United States of America*. 111:E4769-4778.
- Shan, J., K. Moran-Jones, T.P. Munro, G.J. Kidd, D.J. Winzor, K.S. Hoek, and R. Smith. 2000. Binding of an RNA trafficking response element to heterogeneous nuclear ribonucleoproteins A1 and A2. *The Journal of biological chemistry*. 275:38286-38295.

- Shelkovnikova, T.A., H.K. Robinson, N. Connor-Robson, and V.L. Buchman. 2013. Recruitment into stress granules prevents irreversible aggregation of FUS protein mislocalized to the cytoplasm. *Cell cycle*. 12:3194-3202.
- Shelkovnikova, T.A., H.K. Robinson, J.A. Southcombe, N. Ninkina, and V.L. Buchman. 2014. Multistep process of FUS aggregation in the cell cytoplasm involves RNA-dependent and RNA-independent mechanisms. *Human molecular genetics*. 23:5211-5226.
- Sherman, D.L., and P.J. Brophy. 2005. Mechanisms of axon ensheathment and myelin growth. *Nature reviews. Neuroscience*. 6:683-690.
- Shifera, A.S., and J.A. Hardin. 2010. Factors modulating expression of Renilla luciferase from control plasmids used in luciferase reporter gene assays. *Analytical biochemistry*. 396:167-172.
- Simons, M., and K. Trajkovic. 2006. Neuron-glia communication in the control of oligodendrocyte function and myelin biogenesis. *Journal of cell science*. 119:4381-4389.
- Simons, M., and J. Trotter. 2007. Wrapping it up: the cell biology of myelination. *Current opinion in neurobiology*. 17:533-540.
- Slobodin, B., and J.E. Gerst. 2010. A novel mRNA affinity purification technique for the identification of interacting proteins and transcripts in ribonucleoprotein complexes. *Rna*. 16:2277-2290.
- Smith, G.S., B. Samborska, S.P. Hawley, J.M. Klaiman, T.E. Gillis, N. Jones, J.M. Boggs, and G. Harauz. 2013. Nucleus-localized 21.5-kDa myelin basic protein promotes oligodendrocyte proliferation and enhances neurite outgrowth in coculture, unlike the plasma membrane-associated 18.5-kDa isoform. *Journal of neuroscience research*. 91:349-362.
- Smith, G.S., L.V. Seymour, J.M. Boggs, and G. Harauz. 2012. The 21.5-kDa isoform of myelin basic protein has a non-traditional PY-nuclear-localization signal. *Biochemical and biophysical research communications*. 422:670-675.
- Smith, R. 2004. Moving molecules: mRNA trafficking in Mammalian oligodendrocytes and neurons. *The Neuroscientist : a review journal bringing neurobiology, neurology and psychiatry*. 10:495-500.
- Snaidero, N., W. Mobius, T. Czopka, L.H. Hekking, C. Mathisen, D. Verkleij, S. Goebbels, J. Edgar, D. Merkler, D.A. Lyons, K.A. Nave, and M. Simons. 2014. Myelin membrane wrapping of CNS axons by PI(3,4,5)P3-dependent polarized growth at the inner tongue. *Cell*. 156:277-290.
- Sobottko, B., U. Ziegler, A. Kaech, B. Becher, and N. Goebels. 2011. CNS live imaging reveals a new mechanism of myelination: the liquid croissant model. *Glia*. 59:1841-1849.
- Spencer, C.M., E. Serysheva, L.A. Yuva-Paylor, B.A. Oostra, D.L. Nelson, and R. Paylor. 2006. Exaggerated behavioral phenotypes in Fmr1/Fxr2 double knockout mice reveal a functional genetic interaction between Fragile X-related proteins. *Human molecular genetics*. 15:1984-1994.
- Sperber, B.R., E.A. Boyle-Walsh, M.J. Engleka, P. Gadue, A.C. Peterson, P.L. Stein, S.S. Scherer, and F.A. McMorris. 2001. A unique role for Fyn in CNS myelination. *The Journal of neuroscience : the official journal of the Society for Neuroscience*. 21:2039-2047.
- Sreedharan, J., I.P. Blair, V.B. Tripathi, X. Hu, C. Vance, B. Rogelj, S. Ackerley, J.C. Durnall, K.L. Williams, E. Buratti, F. Baralle, J. de Belleruche, J.D. Mitchell, P.N. Leigh, A. Al-Chalabi, C.C. Miller, G. Nicholson, and C.E. Shaw. 2008. TDP-43 mutations in familial and sporadic amyotrophic lateral sclerosis. *Science*. 319:1668-1672.
- Staats, K.A., D. Pombal, S. Schonefeldt, L. Van Helleputte, H. Maurin, T. Dresselaers, K. Govaerts, U. Himmelreich, F. Van Leuven, L. Van Den Bosch, J. Dooley, S. Humblet-Baron, and A. Liston. 2015. Transcriptional upregulation of myelin components in spontaneous myelin basic protein-deficient mice. *Brain research*. 1606:125-132.
- Staugaitis, S.M., P.R. Smith, and D.R. Colman. 1990. Expression of myelin basic protein isoforms in nonglial cells. *The Journal of cell biology*. 110:1719-1727.
- Stevenson, R.J., S.J. Hamilton, D.E. MacCallum, P.A. Hall, and F.V. Fuller-Pace. 1998. Expression of the 'dead box' RNA helicase p68 is developmentally and growth regulated and correlates with organ differentiation/maturation in the fetus. *The Journal of pathology*. 184:351-359.
- Suzuki, K., and M.N. Rasband. 2008. Molecular mechanisms of node of Ranvier formation. *Current opinion in cell biology*. 20:616-623.
- Suzuki, H.I., K. Yamagata, K. Sugimoto, T. Iwamoto, S. Kato, and K. Miyazono. 2009. Modulation of microRNA processing by p53. *Nature*. 460:529-533.
- Takahashi, N., A. Roach, D.B. Teplow, S.B. Prusiner, and L. Hood. 1985. Cloning and characterization of the myelin basic protein gene from mouse: one gene can encode both 14 kd and 18.5 kd MBPs by alternate use of exons. *Cell*. 42:139-148.

- Takanashi, K., and A. Yamaguchi. 2014. Aggregation of ALS-linked FUS mutant sequesters RNA binding proteins and impairs RNA granules formation. *Biochemical and biophysical research communications*. 452:600-607.
- Tanaka, T., T. Ishii, D. Mizuno, T. Mori, R. Yamaji, Y. Nakamura, S. Kumazawa, T. Nakayama, and M. Akagawa. 2011. (-)-Epigallocatechin-3-gallate suppresses growth of AZ521 human gastric cancer cells by targeting the DEAD-box RNA helicase p68. *Free radical biology & medicine*. 50:1324-1335.
- Tasaki, I. 2007. Saltatory conduction. In *Scholarpedia*. Vol. 2.
- Thomas, M.G., L.J. Martinez Tosar, M. Loschi, J.M. Pasquini, J. Correale, S. Kindler, and G.L. Boccaccio. 2005. Staufen recruitment into stress granules does not affect early mRNA transport in oligodendrocytes. *Molecular biology of the cell*. 16:405-420.
- Tissera, H., M. Kodiha, and U. Stochaj. 2010. Nuclear envelopes show cell-type specific sensitivity for the permeabilization with digitonin.
- Tomassy, G.S., D.R. Berger, H.H. Chen, N. Kasthuri, K.J. Hayworth, A. Vercelli, H.S. Seung, J.W. Lichtman, and P. Arlotta. 2014. Distinct profiles of myelin distribution along single axons of pyramidal neurons in the neocortex. *Science*. 344:319-324.
- Toritsuka, M., M. Makinodan, and T. Kishimoto. 2015. Social Experience-Dependent Myelination: An Implication for Psychiatric Disorders. *Neural plasticity*. 2015:465345.
- Torvund-Jensen, J., J. Steengaard, L. Reimer, L.B. Fihl, and L.S. Laursen. 2014. Transport and translation of MBP mRNA is regulated differently by distinct hnRNP proteins. *Journal of cell science*. 127:1550-1564.
- Trapp, B.D., T. Moench, M. Pulley, E. Barbosa, G. Tennekoon, and J. Griffin. 1987. Spatial segregation of mRNA encoding myelin-specific proteins. *Proceedings of the National Academy of Sciences of the United States of America*. 84:7773-7777.
- Trotter, J., D. Bitter-Suermann, and M. Schachner. 1989. Differentiation-regulated loss of the polysialylated embryonic form and expression of the different polypeptides of the neural cell adhesion molecule by cultured oligodendrocytes and myelin. *Journal of neuroscience research*. 22:369-383.
- Tsai, B.P., X. Wang, L. Huang, and M.L. Waterman. 2011. Quantitative profiling of in vivo-assembled RNA-protein complexes using a novel integrated proteomic approach. *Molecular & cellular proteomics : MCP*. 10:M110007385.
- Tyagi, S. 2009. Imaging intracellular RNA distribution and dynamics in living cells. *Nature methods*. 6:331-338.
- Ueki, T., Y. Tsuruo, Y. Yamamoto, K. Yoshimura, H. Takanaga, C. Seiwa, K. Motojima, H. Asou, and M. Yamamoto. 2012. A new monoclonal antibody, 4F2, specific for the oligodendroglial cell lineage, recognizes ATP-dependent RNA helicase Ddx54: possible association with myelin basic protein. *Journal of neuroscience research*. 90:48-59.
- Ueno, S., V.W. Handley, S. Byravan, and A.T. Campagnoni. 1994. Structural features of myelin basic protein mRNAs influence their translational efficiencies. *Journal of neurochemistry*. 62:1254-1259.
- Ule, J., K.B. Jensen, M. Ruggiu, A. Mele, A. Ule, and R.B. Darnell. 2003. CLIP identifies Nova-regulated RNA networks in the brain. *Science*. 302:1212-1215.
- Valegard, K., J.B. Murray, N.J. Stonehouse, S. van den Worm, P.G. Stockley, and L. Liljas. 1997. The three-dimensional structures of two complexes between recombinant MS2 capsids and RNA operator fragments reveal sequence-specific protein-RNA interactions. *Journal of molecular biology*. 270:724-738.
- Valori, C.F., L. Brambilla, F. Martorana, and D. Rossi. 2014. The multifaceted role of glial cells in amyotrophic lateral sclerosis. *Cellular and molecular life sciences : CMLS*. 71:287-297.
- Vance, C., B. Rogelj, T. Hortobagyi, K.J. De Vos, A.L. Nishimura, J. Sreedharan, X. Hu, B. Smith, D. Ruddy, P. Wright, J. Ganesalingam, K.L. Williams, V. Tripathi, S. Al-Saraj, A. Al-Chalabi, P.N. Leigh, I.P. Blair, G. Nicholson, J. de Belleruche, J.M. Gallo, C.C. Miller, and C.E. Shaw. 2009. Mutations in FUS, an RNA processing protein, cause familial amyotrophic lateral sclerosis type 6. *Science*. 323:1208-1211.
- Velumian, A.A., M. Samoilova, and M.G. Fehlings. 2011. Visualization of cytoplasmic diffusion within living myelin sheaths of CNS white matter axons using microinjection of the fluorescent dye Lucifer Yellow. *NeuroImage*. 56:27-34.
- Verkhatsky, A. 2010. Physiology of neuronal-glial networking. *Neurochemistry international*. 57:332-343.
- Wake, H., P.R. Lee, and R.D. Fields. 2011. Control of local protein synthesis and initial events in myelination by action potentials. *Science*. 333:1647-1651.
- Wake, H., F.C. Ortiz, D.H. Woo, P.R. Lee, M.C. Angulo, and R.D. Fields. 2015. Nonsynaptic junctions on myelinating glia promote preferential myelination of electrically active axons. *Nature communications*. 6:7844.

- Wang, E., V. Aslanzadeh, F. Papa, H. Zhu, P. de la Grange, and F. Cambi. 2012. Global profiling of alternative splicing events and gene expression regulated by hnRNP/F. *PLoS one*. 7:e51266.
- Wang, E., and F. Cambi. 2009. Heterogeneous nuclear ribonucleoproteins H and F regulate the proteolipid protein/DM20 ratio by recruiting U1 small nuclear ribonucleoprotein through a complex array of G runs. *The Journal of biological chemistry*. 284:11194-11204.
- Wang, H., X. Gao, Y. Huang, J. Yang, and Z.R. Liu. 2009. P68 RNA helicase is a nucleocytoplasmic shuttling protein. *Cell research*. 19:1388-1400.
- Wang, H., L. Ku, D.J. Osterhout, W. Li, A. Ahmadian, Z. Liang, and Y. Feng. 2004. Developmentally-programmed FMRP expression in oligodendrocytes: a potential role of FMRP in regulating translation in oligodendroglia progenitors. *Human molecular genetics*. 13:79-89.
- Wang, X., J.C. Schwartz, and T.R. Cech. 2015a. Nucleic acid-binding specificity of human FUS protein. *Nucleic acids research*.
- Wang, Y., G. Lacroix, J. Haines, E. Doukhanine, G. Almazan, and S. Richard. 2010. The QKI-6 RNA binding protein localizes with the MBP mRNAs in stress granules of glial cells. *PLoS one*. 5.
- Wang, Z., Z. Luo, L. Zhou, X. Li, T. Jiang, and E. Fu. 2015b. DDX5 promotes proliferation and tumorigenesis of NSCLC cells via activating beta-catenin signaling pathway. *Cancer science*.
- Watanabe, M., J. Yanagisawa, H. Kitagawa, K. Takeyama, S. Ogawa, Y. Arao, M. Suzawa, Y. Kobayashi, T. Yano, H. Yoshikawa, Y. Masuhiro, and S. Kato. 2001. A subfamily of RNA-binding DEAD-box proteins acts as an estrogen receptor alpha coactivator through the N-terminal activation domain (AF-1) with an RNA coactivator, SRA. *The EMBO journal*. 20:1341-1352.
- Weil, T.T., R.M. Parton, and I. Davis. 2010. Making the message clear: visualizing mRNA localization. *Trends in cell biology*. 20:380-390.
- White, R. 2007. The central role of Fyn kinase in axon-glia signalling and translation of myelin proteins. In *Biology Johannes Gutenberg-University Mainz*.
- White, R., C. Gonsior, N.M. Bauer, E.M. Kramer-Albers, H.J. Luhmann, and J. Trotter. 2012. Heterogeneous nuclear ribonucleoprotein (hnRNP) F is a novel component of oligodendroglial RNA transport granules contributing to regulation of myelin basic protein (MBP) synthesis. *The Journal of biological chemistry*. 287:1742-1754.
- White, R., C. Gonsior, E.M. Kramer-Albers, N. Stohr, S. Huttelmaier, and J. Trotter. 2008. Activation of oligodendroglial Fyn kinase enhances translation of mRNAs transported in hnRNP A2-dependent RNA granules. *The Journal of cell biology*. 181:579-586.
- Wilson, B.J., G.J. Bates, S.M. Nicol, D.J. Gregory, N.D. Perkins, and F.V. Fuller-Pace. 2004. The p68 and p72 DEAD box RNA helicases interact with HDAC1 and repress transcription in a promoter-specific manner. *BMC molecular biology*. 5:11.
- Wu, B., J. Chen, and R.H. Singer. 2014. Background free imaging of single mRNAs in live cells using split fluorescent proteins. *Scientific reports*. 4:3615.
- Wu, B., V. Miskolci, H. Sato, E. Tutucci, C.A. Kenworthy, S.K. Donnelly, Y.J. Yoon, D. Cox, R.H. Singer, and L. Hodgson. 2015. Synonymous modification results in high-fidelity gene expression of repetitive protein and nucleotide sequences. *Genes & development*. 29:876-886.
- Xavier, C.P., R.H. Rastetter, M. Blomacher, M. Stumpf, M. Himmel, R.O. Morgan, M.P. Fernandez, C. Wang, A. Osman, Y. Miyata, R.A. Gjerset, L. Eichinger, A. Hofmann, S. Linder, A.A. Noegel, and C.S. Clemen. 2012. Phosphorylation of CRN2 by CK2 regulates F-actin and Arp2/3 interaction and inhibits cell migration. *Scientific reports*. 2:241.
- Yang, L., C. Lin, and Z.R. Liu. 2005a. Phosphorylations of DEAD box p68 RNA helicase are associated with cancer development and cell proliferation. *Molecular cancer research : MCR*. 3:355-363.
- Yang, L., C. Lin, and Z.R. Liu. 2005b. Signaling to the DEAD box--regulation of DEAD-box p68 RNA helicase by protein phosphorylations. *Cellular signalling*. 17:1495-1504.
- Yang, L., C. Lin, and Z.R. Liu. 2006. P68 RNA helicase mediates PDGF-induced epithelial mesenchymal transition by displacing Axin from beta-catenin. *Cell*. 127:139-155.
- Yasuda, K., H. Zhang, D. Loiselle, T. Haystead, I.G. Macara, and S. Mili. 2013. The RNA-binding protein Fus directs translation of localized mRNAs in APC-RNP granules. *The Journal of cell biology*. 203:737-746.
- Yoon, J.H., S. Srikantan, and M. Gorospe. 2012. MS2-TRAP (MS2-tagged RNA affinity purification): tagging RNA to identify associated miRNAs. *Methods*. 58:81-87.

- Young, K.M., K. Psachoulia, R.B. Tripathi, S.J. Dunn, L. Cossell, D. Attwell, K. Tohyama, and W.D. Richardson. 2013. Oligodendrocyte dynamics in the healthy adult CNS: evidence for myelin remodeling. *Neuron*. 77:873-885.
- Zalc, B., D. Goujet, and D. Colman. 2008. The origin of the myelination program in vertebrates. *Current biology : CB*. 18:R511-512.
- Zeisel, A., A.B. Munoz-Manchado, S. Codeluppi, P. Lonnerberg, G. La Manno, A. Jureus, S. Marques, H. Munguba, L. He, C. Betsholtz, C. Rolny, G. Castelo-Branco, J. Hjerling-Leffler, and S. Linnarsson. 2015. Brain structure. Cell types in the mouse cortex and hippocampus revealed by single-cell RNA-seq. *Science*. 347:1138-1142.
- Zeitelhofer, M., D. Karra, P. Macchi, M. Tolino, S. Thomas, M. Schwarz, M. Kiebler, and R. Dahm. 2008. Dynamic interaction between P-bodies and transport ribonucleoprotein particles in dendrites of mature hippocampal neurons. *The Journal of neuroscience : the official journal of the Society for Neuroscience*. 28:7555-7562.
- Zhan, R., M. Yamamoto, T. Ueki, N. Yoshioka, K. Tanaka, H. Morisaki, C. Seiwa, Y. Yamamoto, H. Kawano, Y. Tsuruo, K. Watanabe, H. Asou, and S. Aiso. 2013. A DEAD-box RNA helicase Ddx54 protein in oligodendrocytes is indispensable for myelination in the central nervous system. *Journal of neuroscience research*. 91:335-348.
- Zhang, Y., K. Chen, S.A. Sloan, M.L. Bennett, A.R. Scholze, S. O'Keefe, H.P. Phatnani, P. Guarnieri, C. Caneda, N. Ruderisch, S. Deng, S.A. Liddelow, C. Zhang, R. Daneman, T. Maniatis, B.A. Barres, and J.Q. Wu. 2014. An RNA-sequencing transcriptome and splicing database of glia, neurons, and vascular cells of the cerebral cortex. *The Journal of neuroscience : the official journal of the Society for Neuroscience*. 34:11929-11947.
- Ziemann, A., S. Hess, R. Bhuwania, S. Linder, P. Kloppenburg, A.A. Noegel, and C.S. Clemen. 2013. CRN2 enhances the invasiveness of glioblastoma cells. *Neuro-oncology*. 15:548-561.
- Zinszner, H., J. Sok, D. Immanuel, Y. Yin, and D. Ron. 1997. TLS (FUS) binds RNA in vivo and engages in nucleocytoplasmic shuttling. *Journal of cell science*. 110 (Pt 15):1741-1750.
- Zivraj, K.H., Y.C. Tung, M. Piper, L. Gumy, J.W. Fawcett, G.S. Yeo, and C.E. Holt. 2010. Subcellular profiling reveals distinct and developmentally regulated repertoire of growth cone mRNAs. *The Journal of neuroscience : the official journal of the Society for Neuroscience*. 30:15464-15478.
- Zuchero, J.B., and B.A. Barres. 2011. Between the sheets: a molecular sieve makes myelin membranes. *Developmental cell*. 21:385-386.
- Zuchero, J.B., M.M. Fu, S.A. Sloan, A. Ibrahim, A. Olson, A. Zaremba, J.C. Dugas, S. Wienbar, A.V. Caprariello, C. Kantor, D. Leonoudakus, K. Lariosa-Willingham, G. Kronenberg, K. Gertz, S.H. Soderling, R.H. Miller, and B.A. Barres. 2015. CNS Myelin Wrapping Is Driven by Actin Disassembly. *Developmental cell*.

Appendix

A. Danksagung / Acknowledgements

B. Curriculum Vitae

C. Eidesstattliche Erklärung

Ich erkläre hiermit, dass die vorgelegte Dissertation von mir selbstständig, ohne unzulässige Hilfe Dritter und ohne Benutzung anderer als der angegebenen Hilfsmittel, angefertigt wurde. Alle von mir benutzten Veröffentlichungen, ungedruckten Materialien, sonstige Hilfsmittel sowie Textstellen, die ich wörtlich oder inhaltlich aus gedruckten oder ungedruckten Arbeiten übernommen habe, habe ich als solche gekennzeichnet und mit den erforderlichen bibliographischen Angaben nachgewiesen. Unterstützungsleistungen, die ich von anderen Personen erhalten habe, wurden in der Dissertationsschrift als solche benannt. Die Dissertation wurde bei keiner anderen Fakultät oder einem anderen Fachbereich vorgelegt, weder im In- noch im Ausland. Überdies bin ich nicht im Besitz eines anderen Doktorgrades. Ein bisher erworbener Doktorgrad wurde mir nicht aberkannt. Ich habe bisher kein Promotionsverfahren erfolglos beendet. Mir ist bekannt, dass die Zulassung zur Promotion zu versagen ist, wenn die Unterlagen unvollständig oder die Angaben unrichtig sind. Ich bin darüber informiert, dass ich zur Führung des Dokortitels erst mit Aushändigung der Promotionsurkunde berechtigt bin.

Mainz, den 30.9.2015

Peter Hoch-Kraft